A MOLECULAR, STRUCTURAL, AND CELLULAR MULTIPLE-LEVEL STUDY AIMED AT UNDERSTANDING THE UNIQUE REACTION CATALYZED BY THE LAST ENZYME IN THE HEME-BIOSYNTHESIS PATHWAY OF GRAM-POSITIVE BACTERIA, COPROHEME DECARBOXYLASE (CHDC)

by

Arianna I. Celis Luna

A dissertation submitted in partial fulfillment
of the requirements for the degree

of

Doctor of Philosophy

in

Biochemsitry

MONTANA STATE UNIVERSITY
Bozeman, Montana

July 2018

©COPYRIGHT

by

Arianna I. Celis Luna

2018

All Rights Reserved

DEDICATION

Para mi mami y papi que han dado todo para el bien estar de sus hijas, este trabajo es papa ustedes. El nombre Celis Luna ya tiene Dr!

ACKNOWLEDGEMENTS

The work presented here and the invaluable knowledge and skills obtained while doing this work would not be possible without the help, support, care, and dedication to my development of the great mentors that I have had throughout my academic career. My upmost gratitude to Dr. Jen DuBois for taking me under her wing and giving me the tools to grow as a scientist and as a person-thank you. I also need to thank Coach Mike Barbee, whose mentorship, support, and care were essential to this achievement. I will always hold that close to my heart. I am grateful for all the people who have provided me with experimental and instrument usage help, as well as all other kinds of assistance. A special thanks to Doreen Brown for dealing with all my "special" administrative paper work. I thank my collaborators, Dr. Eric Skaar and Jake Choby, who were vital to the development of the experiments in *S. aureus,* Dr. Kent Rodgers and Dr. Gudrun Lukat-Rodgers who are always excited to hear about our experiments and look at our proteins with rR, and to George Gauss for his mentorship with protein crystallography, molecular biology, and more. To the members of the DuBois Lab, thank you for your companionship, friendship, and conversations. Melodie, I could not have done it without you!

To Nick, thank you for your unconditional love, companionship, support, and patience, and for encouraging me to follow my dreams. Thank you for all you do.

My most heartfelt thank you to my mami and daddy. There are no words to describe how grateful I am to you. This work and achievement is most definitely because of you and for you. This success is not only mine, but yours too. Los quiero mucho.

TABLE OF CONTENTS

SECTION I. AN INTRODUCTION TO HEME B BIOSYNTHESIS AND OUR INTEREST IN THE NOVEL ENZYME CHDC

1. THE TERMINAL THREE CATALYTIC STEPS OF MAKING HEME, A LITERATURE REVIEW 1

Multiple Ways to Make Heme b 2
The PPD Branch can be Further Split into the PPD-(O_2-dependent) and PPD-(O_2-independent) Branches 5
Decarboxylation of the Ring A- and B- Propionate Groups (CgdC, CgdH, and ChdC).6
Oxidation of the Tetrapyrrole Rings (PgoX, PgdH1, PgdH2 and CgoX) 10
Metalation of the Tetrapyrrole Ring (PpfC vs CdfC).......... 16
What Happens After Heme *b* is Synthesized and Final Notes 21
References 23

2. STUDY OF THE NOVEL, LAST ENZYME IN THE HEME B BIOSYNTHESIS PATHWAY OF GRAM-POSITIVE BACTERIA, CHDC (HEMQ) 26
Discovery of ChdC (Formerly Known as HemQ 26
ChdC and the ChdC-Protein Family 28
The ChdC Active Site is Unlike Canonical Peroxidases 31
A Multi-Level Approach to Understanding ChdC and its Unique Reaction 33
Note on the Enzyme Nomenclature Used Here 34
Referenes 35

SECTION II. OXIDATIVE DECARBOXYLATION BY CHDC AT THE MOLECULAR LEVEL

3. UNUSUAL PEROXIDE-DEPENDENT, HEME-TRANSFORMING REACTION CATALYZED BY HEMQ 36
Contribution of Authors and Co-Authors 36
Manuscript Information Page 38
Abstract 39
Introduction 40
Experimental Methods 42
    Reagents and Stocks 42
    Synthesis and Purification of Harderoheme Isomers III and IV 43
    Expression and Purification of *Sa*HemQ Bound to Substrate and Potential Intermediates 43
    UV/Visible and resonance Raman (rR) Spectroscopy 45

TABLE OF CONTENTS CONTINUED

Real-Time Monitoring of Reactions 45
Product Analyses by Pyridine Hemochrome Assay, HPLC, and MS....................46
Results 47
Characterization of SaHemQ Bound to Substrate, Product, and Potential Intermediate 47
Titrimetric Reactions Between *SaHemQ*-coproheme III and H_2O_2.......................49
Time Resolved Reactions Between *Sa*HemQ-coproheme III and H_2O_2 51
Reactions between SaHemQ complexes with harderohemes and H_2O_2................53
Reaction Between *Sa*HemQ-coproheme III and Peracetic Acid 53
Reaction Between *Sa*HemQ-coproheme III and mCPBA or t-Butyl-OOH..........54
Discussion 54
Figures 60
Associated Content...68
Supporting Information..68
Abbreviations..68
References 68

4. REACTIONS OF FERROUS COPROHEME DECARBOXYLASE (HEMQ) WITH O_2 AND H_2O_2 YIELD FERRIC HEME B 72

Contribution of Authors and Co-Authors 72
Manuscript Information Page 73
Abstract...74
Introduction 75
Experimental Methods 77
Preparation of Stocks and pH Buffers 77
Protein Production and Complex Formation 77
Heme Reduction..78
Titrations with Oxidants 78
HPLC 79
EPR 79
Transient Kinetics 80
Testing for Oxygenase Activity 81
Spectroelectrochemical Titrations 81
UV/visible and Resonance Raman Characterization 82
Results 83
The Purified Decarboxylase Forms Stable Complexes with Hardero- and Coproheme..83
UV/Vis Features of the Oxidized and Reduced Enzyme-heme Complexes are Distinct 83

TABLE OF CONTENTS CONTINUED

Reactions between Ferrous Heme Species and O_2 do not Lead to Decarboxylation....83
The Ferrous Enzyme-coproheme Complex and O_2 Rapidly form an Intermediate that Converts to Ferric Coproheme....84
The Oxidative Decarboxylations Do Not Occur via a Monooxygenase Intermediate....84
Decarboxylation of the Ferrous Coproheme or Harderoheme Complexes does not Occur Following Reaction with H_2O_2....85
The Ferrous Coproheme-Decarboxylase Complex Reacts more Rapidly with Air than with H_2O_2....86
A Similar Intermediate Forms whether O_2, H_2O_2, or Peracetic Acid is the Oxidant or Harderoheme is the Tetrapyrrole Substrate....87
Reactions of Ferric Coproheme- or Harderoheme-Decarboxylase Complexes with H_2O_2 are Slow and pH Dependent....88
Reactions between Ferric Coproheme-decarboxylase Complex and Peracetic Acid are Fast and pH-independent....89
Solvent Isotope Effect on the Ferric Coproheme-decarboxylase Reaction Indicates Rate Limiting Proton Transfer....90
Resonance Raman (rR) Spectra for Ferrous Decarboxylase-Coproheme Complex Indicate a Pentacoordinate High-Spin Coproheme with a Neutral His Ligand....91
The Reduction Potential for the Decarboxylase-coproheme Complex is Peroxidase-like and Becomes More Positive as the Propionates Convert to Vinyls....92
Discussion....93
Figures....101
Tables....109
Associated Content....111
Supporting Information....111
Acknowledgement....111
Abbreviations....112
References....112

SECTION III. A PROTEIN STRUCTURE-BASED MECHANISM FOR COPROHEME DECARBOXYLATION BY CHDC

5. A STRUCTURE-BASED MECHANISM FOR OXIDATIVE DECARBOXYLATION REACTIONS MEDIATED BY AMINO ACIDS AND HEME PROPIONATES IN COPROHEME DECARBOXYLASE (HEMQ)....117

TABLE OF CONTENTS CONTINUED

Contribution of Authors and Co-Authors 117
Manuscript Information Page 119
Abstract 120
  Introduction 121
  Experimental Methods 124
    Expression, Purification, and Ligand Binding to WT and Mutant Coproheme Decarboxylases 124
    Structure Determination 125
    Determining Protein-heme Dissociation Constants 126
    Reactions of Decarboxylase-coproheme Complexes Monitored Following Titrimetric Addition of Oxidants 127
    Steady State Kinetics of Catalase Reactions 128
    Resonance Raman (rR) spectroscopy 129
  Results 129
    Co-crystals of the Decarboxylase with Mn-Coproheme Diffracted to 1.8 Å Resolution 129
    Structural changes associated with substrate binding to coproheme decarboxylase are confined to the C-terminus 130
    Coproheme binding site structure: Implications for mechanism 132
    Coproheme-bound CO interacts with the conserved distal Gln 140
    Disruption of H-bonding to Propionates 2 and 4 Alters Heme Conformation 142
  Discussion 148
  Associated Content 155
    Supporting Information 155
    Funding Resources 155
    Abbreviations 155
  References 156

6. COPROHEME DECARBOXYLATION VIA A FERRYL, PROPIONATE, AND A TYROSYL IN A RADICAL RELAY YIELDS HEME *B* 161

  Contribution of Authors and Co-Authors 161
  Manuscript Information Page 163
  Abstract 164
  Introduction 165
  Results 167
    Deuterium-labeled Coproheme III Was Generated in High Yield 167
    D-Tyr-labeled Decarboxylase Was Generated in Low Yield and its Reaction Was Less Efficient than Unlabeled Protein 168
    Time Resolved EPR Demonstrated Formation and Decay of an

TABLE OF CONTENTS CONTINUED

Organic Radical Reaction Intermediate 168
The Organic Radical is Localized on a Tyrosine Side Chain 169
The EPR Spectrum for the Intermediate Can Be Simulated with Hyperfine Coupling Due to the Y145 Methylene Protons and Slight G-anisotropy 170
Loss of the EPR Radical Signal Specifically in the Y145S Mutant Suggests That Y145 is the Site of the Radical Intermediate 171
Cleavage of the 2-propionate-β-C-H Bond by the Y145 Radical is Partly Rate Limiting 173
Y145• Formation is Accompanied by Loss of the High Spin Iron Signal 174
Y145• also Catalyzes the Decarboxylation of the Ferric Harderoheme Intermediate 175
Discussion 175
Conclusions 179
Experimental Procedures 180
Preparation of the decarboxylase (HemQ) from *Staphylococcus aureus* 180
Preparation of the Decarboxylase with Deuterated Tyrosine Side Chains 180
Generation of Decarboxylase-Substrate Complexes 181
Biosynthesis, Purification, and Characterization of Deuterium-Labeled Coproheme 182
HPLC 184
MS 184
NMR Spectroscopy 185
Monitoring Decarboxylase Reactions in Real Time with Stopped Flow UV/Visible spectroscopy (UV/Vis) 185
Time resolved EPR Spectroscopic Analyses of the Reaction of Decarboxylase-Tetrapyrrole Complexes with H_2O_2 186
Figures 188
Associated Content 196
Acknowledgments 196
Abbreviations 196
Conflicts of Interest 196
References 196

SECTION IV. ELUCIDATING THE ROLE OF CHDC AT THE CELLULAR LEVEL

7. PRELIMINARY EVIDENCE AND FUTURE DIRECTIONS IN THE INVESTIGATION OF A PROTEIN-PROTEIN INTERACTION BETWEEN CPFC AND CHDC 200
Background and Statement of the Knowledge Gap 200

TABLE OF CONTENTS CONTINUED

Control Over Metabolite Flux in the Heme *b* Biosynthesis Pathway is Essential 200
Regulation and Control in the PPD Branch 202
Regulation and Control in the CPD Branch is Not Known 205
Reasoning 207
Preliminary Studies 208
Methods 208
Reagents and Stocks 208
Preparation of the Coproheme Decarboxylase (ChdC) and Coproporphyrin Ferrochelatase (CpfC) Enzymes from *Staphylococcus aureus* 209
UV-Vis Spectroscopy 210
Determining a copropoprhyin-CpfC-ChdC Complex Dissociation Constant and protein-porphyrin Dissociation Constants 210
Growth Curve Phenotype Analysis of *S. aureus* ChdC Mutants 210
Cellular porphyrin quantification of *S. aureus* ChdC mutants by LC-MS 211
Results 212
Coproporphyrin III can be used as an indicator to visualize a CpfC-ChdC complex 212
Determining the Affinity of the CpfC-ChdC Complex in the Presence of Coproporphyrin 214
The CpfC-ChdC Complex Does Not Enhance Intrinsic Reactivity CpfC 216
The CpfC-ChdC complex does not enhance intrinsic reactivity CpfC 217
The E120L ChdC Residue is Responsible for the CpfC-ChdC Protein-Protein Interaction 219
Future Directions 223
References 225

8. THE TRUE FINAL STEP IN HEME B BIOSYNTHESIS; EXPLORING THE ROLE OF CHDC IN THE DELIVERY OF HEME B TO ITS FINAL DESTINATION 227
Background and Introduction 227
Targeted search for the gram-positive bacterial heme chaperone; Interrogating HemW 227
Preliminary and Proposed Experiments 230
Expression and Purification of *Sa*HemW 230
Characterization of the *Sa*HemW [Fe-S] Cluster via EPR 231
Analysis of SAM Binding and Cleavage Capacity of *Sa*HemW 231

TABLE OF CONTENTS CONTINUED

Characterization of Heme-Binding Properties of *Sa*HemW....................231
Measurement of Heme-Association and Heme-Dissociation Constants..232
In vitro Heme Transfer Experiments by UV-Vis....................................233
In vitro Heme Transfer Analysis by SEC and SDS-PAGE 233
Determining Rate of Heme Transfer...235
Preliminary Studies with N112L ChdC 235
Assessing the Role of the N112 Residue of ChdC in Heme Transfer to HemW...236
An Untargeted Approach to Finding the Gram-Positive Bacterial Heme Chaperone 236
Conclusions 237
References 237

9. CONCLUDING REMARKS...239

REFERENCES CITED...245

LIST OF TABLES

Table Page

1.1 Nomenclature of heme *b* biosynthesis enzymes 2

4.1. UV/vis bands for complexes of HemQ coproheme decarboxylase with substrate, intermediate, or product...109

4.2. Observed oxidation products following addition of defined amounts of H_2O_2 to decarboxylase complexes with ferrous/ferric coproheme or harderoheme, expressed on a per-substrate basis..110

4.3. Rate constants for reactions of decarboxylase complexes with oxidants (pH 7.4, 20 °C)..111

7.1 Summary of coproheme and coproporphyrin UV-Vis spectral features (50 mM Tris, pH 8, 150 mM NaCl) in solution or when enzyme-bound......214

7.2 K_D values calculated for enzyme-porphyrin complexes...............................216

7.3 Point mutations inserted on ChdC’s active site gate.....................................220

LIST OF FIGURES

Figure Page

1.1. Multiple heme *b* biosynthesis pathways 2

1.2. All heme *b* biosynthesis pathways share a common beginning and have uroporphyrinogen III as the final common intermediate.................................3

1.3. The PPD and CPD branches of heme *b* biosynthesis consist of the same chemical transformation but in a different order 5

1.4. Decarboxylation of coproporphyrinogen III to protoporphyrinogen IX in the PPD branch can be catalyzed aerobically or anaerobically by CgdC or CgdH, respectively 7

1.5. Figure 1.5. Decarboxylation of coproheme is the last transformative step in the CPC branch and it is catalyzed by ChdC......................................9

1.6. Three non-homologous, iso-functional enzymes to catalyze the oxidation of protoporphyrinogen IX to PPIX in the PPD branch 11

1.7. CgoX is homologous to PgoX but has a larger active site which allows it to accommodate its larger substrate..14

1.8. PpfC and CpfC share a similar structural fold and reaction mechanism 18

2.1. The PPD and CPD branches of heme *b* biosynthesis 27

2.2. ChdC does not catalyze the chlorite dismutase (cld) reaction and instead catalyzes the last step of the heme *b* biosynthesis pathway in gram-positive bacteria..28

2.3. The Cld family of enzymes (Pfam06778)..29

2.4. ChdC and canonical Clds share a common structural fold 30

2.6. Canonical heme peroxidases contain a highly polar active site which facilitates reactivity with H_2O_2 through a “push” and “pull” mechanism 31

3.1. Characteristic spectra of *Sa*HemQ in complex with hemes............................60

LIST OF FIGURES CONTINUED

Figure Page

3.2. Spectroscopic changes upon titration of the *Sa*HemQ-coproheme III complex with H_2O_2 61

3.3. HPLC analysis of the products of the reaction of the *Sa*HemQ-coproheme III complex with H_2O_2 62

3.4. Time resolved reactions between the *Sa*HemQ-coproheme III and 12 eq H_2O_2....63

3.5. Titration of *Sa*HemQ-coproheme III complex with peracetic acid 64

3.6. Overlay of the structures of a representative heme *b*-bound chlorite dismutase and solvent-bound HemQ 65

3.7. Scheme 3.1. Biosynthetic pathways leading to heme and other tetrapyrroles....66

3.8. Scheme 3.2. Substrate, possible intermediates, and product of the HemQ-catalyzed 66

3.10. Scheme 3.3. Possible reaction pathways following from Compound 0 67

4.1. The reaction between the ferrous coproheme-decarboxylase complex and O_2 leads to an intermediate, followed by oxidation of the coproheme iron 101

4.2. The ferrous coproheme-decarboxylase complex reacts faster with O_2 in air than with H_2O_2.....102

4.3. Oxidative decarboxylation of ferric coproheme occurs slowly and without observable intermediates when H_2O_2 is the oxidant....103

4.4. The rates of reactions between the ferric coproheme-decarboxylase and H_2O_2 are pH and solvent-isotope dependent....104

4.5. Vibrational characterization of the ferrous iron tetrapyrrole complexes of the coproheme decarboxylase....105

LIST OF FIGURES CONTINUED

Figure Page

4.6. The Fe(III)/(II) redox potential for decarboxylase-bound coproheme is peroxidase-like, and becomes more positive as each propionate is converted to a vinyl........106

4.7. Scheme 4.1. Possible coproheme decarboxylase pathways starting from Fe(II)coproheme........107

4.8. Scheme 4.2. Possible pathways for oxidative decarboxylation........108

5.0. Scheme 1. Reaction catalyzed by coproheme decarboxylase........124

5.1. Superposition of the apo and ligand-bound forms of coproheme decarboxylase illustrate the effects of tetrapyrrole binding........132

5.2. The structure of the coproheme binding site in coproheme decarboxylase has important implications for the chemical mechanism.......135

5.3. Low frequency rR spectra report on the core and peripheral environment of hemes bound to decarboxylases........137

5.4. rR characterization of ferrous CO complexes of the *Sa* decarboxylase report on their proximal ligands and distal environments........141

5.5. Mutations at Lys149 and Tyr145 prevent decarboxylation of one or both propionic acid substrates, respectively........144

5.6. The catalase activity of coproheme decarboxylase is strongly enhanced in the Lys149Ala and Tyr145Ser mutants........148

5.7. Scheme 2. Proposed mechanisms consistent with the available data........151

6.1. Coproheme decarboxylase subunit and active site with the substrate analog, manganese coproporphyrin, bound........188

6.2. Properties of the side chain radical intermediate generated along the pathway to coproheme decarboxylation........189

LIST OF FIGURES CONTINUED

Figure Page

6.3. The side chain radical intermediate formed in W157F, W198F, and Y113S decarboxylase mutants has similar properties to WT decarboxylase, while Y145S is distinct 190

6.4. The decarboxylation of CβD$_2$-coproheme is ~2-fold slower than CβH$_2$-coproheme and results in substantially greater accumulation of Y145• 191

6.5. Time resolved EPR spectra show a ferric S=5/2 component that diminishes in intensity as the S=1/2 signal due to Y145• forms 193

6.6. The ferric decarboxylase-harderoheme complex is also decarboxylated via a Y145 radical 194

6.7. Scheme 6.1 195

6.8. Scheme 6.2. Proposed mechanism for coproheme decarboxylation.............196

7.1. The PPD and CPD branches of heme *b* biosynthesis both produce toxic intermediates during the process 200

7.2 .The Fenton reaction 201

7.3. Eukaryotic cells and gram-negative bacteria can compartmentalize the cytotoxic metabolites of heme *b* biosynthesis in their membrane-bound spaces 203

7.4. Gram-positive bacterial heme *b* biosynthesis occurs in the cytoplasm without membrane compartmentalization of cytotoxic intermediates 206

7.5. UV-Vis spectra of coproporphyrin and coproheme in the absence and presence of CpfC or ChdC 212

7.6. UV-Vis spectra of coproporphyrin can be used to visualize the formation of a CpfC-ChdC complex 213

LIST OF FIGURES CONTINUED

Figure Page

7.7. The affinity of the CpfC-ChdC complex in the presence of coproporphyrin is consistent with a transient protein-protein interaction 214

7.8. The CpfC-ChdC complex does not affect the intrinsic reactivity of CpfC....217

7.9. The CpfC-ChdC complex does not affect the intrinsic reactivity of ChdD....218

7.10. ChdC's active site gate may play a role in a CpfC-ChdC protein-protein interaction....220

7.11. E120L and N112L ChdC protein variants in *ΔchdC S. aureus* exhibit a growth deficiency relative to WT....221

7.12. Porphyrin profiles for the E120L and N112L ChdC *S. aureus* strains....222

8.1. Clustal O (1.2.4) Sequence alignment of canonical *Ec*CgdH, *Ll*HemW *Sa*CgdH, and *Bs*CgdH....229

8.2. Sample figure showing analysis of heme-transfer from PhuS to pa-HO or BpHO by SEC and SDS-PAGE analysis 234

ABSTRACT

Heme *b* is one of nature's most ancient and versatile co-factors and is essential for aerobic life. As such, heme *b* is synthesized by almost every living organism and plays a major role in bacterial virulence. A pathway for heme *b* biosynthesis, which is unique to some of the most primitive gram-positive bacteria including many important pathogens, was recently discovered. This pathway, now known as the coproprophyrin-dependent (CPD) branch, ends in a step catalyzed by an unusual enzyme known alternately as coproheme decarboxylase (ChdC) or HemQ. This research aimed to understand ChdC function at the molecular, structural, and cellular levels. Using the ChdC enzyme from *Staphylococcus aureus* (*Sa*ChdC) and a variety of biochemical and analytical tools (conventional and stopped-flow UV-Vis spectroscopy, resonance Raman, HPLC, LC-MS, site-directed mutagenesis, EPR, and X-ray crystallography), the work presented here describes how the coproheme substrate is accommodated in the *Sa*ChdC active site and poised for reactivity. The cumulative results show that ChdC catalyzes the oxidative decarboxylation of coproheme III to generate heme *b* in a sequential and clock-wise fashion, generating harderoheme III in the process. This reaction is H_2O_2-dependent and the mechanism involves the formation of the high-valent Fe(IV) intermediate (Compound I) and a tyrosine radical (Tyr•). The coproheme-bound ChdC structure revealed a helical-loop that is flexible and moves in towards the active site in the presence of substrate. This loop is hypothesized to act as an "active site gate" which mediates substrate entry and product egress. Due to the cytotoxicity of heme and its porphyrin precursors, we proposed that the metabolite flux in this pathway is controlled by transient protein-protein interactions. Using the UV-Vis characteristics of porphyrins and phenotype characterization of the Δ*chdC* knock-out strain of *S. aureus* complemented with ChdC point mutants, we present preliminary evidence for an interaction between ChdC the preceding enzyme of the pathway, CpfC. The same approaches also implicated potential interactions between ChdC and an unidentified heme-chaperone, which delivers heme to its final cellular destination. We propose that this chaperone is HemW. Experiments to test this hypothesis are outlined. This work elucidates yet different way that nature has equipped cells to perform radical chemistry in order to accomplish essential molecule transformations, such as that of decarboxylation and the simultaneous generation of CO_2, and emphasizes the importance of substrate/product post-catalysis cellular trafficking.

CHAPTER ONE

THE TERMINAL THREE CATALYTIC STEPS OF MAKING HEME, A LITERATURE REVIEW

Multiple Ways to Make Heme *b*

Heme *b* biosynthesis is a highly important process due to the significance of the final cofactor produced, as well as the highly reactive and disease-related intermediates that are formed during this process. As such, the enzymes and porphyrins involved in this pathway had been extensively studied and thought to be well-documented for over 60 years. Increasing accessibility to genome sequencing and the development of bioinformatics tools revealed that the well-characterized, canonical heme *b* biosynthesis pathway was not applicable to all organisms. Over the last 3-5 years, it has been established that this canonical pathway is limited to eukaryotic organisms (namely animals and plants) and gram-negative bacteria (such as *E. coli*), while gram-positive bacteria (like *B. subtilis* and *S. aureus*) and archaea, denitrifying and sulfate-reducing bacteria have a modified, unique pathway to produce the same final product; heme *b*[1,2] (Figure 1.1). As the knowledge about these different pathways evolved, new nomenclature for the enzymes that catalyze each individual step was developed. For clarity, the most recently established nomenclature will be used here (new and former names are listed in Table 1.1)[3].

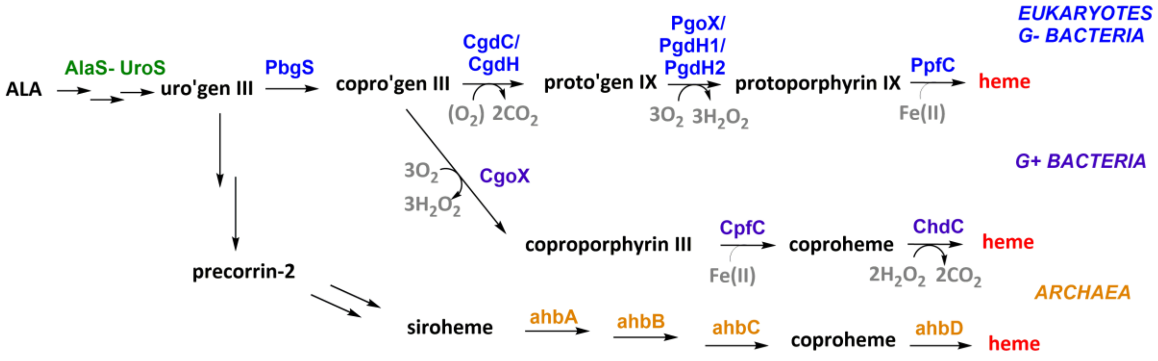
ALA
AlaS- UroS
uro'gen III
PbgS
copro'gen III
CgdC/
CgdH
(O$_2$) 2CO$_2$
proto'gen IX
PgoX/
PgdH1/
PgdH2
3O$_2$ 3H$_2$O$_2$
protoporphyrin IX
PpfC
Fe(II)
heme
EUKARYOTES
G- BACTERIA
3O$_2$
3H$_2$O$_2$
CgoX
G+ BACTERIA
coproporphyrin III
CpfC
Fe(II)
coproheme
ChdC
2H$_2$O$_2$ 2CO$_2$
heme
precorrin-2
ARCHAEA
siroheme
ahbA
ahbB
ahbC
coproheme
ahbD
heme

Figure 1.1. Multiple heme b biosynthesis pathways. Three heme b biosynthesis have been identified, each specific to different organisms. Eukaryotes and gram-negative bacteria share the canonical pathway that was once thought to be universal (blue), while gram-positive bacteria (purple) and archaea (orange) have distinct and unique pathways to synthesize the same molecule.

Table 1. Nomenclature of heme *b* biosynthesis enzymes

Heme biosynthesis enzyme	Former abbreviation (s)	New abbreviation
ALA synthase	HemA	AlaS
Glutamine-tRNA reductase	HemA/GtrA	GtrA
GSA mutase	HemL/GSAM	GsaM
PBG synthase	HemB/ALAD/PBGS	PgbS
HMB synthase	HemC/HMBS/PBGD	HmbS
URO synthase	HemD/UROS	UroS
URO decarboxylase	HemE/UROD	UroD
Coproporphyrinogen decarboxylase	HemF/CPOX	CgdC
Coproporphyrinogen dehydrogenase	HemN/HemZ/CPDH	CgdH
Protoporphyrinogen dehydrogenase 1	HemG	PgdH1
Protoporphyrinogen dehydrogenase 2	HemJ	PgdH2
Protoporphyrinogen oxidase	HemY	PgoX
Protoporphyrin ferrochelatase	HemH	PpfC
Coproporphyrin ferrochelatase	HemH/HemZ	CpfC
Coproporphyrin oxidase	HemY	CgoX
Coproheme decarboxylase	HemQ	ChdC

All pathways share a common beginning and only diverge post generation of uroporphyrinogen III (Figure 1.2). The pathways commence with the irreversible synthesis of 5-aminolevulinic acid (ALA) from glyicine and succinyl-coA by ALA Synthase (ALAS) (metazoans and fungi) or from glutamyl-tRNA via a two-step process catalyzed by glutamyl-tRNA reductase (GtrR) and glutamate-1-semialdehyde-2-1, aminomutase (GsaM) (most bacteria and archaea). Two molecules of ALA can then be used by porphobilinogen synthase (PbdS) to make the monopyrrole porphobilinogen, which can subsequently be used by hydroxymethylbilane synthase (HmbS) to make the first tetrapyrrole intermediate hydroxymethylbilane. Uroporphyrinogen synthase (UroS) then catalyzes the formation of the common intermediate, uroporphyrinogen III (Figure 1.2).

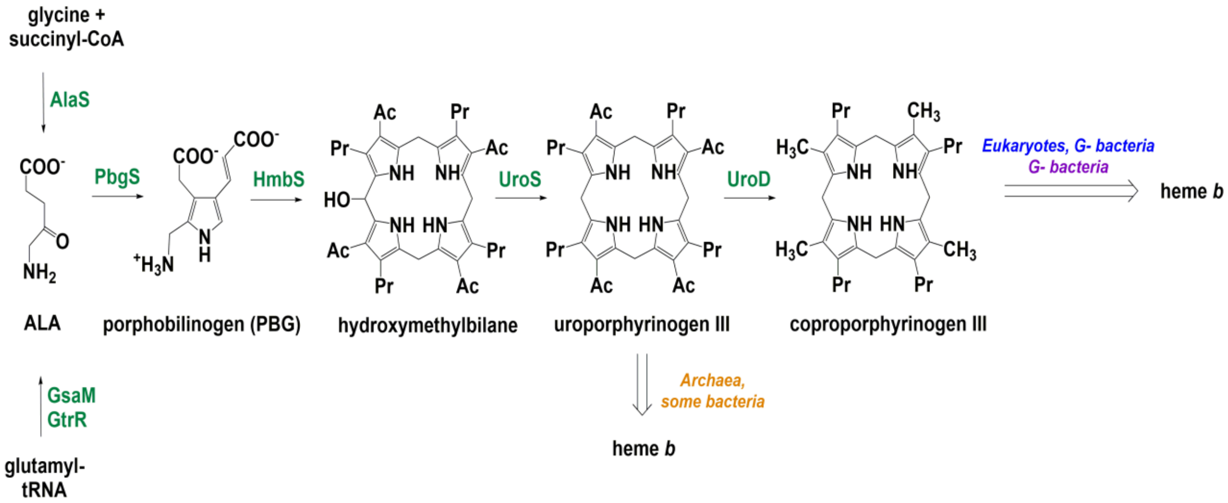
glycine + succinyl-CoA
AlaS
ALA
PbgS
porphobilinogen (PBG)
HmbS
hydroxymethylbilane
UroS
uroporphyrinogen III
UroD
coproporphyrinogen III
Eukaryotes, G- bacteria
G- bacteria
heme b
Archaea, some bacteria
heme b
GsaM
GtrR
glutamyl-tRNA

Figure 1.2. All heme b biosynthesis pathways share a common beginning and have uroporphyrinogen III as the final common intermediate. The eukaryotic, gram-negative, and gram-positive bacterial pathways continue on to make coproporphyrinigen III, while the archaeal pathway branches off after this step.

The archeal/sulfate-reducing/denitrifying bacterial pathway was the first alternate pathway to be discovered and, as such, was called the "Alternate heme biosynthesis" pathway (Ahb pathway)[2]. In this alternate pathway, uroporphyrinogen III is converted into siroheme, the prosthetic group of sulfite and nitrite reductase. Siroheme is "hijacked" in and processed into heme *b* by the enzymes AhbA, AhbB, AhbC, and AhbD (Figure 1.1)[2]. For the other two pathways, coproporphyrinogen III is the last common intermediate and it is obtained by the decarboxylation of uroporphyrinogen III by uroporphyrinogen decarboxylase (UroD). For the simplicity of this discussion, that is all that will be said about the Ahb pathway and we will focus on the canonical pathway and the branch that stemmed off from it for gram-positive bacteria.

To get from coproporphyrinogen III to heme *b*, three chemical transformations must occur; (1) decarboxylation of the A- and B-ring propionate groups, (2) oxidation of two of the four pyrrole rings, and (3) metalation of the tetrapyrrole with iron. Although the set of transformations are the same in both branches of heme *b* biosynthesis, the order in which these transformations occur is what makes them distinct (Figure 1.3). The two pathways diverge by proceeding through either the decarboxylation step to yield protoporphyinogen IX or through the oxidation step to yield coproporphyrin III and thus are now referred to as the protoporphyrin-dependent (PPD) branch or the coproporphyrin-dependent (CPD) branch, respectively.

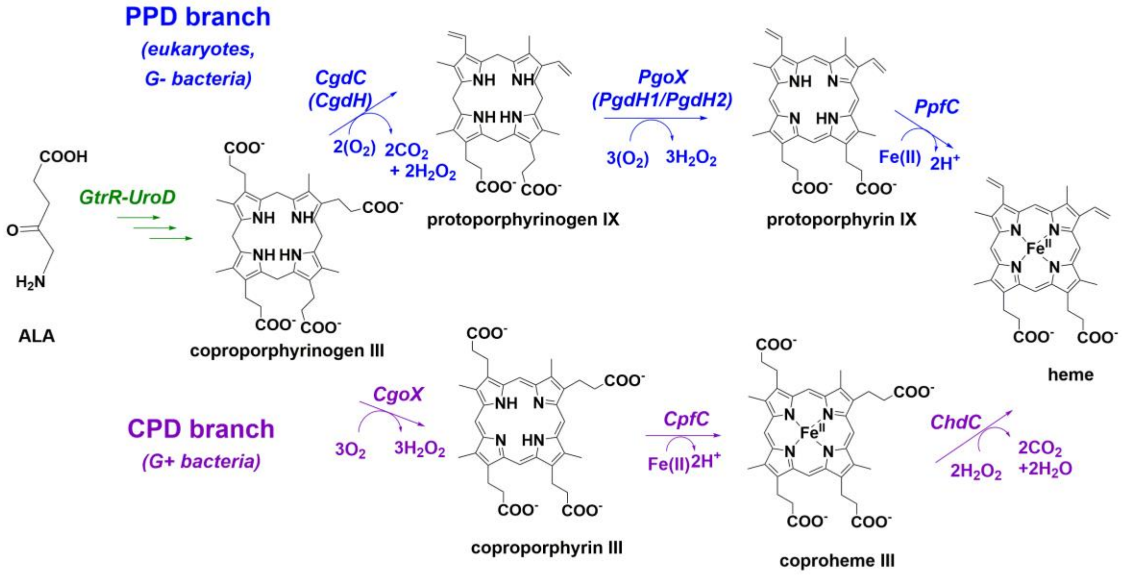
PPD branch
(eukaryotes,
G- bacteria)
CgdC
(CgdH)
2(O2) 2CO2
+ 2H2O2
PgoX
(PgdH1/PgdH2)
3(O2) 3H2O2
PpfC
Fe(II) 2H+
COOH
O
H2N
ALA
GtrR-UroD
COO-
NH NH
NH HN
coproporphyrinogen III
protoporphyrinogen IX
protoporphyrin IX
Fe II
heme
CPD branch
(G+ bacteria)
CgoX
3O2 3H2O2
coproporphyrin III
CpfC
Fe(II)2H+
coproheme III
ChdC
2H2O2 2CO2
+2H2O

Figure 1.3. The PPD and CPD branches of heme b biosynthesis consist of the same chemical transformation but in a different order. Although some of the enzymes between the branches are homologous, a change in the order creates different porphyrin intermediates, making the enzymes that act on these porphyrins intrinsically different. The CPD pathway's unique terminal enzyme is ChdC.

By changing the order of the set chemical transformations, the tetrapyrrole intermediates that are formed also become slightly different. As such, the enzymes that catalyze these steps (although sometimes homologous and/or very structurally similar) are also unique and distinct. Here, we discuss the recently elucidated similarities and differences between the enzymes (and reaction mechanisms) that catalyze these last three chemical transformations of the heme *b* biosynthesis pathway.

The PPD Branch can be Further Split into the PPD-*(O$_2$-dependent)* and PPD-*(O$_2$-independent)* Branches

Biosynthesis of heme *b* has been currently split into two branches. The PPD heme biosynthesis branch (the former canonical pathway), which is only found in eukaryotic organisms and gram-negative bacteria, and the novel CPD branch, which pertains to gram-positive bacteria[1, 3].

In the newly elucidated CPD branch, the order of the terminal steps is (1) oxidation of two of the four pyrrole rings, (2) metalation of the tetrapyrrole, and finally (3) decarboxylation of the A- and B-ring propionates. The PPD branch follows the before mentioned order of (1) decarboxylation of the A- and B-ring propionate groups, (2) oxidation of two of the four pyrrole rings, and lastly (3) metalation of the tetrapyrrole with iron. The terminal steps of the CPD branch are each catalyzed by one enzyme. In the PPD branch however, each step can be catalyzed by one or more enzymes, depending on the organism in which biosynthesis is occurring and on whether oxygen is used during catalysis. We propose that the PPD pathway can be further split into two more branches which we will call the PPD-*(O_2-dependent)* branch and the PPD-*(O_2-independent)* branch (Figure 1.3). This makes heme *b* biosynthesis unique and distinct, not only in gram-positive bacteria, but in all organisms for which it has been described.

Decarboxylation of the Ring A- and B- Propionate Groups (CgdC, CgdH, and ChdC)

The first chemical transformation to occur post coproporphyrinogen III formation in the PPD branch is a decarboxylation to yield protoporphyrinogen IX (Figure 1.3). This reaction can be catalyzed by coproporphyrinogen decarboxylase (CgdC) or coproporphyrinogen dehydrogenase (CgdH) in an oxygen-dependent or in an oxygen-independent manner, respectively.

As part of the PPD-*(O_2-dependent)* branch, CgdC catalyzes the oxidative decarboxylation of the A- and B-ring propionate groups in sequential and clockwise manner. This mitochondrial intermembrane enzyme is dimeric and contains a conserved active site base Asp residue is thought to facilitate reactivity of coproporphyrinogen III with O_2, leaving vinyl groups in those positions[3-4]. This reaction yields two molecules of CO_2 and H_2O_2, one for each round of decarboxylation. CgdC is found almost exclusively in eukaryotic organisms and a very small amount of gram-negative bacteria.

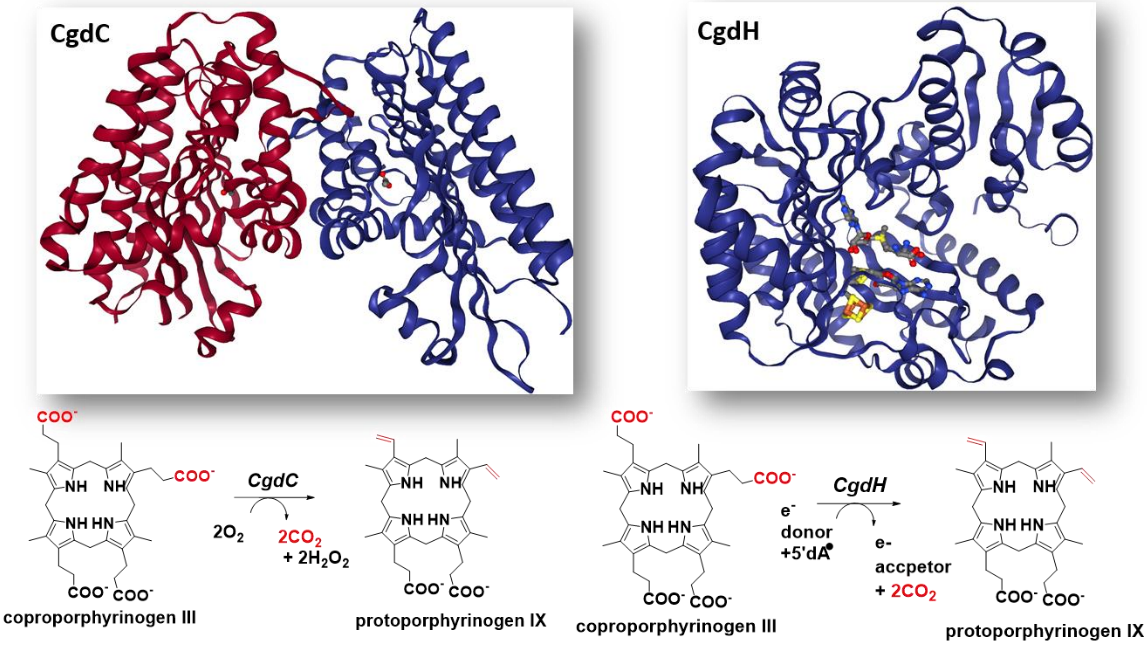
CgdC
CgdH
COO⁻
COO⁻
NH NH
NH HN
COO⁻ COO⁻
coproporphyrinogen III
CgdC
2O₂
2CO₂
+ 2H₂O₂
protoporphyrinogen IX
COO⁻
COO⁻
coproporphyrinogen III
CgdH
e⁻
donor
+5'dA•
e-
accpetor
+ 2CO₂
protoporphyrinogen IX

Figure 1.4. Decarboxylation of coproporphyrinogen III to protoporphyrinogen IX in the PPD branch can be catalyzed aerobically or anaerobically by CgdC or CgdH, respectively. Although CgdC and CgdH catalyze the same chemical transformation, they share no structural nor mechanistic similarity (PDBID 5EO6 and 1OTL). The oxidative decarboxylation reaction requires an electron acceptor. CgdC uses oxygen, while CgdH is a radical SAM enzyme that uses its [4Fe-4S] cluster and SAM for catalysis.

The enzyme that catalyzes this decarboxylation step exclusively in gram-negative bacteria is CgdH. CgdH has no structural nor mechanistic relationship to CgdC and as part of the PPD-*(*O_2*-independent)* branch, CgdH is a soluble, monomeric radical SAM enzyme, containing a [4Fe-4S] cluster [5-6](Figure 1.4). This reaction is facilitated by the formation of the 5'-deoxyadenosyl radical, which is generated through transfer of an electron from the iron-sulfur cluster to one of the SAM molecules and subsequent homolytic cleavage of methionine to yield the reactive radical species[5]. The 5'deoxyadenosyl radical initiates the decarboxylation reaction by stereospecific pro-S-hydrogen-atom abstraction at the beta-position of the propionate side chains, producing a radical in that position[7]. This reaction requires an electron donor at the start of the reaction (to fill the iron-sulfur cluster electron hole) and an electron acceptor at the end of the reaction (to quench the radical), both of which have not yet been identified [5]. As with CgdC, decarboxylation of the ring A- and B- propionate groups in coproporphyrinogen III to yield protoporphyrinogen IX happens in a sequential and clockwise manner and generates two molecules of CO_2 during the process.

In the CPD branch, decarboxylation of the A- and B-ring propionate groups is not the first terminal step, but the last one. In this branch, this chemical transformation occurs with coproheme III as a substrate and yields heme *b* as the final product (Figure 1.2). This reaction is a peroxide-dependent oxidative decarboxylation catalyzed by the novel enzyme coproheme decarboxylase (ChdC)[1, 8]. It is the discovery of this enzyme that led to the deciphering of the novel CPD branch [1, 9]. ChdC also is not homologous nor structurally related to either CgdC or CgdH. Instead this enzyme is a member of the chlorite dismutase (Cld) family of proteins, which are soluble enzymes that share a homopentametic structure[10] (Figure 1.5).

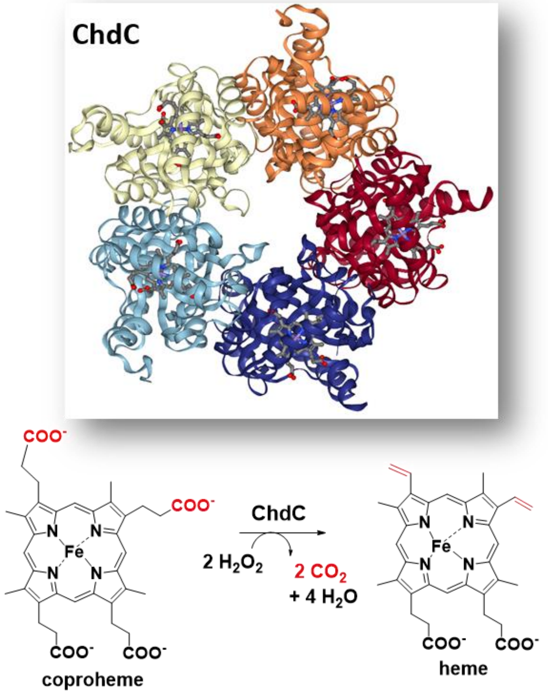

Figure 1.5. Decarboxylation of coproheme is the last transformative step in the CPC branch and it is catalyzed by ChdC. ChdC catalyzes the oxidative decarboxylation of coproheme to heme using coproheme as a substrate and a cofactor and H_2O_2 as an electron acceptor. This enzyme shares no structural relationship to CgdC or CgdH and instead is a homopentamer, binding one molecule of coproheme in each monomer (PDBID 5T2K).

Each monomeric unit in ChdC binds a coproheme III molecule and decarboxylation is facilitated by reactivity with H_2O_2 and a conserved Tyr residue in the active site which forms a radical to induce reactivity[8, 11-12]. ChdC uniquely uses coproheme III both as a substrate and a cofactor. This reaction mechanism is thought to include the formation of the high-valent Fe(IV) intermediate (Compound I) that subsequently acts as an oxidizing agent to the Tyr residue, making it a radical. Slightly similar to the 5'deoxyadeniosyl radical in CgdH, this protein radical performs a hydrogen-atom abstraction at the beta-position of the propionate side chains, producing a radical in that position, and inducing decarboxylation. This process happens twice, to decarboxylate both propionate groups. Decarboxylation by ChdC again occurs in a step-wise and clockwise fashion and generates two molecules of CO_2 and four molecules of H_2O in the process. H_2O_2, is an unusual cellular substrate and its source remains to be elucidated, although it is possible that the preceding enzyme CgoX (Figure 1.2), which generates H_2O_2, could deliver the required molecules directly.

Oxidation of the Tetrapyrrole Rings (PgoX, PgdH1, PgdH2 and CgoX)

The diversity of heme *b* biosynthesis pathways, or branches, in different organisms is most pronounced when looking at the enzymes that catalyze the oxidation of the tertrapyrrole ring. This step is the second terminal step in the PPD branch and three enzymes have been described as being able to catalyze it (Figure 1.6).

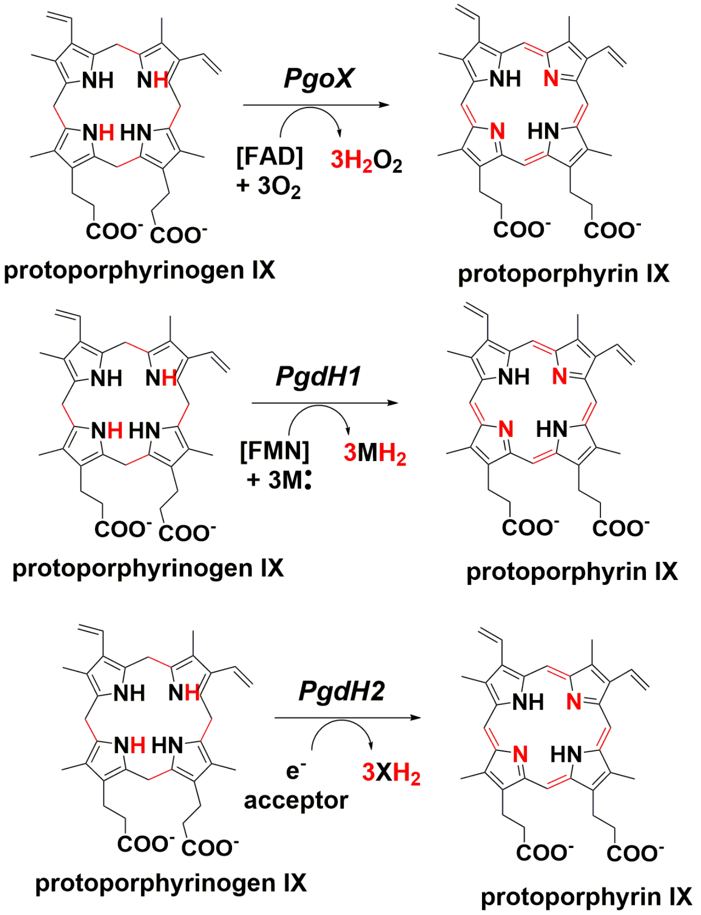
PgoX
[FAD]
+ 3O2
3H2O2
PgdH1
[FMN]
+ 3M:
3MH2
PgdH2
e-
acceptor
3XH2
NH
NH
HN
N
COO-
protoporphyrinogen IX
protoporphyrin IX

Figure 1.6. Three non-homologous, isofunctional enzymes to catalyze the oxidation of protoporphyrinogen IX to PPIX in the PPD branch. The PgoX reaction has been well-characterized and uses O_2 as an electron acceptor to yield 3 molecules of H_2O_2 upon completion of catalysis. PgdH1 catalyzes the same reaction in an O_2-independent manner, by using FMN and electron acceptors from the respiratory chain, such as menadione and ubiquinone. PgdH2 is the most abundant protoprophyrin dehydrogenase enzyme, but has not been structurally or mechanistically characterized.

In the PPD-*(O_2-dependent)* branch, the oxidation of protoporphyrinogen IX to protoporphyrin IX (PPIX) is catalyzed by protoporphyrinogen oxidase (PgoX) (Figure 1.2). This reaction is a six-electron oxidation of the tetrapyrrole ring, leaving double bonds at all *meso*-carbon positions. Oxidation by PgoX occurs in an oxygen-dependent manner, requiring three O_2 molecules and generating three H_2O_2 molecules during the six-electron transfer [13-14]. This enzyme is dimeric, membrane-associated, and contains a single non-covalently bound FAD[3] (Figure 1.7). It is thought that PgoX uses FAD as a co-factor, going through three-rounds of oxidation before the final, fully-oxidized PPIX tetrapyrrole is obtained. PgoX is found almost exclusively in eukaryotes and only in a very small amount of gram-negative bacteria, like *Myxococcus*[15-16]. Of note is that all of the work that has been done to study this oxidation step of the heme *b* biosynthesis pathway has been with the eukaryotic PgoX enzyme.

In the PPD-*(O_2-independent)* branch, oxidation of protoporphyrinogen IX to PPIX can be catalyzed by the O_2-independent enzyme protoporphyrinogen dehydrogenase 1 (PgdH1) or protoporphyrinogen dehydrogenase 2 (PgdH2). The isofunctional enzymes of the PPD branch (PgoX, PgdH1 and PgdH2) are non- homologous and have no structural resemblance[17]. PgdH1 is found mainly in gamma-proteobacteria, like *E. coli.* It is a membrane-bound protein and a member of the “long-chain flavodoxin family”, whose members are known to bind FMN and participate in electron transfer. Unique to PgdH1 is a long-chain insert loop that is essential for its reactivity[15]. PgdH1 is thought to use FMN and members of the cell’s respiratory chain, such as menadione and ubiquinone, for catalysis relieving it of its use of O_2 as a final electron acceptor[3, 15].

PgdH2 also catalyzes the oxidation of protoporphyrinogen to PPIX in an O_2-independent manner. This enzyme is present in heme-synthesizing, non-enteric gram-negative bacteria, such as *Acinetobacter* (gamma-proteobacteria) and *Synechocystis* (cyanobacteria), which lack both *pgoX* and *pgdH1*[3, 15, 18]. Phylogenetic analyses have indicated that *pgdH2* may have originated in alpha-proteobacteria and subsequently became transferred to gamma-proteobacteria and cyanobacteria [17]. Although PgdH2 is the most abundant out of these three isofunctional enzymes, very little is known about its reaction mechanism. Because it is also a membrane-bound protein, it was initially thought that it too could interact with and use molecules of the cell's respiratory chain to catalyze its reaction. However, no co-factor has been identified for PgdH2 and it has been reported that PgdH2 is not able to complement a PgdH1-deificient *E. coli* strain, suggesting that it is clearly distinct from PgdH1[3, 16].

In the CPD branch, oxidation of the tetrapyrrole ring is not the penultimate step of the entire pathway, but the first out of the terminal three. Conversion of coproporphyrinogen III to coproporphyrin III by coproporphyrinogen oxidase (CgoX) is the CPD pathway's committed step. Interestingly, CgoX bears almost identical sequence and structural similarity to PgoX, including the non-covalently bound FAD molecule [17, 19] (Figure 1.7). As such, CgoX has extensively been reported to be the same as PgoX, with the following exceptions; (1) it acts on coproporphyrinogen III instead of on protoporphyrinogen IX, (2) it is monomeric instead of dimeric, and (3) it is cytoplasmic instead of membrane associated[1,19,21].

The most widely studied CgoX has been that from *Bacillus subtilis*, whose crystal structure is known (PDBID 3I6D) [22]. Analysis of the *Bs*CgoX crystal structure and comparison to that of *Mt*PgoX and *Hs*PgoX have shown that CgoX has an active site cavity with a volume 2-3 times larger (1173 Å vs 450-550 Å) and significantly more positively charged than that of PgoX, allowing it to accommodate larger and more negatively charged substrates (namely coproporphyrinogen III) [19]. In addition, although the *Bs*CgoX crystal structure could not be obtained without it, the structure showed that acifluoren, a well-known PgoX inhibitor, binds towards the outside of the CgoX active site, while it is buried deep in that of PgoX[19] (Figure 1.7). This is in agreement with previous reports stating that CgoX is not inhibited by acifluoren (~77 µM), while this compound acts as a very strong inhibitor in PgoX (Ki ~0.2 nM) [20, 22].

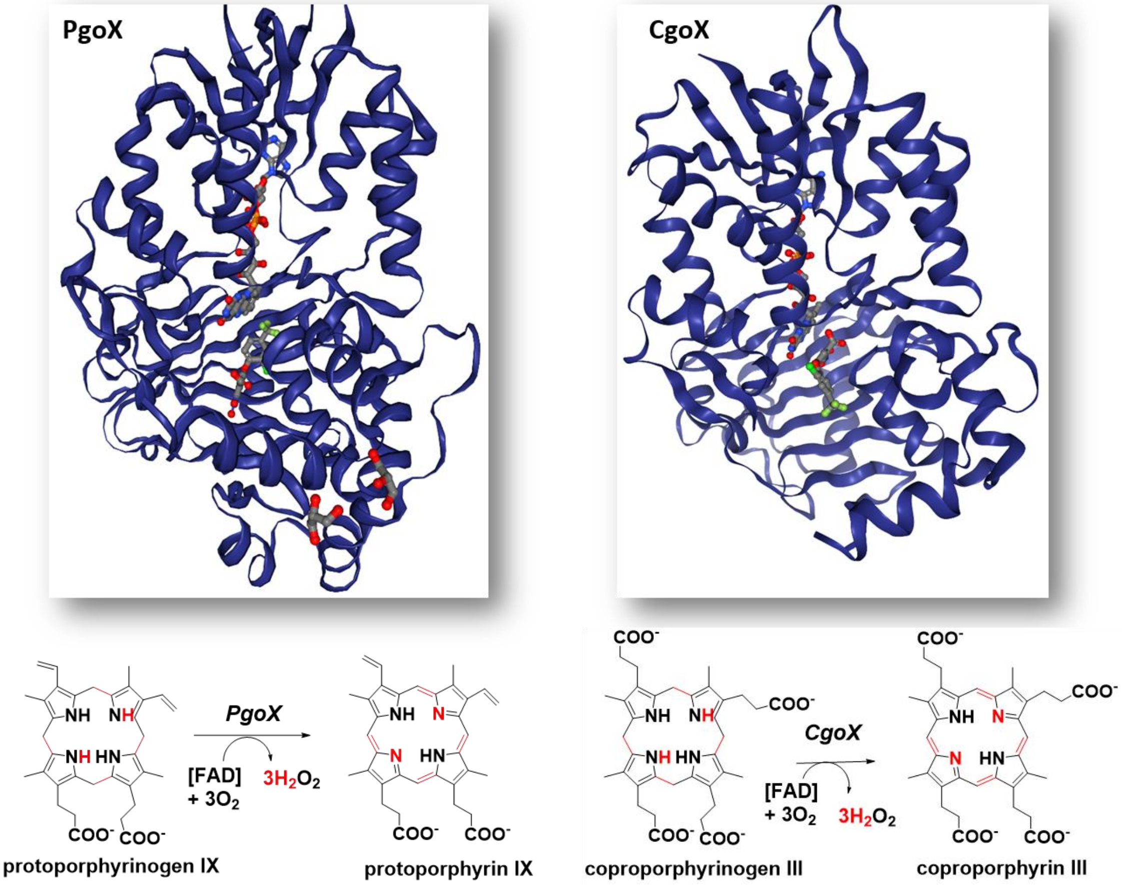
PgoX
CgoX
NH
NH
NH
HN
PgoX
[FAD]
+ 3O2
3H2O2
NH
N
N
HN
COO-
COO-
protoporphyrinogen IX
COO-
COO-
protoporphyrin IX
COO-
COO-
NH
NH
NH
HN
CgoX
[FAD]
+ 3O2
3H2O2
COO-
COO-
COO-
COO-
NH
N
N
HN
COO-
COO-
coproporphyrinogen III
coproporphyrin III

Figure 1.7. CgoX is homologous to PgoX but has a larger active site which allows it to accommodate its larger substrate. The structures of PgoX (PDBID 2IVD) and CgoX (PDBID 3I6D) show that they both bind an FAD cofactor and can bind the acifluofren (AF) molecule (historically a PgoX inhibitor).CgoX is thought to have a very similar reaction mechanism with PgoX. However, CgoX is a monomer (vs a dimer), a soluble enzyme (vs membrane-bound) and has an active site cavity that is ~3-times larger than PgoX. The larger active site allows it to bind its larger porphyrin substrate, its FAD co-factor and still have room to bind other molecules that might help with catalysis.

CgoX has been described as having the same reaction mechanism as PgoX, where 3 molecules of O_2 are used as electron acceptors for the 6-electron oxidation to yield 3 molecules of H_2O_2. However, due to the novelty of the CPD pathway, all mechanistic studies on CgoX have been conducted using protoporphyrinogen IX as a substrate and the requirement of O_2 as an electron acceptor has not been experimentally shown using coproporphyrinogen III[22-23]. This begs the question of whether CgoX can catalyze its reaction in an O_2-independent manner, to best suit the facultative anaerobic organisms in which it is found. The PgoX in *Plasmodium falciparium*, for example, is able to catalyze its oxidation reaction using FAD, NAD, and/or NADP as electron acceptors under anaerobic conditions[24]. It is possible that the much larger active site in CgoX can not only accommodate FAD and its slightly larger coproporphyrinogen substrate, but also an electron acceptor such as NAD(P). Although completely speculative at the moment, the requirement of acifluoren in the crystallization of *Bs*CgoX and its pi-stacking interaction with the bound FAD alludes to this possibility.

Lastly, something to note is that the reports that state that CgoX is a soluble enzyme are inconsistent with the actual biochemical studies that have been conducted. Over the past two decades journal articles and review articles on heme *b* biosynthesis have stated that CgoX, unlike PgoX, is a cytosolic enzyme[1, 3, 20-21]. However, the original biochemical studies of CgoX suggest, and in one case the authors explicitly state, that this is not the case[22-23]. Studies with recombinant *Bs*CgoX showed that this enzyme is found in the insoluble fraction/cell membrane fraction when expressed in *E. coli*, indicating that "CgoX is likely a membrane protein" [23]. A different study reported that, much like other membrane-associated proteins, purification of CgoX required denaturing conditions and the addition of 1% Tween-20 to maintain the enzyme in solution[22]. Finally, although Qin et al. 2010 state that CgoX is a soluble enzyme by citing articles that make the experimentally untested statement, through comparison of *Bs*CgoX and *Mt*- and *Hs*PgoX, they report that CgoX also contains the membrane-binding domain, the so-called "Domain II", that is found in PgoX enzymes, again, indicating that CgoX is likely membrane-associated[19].

A lot remains to be discovered about the enzymes that catalyze this tetrapyrrole ring oxidation step, in both the PPD and CPD pathways. In order to decipher the true nature and mechanism of action of these enzymes it will be important to consider them as individuals which are distinct from each other. In the case of CgoX, it is important that future studies be performed with the appropriate substrate (coproporphyrinogen III) and that its solubility, as well as cellular location, be reassessed.

Metalation of the Tetrapyrrole Ring (PpfC vs CdfC)

The final step left to describe is the metalation of the oxidized tetrapyrrole ring with iron. This is the final step in the PPD branch of heme *b* biosynthesis pathway and it is catalyzed by protoporphyrin IX ferrochelatase (PpfC) (Figure 1.2). PpfC performs a ferrous iron- specific insertion to PPIX and its mechanism has been described as being the same in eukaryotes and in gram-negative bacteria, although very few bacteria PpfCs have been described. The most studied enzyme is that of human (*Hs*PpfC) whose WT form, as well as many protein variant forms, has been crystallographically characterized[25]. PpfC is a homodimer, membrane-bound enzyme that is thought to localize in the inner mitochondrial membrane of eukaryotes, and the inner cellular membrane of gram-positive bacteria[25]. Each monomer contains a [2Fe-2S] cluster that does not participate in catalysis[4, 25-26]. The most notable feature of PpfC is the so-called "active site lip", which gives PpfC two structural conformations (Figure 1.8). This 12 amino acid structure moves in towards the active site upon PPIX binding, creating an enclosed active site and burying the porphyrin deep inside the pocket. In the absence of substrate or upon product formation, the active-site lip is away from the active site, leaving it solvent exposed for substrate entry or product egress.

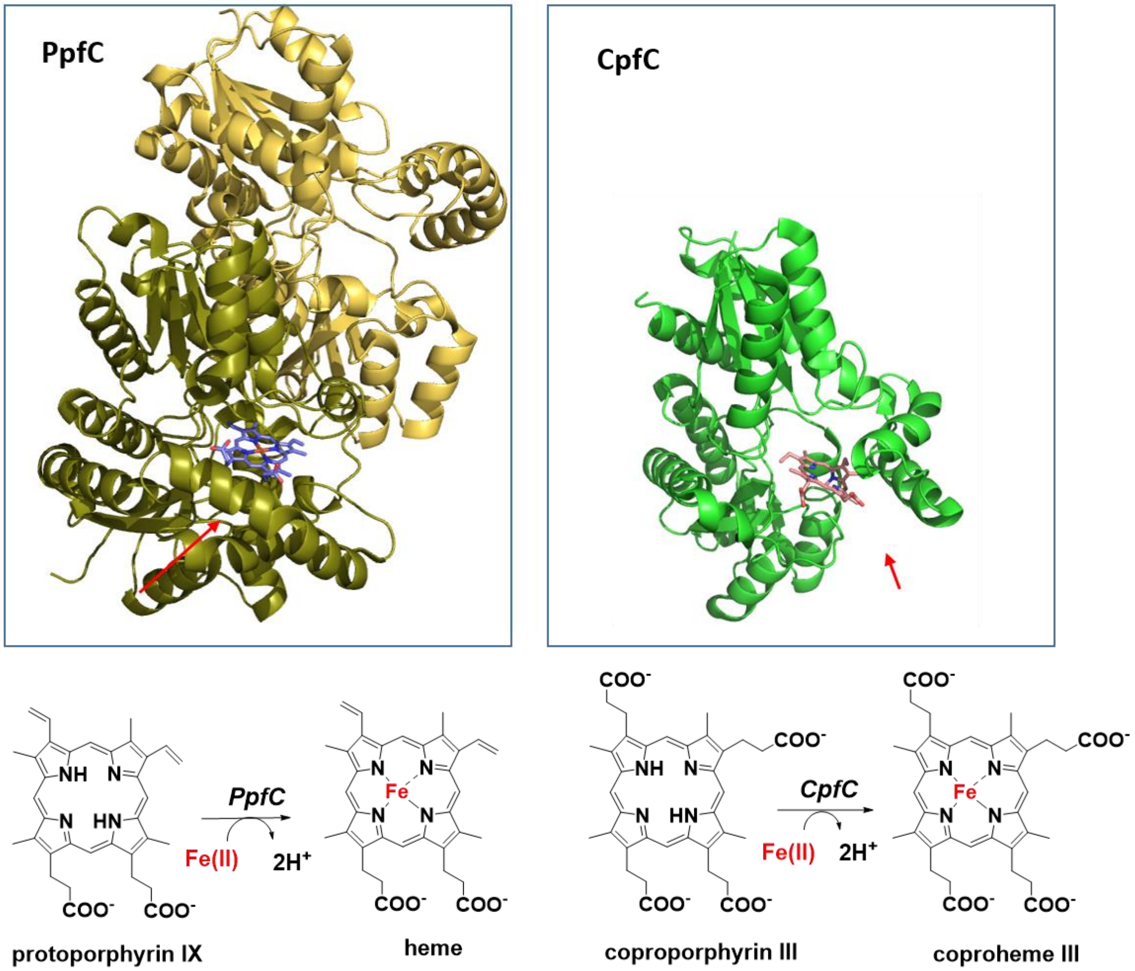
PpfC
CpfC
NH
N
N
HN
PpfC
Fe(II)
2H+
Fe
COO-
protoporphyrin IX
heme
coproporphyrin III
CpfC
coproheme III

Figure 1.8. PpfC and CpfC share a similar structural fold and reaction mechanism. PfpC is a dimer and a membrane associate protein that has a notable (active site lip) that closes in towards the active site upon substrate binding (red arrow, PDBID 3HCO). CfpC lacks this active site lip, leaving the active site more solvent exposed (PDBID 1CH1).

The PpfC reaction mechanism entails (1) Fe^{2+} acquisition and binding by PpfC, (2) binding of PPIX, (3) deprotonation of two pyrrole ring nitrogens in PPIX, and finally (4) Fe^{2+}-insertion into the macrocycle and product release. The current model for this reaction mechanism was proposed by looking at the different *Hs*PpfC crystal structures[25, 27], as well as heavy metal-soaked crystal structures of the structurally homologous enzyme in *Bascillus subtilis* (*Bs*CpfC), in Figure 1.2 and described below)[28-29]. In order to obtain Fe^{2+} in its reduced form, this metal is directly delivered to PpfC by frataxin (*Frda* in human, *Yfh1* in yeast) [30-31]. Frataxin is a membrane-bound enzyme involved in iron storage, iron delivery to [Fe-S] cluster assembly machinery and heme biosynthesis enzymes, its role depending on its oligomeric state, which is induced by metal binding[30-31]. As a trimer, frataxin directly interacts with PpfC and transfers Fe^{2+} to a conserved His and Glu residues found in the active site pocket, which hold the metal in place[28-29]. Upon PPIX binding, the active site lip closes-in tightly around the active site, causing rearrangement of an active site hydrogen-bonding network and distortion to the planarity of the PPIX tetrapyrroles ring [25, 27]. Both of these conformational changes trigger deprotonation and facilitate metal insertion into the porphyrin to yield the final heme *b* product. The hydrogen ions lost from the pyrrole nitrogens are buffered by a well conserved His residue. Protonation of this His residue reorients its side-chain and causes the final conformational change in the PgoX reaction cycle, which is opening of the active site lip to allow for product release[3, 25].

As previously mentioned, although a lot is known about eukaryotic PpfC, very little is known about bacterial PpfC and no bacterial PpfC crystal structures have been obtained. However, because the enzymes in these organisms are so similar in sequence and structural models indicate high structural similarity as well, the reaction mechanism is thought to be the same. As such, for the purpose of this review, catalysis of this reaction is the same in both forms (*O_2-dependent* and *O_2-independent*) of the PPD pathway (Figure 1.2). It is worth noting, that further characterization of the bacterial enzymes is required to confirm their reaction mechanism is truly the same as the eukatyotic PpfC, as other differences have already been documented, such as [2Fe-2S] cluster content and cluster binding motifs, between the enzymes in different organisms[3, 26], and this may very well not be the case.

Elucidation of the CPD branch led to the discovery that this was not the case for gram-positive bacteria. For many years, people documented that the ferrochelatase enzyme from gram-positive organisms like *B. subtilis* were anomalies that had significantly lower binding affinities and reaction rates with PPIX than the well-known *Hs*PpfC1992[23, 28] . It is now recognized that this is because these enzymes are not the same at all. Iron insertion into the oxidized tetrapyrroles is the penultimate step of the CPD heme *b* biosynthesis branch. Coproporphyrin ferrochelatase (CpfC) catalyzes the insertion of iron specifically to coproporphyrin III. This enzyme is very structurally related to PpfC, but shares less than 15% sequence identity with it [1, 25](Figure 1.8). Instead of a membrane-bound dimer, CpfC is a cytosolic monomer, as confirmed by various independent groups[23, 28].

CpfC enzymes does not contain any bound co-factors and, except for in Actinobacteria, do not contain a [2Fe-2S] cluster. Several structures of CpfC from *B. subtilis* have been obtained with either M-methylmesoporphyrin IX or deuteroporphyrin IX bound in the active site, although no substrate/product structure has been obtained. CpfC contains all of the conserved active site residues found in PpfC and but lacks the well noted “active site lip”[25, 28],which is though to allow for the accommodation of a larger substrate, as is coproporphyrin III. Comparison of M-methylmesoporphyrin IX-bound *Bs*CpfC and PPIX-*Hs*PpfC showed that the porphyrin in CpfC binds in a different location than in PpfC and is rotated ~100°. Moreover, the porphyrin is about 4.5Å further from the inside of the active site, leaving two out of four propionate groups exposed to solvent.

Nevertheless, the porphyrin in CpfC still interacts with the well-conserved active site His and CpfC has been shown to bind Fe^{2+} in a similar manner with its respective His-Glu residues[28-29]. Delivery of Fe^{2+} to CpfC is also similar and, at least in *B. subtilis*, is directly delivered by Fra, the *B. subtilis* frataxin homolog[31-32]. Metalation is thus thought to occur through a similar mechanism, although further work with this enzyme and its appropriate substrate is also needed.

What Happens After Heme *b* is Synthesized and Final Notes

The availability of genome sequencing data and bioinformatics led to the realization that there were missing pieces to what was thought to be a well-defined pathway. These pieces, which have now been filled in, have simultaneously created more holes. Of most importance, the questions that come up are (1) what is the true nature of the CgoX and CpfC enzymes? (2) how does metabolite flux happen and how is off-pathway reactivity controlled in gram-positive organisms? and (3) what is the fate of heme *b* after it has been synthesized?

Discovery of the CPD branch led to the realization that CgoX and CpfC act on different substrates and produce different products than the homologous PgoX and PpfC enzymes. Leading off of this, it cannot be assumed that isofunctional, or even homologous, enzymes found in different organisms are the same. In order to understand the true nature of these enzymes in the distinct organisms in which they are found, oligomerization state, solubility, presence and identity of a cofactor, and reaction mechanism must all be experimentally determined for each enzyme. This has been done with ChdC, as it was a novel enzyme, unique to the CPD branch, but remains to be done for CgoX and CpfC. It is currently assumed that CgoX and CpfC have near identical reaction mechanisms to PgoX and PpfC, respectively, however this has not been experimentally tested. It is our belief that CgoX and CpfC could catalyze their reactions using different co-factors/co-substrates, to best suit the organisms in which they are found.

The fact that heme *b* and its porphyrin precursors generated during the last three steps of biosynthesis are cytotoxic, leads to the question of how off-pathway reactivity is regulated in gram-positive organisms. The production and location of these metabolites must be tightly regulated. Eukaryotes and gram-positive bacteria have double membrane structures that allow them to compartmentalize the terminal enzymes of the heme biosynthesis pathway and the toxic molecules they produce. Gram-positive bacteria lack a double membrane and thus must have a different way to create this compartmentalization. Direct protein-protein interactions between CgoX, CpfC, and ChdC could be a way to achieve this. Characterization of these enzymes with their accurate substrates and reconsideration of their structural features (ie. membrane association) will shed light on how the CgoX, CpfC, and ChdC work together to synthesize the final product, heme *b*.

Lastly, an aspect of heme biosynthesis that is not always considered is the delivery of this cofactor to its final cellular destination. Because of its highly reactive nature, it is unlikely that ChdC simply releases heme *b* to the cellular mileu after making it. More likely is that ChdC hands this molecule off to a recipient protein that safely transports heme throughout the cell. Identifying this recipient protein will be essential to understanding gram-positive bacterial heme *b* biosynthesis in totality.

References

1. Dailey, H. A.; Gerdes, S.; Dailey, T. A.; Burch, J. S.; Phillips, J. D., Noncanonical coproporphyrin-dependent bacterial heme biosynthesis pathway that does not use protoporphyrin. *Proc Natl Acad Sci U S A* **2015,** *112* (7), 2210-5.

2. Bali, S.; Lawrence, A. D.; Lobo, S. A.; Saraiva, L. M.; Golding, B. T.; Palmer, D. J.; Howard, M. J.; Ferguson, S. J.; Warren, M. J., Molecular hijacking of siroheme for the synthesis of heme and d1 heme. *Proc Natl Acad Sci U S A* **2011,** *108* (45), 18260-5.

3. Dailey, H. A.; Dailey, T. A.; Gerdes, S.; Jahn, D.; Jahn, M.; O'Brian, M. R.; Warren, M. J., Prokaryotic Heme Biosynthesis: Multiple Pathways to a Common Essential Product. *Microbiol Mol Biol Rev* **2017,** *81* (1).

4. Hamza, I.; Dailey, H. A., One ring to rule them all: trafficking of heme and heme synthesis intermediates in the metazoans. *Biochim Biophys Acta* **2012,** *1823* (9), 1617-32.

5. Layer, G.; Grage, K.; Teschner, T.; Schunemann, V.; Breckau, D.; Masoumi, A.; Jahn, M.; Heathcote, P.; Trautwein, A. X.; Jahn, D., Radical S-adenosylmethionine enzyme coproporphyrinogen III oxidase HemN: functional features of the [4Fe-4S] cluster and the two bound S-adenosyl-L-methionines. *J Biol Chem* **2005,** *280* (32), 29038-46.

6. LaMattina, J. W.; Nix, D. B.; Lanzilotta, W. N., Radical new paradigm for heme degradation in Escherichia coli O157:H7. *Proc Natl Acad Sci U S A* **2016,** *113* (43), 12138-12143.

7. Layer, G.; Pierik, A. J.; Trost, M.; Rigby, S. E.; Leech, H. K.; Grage, K.; Breckau, D.; Astner, I.; Jansch, L.; Heathcote, P.; Warren, M. J.; Heinz, D. W.; Jahn, D., The

substrate radical of Escherichia coli oxygen-independent coproporphyrinogen III oxidase HemN. *J Biol Chem* **2006,** *281* (23), 15727-34.

8. Celis, A. I.; Streit, B. R.; Moraski, G. C.; Kant, R.; Lash, T. D.; Lukat-Rodgers, G. S.; Rodgers, K. R.; DuBois, J. L., Unusual Peroxide-Dependent, Heme-Transforming Reaction Catalyzed by HemQ. *Biochemistry* **2015,** *54* (26), 4022-32.

9. Mayfield, J. A.; Hammer, N. D.; Kurker, R. C.; Chen, T. K.; Ojha, S.; Skaar, E. P.; DuBois, J. L., The Chlorite Dismutase (HemQ) fromStaphylococcus aureusHas a Redox-sensitive Heme and Is Associated with the Small Colony Variant Phenotype. *Journal of Biological Chemistry* **2013,** *288* (32), 23488-23504.

10. Celis, A. I.; DuBois, J. L., Substrate, product, and cofactor: The extraordinarily flexible relationship between the CDE superfamily and heme. *Archives of Biochemistry and Biophysics* **2015,** *574*, 3-17.

11. Celis, A. I.; Gauss, G. H.; Streit, B. R.; Shisler, K.; Moraski, G. C.; Rodgers, K. R.; Lukat-Rodgers, G. S.; Peters, J. W.; DuBois, J. L., Structure-Based Mechanism for Oxidative Decarboxylation Reactions Mediated by Amino Acids and Heme Propionates in Coproheme Decarboxylase (HemQ). *J Am Chem Soc* **2017,** *139* (5), 1900-1911.

12. Streit, B. R., Decarboxylation involving a ferryl, propionate, and a tyrosyl group in a radical relay yields heme b. *Journal of Biological Chemistry* **2018,** *293* (11), 3989-3999.

13. Ferreira, G. C., Organization of the Terminal Two Enzymes of the Heme Biosynthetic Pathway. *The journal of biological chemistry* **1998,** *263* (8), 38835-3839.
14. Koch, M., Crystal structure of protoporphyrinogen IX oxidase: a key enzyme in haem and chlorophyll biosynthesis. *EMBO Journal* **2004,** *23* (8), 1720-1728.

15. Boynton, T. O.; Daugherty, L. E.; Dailey, T. A.; Dailey, H. A., Identification ofEscherichia coliHemG as a Novel, Menadione-Dependent Flavodoxin with Protoporphyrinogen Oxidase Activity. *Biochemistry* **2009,** *48* (29), 6705-6711.

16. Boynton, T. O.; Gerdes, S.; Craven, S. H.; Neidle, E. L.; Phillips, J. D.; Dailey, H. A., Discovery of a gene involved in a third bacterial protoporphyrinogen oxidase activity through comparative genomic analysis and functional complementation. *Appl Environ Microbiol* **2011,** *77* (14), 4795-801.

17. Kobayashi, K.; Masuda, T.; Tajima, N.; Wada, H.; Sato, N., Molecular phylogeny and intricate evolutionary history of the three isofunctional enzymes involved in the oxidation of protoporphyrinogen IX. *Genome Biol Evol* **2014,** *6* (8), 2141-55.

18. Kato, K., Identification of a gene essential for protoporphyrinogen IX oxidase activity in the cyanobacterium Synechocystis sp. PCC6803. *PNAs* **2010,** *107* (36), 16649-16654.

19. Qin, X., Structural insight into unique properties of protoporphyrinogen oxidase from Bacillus subtilis. *Journal of Structural Biology* **2010,** *170* (1), 76-82.

20. Lobo, S. A.; Scott, A.; Videira, M. A.; Winpenny, D.; Gardner, M.; Palmer, M. J.; Schroeder, S.; Lawrence, A. D.; Parkinson, T.; Warren, M. J.; Saraiva, L. M., Staphylococcus aureus haem biosynthesis: characterisation of the enzymes involved in final steps of the pathway. *Mol Microbiol* **2015,** *97* (3), 472-87.

21. Ilka U. Heinemann, M. J., Dieter Jahn, The biochemistry of heme synthesis. *Archives of Biochemistry and Biophysics* **2008,** *474* (2), 238-251.

22. Corrigal, A. V., Purification of and Kinetic Studies on a Cloned Protoporphyrinogen Oxidase from the Aerobic BacteriumBacillus subtilis. *Archives of Biochemistry and Biophysics* **1998,** *358* (2), 251-256.

23. Henderstedt, M. H. a. L., Bacillus subtilis HemY Is a Peripheral Membrane Protein Essential for Protoheme IX Synthesis Which Can Oxidize Coproporphyrinogen III and Protoporphyrinogen IX. *Journal of Bacteriology* **1994,** *176* (19), 5962-5970.

24. Nagaraj, V. A.; Arumugam, R.; Prasad, D.; Rangarajan, P. N.; Padmanaban, G., Protoporphyrinogen IX oxidase from Plasmodium falciparum is anaerobic and is localized to the mitochondrion. *Mol Biochem Parasitol* **2010,** *174* (1), 44-52.

25. Amy Medlock, L. S., Tamara A. Dailey, Harry A. Dailey, and William N. Lanzilotta, Substrate interactions with human ferrochelatase. *Proc Natl Acad Sci U S A* **2001,** *104* (6), 1789-1793.

26. Shepherd, M.; Dailey, T. A.; Dailey, H. A., A new class of [2Fe-2S]-cluster-containing protoporphyrin (IX) ferrochelatases. *Biochem J* **2006,** *397* (1), 47-52.

27. Dailey, H. A., Altered Orientation of Active Site Residues in Variants of Human Ferrochelatase.Evidence for a Hydrogen Bond Network Involved in Catalysis. *Biochem J* **2007,** *46* (27), 7973-7979.

28. Salam Al-Karadaghi, M. H., Stanislav Nikonov, Crystal structure of ferrochelatase: the terminal enzyme in heme biosynthesis. *Structure* **1997,** *5* (11), 1501-1510.

29. Lecerof, D.; Fodje, M. N.; Alvarez Leon, R.; Olsson, U.; Hansson, A.; Sigfridsson, E.; Ryde, U.; Hansson, M.; Al-Karadaghi, S., Metal binding to Bacillus

subtilis ferrochelatase and interaction between metal sites. *J Biol Inorg Chem* **2003,** *8* (4), 452-8.

30. Lesuisse, E., Iron use for haeme synthesis is under control of the yeast frataxin homologue (Yfh1). *Human Molecular Genetics* **2003,** *12* (8), 879-889.

31. Soderberg, C.; Gillam, M. E.; Ahlgren, E. C.; Hunter, G. A.; Gakh, O.; Isaya, G.; Ferreira, G. C.; Al-Karadaghi, S., The Structure of the Complex between Yeast Frataxin and Ferrochelatase: Characterization and pre-steady state reaction of ferrous iron delivery and heme synthesis. *J Biol Chem* **2016,** *291* (22), 11887-98.

32. Mielcarek, A.; Blauenburg, B.; Miethke, M.; Marahiel, M. A., Molecular insights into frataxin-mediated iron supply for heme biosynthesis in Bacillus subtilis. *PLoS One* **2015,** *10* (3), e0122538.

CHAPTER TWO

STUDY OF THE NOVEL, LAST ENZYME IN THE HEME B BIOSYNTHESIS PATHWAY OF GRAM-POSITIVE BACTERIA, CHDC (HEMQ)

Discovery of ChdC (Formerly Known as HemQ)

Prior to genome sequencing and the development of bioinformatics tools, it was believed that there was single heme *b* biosynthesis pathway (now known as the PPD branch), which was universal to all heme-containing organisms (Figure 2.1). As these tools became more available, it was noted that gram-positive bacteria do not code for either enzyme that could catalyze the conversion of coproporphyrinogen III to protoporphyrinogen IX (CgdC or CgdH). However, they did contain a gene in their heme *b* biosynthesis gene cluster whose function had not yet been described. This gene, first annotated as a “putative chloride dismutase enzyme” (*cld*), was renamed *hemQ* and fittingly, was found in gram-positive bacteria but not gram-negative bacteria nor eukaryotes[1-3].

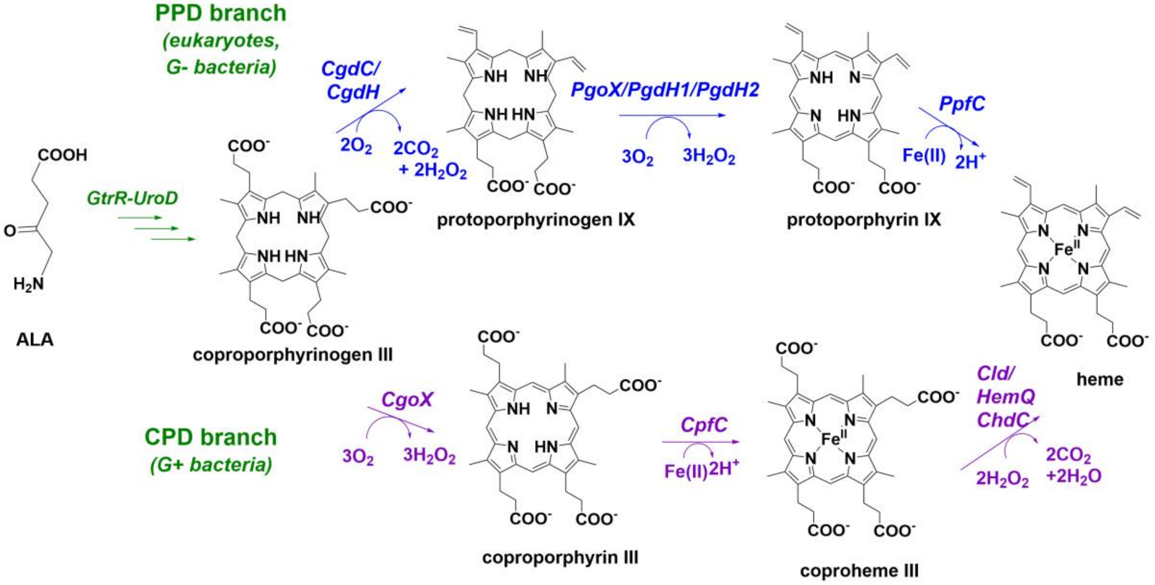
PPD branch
(eukaryotes, G- bacteria)
CgdC/ CgdH
2O2
2CO2 + 2H2O2
PgoX/PgdH1/PgdH2
3O2
3H2O2
PpfC
Fe(II)
2H+
GtrR-UroD
ALA
coproporphyrinogen III
protoporphyrinogen IX
protoporphyrin IX
heme
CPD branch
(G+ bacteria)
CgoX
3O2
3H2O2
coproporphyrin III
CpfC
Fe(II)
2H+
coproheme III
Cld/ HemQ ChdC
2H2O2
2CO2 +2H2O

Figure 2.1. The PPD and CPD branches of heme *b* biosynthesis. Discovery of ChdC allowed for elucidation of a new heme *b* biosynthesis pathway that is unique to gram-positive bacteria. For the different intermediates that are generated in the unique branches, one was called the porphyrin-dependent (PPD) branch and the other the coproporphyrin-dependent (CPD) branch. The PPD branch is found in eukaryotic and gram-negative bacteria only.

Eager to decipher the function of HemQ, studies of the *S. aureus* and the *B. subtilis* HemQ enzymes by separate groups revealed that HemQ did not catalyze the chlorite dismutase (cld) reaction (Figure 2.2A) nor did it catalyze the reaction required to substitute for the missing CgdC/CgdH heme biosynthesis enzymes[2-3]. Its link to heme biosynthesis, however, was clear. Not only was its gene location suggestive of this, but *in cellulo* experiments also indicated it. The removal of *hemQ* in *S. aureus* made this organism a heme auxotroph[3] and co-expression of the *cgoX* + *cpfC* + *hemQ* proved to be able to complement the heme auxothrophy of an *E. coli pgoX or ppfC* knock-out, while it had been long documented that (although *cdgH* is present in this organism) *cgoX* and *cfpC* alone did not[2]. These results led to the realization that the well-characterized heme *b* biosynthesis pathway was not universal and needed to be re-examined for gram-positive organisms. It is now known that HemQ catalyzes the oxidative decarboxylation of coproheme III to yield heme *b* (Figure 2.2B). The discovery of *hemQ* led to the deciphering of the novel CPD branch of heme *b* biosynthesis and during the renaming of all the other enzymes, HemQ became Coproheme Decarboxylase, or ChdC[2-3] (Figure 2.1,Table 1.1).

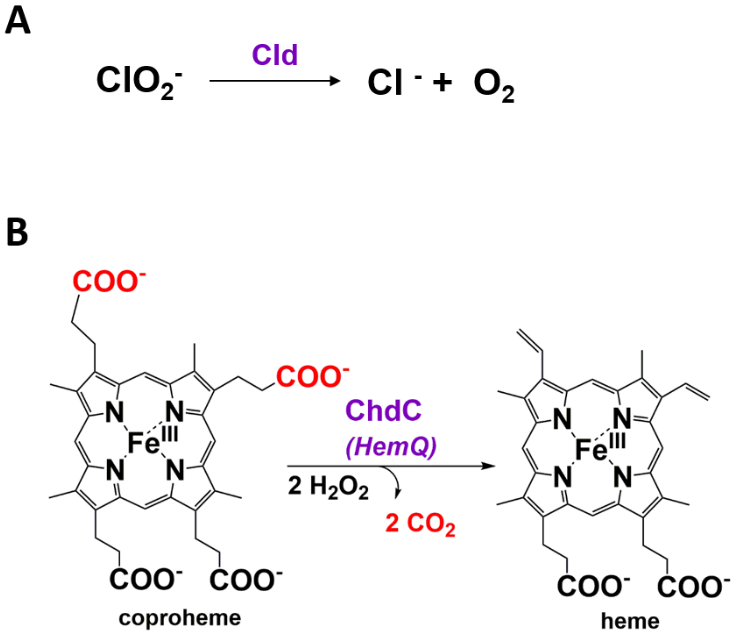

Figure 2.2. ChdC does not catalyze the chlorite dismutase (cld) reaction and instead catalyzes the last step of the heme b biosynthesis pathway in gram-positive bacteria. (A) Canonical Cld enzymes convert ClO_2^- to Cl^- and O_2, using heme as a cofactor. (B) ChdCs (formerly HemQs) bind coproheme as a substrate and catalyze the H_2O_2-dependent oxidative decarboxylation of the ring A- and ring B-propionate groups to yield heme.

ChdC and the ChdC-Protein Family

ChdC was first annotated as a chlorite dismutase enzyme. Chlorite dismutase enzymes (Clds) were first noted for their ability to convert ClO_2^- into Cl^- and O_2 using heme as a tightly bound cofactor (Figure 2.2A). The Cld family of enzymes is quite large and diverse, with members in almost all bacterial and archeal phyla[4] (Figure 2.3).ChdCs share such a high sequence similarity to canonical Clds that the Pfam protein family database still groups Clds and ChdCs as a single family and only separates the two at high stringencies [4]. Their taxonomic distribution, however, is rather distinct and reflects the different biological roles of these enzymes. While canonical Clds are found within perchlorate or chlorate reductase operons in gram-negative proteobacteria, ChdCs are exclusively found within heme *b* biosynthesis operons of gram-positive bacteria.

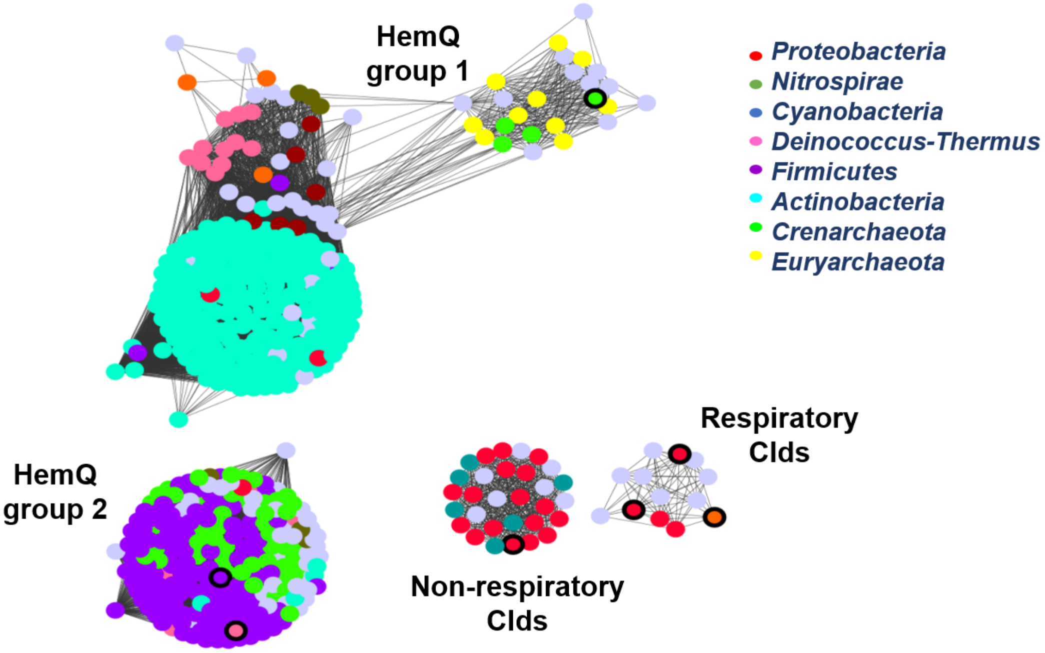
HemQ group 1
Proteobacteria
Nitrospirae
Cyanobacteria
Deinococcus-Thermus
Firmicutes
Actinobacteria
Crenarchaeota
Euryarchaeota
Respiratory Clds
HemQ group 2
Non-respiratory Clds

Figure 2.3. The Cld family of enzymes (Pfam06778). ChdC's belong to the Cld family of proteins and share high sequence and structural similarity with canonical Clds. The Cld family of proteins is taxonomically diverse with members in almost all phyla.

ChdCs and Clds are not only similar in sequence, but also in secondary and tertiary structure (Figure 2.4B). The N-terminal, heme/coproheme-binding portion of these structures mutually align to form a homopentamer with an opening in the center (Figure

2.4A). With the exception of a large helix loop segment around the active site, the superimposed structures of canonical Clds and ChdC display almost complete overlap. This helix-loop, composed of amino acid residues ~110-140, is away from the active site in ChdC and is thought to have important implications for substrate binding, product-egress, and/or interactions with other proteins. A defining feature of canonical Clds is a well-conserved distal (above the heme plane) Arg residue that is substituted by a neutral Glu or Ser in ChdCs (Figure 2.4C).

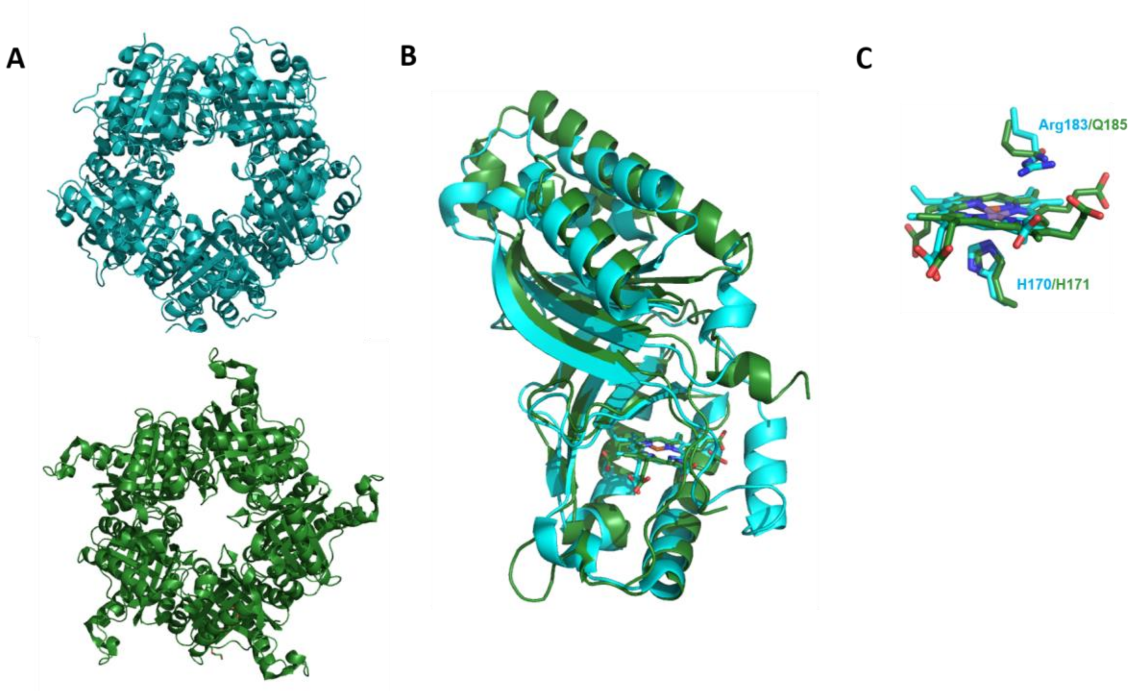

Figure 2.4. ChdCs and canonical Clds share a common structural fold. (A) Canonical Clds (top, PDBID 3Q09) and Chds (bottom, PDBID 5T2K) share a homopentameric quaternary structure. (B) Superimposing their monomers show almost complete overlap with heme or coproheme binding in a similar position. (C) The coproheme substrate in ChdCs is rotated about 90 relative to the heme in Clds, positioning the non- reactive propionate groups facing towards solvent and the reactive A- and B-ring propionate groups buried deep within the ChdC active site. Canonical Clds have a conserved distal Arg, which is essential for reactivity with ClO_2^-. This residue is replaced by a non-polar Glu in ChdCs.

The absence of a polar distal charge, along with the rest of the surrounding non-polar residues, makes the ChdC binding pocket highly hydrophobic. Without the ability to recruit anionic substrates, it is hypothesized that this could be the reason why the function of these two enzymes diverged.

The ChdC Active Site is Unlike Canonical Peroxidases

Early in the discovery of ChdC, preliminary studies suggested that this reaction was H_2O_2-dependent, making ChdC a peroxidase. Canonical peroxidases are enzymes that catalyze the oxidation of wide variety of organic and inorganic substrates using H_2O_2 and heme *b* as a cofactor. The axial ligands to the heme in these enzymes are a tyrosyl residue or a histidyl residue on the proximal side and water on the distal side, which is replaced by H_2O_2 during the catalytic reaction[5] (Figure 2.6A, in red). Also within the active site are His and Arg or Asn side chains on the distal side that interact with H_2O_2 when it is bound to the iron (Figure 2.6A, in blue).

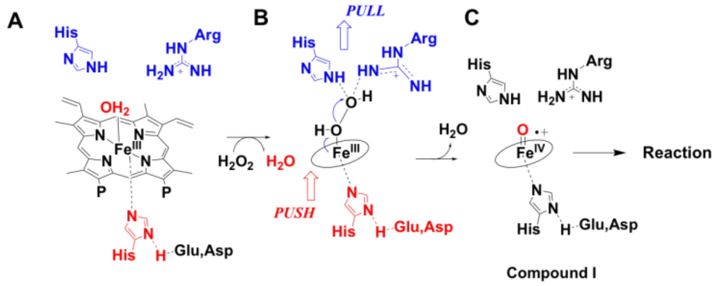
A
His
N
NH
HN
Arg
H₂N
NH
OH₂
N
N
Fe^III
N
N
P
P
N
N
His
H
Glu,Asp
H₂O₂
H₂O
B
PULL
His
N
NH
HN
Arg
HN
NH
O
H
H-O
Fe^III
PUSH
N
N
His
H
Glu,Asp
H₂O
C
His
N
NH
HN
Arg
H₂N
NH
O
Fe^IV
Reaction
N
N
His
H
Glu,Asp
Compound I

Figure 2.6. Canonical heme peroxidases contain a highly polar active site, which facilitates reactivity with H_2O_2 through a "push" and "pull" mechanism. (A) In the resting state, peroxidase enzymes have a water molecule bound to the iron. (B) This water molecule is replaced by H_2O_2 during catalysis. A push and pull of electrons by conserved distal and proximal residues to the O-O bond in the bound H_2O_2 creates polarization of this bond and leads to subsequent heterolytic cleavage. (C) This creates a high-valent Fe (IV) intermediate known as compound I, which is the reactive species in these enzymes.

These residues play an important role in the reaction mechanism. The distal His and Arg/Asn residues activate peroxide by catalyzing proton transfer from the α-oxygen to the β-oxygen in the heme bound H_2O_2, polarizing the O-O bond[6] (Figure 2.6B). The modulation of the ionization state (and thus pKa) of the distal His by Arg/Asn and the potential acid/base catalysis of this residue also polarizes the O-O bond by what is known as the "pull" mechanism of electrons. The proximal Tyr or His residue, where the latter is strongly H-bonded to another residue and therefore anionic in character, donates electrons to the heme iron and the bound α-oxygen atom of H_2O_2, again polarizing the O-O bond by what is called the "push" mechanism (Figure 2.6B). Deprotonation of H_2O_2, charge separation in the hydroperoxy intermediate (Compound 0) and the formation and stabilization of Compound I, allow for reactivity with H_2O_2 (Figure 2.6C). The ability of canonical peroxidase enzymes to do this is attributed to the polar residues contained in their active site pocket.

The fact that the active site of ChdC lacks the polar residues described to be essential for reactivity with H_2O_2 indicates that the ChdC reaction mechanism is not like a typical peroxidase.

A Multi-Level Approach to Understanding ChdC and its Unique Reaction

As a newly discovered enzyme, very little was known about ChdC. The oxidizing agent required for this reaction, although hypothesized to be H_2O_2, required further scrutiny. The active site of ChdC lacks essential elements of canonical peroxidase enzymes and thus the mode of H_2O_2 activation needed to be defined. While a mechanism for oxidative decarboxylation of a tetrapyrrole has already been well described in the PPD branch of the heme *b* biosynthesis pathway (by CgdC/CgdH), the fact that the substrate of ChdC is metalated, suggested that the method of catalysis must be intrinsically different and that ChdC could use coproheme as both a substrate and a cofactor. The great structural similarity, yet widely different catalyzed reaction, between ChdC and canonical Clds was also of great interest. We wished to identify the specific amino acid residues in ChdC responsible for substrate-binding, catalysis, and product egress and determine how two highly homologous structures could catalyze completely different reactions. Further, how a peroxide-dependent reaction could occur in a highly hydrophobic site, was not determined. We wished to characterize this unusual, peroxide-dependent catalysis site. Lastly, heme *b* and the porphyrin precursors that are generated during its biosynthesis are highly reactive and cytotoxic. Also harmful to the cell if its location and concentration are not tightly controlled, is H_2O_2. The presence of ChdC exclusively in gram-positive organisms and the differences in the last three terminal enzymes between the PPD and CPD branch, suggest that the collaborative work of these terminal enzymes to synthesize heme and regulate precursor metabolite flux, must also be unique and distinct to gram-negative bacteria and eukaryotes.

The goal of this thesis project was to characterize ChdC and its catalytic reaction at (1) the molecular level, (2) the protein-structure level, and (3) the cellular level. Contained in the chapters of this thesis are the experiments performed to answer questions at all of the three biochemical levels mentioned above. The conclusions made have, one step at a time, added a valuable piece of knowledge about the novel, unusual, and unique enzyme ChdC and a significant contribution to the field of heme *b* biosynthesis.

Note on the Enzyme Nomenclature Used Here

During the chronological time of this study, the nomenclature of the heme *b* biosynthesis enzymes was evolving. “HemQ” was used in our publications to refer to ChdC and this is reflected in the title of the first three sections of this thesis. In the fourth section, as well as in the Literature Review chapter, the new nomenclature is used to avoid confusion between the PPD and CPD enzymes. The reader should note that HemQ and ChdC is the same enzyme, and that HemY and HemH (unless otherwise stated) refer to CgoX and CpfC, respectively. Table 1.1 in Chapter 1 of this thesis lists the former and current names used for these enzymes and can be used as a reference when needed.

References

1. Dailey, H. A.; Gerdes, S.; Dailey, T. A.; Burch, J. S.; Phillips, J. D., Noncanonical coproporphyrin-dependent bacterial heme biosynthesis pathway that does not use protoporphyrin. *Proc Natl Acad Sci U S A* **2015,** *112* (7), 2210-5.

2. Dailey, T. A.; Boynton, T. O.; Albetel, A. N.; Gerdes, S.; Johnson, M. K.; Dailey, H. A., Discovery and Characterization of HemQ: an essential heme biosynthetic pathway component. *J Biol Chem* **2010,** *285* (34), 25978-86.

3. Mayfield, J. A.; Hammer, N. D.; Kurker, R. C.; Chen, T. K.; Ojha, S.; Skaar, E. P.; DuBois, J. L., The Chlorite Dismutase (HemQ) fromStaphylococcus aureusHas a Redox-sensitive Heme and Is Associated with the Small Colony Variant Phenotype. *Journal of Biological Chemistry* **2013,** *288* (32), 23488-23504.

4. Celis, A. I.; DuBois, J. L., Substrate, product, and cofactor: The extraordinarily flexible relationship between the CDE superfamily and heme. *Archives of Biochemistry and Biophysics* **2015,** *574*, 3-17.

5. Valentine, J. S., Dioxygen Reactions. In *Bioinorganic Chemistry*, University Science Books: Mill Valley, CA, 1994; pp 253-311.

6. Rodriguez-Lopez, J. N. L., D.J.; Hernandez-Ruiz, J.; Hiner, A.N.P.; Garcia-Canovas, F.; Thorneley, R.N.F Mechanism of Reaction of Hydrogen Peroxide with Horseradish Peroxidase: Identification of Intermediates in the Catalytic Cycle. *J Am Chem Soc* **2001,** *123* (48), 11838-11847.

CHAPTER THREE

UNUSUAL PEROXIDE-DEPENDENT, HEME-TRANSFORMING REACTION CATALYZED BY HEMQ

Contribution of Authors and Co-Authors

Author: Arianna I. Celis

Contributions: Expressed, purified, and prepared apo-, harderoheme III/IV- and coproheme III-bound HemQ enzyme. Measured and calculated extinction coefficients. Performed real-time reaction monitoring by UV-Vis and product analysis by pyridine hemochrome, HPLC, and MS. Contributed to the writing and preparation of this manuscript.

Co-Author: Bennett R. Streit

Contributions: Contributed to analysis and interpretation of all reaction data. Provided support and very valuable insight in preparation of manuscript.

Co-Author: Garrett C. Moraski

Contributions: Synthesized, purified and characterized harderoheme III and harderoheme IV.

Co-Author: Timothy D. Lash

Contributions: Provided harderoporphyrin trimethyl esters and essential insight for synthesis of harderoheme III/IV.

Co-Author: Gudrun S. Lukat-Rodgers

Contributions: Measured and analyzed rR data. Provided support and very valuable insight in preparation of manuscript. Contributed to the writing and preparation of this manuscript.

Co-Author: Kenton R. Rodgers

Contributions: Measured and analyzed rR data. Provided support and very valuable insight in preparation of manuscript. Contributed to the writing and preparation of this manuscript.

Co-Author: Jennifer L. DuBois

Contributions: Provided important insight and overview of the preparation of samples, experiment design and interpretation of results. Contributed largest part to the writing and preparation of this manuscript.

Manuscript Information Page

Arianna I. Celis, Bennett R. Streit, Garrett C. Moraski, Timothy D. Lash, Gudrun S. Lukat-Rodgers, Kenton R. Rodgers, Jennifer L. DuBois

Biochemistry

Status of Manuscript:
____ Prepared for submission to a peer-reviewed journal
____ Officially submitted to a peer-review journal
__ _ Accepted by a peer-reviewed journal
__X_ Published in a peer-reviewed journal

Publisher: American Chemical Society

Reprinted with permission from Celis, A. I.; Streit, B. R.; Moraski, G. C.; Kant, R.; Lash, T. D.; Lukat-Rodgers, G. S.; Rodgers, K. R.; DuBois, J. L., Unusual Peroxide-Dependent, Heme-Transforming Reaction Catalyzed by HemQ. *Biochemistry* **2015,** *54* (26), 4022-32. Copyright 2015 American Chemical Society.

CHAPTER THREE

UNUSUAL PEROXIDE-DEPENDENT, HEME-TRANSFORMING REACTION CATALYZED BY HEMQ

Arianna I. Celis,[1] Bennett R. Streit,[1] Garrett C. Moraski,[1] Timothy D. Lash,[2] Gudrun S. Lukat-Rodgers,[3] Kenton R. Rodgers,[3] Jennifer L. DuBois[1]

[1]*Department of Chemistry and Biochemistry, Montana State University, Bozeman, MT 59715-3400, USA*
[2]*Department of Chemistry, Illinois State University, Normal, IL 61761-4160, USA*
[3]*Department of Chemistry and Biochemistry, North Dakota State University, Fargo, North Dakota 58102-6050, USA*

Abstract

A recently proposed pathway for heme *b* biosynthesis, common to diverse bacteria, has the conversion of two of the four propionates on coproheme III to vinyl groups as its final step. This reaction is catalyzed in a cofactor-independent, H_2O_2-dependent manner by the enzyme HemQ. Using the HemQ from *Staphylococcus aureus* (*Sa*HemQ) the initial decarboxylation step was observed to rapidly and obligately yield the three-propionate harderoheme isomer III as the intermediate, while the slower second decarboxylation appeared to control the overall rate. Both synthetic harderoheme isomers III and IV reacted when bound to HemQ, the former more slowly than the latter. While H_2O_2 is the assumed biological oxidant, either H_2O_2 or peracetic acid yielded the same intermediates and products, though significantly greater than the expected two equivalents were required in both cases and peracetic acid reacted faster. The ability of

peracetic acid to substitute for H_2O_2 suggests that, despite the lack of catalytic residues conventionally present in heme peroxidase active sites, reaction pathways involving high valent iron intermediates cannot be ruled out.

Introduction

Heme, the complex of protoporphyrin IX with iron, is fundamentally important for life. A diverse set of metal-chelating cofactors including F430 (Ni), vitamin B12 (Co), siroheme (Fe,S), and chlorophyll (Mg) additionally share a common tetrapyrrole scaffold and hence biosynthetic and evolutionary roots with heme. In humans and other eukaryotes, the biosynthesis of chemically unfunctionalized heme *b* occurs via 8 well-known enzymatic steps.[1,2] A little more than a decade ago, however, a manual survey of the available prokaryotic genomes indicated that genes encoding many of these steps were absent from diverse species, suggesting the evolutionary history of the pathway may be complex.[3]

Sophisticated bioinformatics methods and a substantially expanded pool of genomic data in conjunction with experimental approaches have since allowed many holes in the pathways to heme and related tetrapyrrole cofactors to be filled (Scheme 1). A complete route to heme biosynthesis in Archaea and sulfate-reducing bacteria has been identified.[4] Recently, a new ending for the pathway in gram-positive bacteria from the Actinobacteria and Firmicutes phyla – a large group of organisms characterized by their lack of an outer membrane – was proposed.[5] This and the canonical pathway effect the same three chemical transformations on the metabolic intermediate coproporphyrinogen III.

However, the reactions in the two pathways occur in a different order, yield distinct intermediates, and invoke distinct enzymes for the oxidative decarboxylation step.[5]

In the gram-positive bacteria, this step occurs at the terminus of the pathway, after a step analogous to the well-known ferrochelatase reaction.[6] It is catalyzed by HemQ, an enzyme which uses coproheme III as both substrate and cofactor in the H_2O_2-dependent oxidative decarboxylation of the propionate side chains at β-pyrrole positions 2 and 4 (Scheme 2).[6] Cofactor-independent, O_2-dependent enzymes have been described, including coproporphyrinogen III oxidase (HemF).[7,8] However, this is to our knowledge the first example of a cofactor-independent transformation involving H_2O_2. In contrast with coproporphyrinogen III, the metallosubstrate used by HemQ offers the possibility of mechanistically distinct, iron-mediated activation of H_2O_2 for the oxidative decarboxylation step. Interestingly, the conversion of coproheme to heme *b* is also catalyzed anaerobically by AhbQ, a radical S-adenosyl-methionine- and iron sulfur cluster--dependent enzyme at the terminus of the biosynthetic pathway in Archaea and sulfate-reducing bacteria (Scheme 1).[4,10] Homologs are also found in some gram-positive and possibly other bacteria along with *hemQ* genes, affording a possible anaerobic alternative for this step.

HemQs are part of the chlorite dismutase family (Clds, Pfam 06778).[9,23] This family is best known for the minority of its members that use heme *b* to catalytically convert ClO_2^- to Cl^- and O_2 at the terminus of perchlorate respiratory pathways.[24] The reaction of HemQs, by contrast, has not been well studied. It has been previously shown that HemQ is not highly active toward H_2O_2 in its heme *b*-bound form, but instead fairly readily undergoes heme degradation.[9] Further, the reaction appears to be dependent on H_2O_2 and not O_2. In its coproheme III bound state, the HemQ from *Mycobacterium tuberculosis* was shown to react with H_2O_2 rather than various O_2/reductant combinations, fully converting coproheme III to heme *b*.[5]Here, using the enzyme from *Staphylococcus aureus* (*Sa*HemQ), we sought to identify the likely tetrapyrrole-intermediates on the reaction pathway in order to narrow down the possible reaction mechanisms. We aimed to determine whether the reactions with the propionates occur in an ordered fashion and with what time course, and whether a specific three-propionate harderoheme isomer could be identified as a reaction intermediate. Finally, in order to set limits on possible iron-intermediates, we examined whether the same intermediates and products would be generated with organic peroxides and peracids as, and to establish the stoichiometry of the reaction in each case.

Experimental Methods

Reagents and Stocks

Ferric coproporphyrin III chloride (coproheme III, Frontier Scientific) and hemin chloride (Sigma) were obtained in 10 mg ampules and used to generate 5-10 mM stock solutions in dimethylsulfoxide (DMSO). Harderohemes III and IV prepared in house were rigorously dried in tared glass ampules and weighed on an analytical balance. 5 mM stocks were prepared in DMSO in the ampules based on the measured masses.

Hydrogen peroxide (H_2O_2), *tert*-butyl-peroxide, *meta*-chloroperbenzoic acid (*m*CPBA) and peracetic acid stock solutions were prepared at 100 µM concentrations in

50 mM potassium phosphate (KPi) buffer, pH 7.4. H_2O_2 concentrations were ascertained by titration with freshly prepared 0.02 M $KMnO_4$ under acidic conditions (concentrated H_2SO_4). Titrations were monitored for loss of the characteristic pink color of permanganate as it is reduced to the nearly colorless Mn^{2+} ion. Peracetic acid stocks were analyzed with MQuant Peracetic acid test strips (EMD Millipore).

Biochemicals (lysozyme, catalase, DNAse, etc.) were purchased from New England Biolabs. Reagents and media for bacterial growth, protein purification, and analysis were obtained from Fisher or GE Healthcare and used without further purification.

Synthesis and Purification of Harderoheme Isomers III and IV

Harderoporphyrin trimethyl esters were prepared as previously described,[7, 8] then metallated in a solution of acetic acid/2% pyridine under argon. The resulting harderohemes were saponified using NaOH and analyzed by high pressure liquid chromatography (HPLC) coupled to electrospray time of flight mass spectrometry (ESI-MS). See Supplementary Information and Scheme 1S for synthetic and related analytical details.

Expression and Purification of *Sa*HemQ Bound to Substrate and Potential Intermediates

*Sa*HemQ protein expression and purification were carried out as previously described.[9] (See Supplementary information.) The protein was incubated at 4°C for 12-24h with ferric coproheme III or harderoheme [isomer III or IV] in an approximate 1:1 (protein monomer:heme) ratio, based on the protein concentration estimated by the Bradford assay and SDS-PAGE. To remove unbound substrate and further purify the protein, coproheme-bound *Sa*HemQ was concentrated to 5 mL and loaded onto an S-200 Sephacryl gel filtration column (run at 0.4 mL/min in 50 mM KPi buffer, pH 7.4). Fractions were collected using an AKTA Purification System. Fractions with an $R_z \geq 0.5$ were pooled ($R_z = \text{Absorbance}_{\text{Soret}}/\text{Absorbance}_{280}$), concentrated, flash frozen, and stored at -80°C. A PD-10 desalting column (GE Healthcare) was used to remove unbound harderoheme from the protein before concentration and storage.

Extinction coefficients for the coproheme III- and heme *b*-bound *Sa*HemQ at the Soret absorbance band maxima ($\varepsilon_{\text{Soret}}$) were determined by the pyridine hemochrome assay.[10] Briefly, 200 μL of heme-containing solution was mixed with 800 μL of 50 mM NaOH containing 20% pyridine by volume. 3 μL 0.1 M $K_3Fe(CN)_6$ were added and the oxidized spectrum measured. 3-5 mg of solid $Na_2S_2O_4$ were then added to obtain the spectra of the reduced pyridine-bound hemes. Difference spectra (reduced minus oxidized) are reported. Changes in absorbance at observed λ_{max} values were plotted against [heme] and the data fit to a line from which extinction coefficients were obtained. Protein-bound hemes were released by suspension in 50 mM NaOH/20% pyridine and their pyridine hemochrome spectra obtained similarly. Beer's law was used to estimate ε at the UV/visible absorbance maximum for the protein-associated coproheme III or heme *b* (Soret band λ_{max}).

UV/Visible and resonance Raman (rR) Spectroscopy

UV/vis spectra were measured on a temperature-controlled Cary60 instrument in scanning mode at 20 °C. Samples contained 15-35 μM *Sa*HemQ-coproheme (III) monomer in 50 mM KPi buffer, pH 7.4. Resonance Raman spectra were obtained with 406.7 nm excitation from a Kr^+ laser using the 135° backscattering geometry for collection of Raman scattered light. The spectrometer was calibrated against Raman frequencies of toluene, dimethylformamide, acetone, and methylene bromide. Spectra were recorded at ambient temperature from samples prepared at 10-20 mM SaHemQ-coproheme III monomer in 50 mM KPi in spinning 5 mm NMR tubes. UV/vis absorbance spectra were recorded from the rR samples before and after spectral acquisition to assess whether sample integrity had been compromised by exposure to the laser beam. Laser power at the samples ranged from 5-10 mW; no spectral artifacts due to photoinduced chemistry were observed at these powers.

Real-Time Monitoring of Reactions

Solutions of *Sa*HemQ in complex with coproheme III or harderoheme III/IV (5-10 μM) in 50 mM KPi (pH 7.4) were manually mixed with oxidant from a freshly made and titrated stock (H_2O_2, peracetic acid, *m*CPBA, *t*-butyl-peroxide). UV/vis spectra were scanned every 0.25-0.5 min. Absorbances at a given wavelength were plotted versus time, then fit by linear regression to single exponential curves using KaleidaGraph. Rate constants are averages of 3 measurements (error = standard deviation). Resonance Raman spectra were acquired at 30 s intervals with 406.7 nm excitation. Difference spectra were generated by subtraction of the starting *Sa*HemQ-coproheme III spectrum from that at each reaction time.

For discontinuous kinetic analyses, 10 μM *Sa*HemQ-coproheme III complex was mixed with oxidant in a 1 mL reaction mixture and aliquots removed and quenched with

10 mM aqueous KCN (1:1 v/v ratio) every 0.3 min. The quenching solution was sufficient to completely inhibit the enzymatic reaction. The heme content of quenched samples was quantitatively analyzed by HPLC (below).

Product Analyses by Pyridine Hemochrome Assay, HPLC, and MS

Pyridine-hemochrome spectra were measured as described above. HPLC analyses were carried out using an Agilent 1100 series system with diode array UV/vis detection (300-700 nm). 25-50 µL aliquots of analyte were injected into a Phenomenex Luna 3c C18 (2) column (150 x 4.6 mm) at a flow rate of 0.9 mL/min, 45° C. Solvent A was 1M ammonium acetate + 10% acetonitrile; solvent B was methanol + 10% acetonitrile. Elution followed a linear gradient from 35-95% B over 15 min. The column was washed with 95% B (2 min) and equilibrated with 35% (6 min) between runs.[30]

Standards in 50 mM KPi, pH 7.4, were suspended 1:1 (v/v) in a 65:35 mixture of solvents A and B. For analysis of products, the same solvent was added 1:1 (v/v) to reaction mixtures (100 µL, 10 µM protein subunit). Precipitated protein was removed by centrifugation and supernatant was loaded into the column. Integration of the resulting peaks (400 nm) was used for construction of standard curves and quantification of the respective heme. Due to limited availability of and small impurities (<15%) in the harderoheme standards, these were not explicitly quantified; rather, integrated peak intensities from HPLC traces are reported. The exact masses of intermediates and products were verified using ESI-MS carried out on an Agilent 6538 Q-TOF instrument with dual-ESI source (resolution approximately 20,000; accuracy 1 ppm). Source parameters: drying gas 12 L/min, nebulizer 60 psi, capillary voltage 3500 V, capillary exit 120 V. Spectra were collected in positive mode from 50 to 1000 m/z at a rate of 1 Hz.

Results

Characterization of SaHemQ Bound to Substrate, Product, and Potential Intermediates

Pure *Sa*HemQ was obtained in yields of 15-20 mg per L of culture. Distinct UV/vis spectra for the protein reconstituted with coproheme III, harderohemes III/IV, and heme *b* are shown in Figure 1A. *Sa*HemQ in complex with coproheme III has a slightly asymmetric Soret band with a maximum absorbance at 394 nm. Asymmetry may be due to partial conversion of coproheme III to harderoheme inside the protein environment even without the addition of an oxidant, as indicated by HPLC and MS of the *Sa*HemQ-coproheme III complex (see below).

Values for absorption maxima and spectral extinction coefficients have been previously reported for the pyridine hemochrome of heme *b* (λ_{max} = 556 nm; ε_{556} = 33.3 $mM^{-1}cm^{-1}$) and coproheme III (λ_{max} = 546 nm; ε_{546} = 32.2 $mM^{-1}cm^{-1}$).[10] Pyridine hemochrome absorption maxima for the harderohemes III and IV were both at 549 nm (Figure S1A). Overlap in the pyridine hemochrome spectra for coproheme III and the harderohemes suggested that their separation and analysis by HPLC would be essential. Distinct HPLC retention times for all 4 hemes were obtained with the method described above (Figure S1B).

Using the pyridine hemochrome assay to quantify released coproheme III, ε_{Soret} for the *Sa*HemQ-coproheme III complex was determined to be 139.9 ± 3.0 mM^{-1} cm^{-1}. Visible α/β and charge transfer (CT) bands occurred at 497/533 and 630 nm. The spectrum for *Sa*HemQ-heme *b* measured here was consistent with previously reported data.[9] An extinction coefficient for the Soret band maximum at 406 nm was determined: $\varepsilon = 76.6$ mM^{-1} cm^{-1} Visible bands were recorded at: 510/527 nm (α/β), 630 nm (CT). Absorbance maxima for *Sa*HemQ-harderoheme III were: 396 nm (Soret), 495/533 nm (α/β), 610 nm (CT); for SaHemQ-harderoheme (IV): 398 nm (Soret), 490/530 nm (α/β), 610 nm (CT). Notably, the increasingly red-shifted Soret peak maxima for the SaHemQ complexes with substrate, intermediate(s), and product are distinct.

The low frequency rR spectra of SaHemQ complexed with coproheme III, harderohemes III/IV, and heme *b* are shown in Figure 1B; modes involving motions of the propionate and vinyl substituents of the various hemes are observed in this low-wavenumber region. In addition to distortions of the propionate or vinyl groups, it has been demonstrated that movement of the methyl and core atoms of the porphyrin are also involved; thus they actually occur along with pyrrole ring deformations in these modes. Nevertheless, for the purposes of this discussion, they will be termed propionate ($\delta(C_\beta C_c C_d)$) and vinyl ($\delta(C_\beta C_a C_b)$) bending.

Bands due to propionate bending modes were identifiable in all four spectra between 378 and 390 cm^{-1}. The four propionate groups on coproheme III present as a broad envelope with peaks at 378 and 390 cm^{-1} in the *Sa*HemQ complex. The three propionate groups in *Sa*HemQ-harderoheme III give rise to an even less defined feature, a broad band centered at 387 cm^{-1}. The two broad features assigned to propionate modes for *Sa*HemQ-harderoheme IV (378 and 392 cm^{-1}) are similar in frequency to those of the coproheme complex. In the case of heme *b*, the single band at 380 cm^{-1} is assigned to a propionate bending mode for its two propionate groups. Bands associated with vinyl bending motions appear in the harderoheme and heme *b* spectra between 400 and 420 cm^{-1}; notably, these bands are absent from the *Sa*HemQ-coproheme III spectrum. Single $\delta(C_\beta C_a C_b)$ bands are observed at 406 and 412 cm^{-1} for harderohemes III and IV, respectively. While two vinyl bending bands are observed for some heme proteins, such as myoglobin, only a single feature at 414 cm^{-1} is observed for *Sa*HemQ-heme *b*.[12, 13]

Titrimetric Reactions Between *SaHemQ*-coproheme III and H_2O_2

The conversion of a propionate substituent to a vinyl group plus CO_2 is a net two electron oxidation. Two molecules of H_2O_2 (one per reactive propionate) were therefore expected to be required for the complete conversion of coproheme III to heme *b*, while addition of fewer than 2 eq could potentially result in the accumulation of an intermediate. However, UV/vis and rR titrations (Figure 2A-B) indicated only partial conversion of the starting material to the heme *b* complex with < 10 eq H_2O_2. Ten eq were required to affect the complete shift of the UV/vis Soret band from 394 nm (*Sa*HemQ-coproheme III) to 406 nm (*Sa*HemQ-heme *b*). Net changes were the same whether the H_2O_2 was added at once or in increments.

Direct observation of H_2O_2-mediated vinyl group formation was possible by monitoring the *Sa*HemQ-coproheme III titration by rR (Figure 2B). Appearance of a vinyl bending band at 416 cm^{-1} with diminution in the intensity of the propionate bending modes at 378/390 cm^{-1} is consistent with the expected oxidative decarboxylation reaction. Other features typically assigned to vibrations involving the porphyrin pyrrole rings also track the extent of oxidative decarboxylation, including: the increase in ν_7 (pyrrole deformation mode), ν_8 (iron-pyrrole nitrogen stretch), and ν_{11} (pyrrole asymmetric folding mode) intensities and the loss in intensity of ν_{15} and ν_5 (pyrrole symmetric fold).[14-18] These observations are consistent with changes occurring in response to oxidative decarboxylation of propionate groups to yield vinyl substituents at the same positions.

As the buildup of harderoheme was not clear in the parent rR spectra recorded with intermediate H_2O_2 stoichiometries, rR difference spectra were examined. At each point in the rR titration with H_2O_2, a single, broad band at 416 cm^{-1} was observed, consistent with appearance of one or more modes having vinyl bending character. Given that the vinyl bending bands in the spectra of the coproheme III, harderoheme and heme *b* complexes of *Sa*HemQ (Figure 1B) are broad and within 8 cm^{-1} of one another, they likely fall within the observed 416- cm^{-1} difference envelope. However, when difference spectra generated by subtraction of the *Sa*HemQ-coproheme III spectrum from those of the reconstituted harderoheme complexes (Figure S2) are compared to those observed during the reaction, the multiple features of both harderoheme spectra in this frequency range (Figure 1B) are absent. This suggests that the *Sa*HemQ-harderoheme complex generated via the enzymatic reaction differs from the reconstituted complex in its vinyl conformation.

HPLC analysis (Figure 3) illustrated the progress of the reaction with increasing eq of H_2O_2 and allowed for isolation of the intermediate. Determination of its exact mass by ESI-MS (708.16 amu) and comparison with retention times established for authentic harderoheme standards (Figure S1B) confirmed the intermediate's identity as harderoheme isomer III (Figure 3). Integration of HPLC peaks and comparison to standard curves (Figure S3) indicated loss of roughly 70% of the initially present substrate following addition of 2 eq of H_2O_2. This converted to a mixture of harderoheme III and heme *b*. These observations are consistent complete loss of coproheme III and harderoheme III features in the UV/vis spectrum and maximum vinyl band intensities in the rR spectrum upon reaction with 8 to 10 eq of H_2O_2.

Quantification of the heme *b* products of the 2, 8, and 10 eq reactions (~30 ± 2, 80 ± 1, and 75 ± 15% yields, Figure S3) indicated that a full equivalent of heme was not produced. Titrimetric addition of H_2O_2 in excess of 8 eq resulted in gradual diminution of the Soret band and complete loss of the heme by 110 eq H_2O_2 as measured spectroscopically and by HPLC, Figures 3 and S4. Titration of an independently generated *Sa*HemQ-heme *b* complex with H_2O_2 resulted in heme destruction following addition of 100 eq, consistent with prior work (data not shown).[9]

Time Resolved Reactions Between *Sa*HemQ-coproheme III and H_2O_2

Following addition of sufficient H_2O_2 to effect reaction (12 eq), UV/vis spectra measured over time showed the gradual conversion of the substrate to product complex (Figure 4A). The change in absorbance at 394 nm (Soret band maximum) versus time, likely representing a composite of several events, could be fit to a single exponential (k = 0.30 ± 0.01 min^{-1}).

The reaction was subsequently monitored over time via a discontinuous method in which substrate, intermediate, and product could be independently monitored as function of reaction time (chemical quench followed by HPLC, Figure 4B). These data clearly showed that loss of coproheme III and appearance of harderoheme III occurred at about the same rate (single exponential decay, $k = 2.0 \pm 0.3$ min^{-1}). These rate constants were observed to be ~4× greater than those for loss of harderoheme III and appearance of heme *b* (0.58 ± 0.05 min^{-1} and (0.5 ± 0.1 min^{-1}, respectively). Thus, consistent with the titration data in Figure 3, harderoheme III appears as the intermediate oxidative decarboxylation product. Additionally, the rates of its appearance and decay are consistent with the rate of substrate, coproheme III, decay and product, heme *b*, appearance, respectively.

Formation of vinyl groups was monitored over time via rR spectroscopy (Figure 4C). Assuming that the vinyl group bending modes of harderoheme III and heme *b* have similar resonance enhancements and frequencies, time dependence of the 416 cm^{-1} difference band intensity represents a composite rate of vinyl group appearance (harderoheme III formation and conversion to heme *b*). The data can nonetheless be modeled by a single-term exponential function to yield $k_{\text{app}} = 1.04 \pm 0.10$ min^{-1}. Although scatter in the rR and HPLC data do not support a detailed rate analysis, this apparent rate constant falls between those governing the appearances of harderoheme III and heme *b*. (i.e. $1/k_{\text{harIII}} < 1/k_{\text{app}} < 1/k_b$) and is therefore in keeping with all the kinetic results reported here.

Reactions between SaHemQ complexes with harderohemes and H_2O_2

*Sa*HemQ complexes with harderohemes III and IV were subsequently titrated with H_2O_2. Monitoring by both UV/vis and HPLC indicated conversion of each to heme *b* following addition of 8 and 2 eq of H_2O_2, respectively (Figure S5). The rates of each reaction were monitored via changes at the Soret band maximum (Figure S6) over time following addition of 12 eq H_2O_2. The harderoheme III complex reacted with a time course comparable to coproheme III ($k = 0.28 \pm 0.07$ min^{-1}). The harderoheme IV isomer reacted within the mixing time.

Reaction Between *Sa*HemQ-coproheme III and Peracetic Acid

Titration of the *Sa*HemQ-coproheme III complex with peracetic acid (PAA) gave very similar spectroscopic results to those obtained with H_2O_2 (Figure S7). The completeness of each reaction and identity of the products were clear from the HPLC and rR spectra (Figure 5). Comparison of the integrated HPLC peaks to standard curves indicated that 2 eq of PAA resulted in decomposition of 70% ± 2% of the initially available coproheme III. Eight eq fully degraded the substrate, which was converted to heme *b* in 85% ± 8 % yield. Similar behavior was observed in the rR titration; spectral features were consistent with the products of the reaction being the same as in the H_2O_2 reaction as growth of the vinyl bending band was observed at the same frequency and all other difference features were identical to those obtained with H_2O_2.

The reaction of *Sa*HemQ-coproheme III following addition 12 eq of PAA was subsequently monitored by time resolved UV/vis (Figure S8). The spectral changes were similar to those shown in Figure 4 but occurred with a 6-fold larger rate constant ($k = 2.4 \pm 0.04$ min^{-1}).

Reaction Between *Sa*HemQ-coproheme III and mCPBA or t-Butyl-OOH

Both oxidants were tested as potential HemQ cosubstrates. However, neither resulted in conversion of the *Sa*HemQ-bound coproheme III to an identifiable harderoheme isomer or heme *b*. Instead, following addition of 10 eq of either oxidant, the UV/vis spectrum of the bound coproheme III appeared to recede slightly toward the baseline, with higher numbers of equivalents producing a similar effect that was more pronounced in magnitude. HPLC analysis confirmed that heme *b* was not produced (Figure S9).

Discussion

Nature has devised at least three routes for the biosynthesis of heme *b* [3, 4, 5] one of which appears to be common to a large group of bacteria.[5] The terminal step of this process, catalyzed in a cofactor-independent manner by the enzyme HemQ, was studied here using time resolved methods, synthetically prepared intermediates, and alternate oxidants with the goal of identifying possible tetrapyrrole and iron intermediates.

Only two eq of H_2O_2 are in principle necessary for the oxidation of two propionates to vinyl groups; however, 10 eq were required here to completely convert *Sa*HemQ-coproheme III to the –heme *b* complex, with 2 CO_2 and water as the presumptive co-products (Figure 2). This requirement for a stoichiometric excess suggested that some of the H_2O_2 reacts non-productively. Consistent with that conclusion, a full eq of the product heme *b* was not observed with a stoichiometric addition of H_2O_2 (Figure 3), suggesting concurrent conversion of coproheme III, H_2O_2-mediated degradation of heme *b*, and possible catalytic disproportionation of H_2O_2.[9,20] Heme *b* degradation was driven to completion with the addition of ~ 100 eq of H_2O_2 (Figure S4).

The observed inefficiency of the reaction as well as the degradation of the product with exogenously added H_2O_2 could point toward the upstream catalyst, HemY (Scheme 1), as the endogenous source of H_2O_2. This idea is consistent with the previously documented interplay of HemY, HemH, and HemQ, where the kinetics of HemH/Y are altered by the presence of HemQ[20] It could also explain how a catalase positive organism like *S. aureus*, which avidly detoxifies H_2O_2, might be able to manage and use H_2O_2 as an essential enzymatic substrate.

With <10 eq H_2O_2, most of the initially present coproheme III was converted to a species with several of the anticipated spectral properties of harderoheme (Scheme 2). These include rR bands associated with both vinyl and propionate bends in the "northern" heme pyrroles, rings A and B (Figure 1). MS corroborated the identity of the product as a harderoheme, and comparison to synthetic standards showed it was exclusively isomer III (Figure 3, S5). This suggests that, as in heme-biosynthesis-associated coproporphrinogen and uroporphyrinogen oxidases,[21, 22] the reaction occurs in an obligate clockwise direction, viewing from the distal heme pocket, with the ring A propionate converting to a vinyl first, and the ring B propionate second.

This reaction order is consistent with our proposed model for coproheme III binding,[23] based on published crystal structures of HemQ in the absence of bound substrate and related chlorite dismutases bound to heme *b*.[24, 25] An overlay of two representative structures illustrates the conservation of hydrogen bonding contacts to the non-reactive ring D propionate. By contrast, a key tyrosine residue that forms hydrogen bonds to the ring C propionate in Clds (Y118, Figure 6) is conserved in the primary sequences of HemQs; however, in the substrate-free HemQ structure, this tyrosine (Y124) is part of a ~40 amino acid stretch of the HemQ monomer (residues 100-140) that is clearly out of alignment with the Cld structure. This stretch instead forms the upper part of a large opening in the subunit, which may be important for gating substrate entry/product egress. In addition to the conserved tyrosine, the putative gate contains a triad of positively charged residues (arginine or lysine, R128-130 in Figure 6) that are conserved in HemQs but not Clds. These could form hydrogen bonds to the ring B propionate when the gate closes. A binding geometry which places coproheme III "face up" relative to the Clds' "face down" heme *b* would allow such hydrogen bonding contacts to form, while avoiding potential steric clashes between a HemQ-conserved tyrosine residue (Y144).

The overall conversion of the coproheme III to heme *b*, monitored by changes in the UV/vis spectrum, is relatively slow ($t_{1/2}$ = 4.3 min, pH 7.4, 20 °C; Figure 4). Time-resolved HPLC suggested that the initial decarboxylation reaction at ring A is fast, while the ring B decarboxylation limits the overall reaction rate. This conclusion is consistent with the observed accumulation of harderoheme III in the reaction between *Sa*HemQ-coproheme III and <10 eq of H_2O_2 (Figure 3). If the second decarboxylation were appreciably faster than the first, then only unreacted coproheme III and heme *b* would have been expected. A slower second decarboxylation from ring B is also consistent with the structure-based hypothesis that loss of this propionate, and its hydrogen bonding contacts with the active site gate, helps to trigger opening of the active site and release of heme *b*.

In spite of the fact that harderoheme III is the apparent reaction intermediate, *Sa*HemQ complexes with both harderoheme isomers III and IV were converted to heme *b* upon reaction with H_2O_2 (Figures S5, S6). The reaction with isomer III was slow, with a rate constant similar to the *Sa*HemQ-coproheme III reaction under similar conditions. By contrast, the reaction with isomer IV was complete within the experimental mixing time. This observed pattern, in which removal of the CO_2 from ring B (harderoheme III) is slow and from ring A (harderoheme IV) is fast, mirrors what is observed when coproheme III is the substrate.

Why the reaction at ring A is so much faster is not clear. One possibility is that the ring B propionate is both stabilized and solvent-protected by salt bridges to conserved arginine residues (R128-130) when the active site closes around the substrate. Greater solvent access to ring A could accelerate the initial steps of the reaction of harderoheme IV with H_2O_2. These steps are expected to require the movement of protons and, in principle, could lead to the production of H_2O. An active site base over the open (distal) coordination position, usually a histidine adjacent to an arginine, helps facilitate the Fe(III)/H_2O_2 reaction in typical heme peroxidases.[26] The neutral imidazole side chain acts as a base toward H_2O_2, catalyzing formation of the initial ferric-OOH (Compound 0) intermediate. In peroxidase mutants lacking an active site base, formation of Compound 0 can be slowed up to 5-orders of magnitude.[27, 28] The HemQ active site is remarkably hydrophobic and lacks either a conserved basic residue or an identifiable route for proton entry/departure. Hence, the formation of Compound 0, the most plausible initial reaction product for H_2O_2 and either the coproheme III or harderoheme complexes of HemQ, might be expected to be slow or even rate limiting, but potentially faster if water gains access to the active site.

Once formed, a Compound 0 intermediate can have at least three fates. First, with the input of a proton, the FeO-OH bond can break heterolytically to form water and a high valent iron-oxo intermediate (Scheme 3, pathway a). This intermediate (Compound I) is formally described as $Fe^{IV}=O$ with an oxidizing equivalent on either the porphyrin or the side chain of an amino acid, such as tyrosine or tryptophan, capable of supporting a radical. In heme peroxidases, the protonated active site base acts as the acid in the Compound I-forming reaction. The conserved arginine polarizes the FeOOH moiety, electrostatically promoting movement of both of the electrons from the O-O bond toward the water leaving group.[26] On the other (proximal) side of the porphyrin plane, the heme's histidine ligand is hydrogen bonded to an aspartic or glutamic acid. The anionic character of the ligand supports an additional electrostatic push toward heterolytic cleavage of the Fe(III)O-OH bond.[29] The HemQ active site lacks both the distal His-Arg and proximal His-Glu/Asp motifs of a typical peroxidase. Instead, it has a conserved distal glutamine surrounded by nonpolar residues, and an apparently neutral proximal histidine due to the lack of a hydrogen-bonding Asp or Glu. In short, the HemQ active site appears to lack the ordinary equipment for catalyzing FeO-OH heterolysis.

However, peracetic acid, an oxygen atom donor, was nonetheless able to rapidly convert *Sa*HemQ-coproheme III to –heme *b* with harderoheme III as an intermediate.

Because Compound I is expected to form when these ferric species react with a peracid, these results suggest that a species isoelectronic with Compound I may be able to form, effecting the transformation of coproheme III to harderoheme III and then heme *b*. Whether a similar iron intermediate proceeds from *Sa*HemQ's reactions with H_2O_2, however, is not clear. Notably the larger oxygen atom donor *m*CPBA and an organic peroxide (*t*-butyl-OOH) were both ineffective at converting coproheme III to heme *b* (Figure S9).

Alternatively, the FeO-OH bond of Compound 0 could break homolytically, generating Fe^{IV}=O, water, and a propionyl β-carbon radical in a stepwise (Scheme 3, pathway b) or concerted manner (pathway c). Transient generation of a propionyl β-carbon radical is an early step in some proposed mechanisms for coproporphyrinogen oxidase,[30] in which the ring A and B propionates are converted to vinyls in an O_2-dependent fashion. These pathways both have the advantage of producing less-charged intermediates which are more consistent with the hydrophobic active site. A stepwise homolytic pathway is currently favored in heme oxygenases,[31] another enzymatic class where a heme acts as both substrate and cofactor.

Interestingly, HemQs are evolutionarily and structurally related to IsdGs, which catalyze the heme oxygenase reaction specifically in several groups of gram-positive bacteria.[32, 33] The two proteins both possess hydrophobic heme binding domains characterized by a mutually conserved distal glutamine (HemQ) or asparagine (IsdG) and proximal histidine and tyrosine residues.[34] Why nature evolved pathways for heme biosynthesis and degradation that are particular to gram-positives is not clear.

Figures

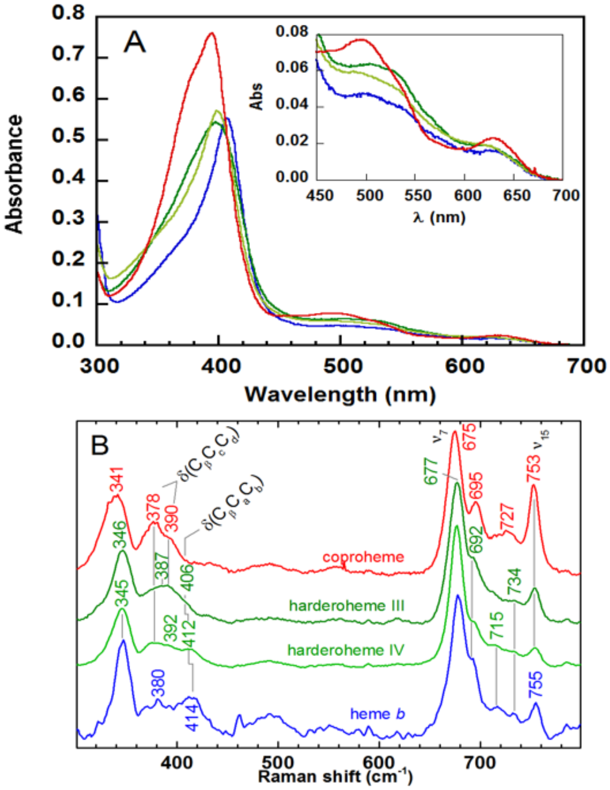

Figure 3.1. Characteristic spectra of *Sa*HemQ in complex with hemes. (A) UV/vis spectra of *Sa*HemQ in complex with ferric coproheme III (red), harderohemes III and IV (dark and light green, respectively), and heme *b* (blue) (5 µM coproheme, 10 µM harderoheme isomers and heme, 50 mM KPi, pH 7.4). The inset shows the visible bands on an expanded scale. (B) Low frequency rR spectra of *Sa*HemQ in complex with the various hemes are shown in the same colors as in A. Spectra were obtained with 406.7 nm excitation of 20 µM samples in 50 mM NaPi, pH 6.8; the propionate and vinyl bending modes are labeled.

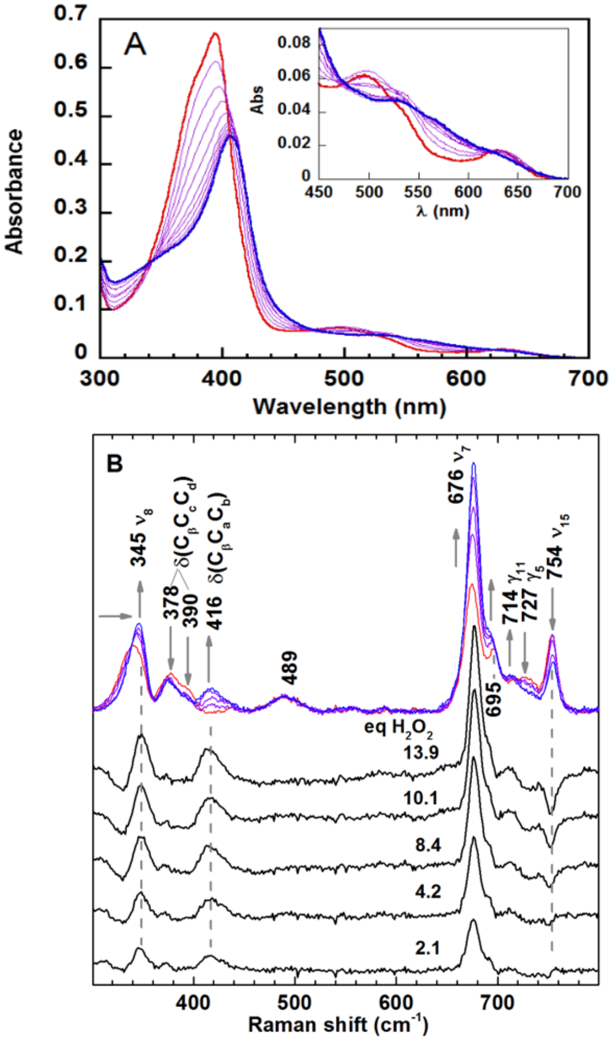

Figure 3.2. Spectroscopic changes upon titration of the *Sa*HemQ-coproheme III complex with H_2O_2. Reactions were monitored by (A) UV/vis spectra following the addition of 0-10 eq H_2O_2 (2 eq increments) to 5 µM *Sa*HemQ-coproheme III, 50 mM KPi, pH 7.4 and (B) rR spectral titration of 15 mM *Sa*HemQ-coproheme III under the same buffer conditions as A with 406.7 nm excitation. H_2O_2 eq are marked on the figure and shown underneath the superimposed spectra for clarity. For both A and B, spectra for the *Sa*HemQ-coproheme III complexes are in red. Partially decarboxylated species are in purple with the final spectrum [λ_{max} (Soret) =406 nm)] in blue. The difference spectra in B were generated by subtracting the spectrum of *Sa*HemQ-coproheme III from the product spectrum obtained from the reaction with the indicated molar eq of H_2O_2.

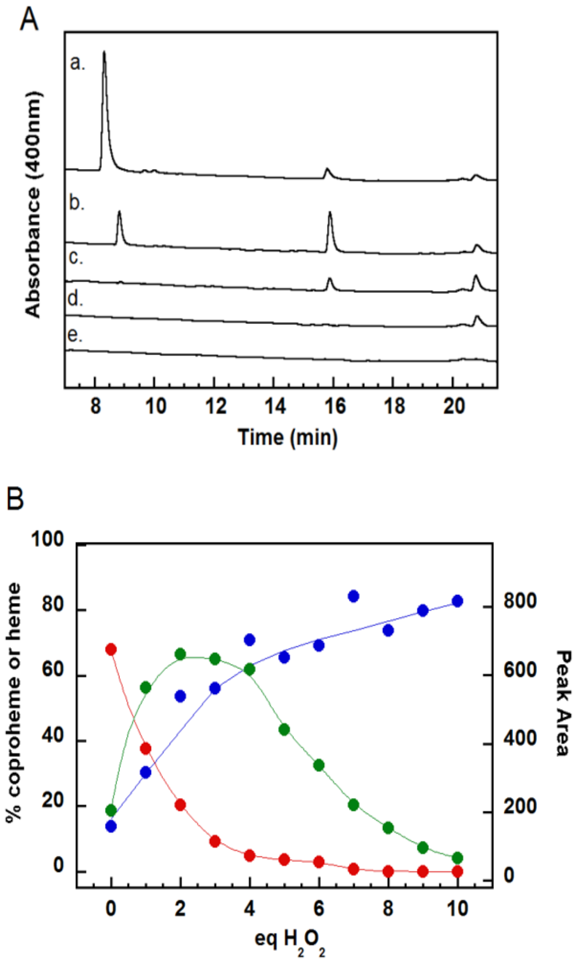

Figure 3.3. HPLC analysis of the products of the reaction of the *Sa*HemQ-coproheme III complex with H_2O_2. (A) Representative HPLC traces showing protein-free products of the reaction with 0, 2, 8, 10, and 100 eq H_2O_2 (a–e) are plotted. Comparison of the retention times to standards (Figure S1B) identified harderoheme isomer III as the reactive intermediate. Note that the absorbance wavelength (400 nm) used for detection is closer to the λ_{max} for free coproheme III, which also has a higher extinction coefficient. (B) Relative (harderoheme, green) or quantitative (coproheme, red; heme *b*, blue) amounts of each heme species discerned from integrated peak intensities are plotted versus the number of H_2O_2 eq. Points are averages of 3 values (standard deviations all within ± 15%). Solid lines are spline curves intended to qualitatively illustrate trends in the data.

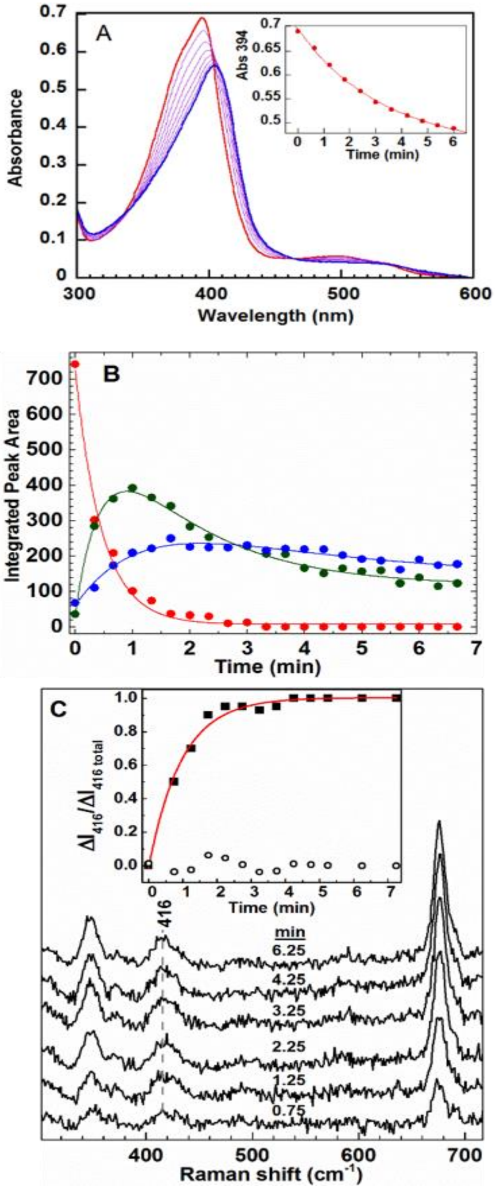

Figure 3.4. Time resolved reactions between the *Sa*HemQ-coproheme III and 12 eq H_2O_2. (A) Reaction monitored by UV/vis (8 μM enzyme, 50 mM KPi, pH 7.4). *Sa*HemQ-coproheme III complex (red), spectra measured every 0.25 min (purple), and final spectrum (Soret band λ_{max} = 406 nm, blue) are shown. The absorbance at 394 nm versus time and fitted to a single exponential is shown as an inset. (B) Reaction monitored by HPLC: red, coproheme III; green, harderoheme III; blue, heme *b*. Kinetic phases were fitted to single exponentials to obtain rate constants. (C) Reaction (15 μM enzyme) monitored continuously by rR. Difference spectra recorded at the indicated times are plotted. Δ rR intensity at 416 cm^{-1} [time t]/total Δ 416 cm^{-1} intensity represents vinyl formation and is plotted versus time in the inset. Red line: single exponential fit; open circles: residuals.

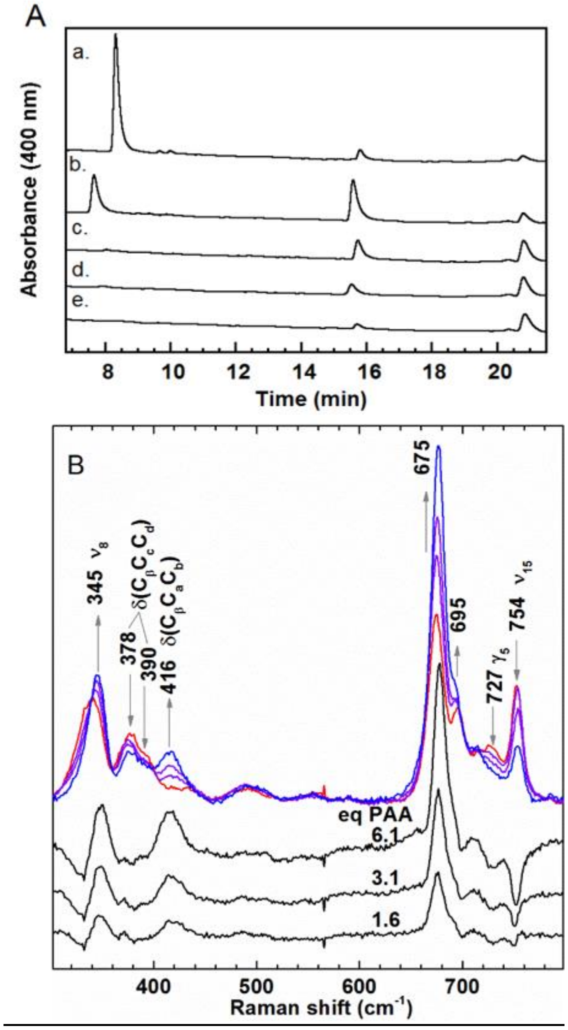

Figure 3.5. Titration of *Sa*HemQ-coproheme III complex with peracetic acid. (A) HPLC analyses of the products of the reaction of the *Sa*HemQ-coproheme III complex with 2, 8, or 10 eq of peracetic acid are shown. Full conversion of coproheme III to products followed addition of 10 eq of PAA. Comparison of the retention times to pure standards (Figure S1B) identified harderoheme isomer III as the reactive intermediate and heme *b* as the final product. Note that the absorbance wavelength (400 nm) used for detection is closer to the λ_{max} for free coproheme III, which also has a higher extinction coefficient. (B) Peracetic acid titration monitored by changes in the Soret-excited rR spectrum. The spectrum for *Sa*HemQ-coproheme III is red; partially decarboxylated complexes are shown in purple and the final spectrum is blue. Difference spectra were generated by subtracting the spectrum of *Sa*HemQ-coproheme III from the spectrum obtained from the reaction mixture at equilibrium with the given molar equivalents of PAA.

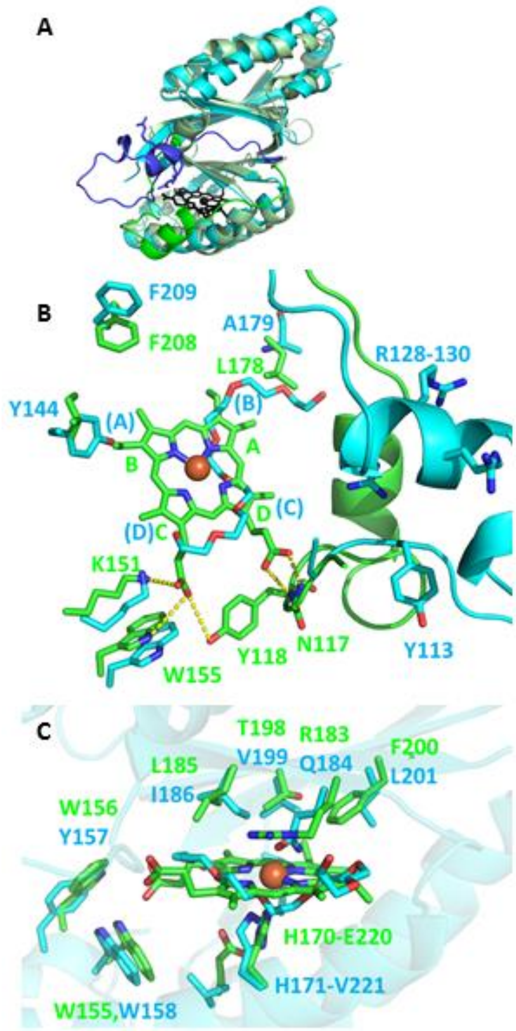
A
B
F209
F208
A179
L178
R128-130
Y144
(A)
(B)
B
A
(C)
D
(D)C
K151
W155
Y118
N117
Y113
C
T198
R183
V199
Q184
F200
L201
L185
I186
W156
Y157
H170-E220
H171-V221
W155,W158

Figure 3.6. Overlay of the structures of a representative heme *b*-bound chlorite dismutase (carbon green, PDB ID 3Q08)[24] and solvent-bound HemQ (carbon cyan, PDB ID 1T0T).[25] (A) The monomeric subunit structures are very similar with the exception of a loop-helix region, highlighted in darker shades of blue/green. This region is located on the exterior of the HemQ homopentamer. (B) Key residues surrounding the heme *b*/coproheme III binding sites are indicated in this view overlooking the distal pocket. The placement of tetrapyrrole rings A-D in the expected orientation of the coproheme III is shown. K151, W155, N117, and Y113 (Cld numbering) are conserved in both HemQs and Clds and form contacts to the ring C/D propionates. Y113 (HemQ) is at the same sequence position as Y118 (Cld). It is part of the loop-helix region in HemQ. (C) Conserved active site Cld/HemQ residues (side view).

Scheme 3.1. Biosynthetic pathways leading to heme and other tetrapyrroles[†]

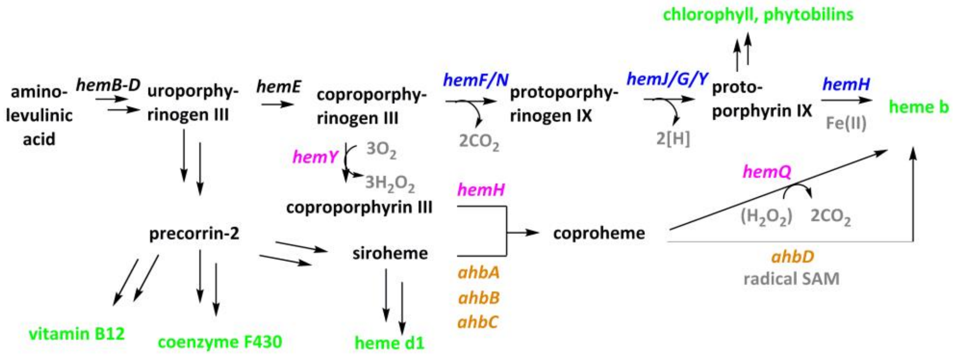
chlorophyll, phytobilins
amino-levulinic acid
hemB-D
uroporphy-rinogen III
hemE
coproporphy-rinogen III
hemF/N
$2CO_2$
protoporphy-rinogen IX
hemJ/G/Y
2[H]
proto-porphyrin IX
hemH
Fe(II)
heme b
hemY
$3O_2$
$3H_2O_2$
coproporphyrin III
hemH
coproheme
hemQ
(H_2O_2)
$2CO_2$
ahbD
radical SAM
precorrin-2
siroheme
ahbA
ahbB
ahbC
vitamin B12
coenzyme F430
heme d1

[†]The genes encoding catalysts for the canonical steps common to eukaryotes and many gram-negative bacteria are designated in blue. The pathway used by Archaea and sulfur-reducing bacteria are in orange.[4] The recently proposed terminus of the pathway, found in gram-positive members of Actinobacteria and Firmicutes, is shown in purple.[5] Note that HemF or HemN can catalyze the indicated step in different organisms under aerobic and anaerobic conditions, respectively. Similarly, HemJ, G, or Y catalyze the removal of 2 H-atoms ([H]).

Scheme 3.2. Substrate, possible intermediates, and product of the HemQ-catalyzed reaction

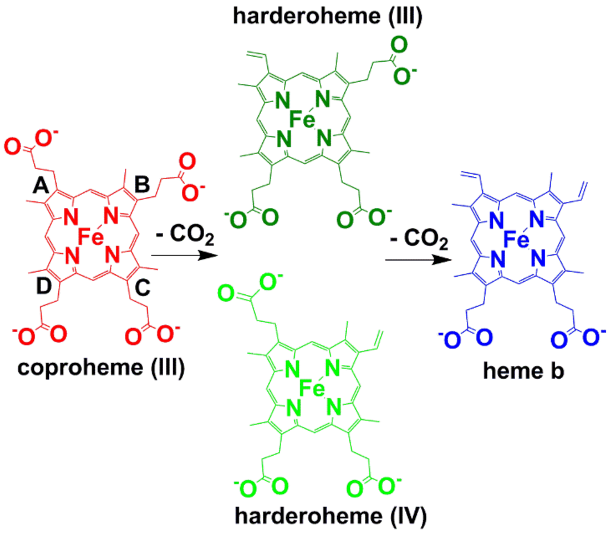
harderoheme (III)
A
B
C
D
Fe
N
$-CO_2$
$-CO_2$
coproheme (III)
heme b
harderoheme (IV)

Scheme 3.3. Possible reaction pathways following from Compound 0

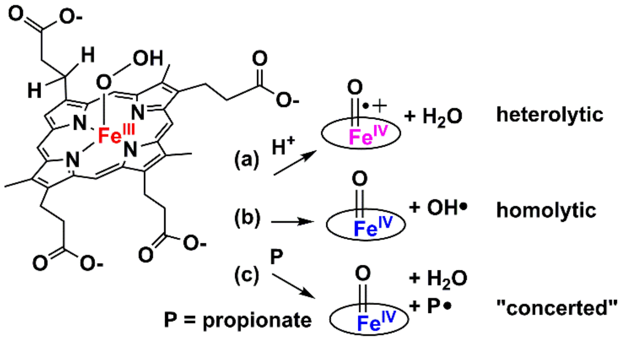
O
O-
H
H
O
OH
N
N
Fe^{III}
N
N
O
O-
O
O-
O
O-
(a)
H$^+$
O
•+
Fe^{IV}
+ H$_2$O
heterolytic
(b)
O
Fe^{IV}
+ OH•
homolytic
(c)
P
O
Fe^{IV}
+ H$_2$O
+ P•
"concerted"
P = propionate

Associated Content

Supporting Information

Includes (1) details of the metalation and deprotection of harderoporphyrins III and IV; (2) details of the purification of *Sa*HemQ; (3) HPLC and pyridine hemochrome analyses of the various hemes; (4) titrations of the *Sa*HemQ-coproheme III complex with H_2O_2 and peracetic acid; (5) titrations and kinetic data describing the reaction of the *Sa*HemQ-harderoheme complexes with H_2O_2; data showing the reaction of *Sa*HemQ-coproheme III with *m*CPBA and *t*-butyl-OOH. This material is available free of charge via the Internet at http://pubs.acs.org.

Abbreviations

Cld, chlorite dismutase; DMSO, dimethylsulfoxide; HPLC, high performance liquid chromatography; *m*CPBA, *meta*-chloroperbenzoic acid; LB, lysogeny broth; KPi, potassium phosphate; rR, resonance Raman; *Sa*, Staphylococcus aureus; SDS-PAGE, sodium dodecylsulfonate polyacrylamide gel electrophoresis; UV/vis, ultraviolet-visible.

References

(1) Dailey, H. A. (1997) Enzymes of heme biosynthesis, *J. Biol. Inorg. Chem. 2*, 411-417.

(2) Layer, G.; Reichelt, J.; Jahn, D.; Heinz, D. W. (2010) Structure and function of enzymes in heme biosynthesis, *Protein Sci. 19*, 1137-1161.

(3) Panek, H.; O'Brian, M. R. (2002) A whole genome view of prokaryotic haem biosynthesis, *Microbiology 148*, 2273-2282.

(4) Bali, S.; Lawrence, A. D.; Lobo, S. A.; Saraiva, L. M.; Golding, B. T.; Palmer, D. J.; Howard, M. J; Ferguson, S. J.; Warren, M. J. (2011) Molecular hijacking of siroheme for the synthesis of heme and d1 heme, *Proc. Nat. Acad. Sci. USA 108*, 18260-18265.

(5) Dailey, H.; Gerdes, S.; Dailey, T.; Burch, J.; Phillips, J. (2015) Noncanonical coproporphyrin-dependent bacterial heme biosynthesis pathway that does not use protoporphyrin, *Proc. Nat. Acad. Sci. USA 112*, 2210-2215.

(6) Dailey, H. A. (2002) Terminal steps of haem biosynthesis, *Biochem. Soc. Trans. 30*, 590-595.

(7) Lash, T. D.; Mani, U. N.; Drinan, M. A.; Zhen, C.; Hall, T.; Jones, M. A. (1999) Normal and abnormal heme biosynthesis. 1. Synthesis and metabolism of di- and monocarboxylic porphyrinogens related to coproporphyrinogen-III and harderoporphyrinogen: A model for the active site of coproporphyrinogen oxidase, *J. Org. Chem. 64*, 464.

(8) Lash, T. D.; Mani, U. N.; Keck, A.; Jones, M. A. (2010) Normal and abnormal heme biosynthesis. 6. Synthesis and metabolism of a series of monovinylporphyrinogens related to harderoporphyrinogen. Further insights into the oxidative decarboxylation of porphyrinogen substrates by coproporphyrinogen oxidase, *J. Org. Chem. 75*, 3183-3192.

(9) Mayfield, J. A.; Hammer, N. D.; Kurker, R. C.; Chen, T. K.; Ojha, S.; Skaar, E. P.; DuBois, J. L. (2013) The chlorite dismutase (HemQ) from Staphylococcus aureus has a redox-sensitive heme and is associated with the small colony variant phenotype, *J. Biol. Chem. 288*, 23488-23504.

(10) Kuhner, M.; Haufschildt, K.; Neumann, A.; Storbeck, S.; Streif, J.; Layer, G. (2014) The alternative route to heme in the methanogenic archaeon *Methanosarchia barkeri*, *Archaea. ecollection 2014*

(11) Berry, E.A.; Trumpower, B.L. (1987) Simultaneous determination of hemes a, b, and c from pyridine hemochrome spectra, *Anal. Biochem. 161*, 1-15.

(12) Rand, K.; Noll, C.; Schiebel, H. M.; Kemken, D.; Duelcks, T.; Kalesse, M.; Heinz, D. W.; Layer, G. (2010) The oxygen-independent coproporphyrinogen III oxidase HemN utilizes harderoporphyrinogen as a reaction intermediate during conversion of coproporphyrinogen III to protoporphyrinogen IX, *Biol. Chem. 391*, 55-63.

(13) Hu, S.; Smith, K.; Spiro, T. (1996) Assignment of protoheme resonance raman spectrum by heme labeling in myoglobin, *J. Am. Chem. Soc. 118*, 12638-12646.

(14) Uchida, K.; Susai, Y.; Hirotani, E.; Kimura, T.; Yoneya, T.; Tekeuchi, H.; Harada, I. (1988) 4-vinyl and 2,4-divinyl deuteration effects on the low frequency

resonance Raman bands of myoglobin: correlation with the structure of vinyl group, *J. Biol. Chem. 103*, 979-985.

(15) Rwere, F.; Mak, P.; Kincaid, J. (2014) Resonance Raman determination of vinyl group disposition in different derivatives of native myoglobin and its heme-disoriented form, *J. Raman Spec. 45*, 97-104.

(16) Rwere, F.; Mak, P.; Kincaid, J. (2008) Resonance raman interrogation of the consequences of heme rotational disorder in myoglobin and its ligated derivatives, *Biochemistry 47*, 12869-12877.

(17) Rwere, F.; Mak, P.; Kincaid, J. (2008) The impact of altered protein-heme interactions on the resonance Raman spectra of heme proteins. Studies of heme rotational disorder, *Biopolymers 89*, 179-186.

(18) Podstawka, E.; Mak, P.; Kincaid, J., Proniewicz, L. (2006) Low frequency resonance Raman spectra of isolated alpha and beta subunits of hemoglobin and their deuterated analoges, *Biopolymers 83*, 455-466.

(19) Mak, P.; Podstawka, E.; Kincaid, J.; Proniewicz, L. (2004) Effecrs of systematic peripheral group deuteration on the low-frequency resonance Raman spectra of myoglobin derivatives, *Biopolymers 75*, 217-228.

(20) Dailey, T. A.; Boynton, T. O.; Albetel, A.-N.; Gerdes, S.; Johnson, M. K.; Dailey, H. A. (2010) Discovery and characterization of HemQ an essential heme biosynthetic pathway component, *J. Biol. Chem. 285*, 25978-86.

(21) Luo, J.; Lim, C. K. (1993) Order of uroporphyrinogen III decarboxylation on incubation of prophobilinogen and uroporphyrinogen III with erythrocyte uropophyrinogen decarboxylase, *Biochem. J. 289*, 529-532.

(22) Stephenson, J. R.; Stacey, J. A.; Morgenthaler, J. B.; Friesen, J. A.; Lash, T. D.; Jones, M. A. (2007) Role of aspartate 400, arginine 262, and arginine 401 in the catalytic mechanism of human corpoporphyrinoen oxidase, *Protein Sci. 16*, 401-410.

(23) Celis, A. I.; DuBois, J. L. (2015) Substrate, product, and cofactor: The extraordinary flexible relationship between the CDE superfamily and heme, *Arch. Biochem. Biophys. 574*, 3-17.

(24) Goblirsch, B. R.; Streit, B. R.; DuBois, J. L.; Wilmot, C. M. (2010) Strunctural features promoting dioxygen production by Dechloromonas aromatica chlorite dismutase, *J. Biol. Inorg. Chem. 15*, 879-889.

(25) Gilski, M.; Borek, D.; Chen, Y.; Collart, F.; Joachimiak, A.; Otwinowski, Z. (2004) Crystal structure of apc35880 protein from bacillus stearothermophillus**,** *to be published*.

(26) Poulos, T. L.; Fenna, R. E. (1994) Metalloenzymes involving amino acid residue related radicals, *Metal Ions Biol. Syst, 30*, 25-75.

(27) Hiner, A. N.; Raven, E. L.; Thorneley, R. N.; García-Cánovas, F.; Rodríguez-López, J. N. (2002) Mechanisms of compound I formation in heme peroxidases, *J. Inorg. Biochem. 91*, 27-34.

(28) Erman, J. E.; Vitello, L. B.; Miller, M. A.; Shaw, A.; Brown, K. A.; Kraut, J. (1993) Histidine 52 is a critical residue for rapid formation of cytochrome c peroxidase compound I, *Biochemistry 32*, 9798-9806.

(29) Choudhury, K.; Sundaramoorthy, M.; Hickman, A.; Yonetani, T.; Woehl, E.; Dunn, M. F.; Poulos, T. L. (1994) Role of the proximal ligand in peroxidase catalysis. Crystallographic, kinetic, and spectral studies of cytochrome c peroxidase proximal ligand mutants, *J. Biol. Chem. 269*, 20239-20249.

(30) Lash, T. D. (2005) The enigma of coproporphyrinogen oxidase: how does this unusual enzyme carry out oxidative decarboxyations to afford vinyl groups? *Bioorg. Med. Chem. Lett. 15*, 4506-4509.

(31) Matsui, T.; Iwasaki, M.; Sugiyama, R.; Unno, M.; Ikeda-Saito, M. (2010) Dioxygen activation for the self-degradation of heme: reaction mechanism and regulation of heme oxygenase, *Inorg. Chem. 49*, 3602-3609.

(32) Wilks, A., Heinzl, G. (2014) Heme oxygenation and the widening paradigm of heme degradation, *Arch. Biochem. Biophys. 544*, 87-95.

(33) Skaar, E. P.; Gaspar, A. H.; Schneewind, O. (2004) IsdG and IsdI, heme-degrading enzymes in the cytoplasm of Staphyloccocus aureus, *J. Biol. Chem. 279*, 436-443.

(34) Lee, W. C.; Reniere, M. L.; Skaar, E. P.; Murphy, M. E. P. (2008) Ruffling of metalloporphyrins bound to IsdG and IsdI, two heme-degrading enzymes in *Staphylococcus aureus*, *J. Biol. Chem. 283*, 30957-30963.

(35) Lobo, S.A.L.; Scott, A.; Videira, M. A. M.; Winpenny, D.; Gardner, M.; Palmer, M.J.; Schroeder, S.; Lawrence, A. D.; Parkinson, T.; Warren, M.J.; Saraiva, L.M. (2015) *Staphyloccocus aureus* haem biosynthesis: characterisation of the enzymes involved in final steps of the pathway, *Mol. Microbiol., Epub ahead of print*

CHAPTER FOUR

REACTIONS OF FERROUS COPROHEME DECARBOXYLASE (HEMQ) WITH O_2 AND H_2O_2 YIELD FERRIC HEME *B*

Contribution of Authors and Co-Authors

Author: Bennett R. Streit

Contributions: Performed UV-Vis, stopped-flow, HPLC, and spectrochemical experiments. Analyzed and interpreted data. Contributed to the writing and preparation of this manuscript.

Co-Author: Arianna I. Celis

Contributions: Expressed, purified, and prepared apo-, harderoheme III/IV- and coproheme III-bound HemQ enzyme. Contributed to the writing and preparation of this manuscript.

Co-Author: Krista Shisler

Contributions: Performed EPR experiments. Analyzed and helped interpret EPR data.

Co-Author: Kenton R. Rodgers

Contributions: Measured and analyzed rR data. Provided support and very valuable insight in preparation of manuscript. Contributed to the writing and preparation of this manuscript.

Co-Author: Gudrun S. Lukat-Rodgers

Contributions: Measured and analyzed rR data. Provided support and very valuable insight in preparation of manuscript. Contributed to the writing and preparation of this manuscript.

Co-Author: Jennifer L. DuBois

Contributions: Provided important insight and overview of the preparation of samples, experiment design and interpretation of results. Contributed largest part to the writing and preparation of this manuscript.

Manuscript Information Page

Bennett R. Streit, Arianna I. Celis, Krista Shisler, Kenton R. Rodgers, Gudrun S. Lukat-Rodgers, Jennifer L. DuBois

Biochemistry

Status of Manuscript:
____ Prepared for submission to a peer-reviewed journal
____ Officially submitted to a peer-review journal
____ Accepted by a peer-reviewed journal
__X_ Published in a peer-reviewed journal

Publisher: American Chemical Society

Reprinted with permission from Streit, B., Celis, A., Shisler, K., Rodgers, K., Lukat-Rodgers, G., and DuBois, J. (2017) Reactions of ferrous coproheme decarboxylase (HemQ) with O-2 and H_2O_2 yield ferric heme *b*. *Biochemistry* **56**, 189-201. Copyright 2017 American Chemical Society.

CHAPTER FOUR

REACTIONS OF FERROUS COPROHEME DECARBOXYLASE (HEMQ) WITH O_2 AND H_2O_2 YIELD FERRIC HEME *B*

Bennett R. Streit,[1] Arianna I. Celis,[1] Krista Shisler,[1] Kenton R. Rodgers,[2] Gudrun S. Lukat-Rodgers,[2] Jennifer L. DuBois,[1]*

[1]Department of Chemistry and Biochemistry, Montana State University, Bozeman, Montana 59715, USA
[2]Department of Chemistry and Biochemistry, North Dakota State University, Fargo, North Dakota 58102, USA

Abstract

A recently discovered pathway for the biosynthesis of heme *b* ends in an unusual reaction catalyzed by coproheme decarboxylase (HemQ), where the Fe(II)-containing coproheme acts as both substrate and cofactor. Because both O_2 and H_2O_2 are available as cellular oxidants, pathways for the reaction involving either can be proposed. Analysis of reaction kinetics and products showed that, under aerobic conditions, the ferrous coproheme-decarboxylase complex is rapidly and selectively oxidized by O_2 to the ferric state. The subsequent second-order reaction between the ferric complex and H_2O_2 is slow, pH dependent, and further decelerated by D_2O_2 (average KIE = 2.2). The observation of rapid reactivity with peracetic acid suggested the possible involvement of Compound I (ferryl porphyrin cation radical), consistent with coproheme and harderoheme reduction potentials in the range of heme-proteins that heterolytically cleave H_2O_2. Resonance Raman spectroscopy nonetheless indicated a remarkably weak Fe-His interaction; how

the active site structure may support heterolytic H_2O_2 cleavage is therefore unclear. From a cellular perspective, the use of H_2O_2 as an oxidant in a catalase-positive organism is intriguing, as is the unusual generation of heme *b* in the Fe(III) rather than Fe(II) state as the end product of heme synthesis.

Introduction

Tetrapyrroles - hemes, corrins, and chlorophylls - give rise to many of the colors of life and mediate processes from respiration to photosynthesis. The biosynthetic routes to tetrapyrroles have evolved and diversified alongside the transitions from anaerobic to aerobic Earth and uni- to multi-cellular life. In addition to the well-known, textbook pathway for heme biosynthesis, at least two more ancient routes have been described.[1, 2]

In the final steps of the well-described pathway, which is shared by eukaryotes and gram-negative bacteria, coproporphyrinogen undergoes decarboxylation, macrocycle oxidation, and metalation to give heme *b*.[3, 4] By contrast, in gram-positive bacteria (Actinobacteria, Firmicutes), the same intermediate is initially oxidized and then metalated to give coproheme (isomer III). In the final step, two propionate substituents on the coproheme III (referred to as *coproheme* herein) are oxidatively decarboxylated to vinyls to produce heme *b*. The oxidation and metalation steps are catalyzed by homologs to their canonical counterparts, which act on different substrates in the non-canonical pathway. The final step, however, is catalyzed by a novel decarboxylase encoded by the *hemQ* gene.[1] Functionally, the coproheme decarboxylase (HemQ) is part of a collection of enzymes that includes heme oxygenases where the same molecule acts as both substrate and cofactor.

It was previously observed that the decarboxylation can proceed with the coproheme in the ferric (Fe(III)) oxidation state and with hydrogen peroxide as the cosubstrate.[1, 5, 6] However, whether this reaction is biologically relevant is not clear because, under biological conditions, iron is inserted into porphyrins as Fe(II).[7] Because ferrous hemes can react with O_2, the cellular process could use O_2 and ferrous coproheme as cosubstrates, yielding H_2O_2 as a product (Scheme 1A). An O_2-dependent reaction of this kind is consistent with known biological oxidative decarboxylases, including those used in the canonical pathway to decarboxylate heme intermediates.[8-11] Alternatively, a reaction between O_2 and Fe(II)-coproheme could occur by a monooxygenase pathway via a hydroxylated intermediate (Scheme 1B). This mechanism is analogous to the heme oxygenase reaction, which begins with an O_2-mediated hydroxylation of the porphyrin ring.[12, 13] Finally, the enzyme might catalyze a reaction involving Fe(II) and H_2O_2 (Scheme 1C). While not completely unprecedented,[14, 15] such a reaction would be highly unusual since hemes generally react with H_2O_2 when the iron is in the ferric oxidation state.[16] The conversion of H_2O_2 to OH- and OH▪, which is readily catalyzed by ferrous iron, would have to be excluded.

We sought to determine which if any of these pathways is followed by the coproheme decarboxylase in the presence of both O_2 and H_2O_2. Using the *hemQ*-encoded decarboxylase from *Staphylococcus aureus*, we examined complexes of the protein with its substrate coproheme and intermediate harderoheme III (here referred to as *harderoheme*), and their reactions with both oxidants from the ferrous or ferric state (Scheme 1). The results presented here support the conclusion that the enzyme facilitates

O_2-mediated oxidation of the ferrous coproheme under aerobic conditions and then acts as a peroxide-dependent decarboxylase. Distinct from the canonical pathways, the coproheme decarboxylase yields ferric heme *b*. These findings have implications for how *S. aureus* and potentially other gram-positive bacteria have evolved to survive in and exploit an aerobic environment.

Experimental Methods

Preparation of Stocks and pH Buffers

Ferric coproporphyrin III chloride (coproheme, Frontier Scientific) and hemin chloride (Sigma) were dissolved in dimethyl sulfoxide (DMSO) to generate 5−10 mM stocks. Harderoheme III was synthesized and purified as described previously.[5] Hydrogen peroxide (H_2O_2) and peracetic acid working solutions (0.5– 5 mM) were prepared from 50 mM stocks in 50 mM potassium phosphate (KPi) buffer (pH 7.4). Working solutions were kept on ice and replaced with fresh stocks every 2 h. Oxidant stocks were titrated with acidified $KMnO_4$, which had itself been titrated against ultrapure oxalic acid, to verify their concentrations. Biochemicals (lysozyme, catalase, DNase, etc.) were from New England Biolabs. Reactions were carried out over a range of pH values in either 50 mM KPi (pH 5.8, 6.6, and 7.4) or 50 mM Tris-Cl (pH 8.2 or 8.8). For the solvent isotope studies, the 50 mM Tris-Cl buffers were made in D_2O (Cambridge isotopes, 99.8 % D) with addition of DCl (Acros Organics 99% + D) to give final pD values 6.1, 6.5, 6.8, 7.3, 8.1, 8.7, and 9.2 (pD = pH* + 0.41, where pH* is the apparent pH measuring using a standard glass electrode).[17] Protein samples were prepared through multiple rounds of concentration and resuspension in deuterated buffer, resulting in only 0.1 % or less of the original buffer solution present in the final solution. D_2O_2 solutions were made from a 10.6 M H_2O_2 stock diluted 1:100 in D_2O, producing a 108 mM stock with ≥98 % deuterium enrichment.

Protein Production and Complex Formation

Expression, purification, and ligand complexation with coproheme decarboxylase were carried out as previously reported.[5] Porphyrin concentrations were determined by the pyridine hemochrome methods. Briefly: 50 µL of protein solution (at 50-300 µM) was mixed with 200 µL of 50 mM NaOH containing 20% pyridine by volume. 3 µL of 0.1 M $K_3[Fe(CN)_6]$ was added and the oxidized spectrum was measured; 3−5 mg of solid sodium dithionite ($Na_2S_2O_4$) was then added to yield spectra for the reduced pyridine-bound hemes. Difference spectra (reduced minus oxidized, r-o) were used to determine the concentration of metalloporphyrin released from the protein. For coproheme: □$_{\text{r-o}}$ 546 nm = 23.2 mM^{-1} cm^{-1}; for heme *b*, □$_{\text{r-o}}$ 556 nm = 28.4 mM^{-1} cm^{-1}.

Heme Reduction

Solutions were made anaerobic using a double manifold Schlenk line with alternating cycles of argon gas purging and evacuation. Protein-coproheme complexes were reduced in an anaerobic chamber (Coy) using solutions of sodium dithionite prepared by dissolving the solid in deoxygenated buffer. The dithionite concentration was determined via anaerobic titration with potassium hexacyanoferrate(III) in the presence of methylene blue as indicator.[18] A 1.5 molar excess of dithionite relative to coproheme was added and reduction of the heme species was monitored by UV/visible spectroscopy (UV/vis, Agilent 8453 spectrometer). Excess unreacted dithionite and dithionite oxidation products were removed using a PD-10 desalting column (GE Healthcare).

Titrations with Oxidants

Complexes of coproheme decarboxylase with either coproheme or harderoheme (ferrous and ferric, pH 7.4, 20 °C) were mixed anaerobically with H_2O_2 or peracetic acid (0, 0.5, 1, 1.5 or 2 eq) inside an anaerobic chamber. Products were analyzed by UV/vis, high performance liquid chromatography (HPLC) (samples 10 μM in the heme species), and electron paramagnetic resonance spectroscopy (EPR) (described below). Reactions with O_2 were carried out by exposing ferrous complexes to atmosphere (240 μM O_2, pH 7.4, 20 °C) or mixing with aliquots of O_2-saturated buffer inside septum-sealed vials to achieve the desired final O_2 concentration. In reactions involving either O_2 or peracid, catalase was included at 1000 U/mL to remove any H_2O_2.

HPLC

Reactions were analyzed for coproheme, harderoheme, and heme *b* by HPLC on an Agilent 1100 series instrument with a Phenomenex Luna C18 3μm column (150 mm x 4.6 mm). The solvents were H_2O with 0.1% TFA (trifluoroacetic acid) (Solvent A) and acetonitrile (ACN) with 0.1% TFA (Solvent B). All samples were run at a flow rate of 1.5 mL/min starting with isocratic 80% A for 3 min, followed by a linear gradient transitioning to 5% A over 12 min. This was followed by 5% A for 5 min and a final isocratic run of 20 % A for 3 min. UV/vis detection was at 411 nm. Standard curves (0 –

500 pmol) were generated for quantifying heme species via integration of the peak areas. Samples were quantified in triplicate and error bars are ± 1 standard deviation.

EPR

250 μL aliquots of coproheme decarboxylase in complex with its ferrous/reduced substrate (pH 7.4, 90 μM) were mixed with 0-2 eq of H_2O_2 from a 5 mM stock, loaded into EPR tubes, sealed, and removed from the anaerobic chamber in a sealed glove bag. The samples were immediately frozen and stored in liquid N_2. Spectra were measured on a Bruker EMX EPR spectrometer (X-band, 9.37 MHz) at 12 K using a Bruker Cold Edge (Sumitomo Cryogenics) cryogen-free system with a Mercury iTC controller unit. Instrument parameters were: 3.18 MW microwave power, 100 kHz modulation frequency, and 5 G modulation amplitude. Averages of 4 scans are reported. For spin quantitation, horse heart myoglobin (Sigma) was used as a standard. Spectra were double integrated over 500-4000 gauss (OriginLab) to include the range of Fe(III) species produced during the reaction with H_2O_2.

Transient Kinetics

Data were measured using KinetAssyst stopped-flow spectrometer (Hi-Tech Scientific) in single mixing mode with diode array detection. For the ferric substrates, the decarboxylase-coproheme complex (5 μM) was rapidly mixed (< 5 ms) with variable concentrations of H_2O_2 or peracetic acid prior to measurement of spectra. For ferrous substrates, the spectrometer was made anaerobic by overnight incubation with protocatechuate dioxygenase (PCD) and its substrate, protocatechuic acid (PCA).[19]

Dithionite-reduced anaerobic samples were prepared in an anaerobic chamber as described above and sealed in an airtight tonometer that interfaced with the stopped flow sample handling unit. Deoxygenated buffer, H_2O_2, and peracetic acid solutions were prepared in the glove box, sealed in gastight syringes, and then introduced to the sample handling unit for reaction. Data were measured at varying time points and fit using the Kinetic Studio (Hi-Tech Scientific) software to exponential decay functions to determine rate constants (k_{obs}). For each experimental condition, all data were measured in at least triplicate and averaged. Plots of k_{obs} versus oxidant concentration were fit with linear least squares regression analysis to determine second order rate constants (Kaleidagraph).

Testing for Oxygenase Activity

To test for oxygenase activity in the ferric state, 5 μM ferric coproheme-decarboxylase complex was treated with 5 mM (1000 eq) ascorbate in the presence of 100 U catalase (50 mM KPi, pH 7.4) and spectral changes were monitored every min for 30 min. The same assay conditions led to complete oxidation of the heme *b* substrate in studies of bacterial IsdG-type heme oxygenases.[20] To screen for oxygenase activity from the ferrous state, 10 μM coproheme-bound decarboxylase was reduced with dithionite under anaerobic conditions (excess reductant removed as described above). The complex was mixed 1:1 v/v in the stopped flow with freshly prepared aerobic solutions of reductant (2 mM dithionite or 20 mM ascorbate, 50 mM KPi, pH 7.4) and spectral changes monitored over time via diode array detection. The products in each case were quantified by HPLC.

Spectroelectrochemical Titrations

Fe(III)/Fe(II) reduction potentials (E) were determined via titration of the decarboxylase bound to coproheme, harderoheme, or heme *b* (6 μM) with dithionite in the presence of the redox mediator methyl viologen (2 μM) and a reducible dye (10-15 μM) in an anaerobic glove box (50 mM KPi, pH 7.0, 20 °C). The dyes used were indigo disulphonate (-125 mV, coproheme and harderoheme complexes) and indigo trisulphonate (-85 mV, heme *b*) (all potentials are reported versus the standard hydrogen electrode, SHE, at pH 7).[21] Changes in the UV/vis spectrum were recorded following each dithionite addition. Absorbances for the oxidized and reduced dyes (dye_{ox}, dye_{red}) and the ratio of the oxidized/reduced protein-heme absorbances ($\text{Enz}_{\text{ox}}/\text{Enz}_{\text{red}}$) were recorded at their maxima: 612 nm, oxidized indigo disulphonate; 593 nm, indigo trisulphonate; 424 nm, coproheme; 418 nm, harderoheme; 428 nm heme *b*. Plots of $\ln(\text{P}_{\text{ox}}/\text{P}_{\text{red}})$ versus $\ln(\text{dye}_{\text{ox}}/\text{dye}_{\text{red}})$ were fit to a modified Nernst equation:

$$\ln(\text{Enz}_{\text{ox}}/\text{Enz}_{\text{red}}) = (nF/RT)(E_{\text{dye}} - E_{\text{P}}) + \ln(\text{dye}_{\text{ox}}/\text{dye}_{\text{red}}) \qquad (1)$$

R is the universal gas constant, F is Faraday's constant, and n is the number of reducing equivalents involved. Titrations were carried out in triplicate, averaged, and ±1 standard deviation reported as the error.

UV/visible and Resonance Raman Characterization

UV/vis spectra were measured on either a Cary 50 spectrometer under ambient atmosphere, or an Agilent 8453 spectrometer housed inside an anaerobic chamber. Resonance Raman (rR) spectra were obtained from enzyme samples ranging from 20 to

100 μM in coproheme at 20 °C. Spectra were recorded using the 135° backscattering geometry and f1 collection. Excitation of Raman scattering was achieved with either 441.6-nm emission from a HeCd laser, or the 413.1-nm line from a Kr^+ laser. The laser beam was focused to a line on a spinning 5 mm NMR tube. Scattered light was passed through a holographic notch filter and a polarization scrambler then -matched to a 0.67-m, f/4.7 Czerny-Turner spectrograph fitted with a 1200 groove/mm grating. The Raman spectrum was detected using a liquid N_2 cooled CCD camera (1340×400 array of 20×20 μm pixels, 26.8×8.0 mm^2 image area). Dimethylformamide, toluene, acetone, and methylene bromide were used as external standards for spectral calibration. Laser power at samples ranged from 2 to 8 mW; no spectral artifacts due to photoinduced chemistry were observed with these irradiation powers.

Results

The Purified Decarboxylase Forms Stable Complexes with Hardero- and Coproheme

The decarboxylase purified in yields of 15-20 mg/L culture. Following incubation with either coproheme or harderoheme and further purification by gel filtration chromatography, nearly 1:1 ratios of protein monomer:heme species were measured.[5]

UV/Vis Features of the Oxidized and Reduced Enzyme-heme Complexes are Distinct

Spectra for the oxidized and reduced complexes of the decarboxylase with its substrate (coproheme), intermediate (harderoheme), and product (heme *b*) were measured and their features summarized in Table 1 (Supplementary Information Figure S1). As previously noted,[5] the ferric complexes had Soret and visible bands typical of five coordinate high spin (S = 5/2) Fe porphyrins with the Soret bands shifting to the red as the number of propionates (and therefore the charge) of the tetrapyrrole diminished (coproheme to harderoheme to heme b). Reduction of the iron led to a significant red shift of the Soret band (>20 nm) for each ferrous complex relative to the ferric value and the appearance of a prominent visible band near 550 nm with a higher energy shoulder. These spectral changes are consistent with those observed for other histidine-ligated heme proteins, and are suggestive of the formation of five coordinate high spin (5cHS) ferrous complexes.[22, 23]

Reactions between Ferrous Heme Species and O_2 do not Lead to Decarboxylation

Complexes of the decarboxylase with coproheme or harderoheme were reduced to their ferrous forms under anaerobic conditions. Following exposure to air in the presence of catalase, both ferrous complexes converted to ferric within the manual mixing time (≤ 5 s, pH 7.4, 20 °C, Figure S2). HPLC analysis of the tetrapyrrole products indicated no conversion of the propionate side chains to vinyls (data not shown). It was concluded that propionates 2 and 4 are not converted to vinyls via an Fe(II)/O_2 mediated oxidation (Scheme 1A).

The Ferrous Enzyme-coproheme Complex and O_2 Rapidly form an Intermediate that Converts to Ferric Coproheme

Reactions between the ferrous enzyme-coproheme complex and O_2 were monitored via UV/vis stopped flow (pH 7.4, 20 °C). An intermediate with a Soret band at 408 nm (350 nm shoulder) and visible bands at 539 and 573 nm (Table 1) formed rapidly (100 ms, Figure 1A). The rate constant for intermediate formation depended linearly on O_2

concentration under pseudo first order conditions, yielding second order rate constant k = $1.2\text{x}10^6$ $M^{-1}s^{-1}$ (Figure 1B, Table 2). The intermediate converted in a slower, O_2-independent, single-exponential phase to a final product (k = 0.20±0.02 s^{-1}, Table 2) with UV/vis features closely resembling the ferric enzyme-coproheme complex. A two-intermediate model (sum of 3 exponentials) was tested but did not substantially improve the quality of the data fit. The identity of the product as coproheme was confirmed via comparison of its HPLC retention time with those of standards[5] (data not shown).

The Oxidative Decarboxylations Do Not Occur via a Monooxygenase Intermediate

A monooxygenase reaction starting from complexes of the decarboxylase with ferric states of coproheme or harderoheme and leading to hydroxylation of the propionate side chain may require both O_2 and additional electrons. In studies of both canonical and IsdG-type heme oxygenases, the electrons have been supplied by excess ascorbate, dithionite, or other surrogate donors, as the physiological source is unknown.[13, 20, 24] Under conditions that led to reactivity in IsdG-type heme oxygenases (excess ascorbate, O_2 and catalase to consume H_2O_2),[13, 20] no reaction was observed for the decarboxylase-coproheme complex (data not shown). Reactions were subsequently carried out starting from the ferrous coproheme-decarboxylase complex. Upon addition of O_2 and either 10 mM ascorbate or 1 mM dithionite (data not shown) the same intermediate formed that was observed in the Fe(II)/O_2 reaction in the absence of reductants (Figure 1A, Table 1). No changes in the rate of intermediate formation or decay were detected, and the only observable product (via UV/vis and HPLC) was ferric coproheme. This suggests that the presence of excess reducing equivalents along with O_2 is not sufficient to promote oxidative decarboxylation. This further suggests that the coproheme decarboxylase either does not react as a monooxygenase (Scheme 1), or that, unlike known heme oxygenases, it has an obligate requirement for a specific physiological reductant.

Decarboxylation of the Ferrous Coproheme or Harderoheme Complexes does not Occur Following Reaction with H_2O_2

We next examined the possibility of a ferrous decarboxylase reaction using H_2O_2. If the enzyme acts efficiently, then 0-1 eq of H_2O_2 should result in stoichiometrically equivalent amounts of vinyl groups forming with no oxidation of the iron. To test this hypothesis, ferrous complexes of the coproheme decarboxylase with both the substrate and intermediate harderoheme were prepared, mixed anaerobically with 0-2 eq of H_2O_2, and the tetrapyrrole and Fe(III) products quantified by HPLC, EPR, and UV/vis spectroscopy (pH 7.4, 20 °C, Table 2).

UV/vis spectra did not exhibit changes consistent with the oxidation of the propionates; rather, both UV/vis and EPR spectra indicated that the substrate Fe(II) was oxidized to Fe(III) (Figure S3). Iron oxidation did not occur stoichiometrically with added H_2O_2. Instead, full oxidation of the iron for either the coproheme or harderoheme complex required 1.5 eq of H_2O_2, at which point 0.58 or 0.14 vinyl groups (per coproheme or harderoheme molecule, respectively, Table 2) had also formed, with both harderoheme and heme *b* as products. We note that, though the mechanism of propionate oxidation is not possible to discern from these experiments, 0.45 vinyl groups formed following addition of 0.5 eq of H_2O_2 to the ferric coproheme-decarboxylase complex, suggesting that the observed propionate oxidation could have occurred following oxidation of the coproheme iron. Together, these results demonstrated that H_2O_2 preferentially oxidized Fe(II), accompanied by a small amount of oxidation of the propionates of either coproheme or harderoheme.

The Ferrous Coproheme-Decarboxylase Complex Reacts more Rapidly with Air than with H_2O_2

Even though it does not lead to stoichiometric decarboxylations, we asked whether H_2O_2 might nonetheless kinetically outcompete O_2 for reaction with the ferrous iron of coproheme or harderoheme bound to the decarboxylase. The reactions between these complexes and H_2O_2 were therefore examined in the absence of O_2 by stopped flow.

After mixing the enzyme-coproheme complex with 1 eq H_2O_2, an intermediate spectrum with UV/vis features similar to the Fe(II)/O_2 intermediate formed (maximizing at ~100 ms, pH 7.4, Table 3, Figure 2A). This intermediate slowly converted to a ferric product (within 20 s at pH 7.4, $k_{obs} = 0.48\ s^{-1}$, Table 3). EPR confirmed that the majority of this end product was in the ferric state (Table 2, Figure S4). Its UV/visible features resembled those measured for ferric decarboxylase-coproheme or –harderoheme complexes, or a mixture of the two (397 nm [Soret]; 508, 632 nm [visible bands]) (Table 1). This result is consistent with HPLC analysis of the products showing predominantly Fe(III) production and incomplete oxidation of the propionates (Table 2).

The reaction was subsequently monitored as a function of [H_2O_2]. The first order rate constants for intermediate formation (average $k_{obs} = 32\ s^{-1}$) or decay were relatively insensitive to [H_2O_2], remaining roughly constant for the two respective phases (Figure S5). This suggested that the initial step leading to intermediate formation is either independent of H_2O_2 or that a saturating value for the rate had been reached at 5 μM H_2O_2 (Table 3). If we take the latter interpretation as more likely, then we may compare this saturating rate constant to the second order rate constant for the ferrous decarboxylase-coproheme/O_2 reaction. At 27 μM of either, the two oxidants yield equivalent values for k_{obs}. Above this concentration, the reaction with O_2 becomes faster than the reaction with H_2O_2. Notably, the value for k_{obs} measured at air-saturating O_2 (300 s^{-1}, Figure 2B) is 10-fold higher than the saturating rate constant for the reaction with H_2O_2. These results suggest that, under the aerobic conditions where *hemQ* is presumed to be expressed,[1] dioxygen is the kinetically preferred (faster) reaction partner for the ferrous decarboxylase-coproheme complex, with $O_2^{\bullet -}$ as the presumed co-product.

A Similar Intermediate Forms whether O_2, H_2O_2, or Peracetic Acid is the Oxidant or Harderoheme is the Tetrapyrrole Substrate

To gain further insight into the likely identity of the intermediate(s) formed in reactions between O_2 or H_2O_2 and ferrous coproheme-decarboxylase, reactions with alternate substrates were examined via stopped flow spectroscopy (Table 3). Peracetic acid ($CH_3(CO)OOH$, PAA) typically reacts as an oxygen atom donor, oxidizing heme species by two electrons and forming a ferryl [from Fe(II)] or ferryl porphyrin pi-cation radical [from Fe(III)]. When peracetic acid was used as the oxidant (1 eq, pH 7.4, 20 °C), an intermediate formed with the same UV/vis bands as the others and on a similar time scale, maximizing at approximately 100 ms (Figure S6). The intermediate converted to ferric coproheme within 10 s ($k_{obs} = 0.47 \pm 0.04$ s^{-1}).

The reaction between the ferrous decarboxylase-harderoheme complex and 1 eq H_2O_2 led to a similar intermediate (408 nm [Soret], 350 nm [shoulder]; 537, 572 nm [visible bands]) (Figure S7, Table 1) that formed on a comparable time scale as the coproheme complex and then converted to the ferric product (first order rate constant $k_{obs} = 0.72\ s^{-1}$, Table 3). The observation of an intermediate with similar UV/vis features with either coproheme or harderoheme as the substrate or in the presence of O_2, H_2O_2, or peracetic acid as oxidants suggests that a similar species formed in each case.

Reactions of Ferric Coproheme- or Harderoheme-Decarboxylase Complexes with H_2O_2 are Slow and pH Dependent

Since the decarboxylase appears to kinetically favor O_2-mediated oxidation of the ferrous coproheme iron in air (Figure 1), both of the decarboxylation reactions are expected to take place in an Fe(III)/H_2O_2 dependent manner under aerobic conditions. The ferric coproheme-decarboxylase reaction with H_2O_2 was monitored as a function of H_2O_2 concentration and at a series of pH values. An intermediate was not clearly detectable under any condition. Instead, the initial reaction phase led to a heme *b* complex that subsequently decomposed (Figure 3A). The two observed phases could be fit to single exponential curves to obtain k_{obs} values. The first phase exhibited a strong, linear dependence on H_2O_2 concentration (Figure 3B) and a sigmoidal dependence on pH, yielding second order rate constants ranging from 110 to 330 $M^{-1}\ s^{-1}$ (pH 5.8-8.8). Fitting the data to eq (2) yielded p*K*a = 7.4 ± 0.3 (Figure 4):

$$\log k = \frac{k_2 \times 10^{(pH\ -\ pKa)} + k_1}{(1 + 10^{pH - pKa})} \qquad (2)$$

The constants k_1 and k_2 describe the low and high pH forms of the enzyme-substrate system.

This value is well below the p*K*a of H_2O_2 (11.7), suggesting that it is due to a deprotonation event on the decarboxylase-coproheme complex rather than deprotonation of free H_2O_2. The second phase was far slower and independent of both H_2O_2 concentration and pH (Figure 4B, Table 3).

The reaction of the ferric harderoheme complex was likewise characterized by two phases. The first led to a complex of the decarboxylase with heme *b* (Soret 408 nm; visible bands 540, 572 nm) and the second to heme destruction (Figure S7). Second order rate constants were slightly faster with harderoheme than coproheme as substrate (190 to 350 M^{-1} s^{-1}, pH 5.8-8.8) and exhibited the same p*K*a (7.3 ± 0.2) (Figure 4). The heme decomposition phases for coproheme or harderoheme as substrates (Figure S8) were indistinguishable kinetically or spectroscopically, suggesting that the degradation process occurred after heme *b* formed.

Reactions between Ferric Coproheme-decarboxylase Complex and Peracetic Acid are Fast and pH-independent

When PAA was used as the oxidant in place of H_2O_2, analogous conversion of the substrate to a heme *b* complex followed by degradation was observed in stopped flow experiments (Figure S9). However, the phase leading to heme *b* was approximately an order of magnitude faster with the peracid than with H_2O_2 (k = 3600-5200 $M^{-1}s^{-1}$). Because PAA is expected to react as an oxygen atom donor, the fact that both it and H_2O_2 are productive oxidants suggests that the ferryl porphyrin pi-cation radical (Fe(IV)=O por▪+, Compound I) is a common intermediate on both the H_2O_2 and peracid pathways. Finally, neither the second order formation nor the first order decay rate constants had a sigmoidal dependence on pH (Figure 4). This may reflect the relatively low pK_a of the peracid (8.2), which would obviate the need for basic residues to catalyze the formation of a ferric-acetylperoxy species.

Solvent Isotope Effect on the Ferric Coproheme-decarboxylase Reaction Indicates Rate Limiting Proton Transfer

The slow second order kinetics of the ferric coproheme reactions suggests that a bimolecular step involving H_2O_2 partly limits the rate at which heme *b* forms. The pH dependence of the rate constant (Figure 4) suggests that this step includes transfer of H^+. To further explore these hypotheses, the decarboxylase-coproheme complex reaction with D_2O_2 was monitored in D_2O at varying pD. The second order rate constants diminished in magnitude, with an averaged solvent kinetic isotope effect (SKIE) on k (k_H/k_D) of 2.2 over the measured pH/pD range. The plot of *k* versus pD adhered closely not to a one but rather a two p*K*a model:

$$\log k = \frac{k_1 \times 10^{(pH-pK1)} + k_2}{(1+10^{(pH-pK1)})} + \frac{k_2 \times 10^{(pH-pK2)} + k_3}{(1+10^{(pH-pK2)})} \tag{3}$$

Here, k_1, k_2, and k_3 describe the rate constants for each of the 3 pH-dependent forms of the enzyme-substrate system. This fit yielded p*K*as of 6.5 and 9.3.

We conclude that D_2O clearly influences both the rate of the second order reaction and the observed number and magnitude of acid dissociation equilibria for the coproheme-decarboxylase complex. Substitution of ^2D for ^1H is known to perturb acid dissociation equilibrium constants by varying amounts depending on the acid's structure (the p*K*a shifts 0.41 units for D_2O versus H_2O, e.g., to 7.41).[25] It is possible that the p*K*as 7.4 and 9.3 measured in H_2O and D_2O, respectively, correspond to the same acid dissociation event, and that the second p*K*a (6.5 in D_2O) was out of the pH range used in protonated buffer. Alternatively, the introduction of deuterium could have altered the rate limiting steps of the mechanism, and therefore the chemical event contributing the most to the second order rate constant. The origins of these p*K*as will be explored further in future work.

Resonance Raman (rR) Spectra for Ferrous Decarboxylase-Coproheme Complex Indicate a Pentacoordinate High-Spin Coproheme with a Neutral His Ligand

The five-coordinate, high-spin (5cHS) nature of the ferrous HemQ complexes was confirmed by the coordination- and spin-state marker bands ν_3 and ν_4 at 1467 and 1353-cm^{-1}, respectively, in the high frequency rR spectra (Figure 5A). The ferrous coproheme, harderoheme, and heme *b* complexes exhibit very similar ν_3 and ν_4 shifts.

Additionally, the rR spectra report on the nature and strength of the proximal iron-ligand bond. In 5cHS ferrous heme proteins having proximal imidazole ligands, 441.6-nm Raman excitation elicits well-enhanced bands attributable to their iron-histidine stretches, ν_{Fe-His}. By virtue of its intensity and frequency, the 215 cm^{-1} band is tentatively assigned to the ν_{Fe-His} mode of 5cHS ferrous decarboxylase-coproheme (Figure 5B). The ν_{Fe-His} frequency for ferrous decarboxylase complexes of harderoheme and heme *b* are within 1 cm^{-1} of that for the coproheme complex.

The 215-cm^{-1} $\nu_{\text{Fe–His}}$ frequency of decarboxylase-coproheme is 7, 11, and 14 cm^{-1} lower than those of the closely related, heme *b*-dependent chlorite dismutases (Clds) from *Dechloromonas aromatica* (*Da*Cld, 222 cm^{-1}), *Nitrospira defluvii* (*Nd*Cld, 226 cm^{-1}), and *Klebsiella pneumoniae* (229 cm^{-1}), respectively.[26-28] Mutation of the distal pocket in *Da*Cld (*Da*Cld(R183Q)) to mimic the predicted pocket in the decarboxylase[29] does not result in a significant change of its $\nu_{\text{(Fe-His)}}$ frequency.[30] The proximal histidine ligands of *Da*Cld and *Nd*Cld have some imidazolate character due to H-bonding interactions with nearby glutamate side chains. Since the H-bond accepting glutamate in the Cld proximal pockets is not conserved in the decarboxylases,[31] Hofbauer and coauthors predicted correctly that the $\nu_{\text{Fe–His}}$ frequency for the heme complexes would be similar to that of *Nd*Cld(E210A) which they reported at 216 cm^{-1}.[27] This result suggests that any proximal hydrogen bond network in the decarboxylases does not include strong participation by the proximal ligand. It further suggests that the electronic "push" exerted by the proximal His is closer to that in the globins than in His-ligated peroxidases.

The Reduction Potential for the Decarboxylase-coproheme Complex is Peroxidase-like and Becomes More Positive as the Propionates Convert to Vinyls

Fe(III)/Fe(II) potentials for coproheme (-190 mV), harderoheme (-170 mV), and heme *b* (-160 mV) bound to the decarboxylase were measured spectroelectrochemically (versus SHE, pH 7. 20 °C, Figures 6 and S10). The value for the coproheme complex is similar to the one recently reported for the same protein (-207 mV) at neutral pH.[32] These positive shifts in reduction potential are consistent with the loss of negative charge from the porphyrin periphery as each propionate is converted to a vinyl group. Other histidine-ligated heme proteins offering relevant comparisons include heme peroxidases, which react in the ferric oxidation state and have heme Fe(III)/(II) reduction potentials ranging from -150 to -300 mV vs SHE.[33] The reduction potential of *Da*Cld, which is homologous (31.4% similarity, EMBOSS Needle alignment) to and structurally superimposable with the decarboxylase/HemQ, is -21 mV.[34] Clds use ferric heme *b* as a catalytic cofactor for converting ClO_2^- to Cl^- and O_2. By contrast, positive potentials are associated with heme proteins that operate in the Fe(II) state. Ferrous myoglobin, which reversibly binds O_2, has a low, positive reduction potential of 45 mV,[35] while the potential for bifunctional dehaloperoxidase, which reversibly binds O_2 and reacts with H_2O_2 in its ferrous form, is 222 mV.[22]

Discussion

The assembly of biological cofactors requires the highly controlled combination of reactive components within the cellular environment. In the final step of heme biosynthesis in many bacteria, including most facultative gram positives,[1] a ferrous-porphyrin precursor undergoes the selective oxidative decarboxylation of two propionate groups under conditions where both cellular O_2 and H_2O_2 are known to be present.[1, 6] Coproheme is the substrate and cofactor in this unusual autocatalytic reaction, carried out by a coproheme decarboxylase encoded by the *hemQ* gene. Because iron is inserted into coproheme as Fe(II),[1, 6, 36] the reaction could, in principle, occur via mechanisms that are oxidase-, oxygenase-, or peroxidase-like (Scheme 1). Each invokes unique chemical steps and distinct biological strategies for directing the reactivity of the redox-active substrates and product. We sought to determine which of these is the most likely pathway for the decarboxylase under biological conditions.

In nearly all cases where decarboxylation is accompanied by C-C bond oxidation, the two electrons from the substrate are funneled into a cofactor (e.g., flavin or pyridoxal phosphate).[*37*] The cofactor electrons may be subsequently discharged onto NAD(P)$^+$ or O_2. The coproheme decarboxylase lacks a cofactor; however, the substrate itself could act as a conduit for removing two electrons from each propionate side chain and delivering them to O_2, generating H_2O_2. This hypothetical reaction (Scheme 1A) is similar to the one catalyzed by coprophorphyrinogen oxidase: the cofactor-free enzyme from the canonical pathway that catalyzes an analogous reaction with a metal-free, reduced, and unconjugated substrate.[*10*] When we examined the ferrous coproheme decarboxylase for oxidase activity, however, none was observed.

In nearly all cases where decarboxylation is accompanied by C-C bond oxidation, the two electrons from the substrate are funneled into a cofactor (e.g., flavin or pyridoxal phosphate).[*37*] The cofactor electrons may be subsequently discharged onto NAD(P)$^+$ or O_2. Although the coproheme decarboxylase lacks such a cofactor, the substrate itself could act as a conduit for removing two electrons from each propionate side chain and delivering them to an exogenous oxidizing agent. One possibility is that electrons are directed to cellular O_2, generating H_2O_2. This hypothetical reaction (Scheme 1A) is similar to the one catalyzed by coprophorphyrinogen oxidase: the cofactor-free enzyme from the canonical pathway that catalyzes an analogous reaction with the metal-free porphyrinogensubstrate.[10] When we examined the ferrous coproheme-bound decarboxylase for oxidase activity, however, none was observed.

Structurally, the decarboxylase closely resembles bacterial heme oxygenases from the IsdG family, which are found in the same bacterial taxa.[38] The heme oxygenase reaction is likewise autocatalytic, with ferrous heme *b* acting concurrently as the substrate and cofactor. In the proposed IsdG mechanism,[13] heme *b* reacts with O_2 to form a ferrous heme-O_2 complex. Addition of H^+ and an electron leads to a ferric-hydroperoxy intermediate, which hydroxylates one of the pyrrole-bridging *meso*-carbons. The biological source of the electron has not been identified for any heme oxygenase, though various surrogates have been used under *in vitro* conditions. Following the initial hydroxylation, a series of further reactions leads to ring opening and release of formaldehyde and the triply oxygenated linear tetrapyrrole product.[20, 39]

An analogous reaction mechanism can be proposed for the coproheme decarboxylase, though with hydroxylation directed not toward a *meso*-carbon, but rather the β-carbon of a reactive coproheme propionic acid (Scheme 1B). Consistent with an oxygenase mechanism, UV/vis spectroscopic evidence suggests that the ferrous coproheme substrate rapidly forms spectroscopically similar intermediates with both O_2 and H_2O_2 (Figures 1A and 2A). However, under conditions that would have resulted in heme oxygenation by IsdG and its homologs, no reaction occurred. Barring the requirement for a yet-unknown physiological reductant, the evidence here suggests that coproheme decarboxylase does not work according to an oxygenase mechanism.

We next considered whether the decarboxylase might react in the ferrous state with H_2O_2, averting the competing, non-productive Fe(II)/H_2O_2 reaction to generate OH^- and cytotoxic $OH^\bullet$. Such a "ferrous peroxidase" mechanism would be highly unusual though not completely unprecedented. The heme-dependent marine worm dehaloperoxidase (DHP) provides the sole example of H_2O_2/heme reactivity occurring under biological conditions from the ferrous state.[14, 15, 23] A ferrous-hydroperoxy heme species forms as the initial intermediate in DHP, followed by heterolytic cleavage of the O-O bond to yield Compound II (Fe(IV)=O porphyrin). Compound II acts as a one-electron oxidant toward each of a pair of exogenous substrates, returning the heme cofactor to the ferrous oxidation state.

Consistent with this pathway, the ferrous coproheme-decarboxylase appeared to form an intermediate in the reaction with H_2O_2, which could in principle be a ferrous-peroxy complex (Figure 2). However, the subsequent steps did not lead to decarboxylation (Table 2). Instead, the reaction with 1-2 eq of H_2O_2 brought about the complete conversion of the coproheme Fe(II) to Fe(III). Moreover, while the maximal second order reaction rate between the ferrous coproheme-decarboxylase and H_2O_2 was fast, the reaction with ambient O_2 (240 μM at pH 7, 20 °C, in Bozeman, MT) was even faster. The ferrous reaction with O_2 is therefore expected to be kinetically favored over H_2O_2 under aerobic conditions or whenever dissolved O_2 exceeds 30 μM (Table 3).

We therefore hypothesized that the decarboxylase might react as an "oxidase-peroxidase." According to this model, the ferrous coproheme reaction with O_2 would generate the ferric coproheme and $O_2^{\bullet -}$ in the first step. Once in the ferric state, the coproheme- and harderoheme-decarboxylase complexes would have to react with H_2O_2, since ferric heme species are not known to be oxidized by O_2.

This is an attractive proposition since heme enzymes generally react with H_2O_2 in the ferric state, and since the decarboxylase reaction can occur in an Fe(III)/H_2O_2-dependent manner.[5] We observed here (Figures 5 and 6) that the Fe(III)/(II) reduction potential and coordination state for these are reminiscent of typical heme peroxidases, suggesting that the enzyme-substrate complex has a sufficient driving force for reacting in the ferric state. We further observed that the reaction between the ferric coproheme-decarboxylase complex and H_2O_2 was second order and pH dependent, growing faster with a pK_a near 7.4 (Figure 4). The observation of a solvent kinetic isotope effect further indicated that a proton transfer – for example, from H_2O_2 or to a ferric-OOH complex to generate water and Compound I – partly limited the rate of this second order step. Acid-base catalysis of Compound I formation, usually involving a His-Arg pair, is a cornerstone of proposed mechanisms for H_2O_2 activation by heme peroxidases.[40]

However, the second order reaction between the decarboxylase-coproheme complex and H_2O_2 was exceedingly slow, with rate constants (110-330 $M^{-1}s^{-1}$) that are 10^2-10^4 times lower than expected for typical peroxidases.[16] Further, instead of forming Compound I as an initially observable intermediate, the first species observed in reactions with either the coproheme- or harderoheme-decarboxylase complex and H_2O_2 is the complex of the protein with ferric heme *b* (Figure 3). Compound I may nonetheless be on the reaction pathway. Peracetic acid, an oxygen-atom donor which typically forms Compound I from ferric heme, very efficiently generates the expected harderoheme intermediate and heme *b* product. We would not expect Compound I to be directly observed if it reacts quickly once it forms. The lifetime of Compound I in peroxidases is highly variable, and appears to depend strongly on the number and proximity of redox-active amino acids that can react with it.[41, 42] The structure of the decarboxylase with coproheme bound is unknown; however, consistent with a short lived intermediate, it has multiple Trp and Tyr residues (5 and 12, respectively) in its 250 amino acid sequence, and its two oxidizable substrates are covalently attached to the heme. Thus, if the oxidative decarboxylation proceeds via Compound I, its lifetime may be anticipated to be fleeting.

Compound I-catalyzed decarboxylations could occur by one of at least two possible mechanisms (Scheme 2**).** The first is analogous to the classic, two-step peroxidase catalytic cycle.[16] In the first step, a net hydrogen atom (H^+ plus e^-) is transferred from the β−carbon of the propionate to the ferryl porphyrin cation radical, filling the hole on the porphyrin to generate Compound II and protonating the ferryl oxygen atom. Second, migration of the remaining unpaired electron from the β−carbon of the propionate to the Fe(IV) might occur with concomitant loss of the carboxylate group as CO_2. A second proton would need to be brought in to make H_2O. Alternatively, one could imagine the same protonated Compound II [Fe(IV)-OH] "rebounding" with the propionyl radical to yield a hydroxylated intermediate. The rebound reaction would likely only take place if the ferryl were adjacent to the reactive propionate. As this is difficult to envision, the rebound mechanism is improbable. The peroxidase-like mechanism, by contrast, could involve amino acid side chains as conduits for the transferred electrons and protons. In either case, the oxidation state of the metal remains unchanged at the beginning/end of the reaction, and the ferric coproheme is first converted to ferric harderoheme. A second catalytic cycle between Fe(III) harderoheme and H_2O_2 would be needed to generate heme *b*. Do the two, sequential oxidative decarboxylation reactions occur in the same manner? The fact that the second order rates for the ferric coproheme/H_2O_2 and harderoheme/H_2O_2 reactions leading to heme *b* are roughly the same suggests that the second propionate conversion (from harderoheme to heme *b*) limits the overall reaction rate. This suggests that the H_2O_2-activating steps for coproheme and harderoheme could be largely similar.

Though a mechanism involving Compound I is plausible, the electronic structure of the coproheme bound to the decarboxylase presents a conundrum. A “push-pull”/distal acid-base model is used to explain heterolytic peroxide cleavage in the peroxidase mechanism.[40] The “push” effect correlates with the basicity of the proximal ligand which, in the case of heme peroxidases, is typically a His side chain whose basicity is modulated by H-bond acceptors. The strongest, anionic H-bond acceptors lead to the most basic His ligands, which in turn stabilize the high-valent iron centers of Compounds I and II. The extent of the “push” effect is reflected in the iron histidine stretching frequency, which ranges from 233-246 cm^{-1} in heme peroxidases.[43, 44] By contrast, the low ν_{Fe-His} frequency of 215 cm^{-1} shows that the imidazole ligand in coproheme decarboxylase is not associated with an anionic H-bond acceptor, predicting a relatively weak proximal “push”. Clds, which are closely related to these HemQ-decarboxylases, also exhibit lower ν_{Fe-His} frequencies (222 - 229 cm^{-1}) than heme peroxidases, suggesting a weaker proximal “push”, but perhaps greater than HemQ.[5, 45, 46] However, their modest push, in conjunction with a strong "pull" from their distal Arg drives heterolytic cleavage of an O−Cl bond in the ClO_2^- substrate. As inthe heme peroxidases, this is thought to direct both oxidizing equivalents of the substrate to the heme cofactor thereby yielding compound I. The distal environment of the coproheme decarboxylase is not known, though it might partly compensate for the weak Fe-His interaction via the "pull" of positive charges. By the same token, it is possible that the negatively charged propionate groups 2 and 4 could act together with the protein environment to stabilize the ferric oxidation state, potentially supporting heterolytic cleavage of bound H_2O_2.[33] Alternatively, heme oxygenases have neutral His heme ligands (ν_{Fe-His} = 216-218 cm^{-1})[47, 48] and do not react via Compound I. Rather, an Fe(III)-OOH species directly hydroxylates one of the pyrrole-bridging carbons, without prior cleavage of the O-O bond,[49, 50] and an analogous mechanism using ferric coproheme can be proposed here (Scheme 2).

A pathway invoking O_2-mediated oxidation of Fe(II) followed by Fe(III)/H_2O_2 dependent decarboxylations has at least three important implications for how heme synthesis is organized in the cells that use this noncanonical mechanism. First, the well-known biosynthetic pathway from gram-negative bacteria and eukaryotes generates ferrous heme *b.* The production of the ferric heme in gram-positives suggests distinct ways of subsequently chaperoning the cofactor and incorporating it into proteins in the cell. Second, a reaction cycle that begins from the ferrous coproheme complex produces a stoichiometric quantity of superoxide per coproheme/heme *b* conversion as the metal oxidizes from Fe(II) to Fe(III). Although the fate of the $O_2^{\bullet -}$ is not clear, catalytic disproportionation of superoxide in the presence of a proton source rapidly yields H_2O_2.[51]

The susceptibility of free ferric coproheme to bleaching in the presence of even small amounts of H_2O_2 suggests that oxidation of the iron occurs inside the decarboxylase rather than freely in the cell.[5] The upstream catalyst, ferrochelatase (HemH), may directly relay the substrate to the decarboxylase, as some existing data already support.[52] Finally, though *S. aureus* like many gram-positives is a catalase-rich organism, this unique oxidative decarboxylation reaction depends on H_2O_2 rather than O_2.

Figures

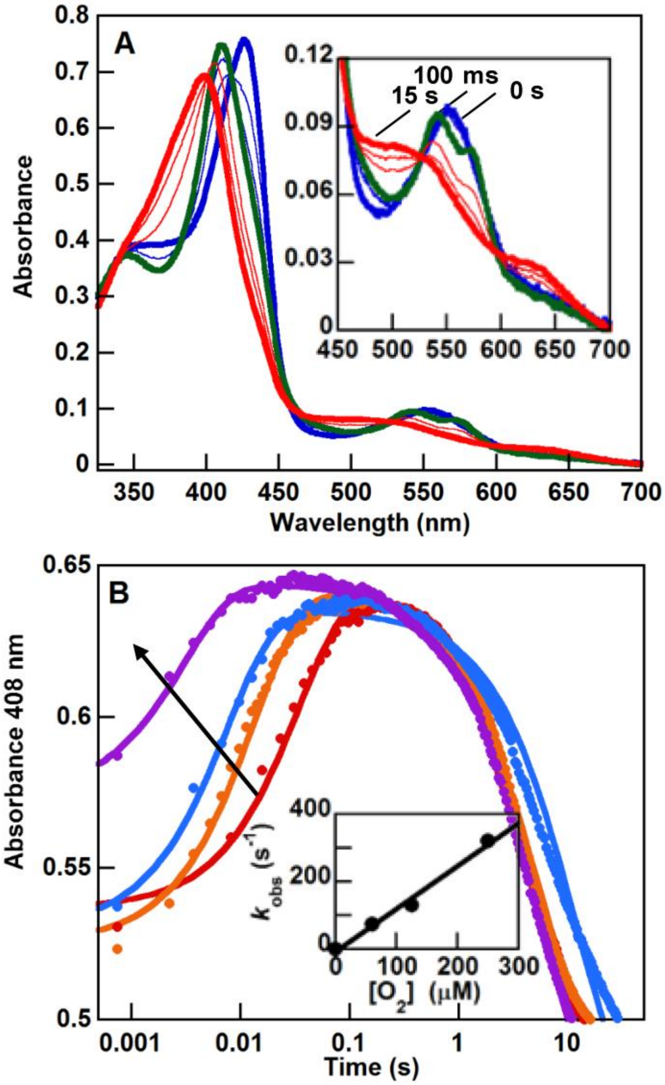

Figure 4.1. The reaction between the ferrous coproheme-decarboxylase complex and O_2 leads to an intermediate, followed by oxidation of the coproheme iron. A. The ferrous coproheme-decarboxylase complex (5 μM, blue line) was rapidly mixed with one eq of O_2 and the reaction monitored by stopped flow UV/vis spectroscopy (50 mM KPi, pH 7.4, 20 °C). Conversion to an initial intermediate after 100 ms (green line) was observed, followed by formation of the ferric coproheme product (15 s, red line). Intervening spectra are shown at 0.015, 0.045, 2, and 5 s (lighter lines). The inset shows the visible bands on an expanded scale. B. The progress of the reaction was monitored over time at 408 nm at varying final concentrations of O_2 (6, 60, 120, and 240 μM, increasing in the direction of the arrow). Each curve was fit to the sum of two exponentials. Inset: values of k_{obs} for the initial phase leading to the green intermediate in (A) were plotted as a function of [O_2], yielding $k = 1.2 \times 10^6$ M^{-1} s^{-1}.

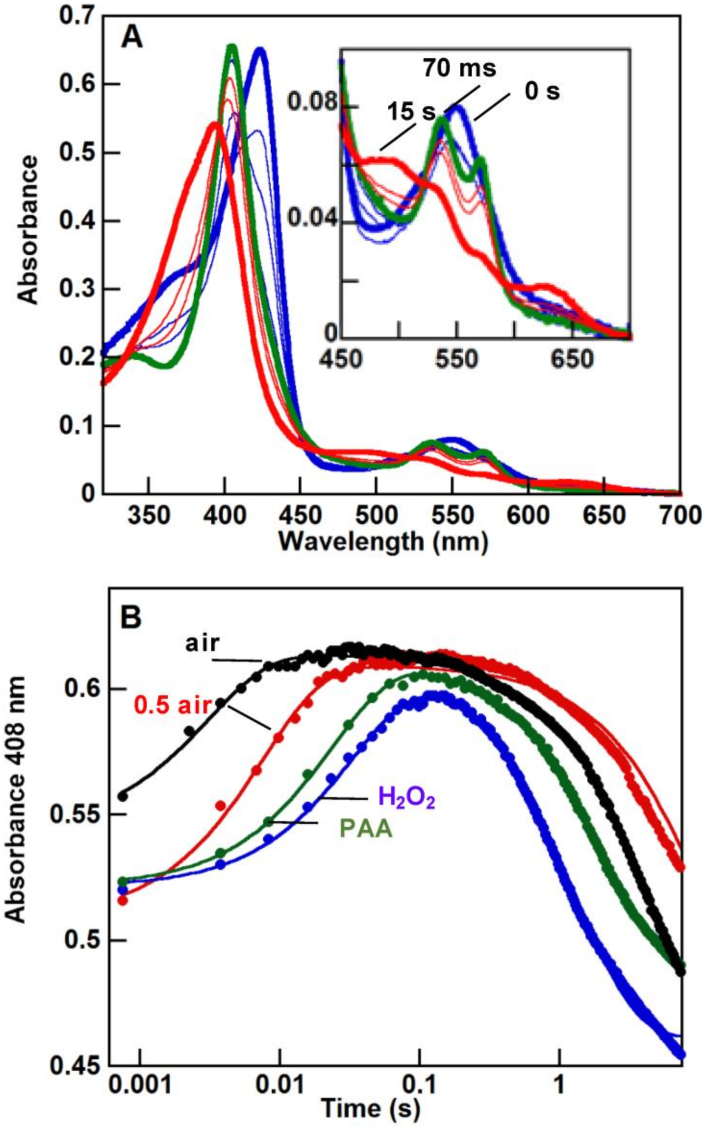

Figure 4.2. The ferrous coproheme-decarboxylase complex reacts faster with O_2 in air than with H_2O_2. A. The ferrous coproheme-decarboxylase complex (5 μM, blue line) was rapidly mixed with one eq of H_2O_2 and the reaction monitored by stopped flow UV/vis spectroscopy (50 mM KPi, pH 7.4, 20 °C). Conversion to an initial intermediate after ~70 ms (green line) was observed, followed by formation of the ferric product (15 s, red line). Intervening spectra are shown at 0.015, 0.045, 2, and 5 s (lighter lines). The inset shows the visible bands on an expanded scale. B. The progress of the reaction monitored over time at 408 nm is shown for the reactions of ferrous coproheme-enzyme complexes with 1 eq H_2O_2 (blue), 1 eq peracetic acid (PAA) (green), or O_2 (half and full air saturation, 120 and 240 μM O_2, red and black points respectively). The data points are shown in fits to sums of two exponential curves. (Fits to the initial phase for the stoichiometric reactions are included as a visual aid.)

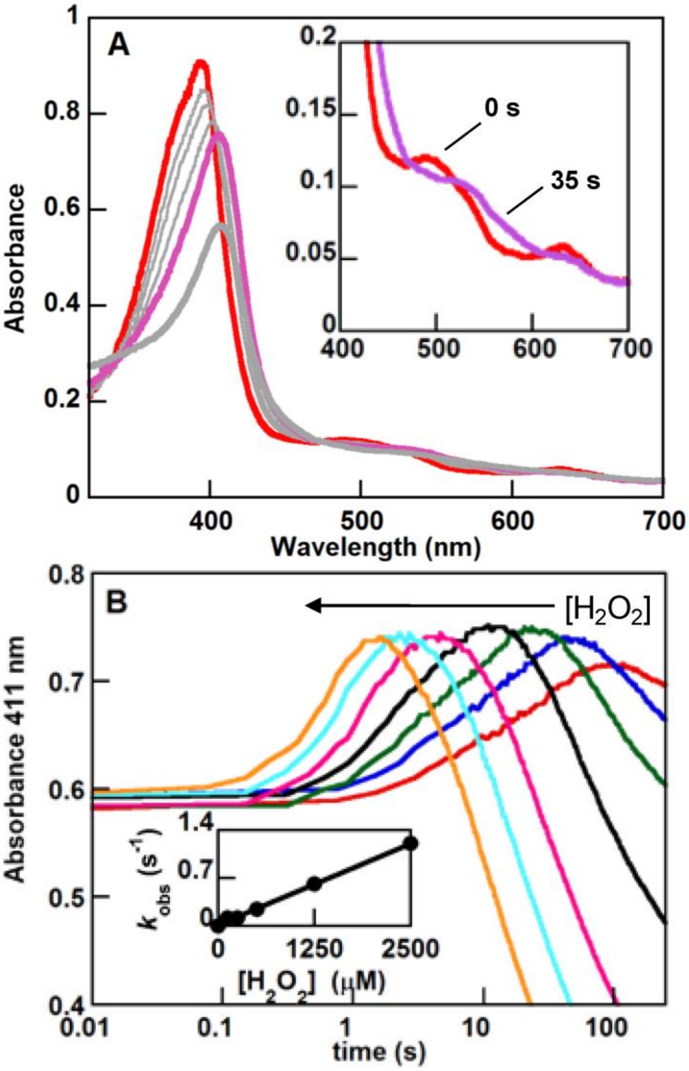

Figure 4.3. Oxidative decarboxylation of ferric coproheme occurs slowly and without observable intermediates when H_2O_2 is the oxidant. A. The ferric coproheme-decarboxylase complex (7 μM, blue line) was rapidly mixed with 10 eq of H_2O_2 and the reaction monitored by stopped flow UV/vis (50 mM KPi, pH 7.4, 20 °C). Conversion to a complex with heme *b* was observed after ~35 s (purple line), followed by heme decomposition over several minutes (illustrated by the 500 s curve, gray). Intervening spectra are shown at 5, 10, and 20 s (lighter lines). The inset shows the visible bands on an expanded scale. B. The progress of the reaction monitored over time at 411 nm is shown for the reaction of ferric coproheme-decarboxylase with increasing concentrations of H_2O_2 (in direction of arrow: 75, 125, 250, 500, 1250, 2500, and 500 μM; 50 mM KPi, pH 7.4, 20 °C). Each curve was fit to the sum of two exponentials. The first kinetic phase corresponded to the generation of a heme *b* complex and the second to heme *b* decomposition (k_{decay}). Inset: Values of k_{obs} for the first phase (red squares) were plotted versus [H_2O_2] and used to generate second order rate constant 210 M^{-1} s^{-1}.

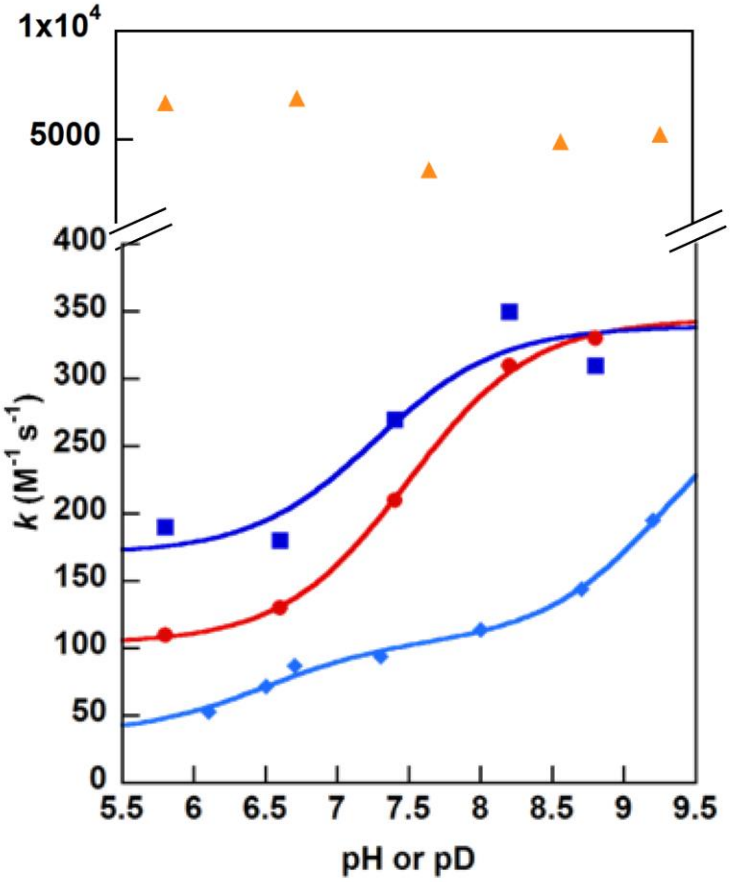

Figure 4.4. The rates of reactions between the ferric coproheme-decarboxylase and H_2O_2 are pH and solvent-isotope dependent. Reactions between the ferric coproheme- and harderoheme-decarboxylase complexes and H_2O_2, D_2O_2 (in D_2O), or PAA were monitored as a function of pH (pD). An initial phase corresponding to heme *b* formation (k_{heme}) followed by heme decomposition (k_{decay}) was observed in every case. A. Second order rate constants measured as shown in Figure 3B were plotted as a function of pH: red circles; coproheme/H_2O_2; blue squares: harderoheme/ H_2O_2. The initial phase grew faster with increasing pH and was fit to a single pK_a equation, yielding pK_a = 7.3 (harderoheme) or 7.5 (coproheme). The same rate constants measured for the coproheme reaction with D_2O_2 (in D_2O) (blue diamonds) were fit to a two-pK_a model yielding 6.5 and 9.3; average SKIE = 2.2. Finally, rate constants for the coproheme reaction with PAA were much larger and did not exhibit a sigmoidal trend. B. Rate constants describing the decay phase did not display sigmoidal dependence on pH (see Figure S8.).

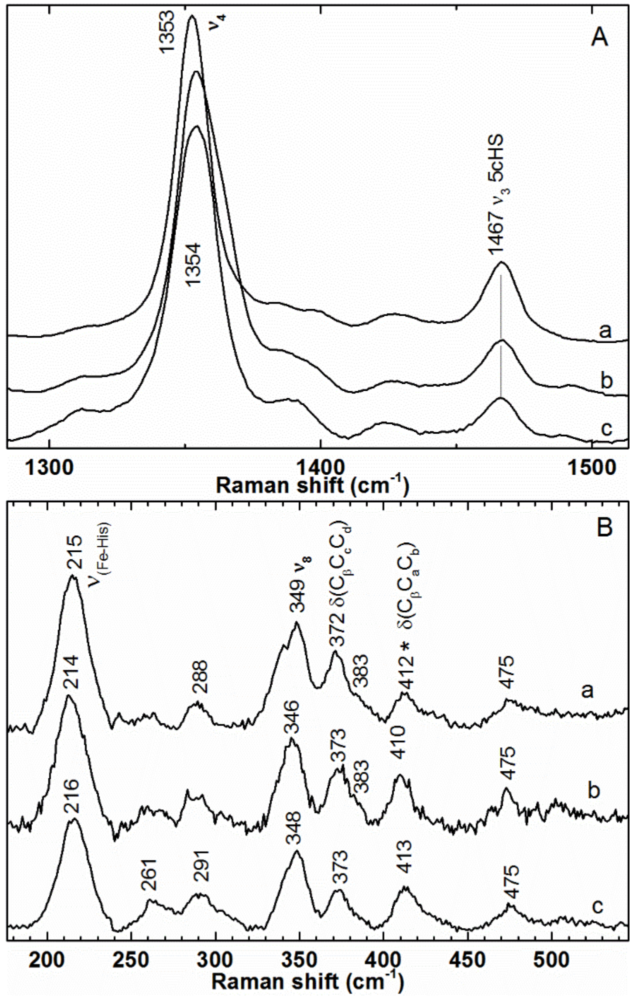

Figure 4.5. Vibrational characterization of the ferrous iron tetrapyrrole complexes of the coproheme decarboxylase. A) High frequency window of the 413.1-nm excited rR spectra of (a) ferrous coproheme-, (b) ferrous harderoheme-, and (c) ferric coproheme-decarboxylase complexes reacted with eight equivalents of H_2O_2 to generate enzyme-heme *b* followed by reduction with sodium dithionite. B) The 441.6 nm excited low frequency rR spectra of (a) ferrous enzyme-coproheme complex, (b) ferrous enzyme-harderoheme and (c) product of ferric enzyme-coproheme with H_2O_2 followed by reduction with dithionite. Note the change in the intensities of the propionate and vinyl bends relative to one another and the ν_8. All samples were prepared in 0.1 M sodium phosphate buffer pH 6.8 and reduced with sodium dithionite. The asterisk indicates a vinyl bending band due to a small amount of decarboxylated coproheme.

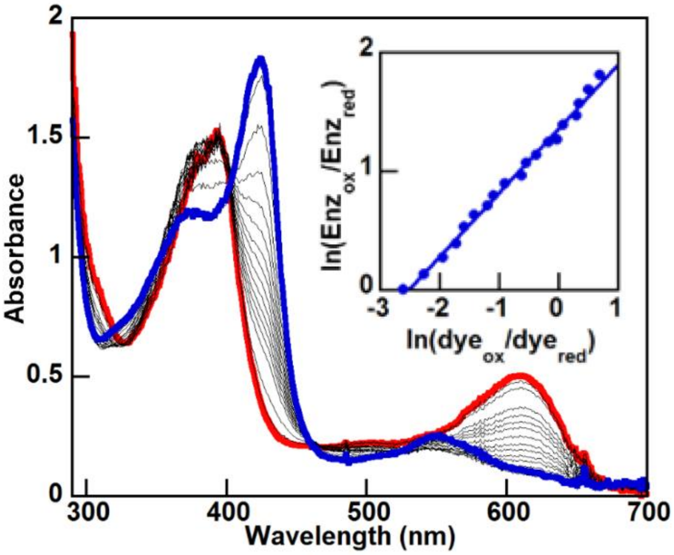

Figure 4.6. The Fe(III)/(II) redox potential for decarboxylase-bound coproheme is peroxidase-like, and becomes more positive as each propionate is converted to a vinyl. Titration of the ferric coproheme-decarboxylase complex with dithionite in the presence of oxidized indigo disulphonate (red) results in the concurrent reduction of both substrate and dye (blue). (Inset) Plotting the $\ln(Enz_{ox}/Enz_{red})$ versus $\ln(Dye_{ox}/Dye_{red})$ allowed for the determination of redox potential of -190 mV from the slope (versus SHE, pH 7. 20 °C). Analogous data measured for the complexes of the decarboxylase with harderoheme and heme *b*, yielded -170 mV, and -160 mV, respectively (see Supplementary Information).

Scheme 4.1. Possible coproheme decarboxylase pathways starting from Fe(II)coproheme‡

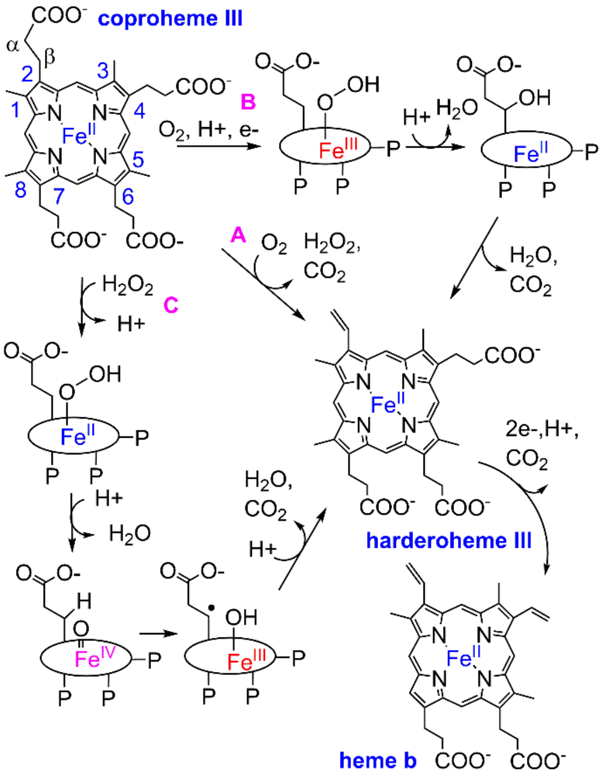
coproheme III
COO⁻
α
β
1
2
3
4
5
6
7
8
Fe^II
B
O_2, H+, e-
Fe^III
H+ H_2O
Fe^II
P
A
O_2
H_2O_2, CO_2
H_2O, CO_2
H_2O_2
C
H+
H+
H_2O
Fe^IV
Fe^III
H_2O, CO_2
H+
2e-,H+, CO_2
harderoheme III
heme b
O-
OH
H
O

‡The ferrous coproheme III substrate is shown with sites of pyrrole ring substituents (methyl or propyl) labeled 1-8. The tetrapyrrole is depicted as an oval and the propionates as "P". Only the reacting propionate 2 is shown, for clarity. A) Oxidase, B) oxygenase and C) peroxide-dependent mechanisms shown. A mechanism for the conversion of the harderoheme III intermediate to heme *b* is not shown but could occur by an analogous mechanism to A-C.

Scheme 4.2. Possible pathways for oxidative decarboxylation.[‡]

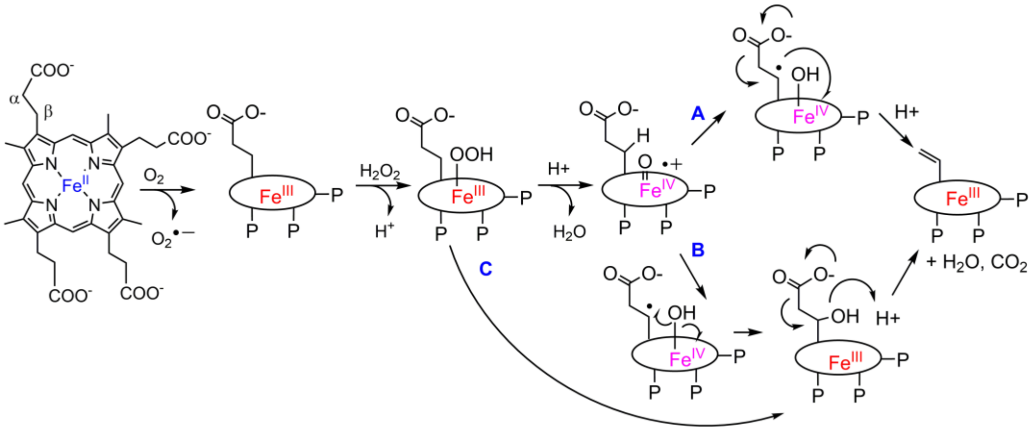
COO-
α
β
COO-
N
N
N
N
Fe II
COO-
COO-
O2
O2•−
O O-
Fe III
P
P
P
H2O2
H+
OOH
H+
H2O
H
O •+
Fe IV
A
B
C
OH
H+
+ H2O, CO2

[‡] Only the first oxidative decarboxylation is shown. O_2-mediated oxidation of the coproheme iron is followed by reaction of the ferric coproheme with H_2O_2 to form a hypothetical Fe(III)-OOH adduct. Two Compound I-dependent pathways are shown. (A) Net H-atom ($H^+ + e^-$) transfer from the propionate β-carbon to Compound I. (B) Net H-atom transfer followed by hydroxyl rebound to yield a hydroxylated intermediate. Direct hydroxylation from the ferric-hydroperoxy species (C) could likewise occur, analogous to heme oxygenase chemistry.

Tables

Table 4.1. UV/vis bands for complexes of HemQ coproheme decarboxylase with substrate, intermediate, or product

Complex	Soret	Visible
Fe(III)		
coproheme	394	497, 533, 630
harderoheme	396	495, 533, 610
heme *b*	406	510, 527, 630
Fe(II)		
coproheme	424	548
harderoheme	418	~520sh, 551
heme *b*	427	560
Fe(II) reaction intermediates		
coproheme + O_2	408	539, 573
coproheme + H_2O_2	408	539, 572
coproheme + peracetic acid	408	539, 572
harderoheme + H_2O_2	408	537, 572
harderoheme + peracetic acid	408	537, 572

Table 4.2. Observed oxidation products following addition of defined amounts of H_2O_2 to decarboxylase complexes with ferrous/ferric coproheme or harderoheme, expressed on a per-substrate basis[a]

heme species	Fe(II) coproheme		Fe(II) harderoheme		Fe(III) coproheme	Fe(III) harderoheme
H_2O_2 (eq)	vinyls[b]	Fe(III)[c]	vinyls	Fe(III)	vinyl groups	vinyl groups
0	0	0	0	0	0	0
0.5	0.32±0.05	0.05	0.07±0.02	ND[d]	0.14±0.02	0.07±0.02
1	0.51±0.07	0.70	0.13±0.02	ND	0.27±0.04	0.11±0.03
1.5	0.58±0.06	0.98	0.14±0.04	ND	0.45±0.07	0.13±0.02
2	0.60±0.1	0.91	0.15±0.03	ND	0.54±0.06	0.14±0.02

[a] Reactions were carried out at 20 °C in pH 7.4 KPi. [b] Conversion of propionates to vinyl groups was determined via HPLC quantification of the total harderoheme and/or heme *b* products of each reaction. Each reaction was carried out in triplicate with the error reported as the standard deviation of the three measurements. [c] Fe(III) was determined by double integration of the EPR spectra and spin quantification, using horse heart myoglobin as a standard (Figure S5). [d] Not determined.

Table 4.3. Rate constants for reactions of decarboxylase complexes with oxidants (pH 7.4, 20 °C)

Substrate	oxidant	k ($M^{-1}s^{-1}$) [a]	k_{decay} (s^{-1})
coprohemeFe(II)	O_2	1.2×10^6	0.20 ± 0.02 s^{-1}
	H_2O_2	32 ± 2 s^{-1} [b]	0.48 ± 0.02 s^{-1}
	PAA	30 ± 3 s^{-1} [b]	0.47 ± 0.04 s^{-1}
harderohemeFe(II)	H_2O_2	41 ± 5 s^{-1} [b]	0.74 ± 0.01 s^{-1}
coprohemeFe(III)	H_2O_2	210	0.00060 $M^{-1}s^{-1}$
	PAA	3600	0.0050 $M^{-1}s^{-1}$
harderohemeFe(III)	H_2O_2	270	0.00090 $M^{-1}s^{-1}$

[a] The second order rate constants in each case describe the conversion of starting material to the first observable species, which is either an intermediate (for Fe(II)/O_2) or heme (for reactions starting with ferric hemes). Formation of ferric coproheme as the final product (in the case of the ferrous starting materials) or heme decomposition (ferric starting materials) is described by k_{decay}. This rate constant is first order for the ferrous substrates and second order for the ferric. [b] These values were insensitive to changes in oxidant concentration and are reported as first-order rate constants. Errors for k_{obs} are standard deviations from ≥3 measurements. Second order plots constructed from similarly measured k_{obs} had linear correlation values >95%.

Associated Content

Supporting Information

Additional supporting data include (S1) UV/vis spectra for all complexes in the manuscript; (S2-S9) further UV/vis and EPR spectroscopic characterization of reactions with O_2 and H_2O_2; (S10) redox titrations of the coproheme decarboxylase in complex with harderoheme and heme *b*. This material is available free of charge via the Internet at http://pubs.acs.org.

Acknowledgement

Support is gratefully acknowledged from the National Institutes of Health grants R01GM090260 (J.L.D.) and GM114787 (G. S. L.-R.).

Abbreviations

Acetonitrile, ACN; Chlorite Dismutase, Cld; Dehaloperoxidase, DHP; Dimethyl Sulfoxide, DMSO; Electron Paramagnetic Resonance Spectroscopy, EPR; Five Coordinate High Spin, 5cHS; High Performance Liquid Chromatography, HPLC; Peracetic Acid, PAA; Protocatechuate Dioxygenase, PCD; Protocatechuic Acid, PCA; Solvent Kinetic Isotope Effect, SKIE; Trifluoroacetic Acid, TFA

References

[1] Dailey, H., Gerdes, S., Dailey, T., Burch, J., and Phillips, J. (2015) Noncanonical coproporphyrin-dependent bacterial heme biosynthesis pathway that does not use protoporphyrin, *Proc. Natl. Acad. Sci. USA 112*, 2210-2215.

[2] Bali, S., Rollauer, S., Roversi, P., Raux-Deery, E., Lea, S. M., Warren, M. J., and Ferguson, S. J. (2014) Identification and characterization of the 'missing' terminal enzyme for siroheme biosynthesis in alpha-proteobacteria, *Mol. Microbiol. 92*, 153-163.

[3] Dailey, H. A. (1997) Enzymes of heme biosynthesis, *J. Biol. Inorg. Chem. 2*, 411-417.

[4] Layer, G., Reichelt, J., Jahn, D., and Heinz, D. W. (2010) Structure and function of enzymes in heme biosynthesis, *Protein Science 19*, 1137-1161.

[5] Celis, A. I., Streit, B. R., Moraski, G. C., Kant, R., Lash, T. D., Lukat-Rodgers, G. S., Rodgers, K. R., and DuBois, J. L. (2015) Unusual Peroxide-Dependent, Heme-Transforming Reaction Catalyzed by HemQ, *Biochemistry 54*, 4022-4032.

[6] Lobo, S. A., Scott, A., Videira, M. A., Winpenny, D., Gardner, M., Palmer, M. J., Schroeder, S., Lawrence, A. D., Parkinson, T., Warren, M. J., and Saraiva, L. M. (2015) *Staphylococcus aureus* haem biosynthesis: characterisation of the enzymes involved in final steps of the pathway, *Mol. Microbiol. 97*, 472-487.

[7] Dailey, H. A. (2002) Terminal steps of haem biosynthesis, *Biochem. Soc. Trans. 30,* 590-595.

[8] Layer, G., Reichelt, J., Jahn, D., and Heinz, D. (2010) Structure and function of enzymes in heme biosynthesis, *Protein Science 19*, 1137-1161.

[9] Layer, G., Pierik, A. J., Trost, M., Rigby, S. E., Leech, H. K., Grage, K., Breckau, D., Astner, I., Jaensch, L., Heathcote, P., Warren, M. J., Heinz, D. W., and Jahn, D. (2006) The substrate radical of Escherichia coli oxygen-independent coproporphyrinogen III oxidase HemN, *J. Biol. Chem. 281*, 15727-15734

[10] Lash, T. D. (2005) The enigma of coproporphyrinogen oxidase: How does this unusual enzyme carry out oxidative decarboxylations to afford vinyl groups? *Bioorg. Med. Chem. Lett. 15*, 4506-4509.

[11] Arnould, S., and Camadro, J. M. (1998) The domain structure of protoporphyrinogen oxidase, the molecular target of diphenyl ether-type herbicides, *Proc. Natl. Acad. Sci. USA 95*, 10553-10558.

[12] Wilks, A., and Heinzl, G. (2014) Heme oxygenation and the widening paradigm of heme degradation, *Arch. Biochem. Biophys. 544*, 87-95.

[13] Matsui, T., Nambu, S., Goulding, C., Takahashi, S., Fujii, H., and Ikeda-Saito, M. (2016) Unique coupling of mono- and dioxygenase chemistries in a single active site promotes heme degradation, *Proc. Natl. Acad. Sci. USA 113*, 3779-3784.

[14] D'Antonio, J., and Ghiladi, R. A. (2011) Reactivity of Deoxy- and Oxyferrous Dehaloperoxidase B from Amphitrite ornata: Identification of Compound II and Its Ferrous–Hydroperoxide Precursor, *Biochemistry 50*, 5999-6011.

[15] Du, J., Sono, M., and Dawson, J. (2010) Functional Switching of Amphit
rite ornata Dehaloperoxidase from O-2-Binding Globin to Peroxidase Enzyme Facilitated by Halophenol Substrate and H_2O_2, *Biochemistry 49*, 6064-6069.

[16] Dunford, H. B. (1999) *Heme Peroxidases*, Wiley-VCH.

[17] Bates, R. G., and Covington, A. K. (1968) Behavior of the glass electrode and other pH-responsive electrodes in biological media, *Ann. N Y Acad. Sci. 148*, 67-80.

[18] Degroot, D. C. (1967) Titrimetric determination of sodium dithionite with potassium hexacyanoferrate(3) as reagent and methylene blue as indicator, *Zeits. Analyt. Chemie Fresenius 229*, 335.

[19] Patil, P. V., and Ballou, D. P. (2000) The Use of Protocatechuate Dioxygenase for Maintaining Anaerobic Conditions in Biochemical Experiments, *Analyt. Bioch. 286*, 187-192.

[20] Streit, B., Kant, R., Tokmina-Lukaszewska, M., Celis, A., Machovina, M., Skaar, E., Bothner, B., and DuBois, J. (2016) Time-resolved Studies of IsdG Protein

Identify Molecular Signposts along the Non-canonical Heme Oxygenase Pathway, *J. Biol. Chem. 291*, 862-871.

[21] Pires, R. H., Venceslau, S. S., Morais, F., Teixeira, M., Xavier, A. V., and Pereira, I. A. C. (2006) Characterization of the Desulfovibrio desulfuricans ATCC 27774 DsrMKJOP complex - A membrane-bound redox complex involved in the sulfate respiratory pathway, *Biochemistry 45*, 249-262.

[22] D'Antonio, J., D'Antonio, E. L., Thompson, M. K., Bowden, E. F., Franzen, S., Smirnova, T., and Ghiladi, R. A. (2010) Spectroscopic and Mechanistic Investigations of Dehaloperoxidase B from *Amphitrite ornata*, *Biochemistry 49*, 6600-6616.

[23] Sun, S. F., Sono, M., Wang, C. X., Du, J., Lebioda, L., and Dawson, J. H. (2014) Influence of heme environment structure on dioxygen affinity for the dual function *Amphitrite ornata* hemoglobin/dehaloperoxidase. Insights into the evolutional structure-function adaptations, *Arch. Biochem. Biophys. 545*, 108-115.

[24] Wilks, A. (2002) Heme oxygenase: Evolution, structure, and mechanism, *Antioxidants & Redox Signaling 4*, 603-614.

[25] Wolfsberg, M., Van Hook, W. A., Paneth, P., and Rebelo, L. P. N. (2014) *Isotope Effects in the Chemical, Geological, and Bio Sciences*, Springer, 484 pp.

[26] Streit, B. R., Blanc, B., Lukat-Rodgers, G. S., Rodgers, K. R., and DuBois, J. L. (2010) How Active-Site Protonation State Influences the Reactivity and Ligation of the Heme in Chlorite Dismutase, *J. Am. Chem. Soc. 132*, 5711-5724.

[27] Hofbauer, S., Howes, B. D., Flego, N., Pirker, K. F., Schaffner, I., Mlynek, G., Djinovic-Carugo, K., Furtmuller, P. G., Smulevich, G., and Obinger, C. (2016) From chlorite dismutase towards HemQ-the role of the proximal H-bonding network in haeme binding, *Biosci. Rep. 36*, art:e00312.

[28] Celis, A. I., Geeraerts, Z., Ngmenterebo, D., Machovina, M. M., Kurker, R. C., Rajakumar, K., Ivancich, A., Rodgers, K. R., Lukat-Rodgers, G. S., and DuBois, J. L. (2015) A dimeric chlorite dismutase exhibits O2-generating activity and acts as a chlorite antioxidant in *Klebsiella pneumoniae* MGH 78578, *Biochemistry 54*, 434-446.

[29] Mayfield, J. A., Hammer, N. D., Kurker, R. C., Chen, T. K., Ojha, S., Skaar, E. P., and DuBois, J. L. (2013) The Chlorite Dismutase (HemQ) from Staphylococcus aureus Has a Redox-sensitive Heme and Is Associated with the Small Colony Variant Phenotype, *J. Biol. Chem. 288*, 23488-23504.

[30] Blanc, B., Mayfield, J. A., McDonald, C. A., Lukat-Rodgers, G. S., Rodgers, K. R., and DuBois, J. L. (2012) Understanding How the Distal Environment Directs Reactivity in Chlorite Dismutase: Spectroscopy and Reactivity of Arg183 Mutants, *Biochemistry 51*, 1895-1910.

[31] Goblirsch, B., Kurker, R. C., Streit, B. R., Wilmot, C. M., and DuBois, J. L. (2011) Chlorite Dismutases, DyPs, and EfeB: 3 Microbial Heme Enzyme Families Comprise the CDE Structural Superfamily, *J. Mol. Biol. 408*, 379-398.

[32] Hofbauer, S., Dalla Sega, M., Scheiblbrandner, S., Jandova, Z., Schaffner, I., Mlynek, G., Djinovic-Carugo, K., Battistuzzi, G., Furtmüller, P. G., Oostenbrink, C., and Obinger, C. (2016) Chemistry and molecular dynamics simulations of heme b-HemQ and coproheme-HemQ, *Biochemistry*, in press.

[33] Ayala, M., Roman, R., and Vazquez-Duhalt, R. (2007) A catalytic approach to estimate the redox potential of heme-peroxidases, *Biochem. Biophys. Res. Commun. 357*, 804-808.

[34] Blanc, B., Mayfield, J. A., McDonald, C. A., Lukat-Rodgers, G. S., Rodgers, K. R., and DuBois, J. L. (2012) Understanding How the Distal Environment Directs Reactivity in Chlorite Dismutase: Spectroscopy and Reactivity of Arg183 Mutants, *Biochemistry 51*, 1895-1910.

[35] Hayashi, T., Dejima, H., Matsuo, T., Sato, H., Murata, D., and Hisaeda, Y. (2002) Blue myoglobin reconstituted with an iron porphycene shows extremely high oxygen affinity, *J. Am. Chem. Soc. 124*, 11226-11227.

[36] Hobbs, C., Dailey, H. A., and Shepherd, M. (2016) The HemQ coprohaem decarboxylase generates reactive oxygen species: implications for the evolution of classical haem biosynthesis, *Biochem J.* in press.

[37] Presi, P., Stark, K. D., Stephan, R., Breidenbach, E., Frey, J., and Regula, G. (2009) Risk scoring for setting priorities in a monitoring of antimicrobial resistance in meat and meat products, In *Int J Food Microbiol*, pp 94-100, Netherlands.

[38] Mayfield, J. A., Hammer, N. D., Kurker, R. C., Chen, T. K., Ojha, S., Skaar, E. P., and DuBois, J. L. (2013) The chlorite dismutase (HemQ) from *Staphylococcus aureus* has a redox-sensitive heme and is associated with the small colony variant phenotype, *J. Biol. Chem. 88*, 23488-23504.

[39] Matsui, T., Nambu, S., Ono, Y., Goulding, C. W., Tsurnoto, K., and Ikeda-Saitot, M. (2013) Heme Degradation by Staphylococcus aureus IsdG and IsdI Liberates Formaldehyde Rather Than Carbon Monoxide, *Biochemistry 52*, 3025-3027.

[40] Poulos, T. L., and Fenna, R. E. (1994) Peroxidases - Structure, Function, And Engineering, In *Metal Ions In Biological Systems, Vol 30*, pp 25-75.

[41] English, A. M., and Tsaprailis, G. (1995) Catalytic Structure–Function Relationships in Heme Peroxidases, *Adv. Inorg. Chem. 43*, 79-125.

[42] Pfister, T. D., Gengenbach, A. J., Syn, S., and Lu, Y. (2001) The role of redox-active amino acids on compound I stability, substrate oxidation, and protein cross-linking in yeast cytochrome c peroxidase, *Biochemistry 40*, 14942-14951.

[43] Teraoka, J., and Kitagawa, T. (1981) Structural implication of the heme-linked ionization of horseradish peroxidase probed by the iron-histidine stretching Raman line, *J. Biol. Chem. 256*, 3969-3977.

[44] Smulevich, G., Feis, A., and Howes, B. D. (2005) Fifteen years of Raman spectroscopy of engineered heme containing peroxidases: What have we learned? *Acct. Chem. Res. 38*, 433-440.

[45] Streit, B. R., Blanc, B., Lukat-Rodgers, G. S., Rodgers, K. R., and DuBois, J. L. (2010) How Active-Site Protonation State Influences the Reactivity and Ligation of the Heme in Chlorite Dismutase, *J. Am. Chem. Soc. 132*, 5711-5724.

[46] Hofbauer, S., Howes, B. D., Flego, N., Pirker, K. F., Schaffner, I., Mlynek, G., Djinović-Carugo, K., Furtmüller, P. G., Smulevich, G., and Obinger, C. (2016) From chlorite dismutase towards HemQ - the role of the proximal H-bonding network in haeme binding, *Biosci Rep 36* in press.

[47] Takahashi, S., Wang, J., Rousseau, D. L., Ishikawa, K., Yoshida, T., Host, J. R., and Ikeda-Saito, M. (1994) Heme-heme oxygenase complex. Structure of the catalytic site and its implication for oxygen activation, *J. Biol. Chem. 269*, 1010-1014.

[48] Sun, J., Wilks, A., Ortiz de Montellano, P. R., and Loehr, T. M. (1993) Resonance Raman and EPR spectroscopic studies on heme-heme oxygenase complexes, *Biochemistry 32*, 14151-14157.

[49] Matsui, T., Unno, M., and Ikeda-Saito, M. (2010) Heme oxygenase reveals its strategy for catalyzing three successive oxygenation reactions, *Acc. Chem. Res. 43*, 240-247.

[50] Wilks, A. (2002) Heme oxygenase: evolution, structure, and mechanism, *Antioxid. Redox Signal., 4*, 603-614.

[51] Valentine, J. S., Foote, C. S., Greenberg, A., and Liebman, J. F. (1995) *Active Oxygen in Biochemistry*, Vol. 3, Springer.

[52] Dailey, T. A., Boynton, T. O., Albetel, A.-N., Gerdes, S., Johnson, M. K., and Dailey, H. A. (2010) Discovery and Characterization of HemQ: an essential heme biosynthetic pathway component, *J. Biol. Chem.285*, 25978-25986.

CHAPTER FIVE

A STRUCTURE-BASED MECHANISM FOR OXIDATIVE DECARBOXYLATION REACTIONS MEDIATED BY AMINO ACIDS AND HEME PROPIONATES IN COPROHEME DECARBOXYLASE (HEMQ)

Contribution of Authors and Co-Authors

Author: Arianna I. Celis

Contributions: Expressed and purified WT- and most *Sa*HemQ and *Gs*HemQ protein variants. Prepared Fe(III)-coproporphyrin III and Mn(III)-coproporphyrin III- HemQ complexes. Performed UV-Vis, HPLC, fluorescence and O_2-electrode measurements. Analyzed and interpreted data. Contributed to optimization of crystallization conditions and crystal structure building. Contributed to the writing and preparation of this manuscript.

Co-Author: George H. Gauss

Contributions: Built *Gs*HemQ crystal structure. Provided invaluable insight and mentoring through crystallization process. Contributed to the writing and preparation of this manuscript.

Co-Author: Bennett R. Streit

Contributions: Expressed and purified and characterized a portion of the *Sa*HemQ protein variants. Contributed to the writing and preparation of this manuscript.

Co-Author: Krista Shisler

Contributions: Expressed and purified and characterized a portion of the *Sa*HemQ protein variants. Performed Mn(III)-coproporphyrin III-HemQ reactivity assays.

Co-Author: Garrett C. Moraski

Contributions: Provided useful discussions about Mn reactivity and drawing the potential reaction mechanism.

Co-Author: Kenton R. Rodgers

Contributions: Measured and analyzed rR data. Provided support and very valuable insight in preparation of manuscript. Contributed to the writing and preparation of this manuscript.

Co-Author: Gudrun S. Lukat-Rodgers

Contributions: Measured and analyzed rR data. Provided support and very valuable insight in preparation of manuscript. Contributed to the writing and preparation of this manuscript.

Co-Author: John W. Peters

Contributions: Provided overview of preparation of samples, interpretation of results, and manuscript preparation.

Co-Author: Jennifer L. DuBois

Contributions: Provided important insight and overview of the preparation of samples, experiment design and interpretation of results. Contributed largest part to the writing and preparation of this manuscript.

Manuscript Information Page

Arianna I. Celis, George H. Gauss, Bennett R. Streit, Krista Shisler, Garrett C. Moraski, Kenton R. Rodgers, Gudrun S. Lukat-Rodgers, John W. Peters, Jennifer L. DuBois

Journal of the American Chemical Society

Status of Manuscript:
____ Prepared for submission to a peer-reviewed journal
____ Officially submitted to a peer-review journal
__ _ Accepted by a peer-reviewed journal
_X_ Published in a peer-reviewed journal

Publisher: American Chemical Society

Reprinted with permission from Celis, A. I.; Gauss, G. H.; Streit, B. R.; Shisler, K.; Moraski, G. C.; Rodgers, K. R.; Lukat-Rodgers, G. S.; Peters, J. W.; DuBois, J. L., Structure-Based Mechanism for Oxidative Decarboxylation Reactions Mediated by Amino Acids and Heme Propionates in Coproheme Decarboxylase (HemQ). *J Am Chem Soc* **2017,** *139* (5), 1900-1911.Copyright 2017 American Chemical Socitety.

CHAPTER FIVE

A STRUCTURE-BASED MECHANISM FOR OXIDATIVE DECARBOXYLATION REACTIONS MEDIATED BY AMINO ACIDS AND HEME PROPIONATES IN COPROHEME DECARBOXYLASE (HEMQ)

Arianna I. Celis,[1] George H. Gauss,[1] Bennett R. Streit,[1] Krista Shisler,[1] Garrett C. Moraski,[1] Kenton R. Rodgers,[2] Gudrun S. Lukat-Rodgers,[2] John W. Peters,[1] Jennifer L. DuBois[1]

[1]*Department of Chemistry and Biochemistry, Montana State University, Bozeman, MT 59717*
[2]*Department of Chemistry and Biochemistry, North Dakota State University, Fargo, ND 58108*

Abstract

Coproheme decarboxylase catalyzes two sequential oxidative decarboxylations with H_2O_2 as the oxidant, coproheme III as substrate and cofactor, and heme *b* as the product. Each reaction breaks a C-C bond and results in net loss of hydride, via steps that are not clear. Solution and solid-state structural characterization of the protein in complex with a substrate analog revealed a highly unconventional H_2O_2-activating distal environment with the reactive propionic acids (2 and 4) on the opposite side of the porphyrin plane. This suggested that, in contrast to direct C-H bond cleavage catalyzed by a high-valent iron intermediate, the coproheme oxidations must occur through mediating amino acid residues. A tyrosine that hydrogen bonds to propionate 2 in a position analogous to the substrate in ascorbate peroxidase is essential for both

decarboxylations, while a lysine that salt bridges to propionate 4 is required solely for the second. A mechanism is proposed in which propionate 2 relays an oxidizing equivalent from a coproheme compound I intermediate to the reactive deprotonated tyrosine, forming Tyr▪. This residue then abstracts a net hydrogen atom (H▪) from propionate 2, followed by migration of the unpaired propionyl electron to the coproheme iron to yield the ferric harderoheme and CO_2 products. A similar pathway is proposed for decarboxylation of propionate 4, but with a lysine residue as an essential proton shuttle. The proposed reaction suggests an unprecedented relay of heme-mediated e^{-}/H^{+} transfers and a novel route for the conversion of carboxylic acids to alkenes.

Introduction

Activation of O_2 or H_2O_2 by heme often leads to the generation of high-valent iron-oxo (ferryl) intermediates.[1] In reactions catalyzed by heme peroxidases, donation of two electrons from the Fe(III)-porphyrin complex results in heterolytic cleavage of the HO-OH bond. The resulting compound I intermediate carries one oxidizing equivalent on the iron and the other in the porphyrin π system, and is consequently described as Fe(IV)=O coupled to a porphyrin radical cation (por•+):[2, 3]

$$\mathrm{Fe(III)por} + \mathrm{H_2O_2} \ \ \bullet\mathrm{Fe(IV){=}O(por}\bullet{+}) + \mathrm{H_2O} \qquad (1)$$

How this central intermediate forms and how it oxidizes compounds, sometimes over long distances, are longstanding questions in catalysis research. In reactions catalyzed by many cytochrome P450s and peroxidases,[4] 1 e- + 1 H^+ are transferred from a substrate to compound I. Such reactions, known as proton coupled electron transfers,[5] can occur in a single concerted proton/electron transfer step. Alternatively, as in the catalytic model for P450s,[3] the proton may migrate to the ferryl oxygen while the electron enters an orbital that is porphyrin-based. The overall reaction is described as hydrogen atom transfer.[6]

The proton and electron may have distinct routes to their separate destinations, though in only few cases have these been rigorously described. In ascorbate peroxidase (APX), the ascorbate substrate binds near and donates a hydrogen bond (H-bond) to one of the heme propionates (Fig. S1).[7, 8] Hydrogen atom transfer from ascorbate, in both APX and a synthetic heme complex designed to mimic it,[9] occurs with the propionate acting both as a base toward the proton and as the conduit for the electron to por•+. The proton is shuttled to an active site arginine and water molecules before finally arriving at the ferryl oxygen,[10] and the resulting Fe(IV)=O + H^+ or Fe(IV)-OH complex is known as compound II.[11] Transfer of a hydrogen atom from a second substrate leads back to the ferric heme and a molecule of water. Representing the substrate as SH gives the general reaction scheme:

$$\mathrm{Fe(IV){=}O(por{\bullet}{+}) + SH \bullet Fe(IV){=}O(por) + H^+ + S{\bullet}} \qquad (2)$$

$$\mathrm{Fe(IV){-}OH(por) + SH \bullet Fe(III)(por) + H_2O + S{\bullet}} \qquad (3)$$

The propionate in APX (Fig. S1) allows the heme to transmit oxidizing equivalents, from the site where the heme iron converts H_2O_2 to its catalytically activated compound I form, to the substrate binding site. In some peroxidases, including cytochrome *c* peroxidase

(CCP) and lignin peroxidase (LnP),[12-14] the sites of heme-Fe(III)/H_2O_2 reaction and substrate oxidation may be quite spatially remote. Redox-active amino acid side chains[15-17] in addition to the propionates[18] act as internal mediators within these enzymes. These supply the means to move oxidizing equivalents away from por•+ and to the site where substrates bind, greatly extending the catalytic reach of heme as an oxidation catalyst.

Here, we describe the combined structural and solution-state characterization of a H_2O_2-activating heme protein in which the iron and the pair of organic substrates have an unusual spatial and electronic relationship. The enzyme uses H_2O_2 as an oxidant in the successive decarboxylations of propionates 2 and 4 of iron coproporphyrin III (coproheme), which serves as both substrate and cofactor in the reactions (Scheme 1). Use of H_2O_2 as the biological oxidant in a decarboxylation or indeed any C-C bond cleavage is a highly uncommon feature of this enzyme,[19] which is encoded by the *hemQ* gene and which is responsible for the last step in heme biosynthesis in many gram positive bacteria.[20] The 1.8 Å resolution structure of the protein in complex with its Mn(III)-containing substrate analog clearly shows the two reactive propionates residing below the coproheme plane, in a position where they cannot directly make contact with a ferryl intermediate. Instead, the structure suggests and the solution data support an electron/proton relay involving the heme, its propionates, and reactive amino acid side chains, leading to net transfers of an electron and a hydrogen atom from the reactive propionates themselves. The structurally-inferred, experimentally supported reaction mechanism is unprecedented in biology. As such, it suggests possible new avenues for extending the catalytic repertoire of synthetic heme complexes.

Scheme 1. Reaction catalyzed by coproheme decarboxylase†

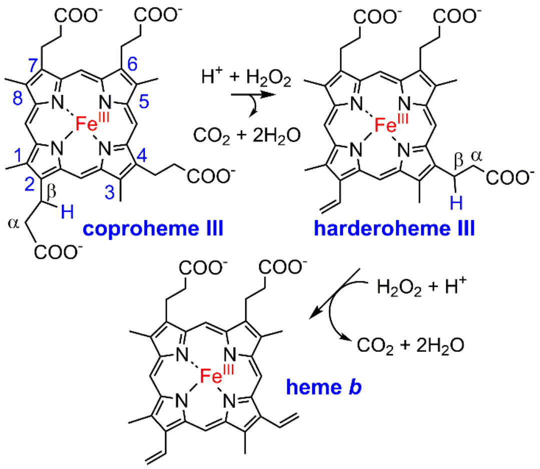

†Net loss of $2e^-$ + H^+ from the Cα-Cβ bond of each propionate occurs along with decarboxylation. Involvement of Fe(III), H_2O_2, and harderoheme III in the reaction scheme was previously verified.[21, 22] The porphyrin species are drawn in their expected protonation states at pH 7.

Experimental Procedures

Expression, Purification, and Ligand Binding to WT and Mutant Coproheme Decarboxylases

The sequence of the protein encoded by the *hemQ* from *Geobacillus stearothermophilus* (*Gs*, NCBI accession WP_053414189, PDB ID: 1T0T)[23] was used to design a codon-optimized synthetic *hemQ* gene for expression in untagged form in *Escherichia coli*. The gene was inserted into a pET14(a) plasmid between the Nde1 and Xho1 restriction sites and used to transform competent *E. coli* Tuner (DE3) cells (Novagen). A similar construct for expressing the untagged, homologous protein from *Staphylococcus aureus* (*Sa*) was previously described.[21] A QuikChange Lightning Site-Directed Mutagenesis Kit (Agilent) was used to generate site-directed mutants of *Sa* decarboxylase using the manufacturer's instructions and primers in Table S1. For residues closer to the protein interior, substitutions were made from Tyr/Ser, or Trp/Phe- in order to retain the hydrophobic/hydrophilic character of the WT residue while dramatically changing its size or chemical functionality. Residues at the solvent interface were substituted by Ala.

Proteins were overexpressed and isolated at >95% purity by reverse-anion exchange and gel filtration chromatography as previously described.[21] Concentrated proteins (Amicon, 10,000 MWCO centrifuge filters) were incubated in the dark with gentle stirring at 4 °C for 24 h with either the substrate ferric coproheme III or the substrate analog Mn(III) coproporphyrinate III (coproporphyrinate III = *tetrakis*-2,4,6,7-propionate-protoporphyrin, Frontier Scientific) in a 1:1 subunit:coproheme ratio. Unbound coproheme was removed and the protein-ligand complexes further purified on an S-200 Sephacryl gel filtration column (0.4 ml/min). Fractions were collected using an AKTA purification system and then screened via UV/Vis spectroscopy (Cary50) for coproheme content. Fractions with Rz values ≥0.8 (Rz = absorbanceSoret/absorbance280nm) were pooled. The Bradford and pyridine hemochrome assays for protein and released coproheme, respectively, were used to determine the coproheme occupancy in the purified complexes. Extinction coefficients determined for the *Gs* coproheme decarboxylase complexes were $\varepsilon_{Soret} = 110.6\ mM^{-1}\ cm^{-1}$ (Fe-coproheme)[21] and $\varepsilon_{Soret} = 69.7 \pm 6.6\ mM^{-1}\ cm^{-1}$ (Mn-coproheme) (Fig. S2).

Structure Determination

The *Gs* decarboxylase in complex with Mn(III)coproheme was crystallized by hanging drop vapor diffusion at 20 °C. Drops were assembled by mixing the complex (7 mg⁄mL in 10 mM HEPES-NaOH pH 7.5) with an equal volume of reservoir solution (0.1 M citrate pH 5.0-5.5, 15-25 % (w/v) polyethylene glycol 3350). Bright red crystals of the complex formed after approximately 2 weeks. Crystals were briefly soaked in reservoir solution supplemented with 15% (w/v) glycerol as a cryoprotectant prior to freezing in liquid N_2. An X-ray diffraction dataset to 1.8 Å was measured at Stanford Synchrotron Radiation Lightsource beamline 14-1 and processed with autoxds.[24] The structure was determined by molecular replacement using Phaser[25] in the CCP4 program suite[26]. Phaser was supplied with the non-substrate bound structure as a search model (PDB ID 1T0T). Model building and refinement and was done using Coot[26] and Phenix.[27] Electron density maps of the Phaser solution showed the presence of a ligand adjacent to His172 (*Sa* sequence numbering, Fig. S3); Mn-coproheme (designated as 76R in the PDB file) was modeled into this electron density. Iterative rounds of model building with Coot and refinement with Phenix[24] yielded the final model (PDB ID 5T2K) with R_{free} = 17.6 % and R_{work} = 15.4 %. The following residues are not included in the final model due to weak electron density: residues 115-123, 114-117, 112-117, 114-119 and 115-123 (all *Gs* numbering) in subunits A, B C, D and E, respectively. Molecular graphics were created with PyMOL (www.pymol.org).

Determining Protein-heme Dissociation Constants

Values of K_D for equilibrium binding of decarboxylases/hemes were determined by fluorescence quenching (Cary). Tryptophan fluorescence (5 µM subunit) was excited at 295 nm and emission monitored at 340 nm. Quenched emission at 340 nm was plotted versus the concentration of added heme ligand. Plots were fitted with the Langmuir-Hill equation to determine the K_D.

$$\theta = \frac{[L]^n}{KD+[L]^n} \qquad (4)$$

θ is the fraction of ligand-binding sites occupied by the ligand, [L] is the ligand concentration, and n is the Hill coefficient describing cooperativity.

Reactions of Decarboxylase-coproheme Complexes Monitored Following Titrimetric Addition of Oxidants

Complexes of decarboxylase with Mn- or Fe-coproheme (pH 7.4, 20 °C) were mixed with aliquots of H_2O_2 or peracetic acid from 1-50 mM stocks. The progress of reactions was monitored by UV/vis spectroscopy (Cary50, samples 10 µL in heme species). Reaction products were analyzed by high performance liquid chromatography (HPLC) and HPLC coupled to electrospray ionization mass spectrometry (HPLC-ESI-MS) (samples 40 µM in the heme species). MS was used to verify the identities of all reactants and products via their exact masses. Fe-bound coproheme, harderoheme (isomers III or IV), and heme *b*, or Mn-bound coproheme/heme *b* were separated and quantified via their integrated HPLC peak intensities referenced to standard curves:

HPLC: 20 µL samples were injected onto a Hypersil Gold PFP 5µm column (150 mm x 4.6 mm, Thermo Fisher) attached to an Agillent1100 series instrument. Solvent A was H_2O with 0.1% trifluoroacetic acid (TFA) and Solvent B was acetonitrile (ACN) with 0.1% TFA. Samples were run at a flow rate of 2 mL/min starting with isocratic 70% A:30% B for 3 min, followed by a linear gradient transitioning from 70% A to 5% A over 12 min. This was followed by isocratic 5% A for 5 min and a final isocratic run of 30 % A for 3 min. UV/vis detection was at 411 nm. Standard curves ranging from 0 – 500 pmol of the tetrapyrroles. HPLC peak areas were determined in triplicate and error bars are reported as ± 1 standard deviation.

HPLC-ESI-MS: The chromatography conditions described above were used were used with an Agilent PLRP-S PSDVB column (PL1312-1300) and 1290 HPLC system. Mass spectra were obtained on an Agilent 6538 quadrupole time of flight (QTOF) instrument with ESI source (drying gas 8.0 L/min, drying gas heat at 350°C, nebulizer 55 psi, capillary voltage 3500 V, capillary exit 100 V). Spectra were collected in negative mode from 50 to 1700 m/z at a rate of 2 Hz.

Steady State Kinetics of Catalase Reactions

The conversion of H_2O_2 to O_2 and water by various decarboxylase-metalloporphyrin complexes was monitored continuously over time via polarography using a Clark O_2 electrode (YSI). The electrode was equilibrated to 20 °C for 1 h using a circulating water bath and calibrated to the concentration of O_2 in air-saturated distilled/deionized water. Reactions were carried out in 2 mL volumes (50 mM potassium phosphate buffer, pH 7.4) with 4 μM of enzyme-porphyrin complex and initiated by addition of 10 -100 mM H_2O_2 stocks via airtight syringe (5-20 μL). Linear initial rates (v_i) were fit by least-squares regression to the first 5–10% of the progress of reaction curves (Kaleidagraph). Plots of v_i versus H_2O_2 concentration were fit to the Michaelis Menton equation:

$$\frac{v}{E} = \frac{k_{cat}[H2O2]}{K_m+[H2O2]} \tag{5}$$

Here, E is the concentration of enzyme-metalloporphyrin complex. Unreacted H_2O_2 was quantified at the end of reactions using horseradish peroxidase (HRP) and a colorimetric substrate (2,2'-Azinobis [3-ethylbenzothiazoline-6-sulfonic acid]-diammonium salt, ABTS). 0.5U/mL HRP and 500 µM ABTS (final concentrations) were added to the samples and incubated (25 °C) for 1hr. The absorbance at 738 nm was recorded and compared with a standard curve generated over 5-100 µM H_2O_2].

Resonance Raman (rR) spectroscopy

Ferric samples for rR experiments were prepared at 25 to 60 µM coproheme-decarboxylase complex in 100 mM sodium phosphate at pH 7.5 Ferrous complexes were prepared anaerobically at 20 °C from ferric enzymes by reduction with an excess of buffered sodium dithionite. The CO complexes were prepared by flushing the ferrous enzymes with ^{12}CO or ^{13}CO (99% ^{13}C).

The rR spectra were recorded using the 135° backscattering geometry and f1 collection using a previously described spectrometer.[21] Either the 406.7-nm or the 413.1-nm emission line from a Kr+ laser was used for Raman excitation, and the laser beam was focused to a line on a spinning 5 mm NMR tube. External spectral calibration standards for the rR spectra were toluene, acetone, methylene bromide, and d^6-

dimethylsulfoxide. Laser power for ferric samples ranged from 4 to 12 mW; ferrous CO complexes required laser irradiation powers of 1 to 3 mW to prevent CO photolysis. To check the integrity of the rR samples, their UV-visible spectra were checked before and after irradiation in the laser beam. Normal mode assignments were made by analogy to other heme proteins. Peak fitting analyses of the rR spectra were based on the minimum number of peaks required to achieve statistically valid fits of the spectra. Band shapes were assumed to be Gaussian and were well modeled by Gaussian line-shape functions.

Results

Co-crystals of the Decarboxylase with Mn-Coproheme Diffracted to 1.8 Å Resolution

Our bio-chemical characterization of the coproheme decarboxylase and its genetic knock out has focused on S. aureus due to the importance of pathogenic strains of that spe-cies.[21, 28] Robotic screening of thousands of crystallization conditions failed to generate diffraction-quality crystals of the enzyme from Sa, either alone or in complex with metalloporphyrins. However, the substrate-free structure of a coproheme decarboxylase from another member of its phylum, *Geobacillus stearothermophilus*, was available through a structural genomics consortium (PDB ID: 1T0T)[23]. The *Gs* and *Sa* proteins have 59% sequence identity (Fig. S3), and solution state spectra (Fig. S4) and reactivity (Fig. S5) for the two are similar. We therefore attempted to generate crystals with Fe(III)coproheme using the *Gs* decarboxylase, which was likewise unsuccessful. The enzyme complex with the substrate analog Mn(III)coproheme, however, yielded large crystals that diffracted to 1.8 Å resolution (Table S2). In solution, the

Mn(III)coproheme-decarboxylase complex did not react with H_2O_2 (up to 50 eq). This complex was stable in the presence of O_2 and ionizing X-ray radiation, conditions under which H_2O_2 may be spontaneously produced. However, the Mn(III) complex reacted with peracetic acid (PAA), yielding the expected Mn-substituted harderoheme intermediate and heme *b* products with similar numbers of eq as the Fe-substrate (Fig. S6).[22] These results suggest that the Mn(III)coproheme binds in the catalytic orientation but is incapable of activating H_2O_2 and therefore forms a stable complex.

Structural changes associated with substrate binding to coproheme decarboxylase are confined to the C-terminus

Like other members of its family (Pfam 06778, which includes both chlorite dismutase [Cld] and coproheme decarboxylase enzymes),[29] the crystal structure of the *Gs* coproheme decarboxylase is a homopentamer where each subunit consists of two ferrodoxin-like α/β domains connected by a pseudo-twofold axis (Fig. 1A). The superimposed structures of the ligand-free (PDB ID 1T0T)[23] and -bound (5T2K) forms of subunit A are shown in Fig. 1B (Cα RMSD = 0.47 Å). The peptide backbone and side chains mostly overlay, with the structural changes accompanying ligand binding confined to the C-terminal region housing the Mn-coproheme. In particular, residues 111-121 form part of a loop on the solvent-exposed exterior of the ligand-free homopentamer, where they might constitute the site of substrate entry/product egress. (*Sa* residue numbering is used except where noted.) The most dramatic rearrangements in the ligand-bound structure occur here (Fig. 1C). Though several of its side chains could not be modeled due to weak electron density in this region for the individual coproheme-bound subunits, the loop as a whole folds inwards toward the coproheme in the ligand-bound structure. This rearrangement brings the side chain of Asn112, which occupies a position inside the substrate-binding pocket, toward the protein exterior in the ligand-bound structure. Tyr113 and Arg131, by contrast, form new contacts with propionates 4 and 6, respectively, which could be significant for the oxidative decarboxylation mechanism (see below).

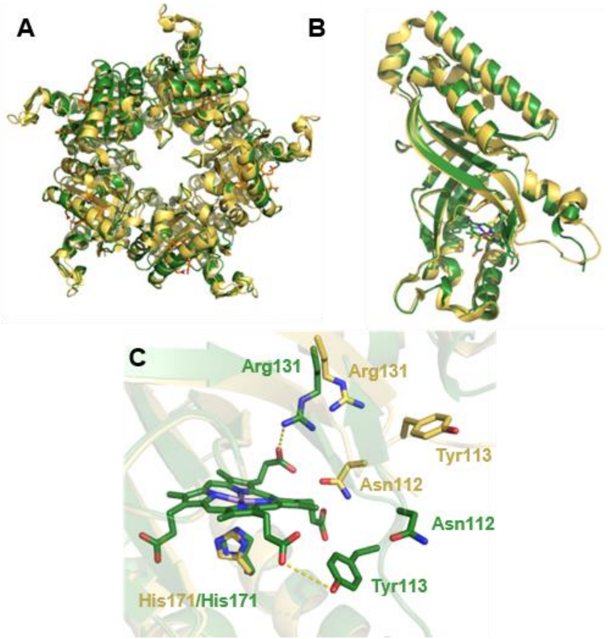

Figure 5.1. Superposition of the apo and ligand-bound forms of coproheme decarboxylase illustrate the effects of tetrapyrrole binding. A. The coproheme-bound decarboxylase homopentamer is shown in green with the bound coproheme ligands as sticks (orange) (5T2K) and the ligand-free structure in yellow (1T0T). The view is down the pseudo-C_5 axis with the coproheme-containing domains oriented toward the viewer. B. Superimposition of an individual subunit of coproheme decarboxylase in the apo (yellow) and ligand-bound (green) forms. Differences are localized around a flexible loop near residues 111-120 and the Mn-coproheme binding site. C. Close-up view of the Mn-coproheme binding site, illustrating prominent shifts in the positions of side chains for Asn112, Tyr113, and Arg131 in the apo (yellow) and ligand-bound (green) forms.

Coproheme binding site structure: Implications for mechanism

The electron density map for Mn-coproheme bound to the active site (Fig. 2A) illustrates the unambiguous assignment of the atomic positions of the porphyrin and all of its side chains in the crystal structure. The porphyrin ring is slightly ruffled, occupying roughly the same position as the molecule of solvent in the ligand-free structure or the heme *b* which serves as a cofactor in Clds. However, the coproheme is rotated approximately 90° about the pseudo-C_4 axis relative to the heme *b* in either Cld (Fig. S7) or energy-minimized predictions of the structure of the decarboxylase-coproheme complex.[30] This orientation positions the two unreactive propionates (6 and 7, Scheme 1) pointing outward from the protein toward the solvent, where they occupy positions on the distal side of the heme plane (Fig. 2B). The two reactive propionates (2 and 4), by contrast, are rotated to the proximal side of the porphyrin plane and well beyond the reach of the open, distal coordination site.

On the other side of the plane (proximal pocket), histidine 172 coordinates the Mn of the coproheme (2.3 Å) via the imidazole-N_ε atom (Fig. 2B). The imidazole-N_ε is H-bonded to a water molecule, which is itself H-bonded to Ser222, Asp219, and the Met216 main chain carbonyl. Most H_2O_2-activating heme enzymes as well as Clds have an aspartic or glutamic acid as the hydrogen bonding donor in the analogous position,[31-33] leading to some degree of negative charge in the proximal ligand. The negatively charged histidine supplies an electronic push that favors heterolytic cleavage of the O-O bond in the heme-Fe(III)-OOH that forms *in trans*. Water is a comparatively weak H-bonding partner;

consistent with previously reported rR spectra,[21] His172 is electronically neutral, leading to a more globin-like metal-His interaction.

The distal pocket (Fig. 2C) is likewise distinct from other H_2O_2-reactive heme proteins. Canonical peroxidases share a distal histidine with a relatively low p*K*a due to a nearby arginine.[33] In its deprotonated form, the distal His acts as a base toward H_2O_2 (p*K*a = 11). Heterolytic bond cleavage in the resulting heme-Fe(III)-OOH complex is catalyzed by proton donation from the His-Arg pair, yielding Compound I and H_2O. By contrast, the distal environment in the coproheme decarboxylase is relatively hydrophobic. Ile187 hovers over the center of the porphyrin plane. Gln185 resides at its side and in the same sequence/structural position occupied by the distal arginine from Clds (Fig. S8). This residue, which distinguishes the decarboxylase- and dismutase-encoding *hemQ* and *cld* genes, is important for the heme-dependent chlorite (ClO_2^-) decomposition mediated by Clds to yield Cl^- and O_2.[34]

At the edge of the distal pocket nearest the solvent interface, the Arg131 side chain sits at the center of a H-bonding network involving propionate 6, Gln185, and a water molecule (Fig 2C). This water occupies a position close to where the terminal oxygen of a coproheme-Fe(III)-OOH intermediate could reside. Though the solution p*K*a of the Arg side chain is high (12.5) and the propionate is low (3.2-3.5), the two together could in principle act as a base toward H_2O_2, an acid toward coproheme-Fe(III)-OOH, or both. An arginine side chain with a similar H-bond to a propionate has been proposed to act as a distal base *in lieu* of His-Arg in dye decoloring peroxidases.[35] Prior work showed that the second order reaction between the decarboxylase-coproheme complex and H_2O_2, which leads to the ferric heme *b* complex, accelerates with pH (~3-fold, p*K*a = 7.4) and is solvent-isotope dependent (average $k(H_2O):k(D_2O) = 2.2$).[22] Both results suggest the involvement of proton movement in the rate limiting step of the H_2O_2 reaction. However, pH has a much larger influence over the analogous, acid-base-catalyzed steps in heme peroxidases.[33, 36] The roles of these residues and of pH therefore remain to be determined.

Reactive propionates 2 and 4 are each converted (net $2e^{-}+1H^{+}$ lost per propionate) to a vinyl group and CO_2 by a H_2O_2-mediated oxidation reaction (Scheme 1). Key residues surrounding each are shown in Figs. 2D and E. Propionate 2, which reacts first,[22] forms H-bonds to the side chain hydroxyls of Ser223 (2.2 Å) and Tyr145 (2.8 Å). The former is part of a H-bonding network leading to the proximal His172. The latter is just 3.1 Å away from the $C_ß$ of the propionate (Scheme 1).

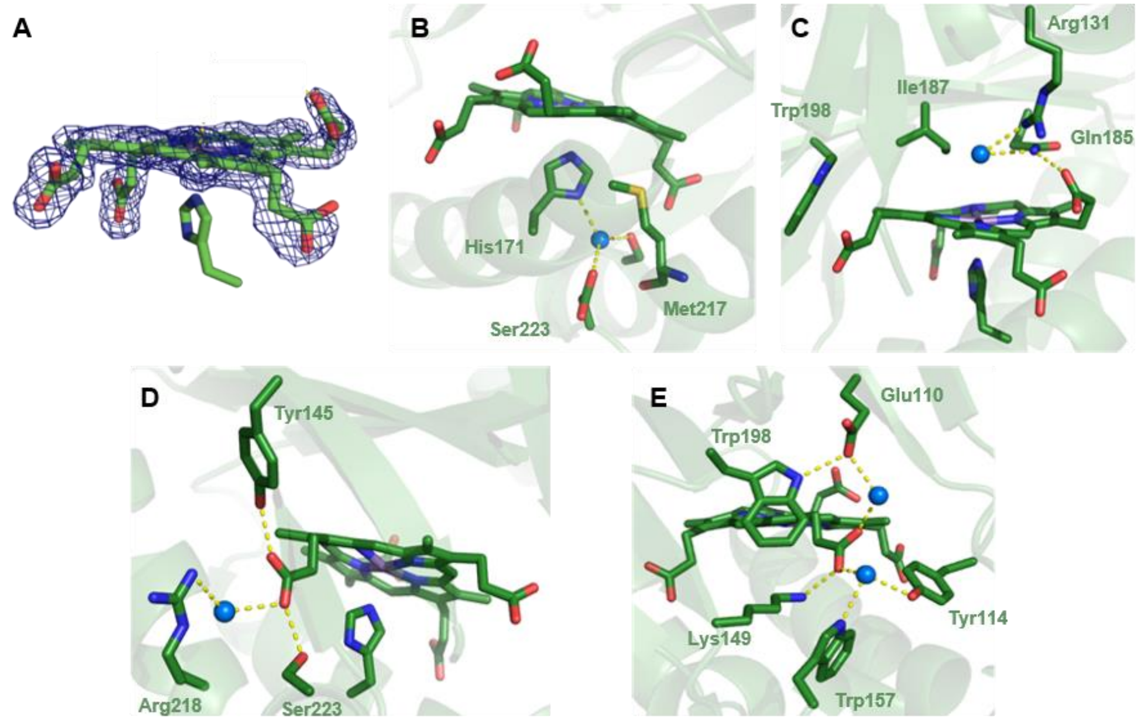

Figure 5.2. The structure of the coproheme binding site in coproheme decarboxylase has important implications for the chemical mechanism. A. View of the Mn-coproheme in subunit B with *F*o-*F*c omit electron density map contoured at 3σ. B. The tetrapyrrole is slightly ruffled, with the two reactive propionates (2 and 4) below its approximate plane. A close-up view of the His171 ligand in the (proximal) pocket beneath the substrate analog shows that it binds to the metal through the imidazole-N_ε. The imidazole-N_δ forms an apparent hydrogen bond to a water molecule, which is itself hydrogen bonded to Ser223 and Asp220. C. The distal region above the coproheme plane is shown, highlighting the pair of unreactive propionates. The R131 side chain is part of a hydrogen bonding network involving propionate 6, Gln185, and a water molecule that occupies a position close to where the terminal oxygen of Fe-OOH might reside. The residue immediately over the coproheme plane is Ile187. The environment surrounding the reactive propionates 2 and 4 is shown in D and E, respectively.

This was the observed site of net hydrogen atom removal catalyzed by coproporphyrinogen oxidase,[37] an enzyme that carries out analogous oxidative decarboxylations on the metal-free, reduced analog of coproheme III. Removal of a hydrogen atom at this position leaves a carbon radical conjugated to, and consequently stabilized by, the tetrapyrrole. Additionally, propionate 2 is H-bonded to a water molecule which is in turn H-bonded to Arg218. Propionate 4 is directly H-bonded/salt-bridged to Lys149 (2.7 Å), and indirectly to Trp156 and Tyr113 by a network of H-bonds including a bridging water molecule. Another H-bond network leads to Trp198 via the $O_{\varepsilon 1}$ atom of Glu109 and a second water molecule. The N_{ε} of Trp198 has the closest through-space approach to the C_{β} of propionate 4 (3.9 Å). The occurrence of multiple residues with possible redox (Tyr, Trp) and proton-translocating activities suggests one or more may be involved in catalyzing the two oxidative decarboxylations.

The solution state Sa and Gs decarboxylase heme environments are similar to one another and distinct from chlorite dismutases. Resonance Raman spectra were measured for the Sa and Gs decarboxylases in complex with ferric coproheme and heme b (Fig. 3A). Comparison of the low frequency spectra of the coproheme complexes demonstrated similarities in their propionate bending ($\delta(C_{\beta}C_{c}C_{d})$, in this nomenclature C_c and C_d correspond to carbons labeled C_{β} and C_{α} in Scheme 1) frequencies (Sa: 374 and 393 cm^{-1}; Gs: 374 and 395 cm^{-1}). Reaction of both coproheme-decarboxylase complexes with H_2O_2 (Fig. S3) yielded comparable rR spectral changes,[21] including the appearance of bands corresponding to vinyl stretching and bending modes with very similar frequencies (1627 and 415-418 cm^{-1}, respectively). The 374-cm^{-1} propionate bending frequency is unaffected by decarboxylation while the second propionate bending frequency decreases by 4 cm^{-1} in both decarboxylases. The similarities between the solution spectra and reactivities of the Gs and Sa enzyme-substrate complexes suggest it is reasonable to expect that their solid state structures, especially the positioning of their reactive coproheme 2- and 4-propionate groups, are comparable.

Prior simulations of coproheme binding to the decarboxylase had the non-reactive propionates 6 and 7 in the same positions as the propionates of the heme *b* in the Cld structures, in contrast with the solid state structure shown here.[30] Unique peripheral substituent environments of ferric heme *b* in decarboxylases and Clds are supported by their propionate and vinyl ($\delta(C_\beta C_a C_b)$) bending mode frequencies. The decarboxylase complexes exhibit $\delta(C_\beta C_c C_d)$ and $\delta(C_\beta C_a C_b)$ frequencies 8-11 cm^{-1} and 4-8 cm^{-1} lower, respectively, relative to those modes in WT *Da*Cld and *Da*Cld Arg183Gln mutant (Fig. 3A).[34] The latter substitution exchanges the Cld-associated distal Arg with the distal Gln of the *Sa* decarboxylase, rendering their distal environments more similar. To further examine the solution state environment of the non-reactive propionates, the rR spectrum for the ferrous *Sa* decarboxylase-heme *b* complex with CO was measured and compared with counterpart spectra from WT *Da*Cld and the *Da*Cld(R183Q) (Fig. 3B). Comparison of the decarboxylase-CO and Cld-CO spectra clearly shows that the bands associated with propionate and vinyl bending, as well as

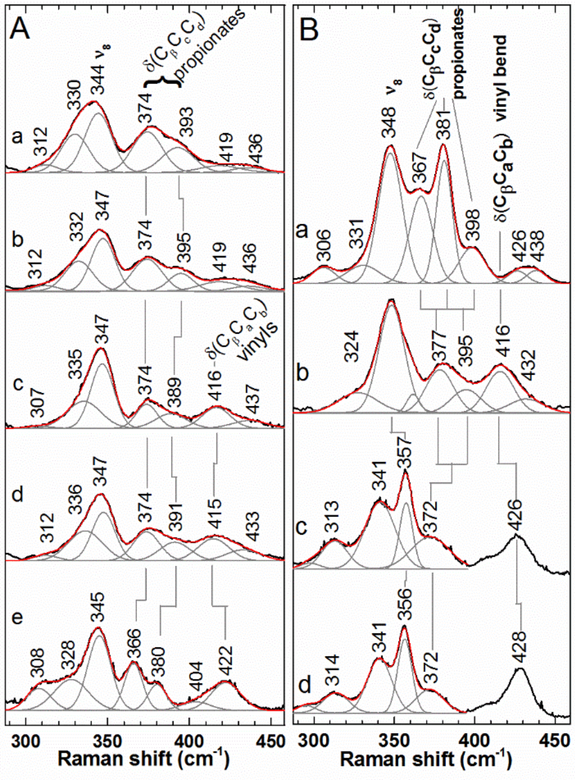

Figure 5.3. Low frequency rR spectra report on the core and peripheral environment of hemes bound to decarboxylases. A) The 406.7-nm excited rR spectra of ferric forms of a) coproheme:*Sa* decarboxylase, b) coproheme:*Gs* decarboxylase c) heme *b*:*Sa* decarboxylase, d) heme *b*:*Gs* decarboxylase, and e) *Da*Cld(R183Q). Ferric samples were in 100 mM potassium phosphate at pH 7.4. B) Soret-excited rR spectra of CO complexes of a) coproheme:*Sa* decarboxylase, b) heme *b*:*Sa* decarboxylase, c) WT *Da*Cld, and d) *Da*Cld(R183Q). Both *Da*Cld enzymes contain heme *b*. Spectra of CO samples in 100 mM potassium phosphate at pH 6.8 were acquired with 413.1 nm excitation and 2 mW power at the sample. Original spectra, black; fit spectra, red; component bands making up the fit spectra, gray.

the porphyrin ring, occur at different frequencies and with different band widths. The bending modes for propionates 6 and 7 of heme *b*:decarboxylase-CO are observed at 377 and 395 cm^{-1}, in contrast to one broad band at 372 cm^{-1} in the *Da*Cld-CO spectrum. The frequency of the vinyl bending mode for heme *b*:decarboxylase-CO is 10 cm^{-1} lower than that of WT *Da*Cld (416 versus 426 cm^{-1}). The *Da*Cld R183Q mutation has little effect on these propionate frequencies, suggesting that the observed differences in the spectra are not due to differences in their distal environments. In addition to these differences in vinyl/propionate-associated frequencies, the ν_8 core size marker band (M-N stretch) of the heme *b*:decarboxylase-CO occurs at 348 cm^{-1}, and 8-9 cm^{-1} higher in frequency in the *Da*Cld spectrum. Finally, a large band at 341 cm^{-1} that is tentatively assigned to the pyrrole tilting mode (γ_6) in *Da*Cld is absent from the decarboxylase spectrum. These differences collectively reveal distinct peripheral and core heme conformations for the decarboxylases and Clds.

Solution-state spectroscopy indicates retention of the weak Fe-His bond but diminishing distal interactions as the propionates are oxidized. The ferrous heme-CO complex is a sensitive probe of heme coordination and the electrostatic character of its binding site inside proteins.[38-41] The CO complexes of the ferrous coproheme-, harderoheme-, and heme b-bound decarboxylase (Sa) were generated and their spectra analyzed for inclusion on a ν_{Fe-C}/ν_{C-O} correlation plot (Fig. 4). Three isotope-sensitive (i.e. ^{12}CO versus ^{13}CO) bands were detected for each of the aforementioned hemes. Based on their frequencies and isotope shifts, they were assigned to the Fe-C and C-O stretching (ν_{Fe-C} and ν_{C-O}) and FeCO bending (δ_{FeCO}) modes for CO-bound forms: coproheme, 513, 1941, and 582 cm^{-1}; harderoheme, 502, 1955, and 579 cm^{-1}; heme b, 498, 1958, and 577 cm^{-1}, respectively (Fig. 4A). The same isotopically sensitive bands were observed for the heme b-CO, whether generated by binding ferric heme b to the enzyme or by the enzymatic activity of the decarboxylase.

All of the CO complexes generated here fell on the inverse correlation line associated with charge-neutral proximal histidine ligands (Fig. 4B), consistent with the proximal pocket structure (Fig. 2B) and with retention of the proximal histidine as the substrate converts to product. However, the location along the histidine correlation line for the three decarboxylase complexes varied, consistent with a changing distal environment. Stronger interactions of the CO ligand with positively charged or H-bond donating residues on the distal side of the heme lead to greater π back bonding and, therefore, to points higher on the imidazole line. The decarboxylase complex with coproheme is highest on the line, in a position consistent with moderate H-bond donation to or electrostatic interaction with the bound CO and the distal pocket. The harderoheme complex is much lower on the correlation line and close to the position of heme *b*, which is lowest of all. The loss of Fe-C π bonding character and increase in the C-O π bonding character in the three CO complexes is consistent with the progressive loss of distal interaction as the substrate is oxidized.

The positions of these complexes on the line can be further interpreted in terms of distal structure using available data from Clds. Two conformers, described as closed and open forms, have been reported for the pH 6.5 and 9 crystal structures of *Da*Cld as well as in rR spectra of *Da*Cld−CO.[44, 45] These have the distal Arg183 oriented toward and away from the open coordination position above the heme plane, respectively. The coproheme:decarboxylase-CO is comparable to the closed form of *Da*Cld(Arg183Gln)-CO, suggesting similar distal environments. The closed form of WT *Da*Cld-CO, with its distal Arg, is higher up on the correlation line; as one would predict, the distal Arg interacts with the bound CO in a stronger manner than the distal Gln in either coproheme:decarboxylase-CO or *Da*Cld(Arg183Gln)-CO. The heme *b*:decarboxylase-CO falls at a position similar to the open form of *Da*Cld-CO and the CO complex of the Cld from *Candidatus Nitrospira defluvii.*[46] The degree of distal pocket interaction with the bound CO in these three complexes is similar and small.

Coproheme-bound CO interacts with the conserved distal Gln

The crystal structure suggests that Gln185 and/or Arg131 could make contact with the terminal oxygen of a ferric coproheme-OOH complex. To examine this hypothesis, rR spectra for the ferrous coproheme-CO complexes were used to assess the distal environment sampled by a bound diatomic ligand inside the Gln185Ala and Arg131Ala variant decarboxylases. The $\nu_{\text{Fe–C}}$ and $\nu_{\text{C–O}}$ frequencies for the Gln185Ala-CO complex (498 and 1953 cm^{-1}, respectively (Fig. S9) dramatically shift the Gln185Ala-CO point down the correlation line away from the WT coproheme complex and to a position close to the heme *b*-decarboxylase (Fig. 4B). This indicates loss of distal interaction when Gln185 is absent and is consistent with a role for Gln185 in the architecture of the distal pocket in solution.

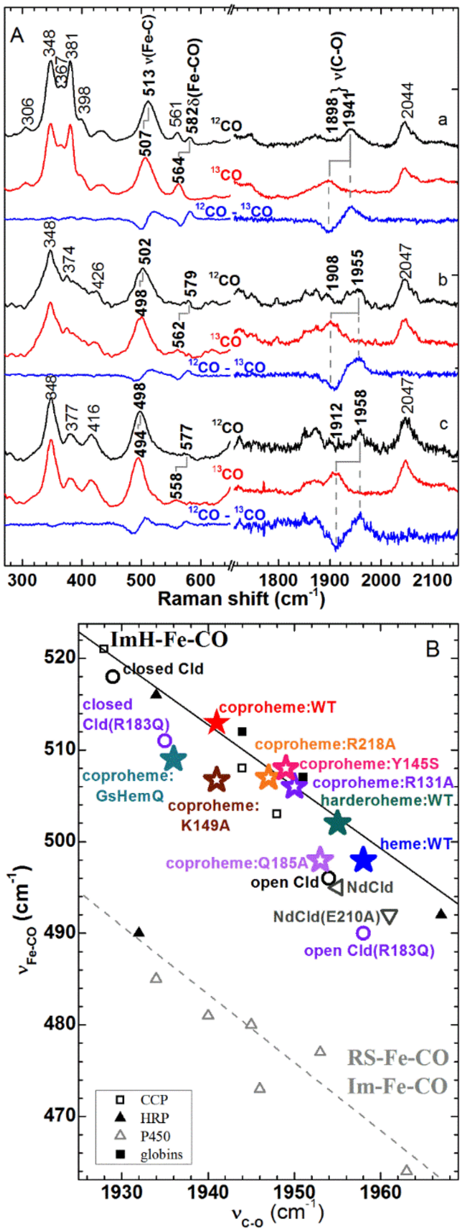

Figure 5.4. rR characterization of ferrous CO complexes of the *Sa* decarboxylase report on their proximal ligands and distal environments. A) Soret-excited rR spectra of the isotopomers of CO complexes of the decarboxylase bound to a) coproheme b) harderoheme III, and c) heme *b* at pH 6.8. Spectra were acquired with 413.1 nm excitation and 2 mW power at the sample. ^{12}CO complex, black; ^{13}CO complex, red; difference spectra ^{12}CO–^{13}CO, blue. B) Backbonding correlation plot of ν_{Fe-C} versus ν_{C-O} for ferrous carbonyls of heme proteins shows the dependences of their positions on axial ligation and distal pocket properties. The black line correlates ν_{Fe-C} with ν_{C-O} for six-coordinate Fe-CO adducts in which the sixth ligand is histidine (neutral imidazole). The gray dashed line represents six-coordinate Fe-CO adducts in which the sixth ligand is a thiolate or and

imidazolate. Points used for these lines are tabulated in Table S1 of reference 42. Data for *Da*Clds and *Nd*Clds are from references 42 and 43, respectively.

The Arg131Ala-CO complex falls between WT and Gln185Ala on the ν_{Fe-C}/ ν_{C-O} correlation plot (Fig. 4B and S8) indicating that this mutation has a smaller effect on the distal pocket interaction than Gln185Ala. Its distal environment is comparable to those observed for mutants in which H-bonds/salt bridges to a propionate group have been disrupted (see below). This suggests that Arg131 plays a role at the periphery of the coproheme instead of in the distal pocket. Loss of the Arg charge could result in either a change in coproheme conformation because of loss of the interaction with propionate 6 or in an increase in solvent accessibility to the pocket. Either could be responsible for the characteristics of Arg131Ala-CO and its decreased activity with H_2O_2 described below.

Disruption of H-bonding to Propionates 2 and 4 Alters Heme Conformation

The presence of H-bonds or salt bridges to propionates 2 (Tyr145, Arg218) and 4 (Lys149) are predicted by the structure (Fig. 2). To test whether these apparent interactions modulate the electronic structure of the coproheme, the site-specific Tyr145Ser, Lys149Ala, and Arg218Ala mutants were generated. The rR spectra of these coproheme:mutant-CO complexes are compared in Fig. 4B and S8 and their νFe−C and νC−O frequencies given in Table S3. As judged by their position on the νFe−C/νC−O correlation plot (Fig. 4B) the mutant:coproheme-CO complexes, like WT coproheme-CO, retain the neutral His as the proximal ligand. The CO interactions with their distal environments, however, have been diminished. If the only role of the H-bonds/salt bridges to the reactive propionates is to position them for decarboxylation, loss of these interactions would not be expected to change exogenous ligand interactions with the distal pocket. This result therefore argues that the roles of the H-bond donors to propionates 2 and 4 are more nuanced than simply positioning their carboxylate groups and the changes in their reactivity could be due, in part, to changes in the distal pocket interactions and/or distortions of the coproheme plane that direct the reactivity of the high-valent intermediate toward oxidative decarboxylation of propionate 2 or 4.

Three bands have been tentatively assigned to propionate bending modes in the CO complexes of WT, Tyr145Ser, Arg218Ala and Lys149Ala coproheme: decarboxylases (Fig. S8B and Table S3). The Tyr145Ser mutant has a propionate bending band at 361 cm−1 that is 6 cm−1 lower than the comparable δ(CβCcCd) band in the WT CO complex; the other two δ(CβCcCd) frequencies are unaffected indicating that the band at 367 cm−1 in the WT CO spectrum is due to propi-onate-2. Loss of the Tyr145 H-bond to propionate 2 results in a significant alteration in its environment. In contrast, all three bands assigned to the propionate bending modes in Arg218Ala and Lys149Ala CO complexes exhibit decreases of 3 cm−1 in their frequencies of relative to WT. This indicates that disruption of the H-bond network between propionate 2 and Arg218 or the salt bridge between Lys149 and propionate 4 lead to more global changes in coproheme environment than the very localized effect of Tyr145 mutation. Interestingly, the ν8 band, a core size marker band that reports Fe-N-pyrrole stretching, exhibits a decrease in frequency for all three mutants. This is consistent with increases in the porphyrin core size upon mutation of the amino acids that interact with the reactive propionates 2 and 4. These features suggest that the interaction of these residues with the coproheme are important in determining the degree to which the heme conformation deviates from planarity. Thus, stepwise changes in the heme planarity may contribute to the structural basis for regioselectivity in oxidizing propionates 2 and 4.

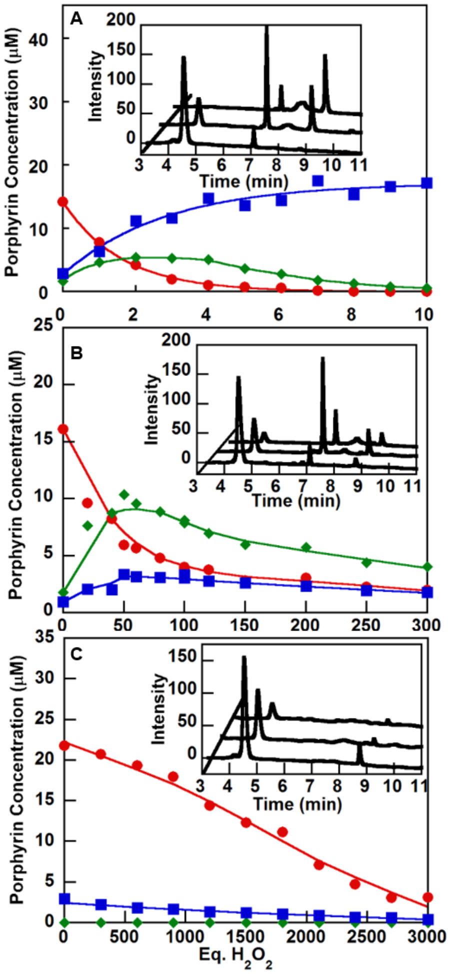

Figure 5.5. Mutations at Lys149 and Tyr145 prevent decarboxylation of one or both propionic acid substrates, respectively. Unreacted coproheme (red), harderoheme III intermediate (green) and the heme *b* product (blue) of the coproheme decarboxylase reaction with increasing eq of H_2O_2 were quantified by HPLC for (top) WT enzyme and the mutants (center) Lys149Ala and (bottom) Tyr145Ser. HPLC traces illustrating the starting material, observable intermediates, and final products are shown as insets. Retention times for unreacted coproheme, the harderoheme III intermediate, and heme *b* product were 4.8, 7.1 and 8.9 min, respectively.

Tyr145 is essential for the decarboxylation of coproheme and harderoheme III; Lys149 contributes to decarboxylation of harderoheme III. Based on their proximity to the substrate and their catalytic roles in other enzymes, we hypothesized that several residues in Fig. 2 may have essential roles in catalysis. We made a series of mutations in the Sa enzyme at a total of eight key positions, including those described above (Table S4). All of the mutants bound coproheme with >80% occupancy, with K_D values similar to WT and varying by less than an order of magnitude (Table S4, Fig. S10-11). The catalytic competence of each mutant-coproheme complex was examined to determine which residues were essential for turnover, specifically whether each generated the expected intermediate (harderoheme III) and product (heme b) and how much oxidant was required.

The WT enzyme required 5 eq of H_2O_2 to turn over 90% of the initially bound coproheme. Harderoheme III was the observed intermediate, maximizing after delivery of 2 eq H_2O_2 (Fig. S5) and fully converting to heme *b* with a total of 10-12 eq H_2O_2. Addition of further oxidant has been observed to bring about the complete degradation of the heme *b* chromophore.[21,]

The most dramatic deviations from WT behavior were obtained for the Tyr145Ser and Lys149Ala mutants (Fig. 5). Tyr145Ser, in which the H-bond to propionate 2 is eliminated, required ~3,000 eq of H_2O_2 to turn over ≥95% of the coproheme substrate (Table S4). Neither harderoheme III nor heme *b* appeared as intermediates or products. Instead, the coproheme degraded without detectable products. The Tyr145Ser mutant readily bound harderoheme so its catalytic competence towards this stable intermediate was investigated. Harderoheme-Tyr145Ser mutant did not form observable heme *b* upon reaction with H_2O_2 (Fig. S12). The Lys149Ala mutant, in which the salt bridge to propionate 4 is removed, required ~300 eq of H_2O_2 to turn over ≥95% of the substrate. However, the major product was harderoheme III, with relatively little turnover of this species to heme *b*. This suggests that Lys149 is essential specifically for the conversion of harderoheme to heme *b*, while Tyr145 appears to play a role in both decarboxylation reactions.

Substitutions of other potentially significant residues surrounding propionate 2 (Arg218Ala) or 4 (Tyr113Ser, Trp157Phe, Trp198Phe), or in the distal pocket (Gln185Ala, Arg131Ala) had far smaller effects, suggesting that none of these on its own is essential for catalysis. Instead, the Gln185Ala and Arg131Ala mutants brought about small increases in the amount of H_2O_2 required to effect substrate conversion (60 and 24 eq, respectively). The Gln185Ala mutant additionally saw exhibited a marked decrease in the amount of harderoheme III accrued, suggesting this mutation had a proportionally greater impact on the first decarboxylation than the second. Arg218Ala, Trp157Phe, and Trp198Phe all behaved very similarly to WT, while the heme *b* product of Tyr113Ser was slightly less stable toward H_2O_2, possibly due to weaker heme *b* binding (Fig. S13).

The excess H_2O_2 required for coproheme turnover can be largely accounted for by catalase activity. The *Sa* decarboxylase containing heme *b* was previously shown to have catalase activity:

$$\text{Fe(III)heme} + H_2O_2 \rightarrow \text{Fe(IV)=O (por}^{\blacksquare +}) \qquad (6)$$

$$\text{Fe(IV)=O (por}^{\blacksquare +}) + H_2O_2 \rightarrow O_2 + H_2O \; (7)$$

This reaction (~50 turnovers) occurs concomitantly with heme *b* degradation.[28] It is possible that some of the excess H_2O_2 required for coproheme conversion to heme *b* might be expended in the catalase reaction. Following addition of 12 eq of H_2O_2 (120 μM) to the decarboxylase-coproheme complex (10 μM), one eq of O_2 (10 μM) (measured by O_2 polarography) (Fig. 6A) was generated over the same time frame in which coproheme converted to heme *b*. In light of the mechanism above, 2 eq of H_2O_2 (likely not a physiologically relevant amount) can be accounted for via the catalase reaction, in addition to the 2 required for the decarboxylation reactions. The remaining 8 of the initial 12 eq, though well within the limits of detection, were not detected by HRP-based colorimetric assays as the end of the reaction. Control reactions in which the ligand-free/apo-protein (5 μM) was mixed with 12 eq H_2O_2 (60 μM) under the same conditions showed that ~8 eq of H_2O_2 (40 μM) were consumed in a heme-independent reaction with the apo-protein without concomitant production of O_2, while 4 eq (22 μM) remained unreacted in solution (Fig. S14).

The large excess of H_2O_2 required to turn over the coproheme bound to the Tyr149Ser and Lys145Ala mutants could likewise be primarily accounted for via the catalase reaction (Fig. S15). Mutation of either residue increases the values of both k_{cat} and $k_{cat}/K_M(H_2O_2)$ relative to WT (Fig. 6B). This suggests that either mutation stabilizes the heme species, thereby enhancing their efficiency as catalases.

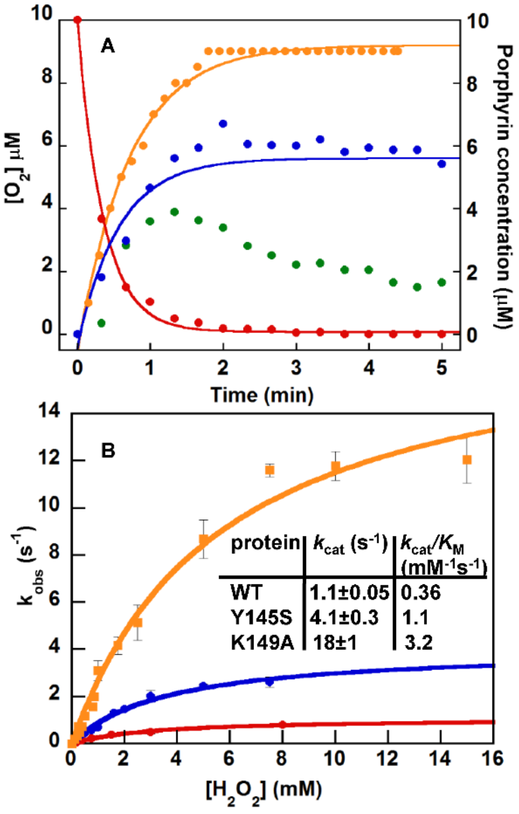

protein	k_{cat} (s^{-1})	k_{cat}/K_M (mM^{-1}s^{-1})
WT	1.1±0.05	0.36
Y145S	4.1±0.3	1.1
K149A	18±1	3.2

Figure 5.6. The catalase activity of coproheme decarboxylase is strongly enhanced in the Lys149Ala and Tyr145Ser mutants. (A) The progress of the coproheme decarboxylase reaction over time [coproheme (red), harderoheme III (green), heme *b* (blue)] measured previously[22] is shown superimposed on the time course for O_2 production (orange) (10 μM enzyme-coproheme, 120 μM H_2O_2, 50 mM KPi, pH 7.4, 25 °C). The generation of ~10 μM O_2 via the catalase reaction suggests that ~20 μM H_2O_2 was consumed during the same time window in which coproheme converted to heme *b*. (B) Initial rates of O_2 production were measured as a function of [H_2O_2] and fit to eqn (5) for the WT (red), Tyr145Ser (blue), and Lys149Ala (orange) decarboxylases. The resulting steady state parameters describing catalase activity are tabulated in the inset.

Discussion

Coproheme decarboxylase catalyzes H_2O_2-dependent C-C bond cleavage reactions to liberate two molecules CO_2 from a pair of propionic acids, converting each to a vinyl (Scheme 1). An analogous reaction is catalyzed by the bacterial cytochrome P450, OleT.[47] Ferric OleT and H_2O_2 react to generate Compound I, which in turn abstracts a hydrogen atom directly from the exogenous carboxylic acid substrate. Unique among P450s, this reaction is not followed by rebound between the substrate radical and Fe(IV)-OH.[19] Instead, the reaction is more peroxidase-like, with the unpaired electron from the nearby substrate reduces the iron to Fe(III), resulting in CO_2 and the alkene. A similar mechanism could be proposed for the coproheme decarboxylase, with the ferryl oxygen most likely interacting for steric reasons with the $C_ß$-H of either propionate 2 or 4 (Scheme 1). However, the 1.8 Å structure of the enzyme in complex with its substrate analog (Fig. 1-2) suggests two complications with any straightforward application of either the peroxidase or OleT model to the coproheme decarboxylase.

The first is that the apparatus for activating H_2O_2 found in most heme peroxidases, including CCP and APX (Fig. S1 and Results),[12] is completely absent in the coproheme decarboxylase. The coproheme is instead ligated by an uncharged proximal His (Fig 2-4) and its open coordination position is flanked by a distal Gln. Both the Gln and the Arg to which it is connected through-water interact with a coproheme-bound CO. Although mutagenesis showed that neither Gln185 nor Arg131 was essential for catalysis, their interactions with bound CO suggests they could play activating roles toward H_2O_2. Some role for the protein is supported by prior studies of the reaction of the coproheme decarboxylase with peracetic acid: an oxygen atom donor that directly converts ferric hemes to Fe(IV)=O(por▪+) or Fe(IV)=O(Trp▪+) without the proton movement or heterolytic bond cleavage associated with H_2O_2.[22] The ferric coproheme decarboxylase reacts rapidly with peracetic acid to form the expected harderoheme intermediate and heme *b* product. The second order rate constant for the same reaction with H_2O_2 is 10-fold slower and, in contrast with the peracid reaction, dependent on both pH and solvent isotope (D_2O).[22] These observations strongly suggest that the reaction proceeds through a ferryl intermediate and that its formation is facilitated by protein-mediated proton transfers (Scheme 2A).

The second issue concerns the presumptive sites of substrate oxidation – the C□ or C□ of propionic acids 2 and 4 – which the structure shows are spatially removed from the site of H_2O_2 activation at the metal. This separation immediately suggests that, in contrast with OleT, the reaction cannot proceed by direct interaction of a ferryl or other iron/oxygen intermediate with either propionate, implying the use of an amino acid side chain or multiple side chains as redox mediators. Inspection of the environment surrounding propionate 2 (Fig. 2C) immediately identified Tyr145 as a possible secondary site of oxidation following the initial generation of a coproheme compound I. The side chain of Tyr145 sits near to and forms an apparent H-bond with the carboxylate moiety of propionate 2, in a position analogous to the ascorbate binding site in APX (Fig. S1).[8] This configuration suggested that Tyr145 might be well-positioned to be oxidized by coproheme compound I (Scheme 2B), and that it may in fact act as the reactive species toward propionate 2. Consistent with that hypothesis, substitution of Tyr145 with Ser led to complete loss of coproheme decarboxylation. A concomitant large increase in catalase activity suggested that, in the absence of Tyr145, the enzyme readily forms Fe(IV)=O(coproporphyrin▪+) with the electron hole localized on the porphyrin.

Scheme 2. Proposed mechanisms consistent with the available data†

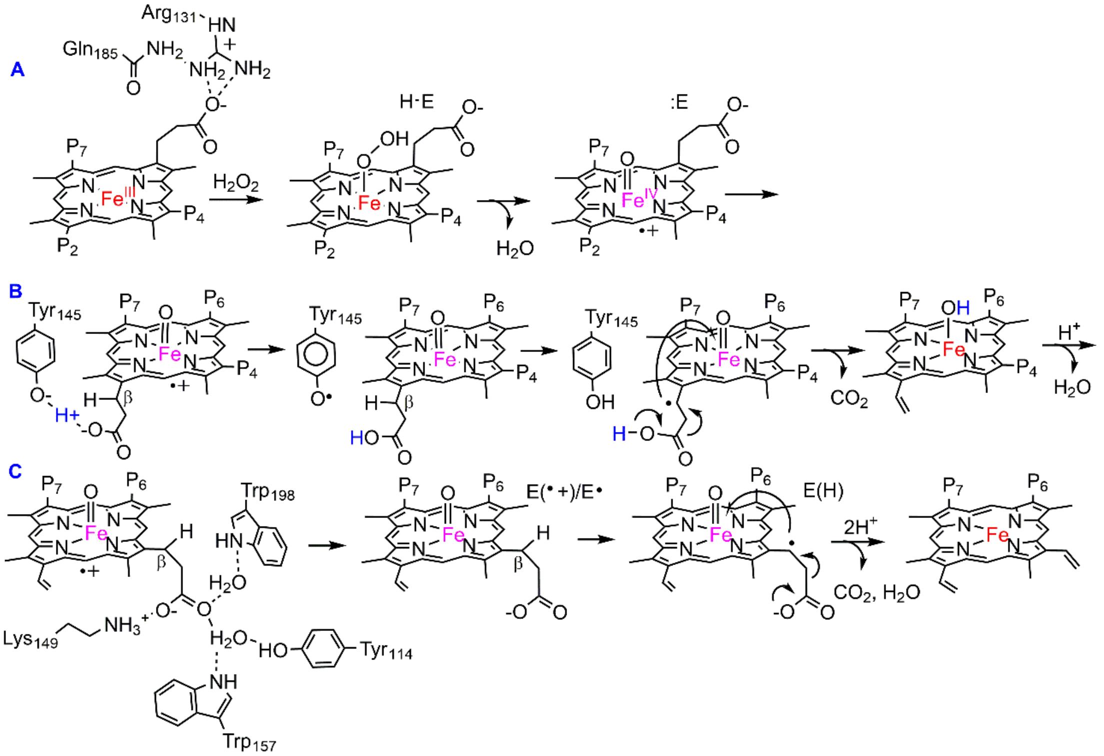
A
Arg131
HN
Gln185
NH2
NH2
NH2
O
O-
P7
P2
P4
FeIII
H2O2
H·E
OH
O-
Fe
H2O
:E
FeIV
•+
B
Tyr145
P6
H+
-O
β
O•
HO
OH
H-O
CO2
H+
H2O
C
Trp198
HN
H2O
Lys149
NH3+
Tyr114
Trp157
E(•+)/E•
E(H)
2H+
CO2, H2O

†A. Formation of Fe(IV)=O(coproporphyrin•+) (coproheme compound I) (E = enzyme; Fe(III) in red and Fe(IV) in purple). B. Oxidative decarboxylation of propionate 2 requires Tyr145. The neutral Tyr145-O• radical is depicted abstracting hydrogen (H•) from the propionate C_β, though this is hypothetical. Transfer of an electron and proton to the ferryl of Compound II then leads to the ferric-OH complex of harderoheme III, from which water can ultimately depart. C. Following another round of H_2O_2-activation analogous to (A), a second Fe(IV)=O(harderoporphyrin•+) complex forms. Three possible redox-active amino acids are connected to propionate 4 via hydrogen bonding through water molecules, though only Lys149 was essential for catalysis. The identity of the mediator for proton coupled electron transfer from the propionate (designated E+• or E•) is unclear. Net uptake of H• by the enzyme is designated via E(H).

Neutral tyrosyl radicals (TyrO▪) are implicated in a variety of reactions, including those catalyzed by class I ribonucleotide reductase,[48] photosystem II,[49] galactose oxidase,[50] and prostaglandin-H synthase.[5] In each case, a metal center is involved in generating the tyrosyl radical, which then acts as the primary recipient of an electron or hydrogen atom from a substrate. The bond dissociation free energy associated with TyrO▪/TyrOH in these systems as well as phenolic model compounds can be quite high[17, 52] and, in the case of the tyrosine Z in photosystem II, thermodynamically sufficient for the oxidation of water. Net transfer of H▪ from the propionate $C_ß$-H to Tyr145-O▪ would result in a resonance-stabilized coproheme propionyl-$C_ß$ radical, suggesting a proportionally lower requisite driving force for carrying out the reaction. Though mutagenesis showed it was not essential for coproheme turnover by the decarboxylase, the side chain of Arg218 is well-positioned to shuttle propionate-derived protons from the active site. A similarly situated arginine residue obligately serves this function in the oxidation of ascorbate by APX (Fig. S1).[10] Transfer of a second electron from the $C_ß$▪ through the porphyrin and to the coproheme Fe(IV) would result in the regeneration of Fe(III) and production of the vinyl and CO_2 (Scheme 2B).

Decarboxylation at propionate 2 is followed by a second, slightly faster[22] H_2O_2-dependent reaction at propionate 4. Inspection of the environment surrounding this group identified three readily oxidizable aromatic residues in its vicinity (Tyr114, Trp198, Trp157) as well as a lysine (Lys149) which like Arg218 could potentially act as an initial recipient or conduit for protons (Fig. 2E). Individual mutations at each of these residues showed that only Lys149 appeared to be essential for coproheme turnover. Substitution of this residue with alanine resulted in the accumulation of the three-propionate intermediate, harderoheme III (Scheme 1). This result suggested that harderoheme maintains the same position as the coproheme substrate, as predicted by solution state rR, and loss of the harderoheme-Lys149 interaction specifically inhibits the decarboxylation of propionate 4.[22] We therefore conclude that H_2O_2 activation by the harderoheme-decarboxylase proceeds in a similar environment as the coproheme complex, though the Fe(III)/(II) reduction potential[22] and the degree of distal pocket interaction with the bound substrate (Fig. 4) have diminished. The pronounced increase in catalase activity in the Lys149Ala mutant likewise suggests that it reacts with H_2O_2 to form Fe(IV)=O(harderoporphyrin▪+).

If this intermediate forms during catalytic turnover, then Tyr114, Trp198, and Trp157 all appear reasonably positioned to form Tyr-O▪ or Trp▪+ radicals by filling the electron hole on (harderoporphyrin▪+). The side chain could then mediate a reaction with propionate 4, where the C□-H electron could migrate to the same (e.g., Tyr114-O▪) or separate destinations. In the latter case, Lys149 could serve an essential role as the proton acceptor in a proton coupled electron transfer. However, mutation of any of these aromatic residues independently had virtually no effect on the efficiency of either propionate decarboxylation. This suggests one of two interpretations. First, it is possible that radical density is spread over two or more of these residues, and that the others can compensate in the event that one is lost. Alternatively, Tyr145-O▪ could act as the enzyme's sole redox mediator toward both propionates 2 and 4. Though the latter is farther from Tyr145, net proton coupled electron transfers can occur across long distances. The reactive Tyr-O▪ in ribonucleotide reductases sets an impressive precedent, reacting with a cysteine-SH over 35 Å away.[48] Supporting this hypothesis in part, we noted that reaction of the Tyr145Ser-coproheme complex with H_2O_2 yielded neither harderoheme nor heme *b*, suggesting that both decarboxylations are impaired by this substitution. Moreover, when a complex of the same mutant was prepared with exogenously supplied harderoheme III, its reaction with with H_2O_2 also yielded no heme *b*. Tyr145 is clearly essential for both propionate oxidations, though whether it acts as a radical mediator in either case is still unknown. How Tyr145 would form the Tyr-O▪ radical in the absence of the conduit provided by propionate 2, once it has converted to vinyl, is an open question, though we note that there is a clear kinetic preference for oxidizing propionate 2 first. This oxidation could be facilitated by the existence of the propionate-Tyr145 interaction.

The chemistry, spectroscopy, and structure reported here constitute an internally consistent account of function and mechanism in this class of decarboxylases. Tyr145 and Lys149 are H-bonded to the reactive propionates 2 and 4, respectively, and play essential roles in the reactivity and regioselectivity of propionates 2 and 4 toward oxidation. These nonbonded interactions differ markedly from those recently reported for the *Listeria monocytogenes* enzyme (*Lm*HemQ), in which coproheme III is oriented such that propionates 2 and 7 are oriented toward the surface of the enzyme while propionates 4 and 6 are directed into the pocket. In the *Lm*HemQ structure, propionate 2 is H-bonded to Gln187, propionate 4 is H-bonded to Tyr147, and the unreactive propionate 6 is H-bonded to Lys151 (comparable to Gln185, Tyr145 and Lys149, respectively, in the *Sa* enzyme). Though there are some differences in crystallization parameters (*Gs* decarboxylase crystals were grown at pH 7.5, for example, whereas the *Lm* decarboxylase crystals were obtained at pH 9.0) the reasons for this different coproheme orientation are unclear. Though it seems unlikely that homologous decarboxylases from different organisms would utilize different coproheme orientations, this possibility cannot be eliminated at this time. More in-depth comparison of the two coproheme-decarboxylase structures is not possible at the time of writing because the *Lm*HemQ structure has yet to be released.[53]

Biological oxidative decarboxylation reactions generally use O_2 as the oxidant. OleT and the coproheme decarboxylase described here are unique for depending on H_2O_2, and coproheme decarboxylase is further distinguished by its evident use of a relay of side chain mediators to convey electrons and protons away from its pair of substrates. This mechanism suggests new approaches for synthetic or semi-synthetic catalysis of the oxidative decarboxylation of fatty acids to generate alkenes, a reaction with significant implications for the production of hydrocarbon fuels from renewable lipid feedstocks.

Associated Content

Supporting Information

A series of 15 data figures and 4 tables is included. This material is available free of charge via the Internet at http://pubs.acs.org.

Funding Sources

This work was supported by funding from the National Institutes of Health, General Medical Sciences R01GM090260 (J.L.D.) and R15GM114787 (G.S.L.-R.). Structural work was supported by the U.S. Department of Energy, Office of Science, Office of Basic Energy Sciences, under Award Number DE-FG02-04ER15563 to J.W.P.

Abbreviations

ABTS, 2,2'-Azinobis [3-ethylbenzothiazoline-6-sulfonic acid]-diammonium salt; ACN, acetonitrile; APX, ascorbate peroxidase; CCP, cytochrome *c* peroxidase; Cld, Chlorite dismutase; Da, *Dechloromonas aromatica*; ESI, electrospray ionization; Gs, *Geobacillus stearothermophilus*; HPLC, High Performance Liquid Chromatography; HRP, horseradish peroxidase; LnP, lignin peroxidase; MS, mass spectrometry; NMR, nuclear magnetic resonance; *Nd*, *Nitrospira defluvii*; PAA, peracetic acid, QTOF, quadrupole time-of-flight, rR, resonance Raman; *Sa*, *Staphyloccocus aureus*; TFA, trifluoroacetic acid;. *Lm*HemQ, *Listeria monocytogenes* decarboxylase; rR, resonance Raman

References

1. Traylor, T. G.; Traylor, P. S., Reactions of dioxygen and its reduced forms with heme proteins and model porphyrin complexes. In *Active Oxygen in Biochemistry*, Valentine, J. S.; Foote, C. S.; Greenberg, A.; Liebman, J. F., Eds. Springer Netherlands: 1995; pp 84-187.

2. Dunford, H. B., *Heme Peroxidases*. Wiley-VCH: 1999; p 528.

3. Ortiz de Montellano P.R., *Cytochrome P450: Structure, Mechanism and Biochemistry*. 3rd ed.; Kluwer Academic/Plenum: New York, 2005.

4. Rittle, J.; Green, M. T., Cytochrome P450 compound I: capture, characterization, and C-H bond activation kinetics. *Science* **2010,** *330* (6006), 933-7.

5. Hammes-Schiffer, S., Proton-coupled electron transfer: Moving together and charging forward. *J Am Chem Soc* **2015,** *137* (28), 8860-71.

6. Reece, S.Y.; Hodgkiss, J.M., Stubbe, J.; Nocera, D.G. Proton-coupled electron transfer: the mechanistic underpinning for radical transport and catalysis in biology. *Philos Trans R Soc Lond B Biol Sci* **2006**, *361* (1472), 1351-1364.

7. Macdonald, I. K.; Badyal, S. K.; Ghamsari, L.; Moody, P. C.; Raven, E. L., Interaction of ascorbate peroxidase with substrates: a mechanistic and structural analysis. *Biochemistry* **2006,** *45* (25), 7808-17.

8. Sharp, K. H.; Mewies, M.; Moody, P. C.; Raven, E. L., Crystal structure of the ascorbate peroxidase-ascorbate complex. *Nat Struct Biol* **2003,** *10* (4), 303-7.

9. Warren, J. J.; Mayer, J. M., Proton-coupled electron transfer reactions at a heme-propionate in an iron-protoporphyrin-IX model compound. *J Am Chem Soc* **2011,** *133* (22), 8544-51.

10. Efimov, I.; Badyal, S. K.; Metcalfe, C. L.; Macdonald, I.; Gumiero, A.; Raven, E. L.; Moody, P. C., Proton delivery to ferryl heme in a heme peroxidase: enzymatic use of the Grotthuss mechanism. *J Am Chem Soc* **2011,** *133* (39), 15376-83.

11. Gumiero, A.; Metcalfe, C. L.; Pearson, A. R.; Raven, E. L.; Moody, P. C., Nature of the ferryl heme in compounds I and II. *J Biol Chem* **2011,** *286* (2), 1260-8.

12. (a) Poulos, T. L., Heme enzyme structure and function. *Chem Rev* **2014,** *114* (7), 3919-62. (b) Cherifi, G.; Baxter, E.L.; Doukov, T.; Cohen, A.E.; McPhillips, S.E.; Song, J.; Meharenna, Y.T; Soltis, S.M.; Poulos, T.L. Crystal structure of the pristine peroxidase ferryl center and its relevance to proton-coupled electron transfer. *PNAS,* **2016**, *112 (5),* 1226-1231.

13. Pelletier, H.; Kraut, J., Crystal-structure of a complex between electron-transfer partners, cytochrome-c peroxidase and cytochrome-c. *Science* **1992,** *258* (5089), 1748-1755.

14. Choinowski, T.; Blodig, W.; Winterhalter, K. H.; Piontek, K., The crystal structure of lignin peroxidase at 1.70 angstrom resolution reveals a hydroxy group on the C-beta of tryptophan 171: A novel radical site formed during the redox cycle. *J Mol BIol* **1999,** *286* (3), 809-827.

15. Colin, J.; Wiseman, B.; Switala, J.; Loewen, P.; Ivancich, A., Distinct role of specific tryptophans in facilitating electron transfer or as [Fe(IV)=O Trp(+▪)] intermediates in the peroxidase reaction of *Bulkholderia pseudomallei* catalase-peroxidase: A multifrequency EPR spectroscopy investigation. *J Am Chem Soc* **2009,** *131* (24), 8557-8563.

16.Sivaraja, M.; Goodin, D. B.; Smith, M.; Hoffman, B. M., Identification by ENDOR of Trp191 as the free-radical site in cytochrome c peroxidase compound ES. *Science* **1989,** *245* (4919), 738-40.

17.Tommos, C.; Skalicky, J. J.; Pilloud, D. L.; Wand, A. J.; Dutton, P. L., De novo proteins as models of radical enzymes. *Biochemistry* **1999,** *38* (29), 9495-9507.

18.Guallar, V., Heme Electron Transfer in Peroxidases: The Propionate e-Pathway. *J Phys Chem B* **2008,** *112* (42), 13460-13464.

19.Grant, J. L.; Mitchell, M. E.; Makris, T. M., Catalytic strategy for carbon-carbon bond scission by the cytochrome P450 OleT. *PNAS* **2016,** *113* (36), 10049-10054.

20. Dailey, H.; Gerdes, S.; Dailey, T.; Burch, J.; Phillips, J., Noncanonical coproporphyrin-dependent bacterial heme biosynthesis pathway that does not use protoporphyrin. *PNAS* **2015,** *112* (7), 2210-2215.

21. Celis, A. I.; Streit, B. R.; Moraski, G. C.; Kant, R.; Lash, T. D.; Lukat-Rodgers, G. S.; Rodgers, K. R.; DuBois, J. L., Unusual peroxide-dependent, heme-transforming reaction catalyzed by HemQ. *Biochemistry* **2015,** *54* (26), 4022-32.

22. Streit, B.R.; Celis, A.I.; Shisler, K.; Rodgers, K.R.; Lukat-Rodgers, G.D.; DuBois, J.L. Reactions of Ferrous Coproheme Decarboxylase (HemQ) with O_2 and H_2O_2 Yield Ferric Heme *b*. *Biochemistry* **ASAP.**

23. Gilski, M.; Borek, D.; Chen, Y.; Collart, F.; Joachimiak, A.; Otwinowski, Z. Crystal Structure of APC35880 protein from *Bacillus stearothermophilus*. *To be published* **2004**.

24.Gonzalez,A.;Tsai,Y.**2010**.http://smb.slac.stanford.edu/facilities/software/xds/#autoxds_script

25. McCoy, A. J.; Grosse-Kunstleve, R. W.; Adams, P. D.; Winn, M. D.; Storoni, L. C.; Read, R. J., Phaser crystallographic software. *J Appl Crystallogr* **2007,** *40* (Pt 4), 658-674.

26. Winn, M. D.; Ballard, C. C.; Cowtan, K. D.; Dodson, E. J.; Emsley, P.; Evans, P. R.; Keegan, R. M.; Krissinel, E. B.; Leslie, A. G.; McCoy, A.; McNicholas, S. J.; Murshudov, G. N.; Pannu, N. S.; Potterton, E. A.; Powell, H. R.; Read, R. J.; Vagin, A.; Wilson, K. S., Overview of the CCP4 suite and current developments. *Acta Crystallogr D Biol Crystallogr* **2011,** *67* (Pt 4), 235-42.

27. Adams, P. D.; Afonine, P. V.; Bunkóczi, G.; Chen, V. B.; Davis, I. W.; Echols, N.; Headd, J. J.; Hung, L. W.; Kapral, G. J.; Grosse-Kunstleve, R. W.; McCoy, A. J.; Moriarty, N. W.; Oeffner, R.; Read, R. J.; Richardson, D. C.; Richardson, J. S.; Terwilliger, T. C.; Zwart, P. H., PHENIX: a comprehensive Python-based system for macromolecular structure solution. *Acta Crystallogr D Biol Crystallogr* **2010,** *66* (Pt 2), 213-21.

28. Mayfield, J. A.; Hammer, N. D.; Kurker, R. C.; Chen, T. K.; Ojha, S.; Skaar, E. P.; DuBois, J. L., The chlorite dismutase (HemQ) from *Staphylococcus aureus* has a redox-sensitive heme and is associated with the small colony variant phenotype. *J Biol Chem* **2013,** *288* (32), 23488-504.

29. Celis, A.; DuBois, J., Substrate, product, and cofactor: The extraordinarily flexible relationship between the CDE superfamily and heme. *Arch Biochem Biophys* **2015,** *574,* 3-17.

30. Hofbauer, S.; Dalla Sega, M.; Scheiblbrandner, S.; Jandova, Z.; Schaffner, I.; Mlynek, G.; Djinovic-Carugo, K.; Battistuzzi, G.; Furtmüller, P. G.; Oostenbrink, C.; Obinger, C., Chemistry and molecular dynamics simulations of heme *b*-HemQ and coproheme-HemQ. *Biochemistry* **2016**.

31. Hofbauer, S.; Howes, B. D.; Flego, N.; Pirker, K. F.; Schaffner, I.; Mlynek, G.; Djinović-Carugo, K.; Furtmüller, P. G.; Smulevich, G.; Obinger, C., From chlorite dismutase towards HemQ - the role of the proximal H-bonding network in haeme binding. *Biosci Rep* **2016,** *36* (2).

32. Choudhury, K.; Sundaramoorthy, M.; Hickman, A.; Yonetani, T.; Woehl, E.; Dunn, M. F.; Poulos, T. L., Role of the proximal ligand in peroxidase catalysis - crystallographic, kinetic, and spectral studies of cytochrome-c peroxidase proximal ligand mutants. *J Biol Chem* **1994,** *269* (32), 20239-20249.

33. Poulos, T. L.; Fenna, R. E., Peroxidases - Structure, Function, And Engineering. In *Metal Ions In Biological Systems, Vol 30*, 1994; Vol. 30, pp 25-75.

34. Blanc, B.; Mayfield, J. A.; McDonald, C. A.; Lukat-Rodgers, G. S.; Rodgers, K. R.; DuBois, J. L., Understanding how the distal environment directs reactivity in chlorite dismutase: Spectroscopy and reactivity of Arg183 mutants. *Biochemistry* **2012,** *51* (9), 1895-1910.

35.Singh, R.; Grigg, J. C.; Armstrong, Z.; Murphy, M. E. P.; Eltis, L. D., Distal heme pocket residues of B-type dye-decolorizing peroxidase, arginine but not aspartate is essential for peroxidase activity. *J Biol Chem* **2012,** *287* (13), 10623-10630.

36. Erman, J. E.; Vitello, L. B.; Miller, M. A.; Kraut, J., Active-site mutations in cytochrome-c peroxidase - a critical role for histidine-52 in the rate of formation of Compound-I. *J Am Chem Soc* **1992,** *114* (16), 6592-6593.

37. Layer, G.; Pierik, A. J.; Trost, M.; Rigby, S. E.; Leech, H. K.; Grage, K.; Breckau, D.; Astner, I.; Jaensch, L.; Heathcote, P.; Warren, M. J.; Heinz, D. W.; Jahn, D., The substrate radical of Escherichia coli oxygen-independent coproporphyrinogen III oxidase HemN. *J Biol Chem* **2006,** *281* (23).

38. Draganova, E. B.; Adrian, S. A.; Lukat-Rodgers, G. S.; Keutcha, C. S.; Schmitt, M. P.; Rodgers, K. R.; Dixon, D. W., Corynebacterium diphtheriae HmuT: dissecting the roles of conserved residues in heme pocket stabilization. *J Biol Inorg Chem* **2016, ASAP**.

39.Spiro, T. G.; Soldatova, A. V.; Balakrishnan, G., CO, NO and O2 as vibrational probes of heme protein interactions. *Coord Chem Rev* **2013,** *257*, 511-527.

40. Lukat-Rodgers, G. S.; Rodgers, K. R.; Caillet-Saguy, C.; Izadi-Pruneyre, N.; Lecroisey, A., Novel heme ligand displacement by CO in the soluble hemophore HasA and its proximal ligand mutants: implications for heme uptake and release. *Biochemistry* **2008,** *47*, 2087-2098.

41.Spiro, T. G.; Wasbotten, I. H., CO as a vibrational probe of heme protein active sites. *J Biol Inorg Chem* **2005,** *99* (1), 34-44.

42. Blanc, B.; Mayfield, J. A.; McDonald, C. A.; Lukat-Rodgers, G. S.; Rodgers, K. R.; DuBois, J. L., Understanding How the Distal Environment Directs Reactivity in Chlorite Dismutase: Spectroscopy and Reactivity of Arg183 Mutants. *Biochemistry* **2012,** *51*, 1895-1910.

43.Hofbauer, S.; Howes, B. D.; Flego, N.; Pirker, K. F.; Schaffner, I.; Mlynek, G.; Djinovic-Carugo, K.; Furtmueller, P. G.; Smulevich, G.; Obinger, C., From chlorite dismutase towards HemQ-the role of the proximal H-bonding network in haeme binding. *Biosci. Rep.* **2016,** *36* , e00312.

44. Goblirsch, B. R.; Streit, B. R.; DuBois, J. L.; Wilmot, C. M., Structural features promoting dioxygen production by *Dechloromonas aromatica* chlorite dismutase. *J Biol Inorg Chem* **2010,** *15* (6), 879-888.

45. Streit, B. R.; Blanc, B.; Lukat-Rodgers, G. S.; Rodgers, K. R.; DuBois, J. L., How active-site protonation state influences the reactivity and ligation of the heme in chlorite dismutase. *J Am Chem Soc* **2010,** *132* (16), 5711-5724.

46. Hofbauer, S.; Gruber, C.; Pirker, K.; Schaffner, I.; Furtmuller, P.; Obinger, C.; Hagmuller, A.; Gysel, K.; Mlynek, G.; Kostan, J.; Djinovic-Carugo, K.; Bellei, M.; Battistuzzi, G.; Daims, H., Understanding chlorite dismutase from *Candidatus Nitrospira defluvii. J Biol Inorg Chem* **2014,** *19*, S253-S253.

47.Grant, J. L.; Hsieh, C. H.; Makris, T. M., Decarboxylation of fatty acids to terminal alkenes by cytochrome P450 Compound I. *J Am Chem Soc* **2015,** *137* (15), 4940-4943.

48. Stubbe, J.; Nocera, D. G.; Yee, C. S.; Chang, M. C. Y., Radical initiation in the class I ribonucleotide reductase: Long-range proton-coupled electron transfer? *Chem Rev* **2003,** *103* (6), 2167-2201.

49. Okamura, M. Y.; Paddock, M. L.; Graige, M. S.; Feher, G., Proton and electron transfer in bacterial reaction centers. *Biochim Biophys Acta* **2000,** *1458* (1), 148-163.
50. Whittaker, J. W., Free radical catalysis by galactose oxidase. *Chem Rev* **2003,** *103* (6), 2347-2363.

51.Tsai, A. L.; Kulmacz, R. J.; Palmer, G., Spectroscopic evidence for reaction of prostaglandin-H synthatase-1 tyrosyl radical with arachidonic-acid. *J Biol Chem* **1995,** *270* (18), 10503-10508.

52. Warren, J. J.; Tronic, T. A.; Mayer, J. M., Thermochemistry of proton-coupled electron transfer reagents and its implications. *Chem Rev* **2010,** *110* (12), 6961-7001.

53. Hofbauer, S.; Mlynek, G.; Millazo, L.; Pühringer, D.; Maresch, D.; Schaffner, I.; Furtmüller, P.G.; Smulevich, G.; Djinović-Carugo, K.; Obinger, C. Hydrogen peroxide-mediated conversion of coproheme to heme *b* by HemQ - Lessons from the first crystal structure and kinetic studies. *FEBS J* **2016**, Ahead of print.

CHAPTER SIX

COPROHEME DECARBOXYLATION VIA A FERRYL, PROPIONATE, AND A TYROSYL IN A RADICAL RELAY YIELDS HEME *B*

Contribution of Authors and Co-Authors

Author: Bennett R. Streit

Contributions: Biosynthesized, purified, and analyzed deuterium labeled coproheme. Performed UV-Vis, HPLC, EPR and MS experiments and data analysis. Contributed to the writing and preparation of this manuscript.

Co-Author: Arianna I. Celis

Contributions: Expressed and purified WT, Y145S *Sa*HemQ, and HemQ with deuterated tyrosine side chains. Contributed to the writing and preparation of this manuscript.

Co-Author: Garrett C. Moraski

Contributions: Performed NMR analysis of biosynthesized deuterated coproheme and its precursors.

Co-Author: Krista Shisler

Contributions: Expressed and purified enzymes required for biosynthesis of deuterium-labeled coproheme.

Co-Author: Eric M. Shepard

Contributions: Significantly contributed to EPR data fitting, analysis, and interpretation. Contributed to the writing and preparation of this manuscript.

Co-Author: Kenton R. Rodgers

Contributions: Measured and analyzed rR data. Provided support and very valuable insight in preparation of manuscript. Contributed to the writing and preparation of this manuscript.

Co-Author: Gudrun S. Lukat-Rodgers

Contributions: Measured and analyzed rR data. Provided support and very valuable insight in preparation of manuscript. Contributed to the writing and preparation of this manuscript.

Co-Author: Jennifer L. DuBois

Contributions: Provided important insight and overview of the preparation of samples, experiment design and interpretation of results. Contributed largest part to the writing and preparation of this manuscript.

Manuscript Information Page

Bennett R. Streit, Arianna I. Celis, Garrett C. Moraski, Krista A. Shisler, Kenton R. Rodgers, Gudrun S. Lukat-Rodgers, Jennifer L. DuBois

The Journal of Biological Chemistry

Status of Manuscript:
____ Prepared for submission to a peer-reviewed journal
____ Officially submitted to a peer-review journal
___ _ Accepted by a peer-reviewed journal
_X_ Published in a peer-reviewed journal

Publisher: American Society for Biochemistry and Molecular Biology

CHAPTER SIX

COPROHEME DECARBOXYLATION INVOLVING A FERRYL, PROPIONATE, AND A TYROSYL GROUP IN A RADICAL RELAY YIELDS HEME *B*

Bennett R. Streit,[1] Arianna I. Celis,[1] Garrett C. Moraski,[1] Krista Shisler,[1] Eric M. Shepard,[1] Kenton R. Rodgers,[2] Gudrun S. Lukat-Rodgers,[2] Jennifer L. DuBois[1,*]

[1]*Department of Chemistry and Biochemistry, Montana State University, Bozeman, MT 59717-3400;*
[2]*Department of Chemistry and Biochemistry, North Dakota State University, Fargo, ND 58108-6050*

Abstract

The H_2O_2-dependent oxidative decarboxylation of coproheme III is the final step in the biosynthesis of heme *b* in many microbes. However, the coproheme decarboxylase reaction mechanism is unclear. The structure of the decarboxylase in complex with coproheme III suggested that the substrate iron, reactive propionates, and an active-site tyrosine convey a net 2e-/2H+ from each propionate to an activated form of H_2O_2. Time-resolved EPR spectroscopy revealed that Tyr-145 forms a radical species within 30 sec of the reaction of the enzyme–coproheme complex with H_2O_2. This radical disappeared over the next 270 sec, consistent with a catalytic intermediate. Use of the harderoheme III intermediate as substrate or substitutions of redox-active side chains (W198F, W157F, or Y113S) did not strongly affect the appearance or intensity of the radical spectrum measured 30 sec after initiating the reaction with H_2O_2, nor did it change the ~270 sec required for the radical signal to recede to ≤ 10% of its initial intensity. These results

suggested Tyr-145 as the site of a catalytic radical involved in decarboxylating both propionates. Tyr-145• was accompanied by partial loss of the initially present Fe(III) EPR signal intensity, consistent with the possible formation of Fe(IV)=O. Site-specifically deuterated coproheme gave rise to a kinetic isotope effect of ~2 on the decarboxylation rate constant, indicating that cleavage of the propionate Cβ-H bond was partly rate limiting. The inferred mechanism requires two consecutive hydrogen atom transfers, first from Tyr-145 to the substrate Fe/H_2O_2 intermediate and then from the propionate Cβ-H to Tyr-145•.

Introduction

Metallotetrapyrroles are among nature's oldest and most versatile catalytic scaffolds. Their functional versatility is due to the macrocycle's capacity for accommodating a variety of metals at the center and organic functional groups around the periphery. Many well-characterized enzymes that use a metallotetrapyrrole as a substrate, such as heme oxygenase (1,2), heme A synthase (3), or some cytochrome P450s (4), take advantage of its intrinsic reactivity, so that these reactions have an autocatalytic character. Coproheme decarboxylase is a metallotetrapyrrole-modifying enzyme that likewise uses a heme as both substrate and cofactor, catalyzing the oxidative decarboxylation of ferric 2,4,6,7-tetrapropionic acid porphyrin (coproheme) to yield ferric 6,7-dipropionic acid-2,4-divinyl porphyrin (heme *b*). This reaction is the final step in the heme biosynthetic pathways of diverse gram-positive bacteria and possibly some

Archaea (5), encoded by a gene alternately referred to as *cld* or *hemQ*, or most recently as *chdC* (5,6).

Each decarboxylation is an oxidation in which a net two electrons and two protons are transferred from the reactive propionate to a molecule of H_2O_2, yielding $2H_2O$, CO_2, and a new vinyl group (7,8). H_2O_2 activation at the open coordination position on the substrate iron (distal pocket) could generate any of a number of well-known reactive species, including a ferric-hydroperoxy [Fe(III)-OOH], ferryl porphyrin π-cation radical [Fe(IV)=O (por+•), compound I], or ferryl complex [Fe(IV)=O or Fe(IV)-OH compound II]. The structure of the decarboxylase bound to coproheme (9), however, showed the reactive propionates are positioned pointing away from the distal pocket; their orientation in the proximal pocket below the porphyrin plane prohibits any direct access of the reactive propionates to an Fe/H_2O_2 species (Fig. 6.1). This suggested a more complicated reaction mechanism where, like in heme-sidechain-modifying enzymes (3,4) or cyclooxygenases (10), electrons or protons might be conveyed from the substrate to a reactive Fe intermediate via a redox-active amino acid side chain. Such transfers of protons and electrons could occur sequentially or by proton-coupled electron transfer (PCET).[3] Alternatively, homolytic scission of an Fe(III)coproheme-OOH bond could yield a hydroxyl radical (•OH) that is channeled by the active site toward a specific C-H bond on the reactive propionate. A mechanism of this type would be consistent with the proposed self-hydroxylation catalyzed by heme oxygenases (1), and with the decarboxylase structure (9), which lacks the typical apparatus of enzymes that activate

H_2O_2 by heterolytic cleavage. How the enzyme would convey a highly reactive •OH to specific sites of reaction on the two propionates is unclear.

To distinguish among these pathways, EPR spectroscopy and kinetic methods were used to monitor the coproheme decarboxylation using WT, mutant, and site-selectively deuterated proteins as well as deuterium labeled substrates. Strong experimental evidence is presented in support of a mechanism where the substrate iron activates H_2O_2, Y145 forms a radical species via hydrogen atom transfer (HAT), and the resulting Y145 radical (Y145•) acts as the unique intermediary for HAT from both reactive propionates.

Results

Deuterium-labeled Coproheme III Was Generated in High Yield

Deuterium labeled coproporphyrinogen III (Fig. S6.1) was prepared in a single step by co-incubating D_4-ALA (3,3,5,5-$^2H_4$-aminolevulinic acid) and the enzymes HemB-E in buffer in an anaerobic chamber. Colorless D-coproporphyrinogen III was subsequently oxidized to pink D-coproporphyrin III using HemY and O_2 from ambient air. The HPLC trace for the HemBCDEY reaction (Fig. S6.1) confirms that the product has a retention time matching a pure coproporphyrin III standard, with minimal detectable contaminants with absorbance in the 300-700 nm range. The predicted exact mass for the $[M+H]^+$ ion (667.3 g/mol, M = $C_{36}H_{26}D_{12}N_4O_8$) is observed in the mass spectrum (Fig. S1), with the same expected isotopic distribution reported previously for D-coproporphyrin (MS, $[M+H]^+$: 667.3 Da, determined distribution: M_{full} – 1.4%; M_{full}-

1D – 5.2%; M_{full}-*2D* – 15.8%; M_{full}-*3D* – 20.2%; M_{full}-*4D* – 20.9%; M_{full}-*5D* – 19.5%; M_{full}-*6D* – 11%; M_{full}-*7D* – 4.6%; M_{full}-*8D* – 1.3%; M_{full}-*9D* – 0.2%). The starting materials and products were subsequently analyzed by ^{1}H-NMR (Fig. S6.2). The data show loss of intensity in peaks associated with the four propionate □-carbons (4.55 ppm) and the four tetrapyrrole-bridging *meso* carbons (11.2-11.3 ppm), indicating that the protons at these positions have been substituted with deuterium. Consistent with prior work (11), substitution at the *meso* positions is not complete, suggesting that a small amount of reintroduction of ^{1}H occurs during the biosynthesis. The molar yield of pure D-coproporphyrin III, based on the amount of D_4-ALA used in the reaction, was 90 ± 5% of the expected theoretical yield.

D-Tyr-labeled Decarboxylase Was Generated in Low Yield and its Reaction Was Less Efficient than Unlabeled Protein

Typical pure protein yields for pure decarboxylase were ~8 mg/l culture. By contrast, pure D-Tyr-labeled enzyme was produced at 2 mg/l culture, due to low levels of expression in the Tyr auxotrophic strain. Complete conversion of substrate to product required 400 eq H_2O_2 (pH 7.4 potassium phosphate, 20 °C). Under those conditions, the reaction was complete within 1 min (Fig. S6.3).

By contrast, prior work showed that approximately 10 eq H_2O_2 was sufficient to convert the WT/unlabeled enzyme-coproheme complex to -heme *b*; the small excess of H_2O_2 was required due to competing side reactions between H_2O_2 and the protein/heme (7,9). A ferric-harderoheme complex accrues with formation rate constant previously fitted to $k = 2.9$ min^{-1} or $t_{1/2} = 14$ s, and heme *b* forms with $k = 0.30$ min^{-1} ($t_{1/2} = 140$ s (pH 7.4 potassium phosphate, 20 °C) (7).

Time Resolved EPR Demonstrated Formation and Decay of an Organic Radical Reaction Intermediate

The decarboxylase-coproheme complex and 10 eq H_2O_2 were manually mixed (pH 8.8, 20 °C) and subsequently freeze-trapped in EPR tubes at time points from 0.5-3 min. The resulting 77K, X-band EPR spectra illustrated the formation of an EPR-active S=1/2 species within 0.5 min that subsequently decayed nearly to baseline over the next 5 min (Fig. 6.2A). Though a full EPR kinetic time course is lacking, the appearance of the S=1/2 species within 0.5 min of mixing and its subsequent decay within 300 s is kinetically consistent with its assignment as an intermediate in the conversion of coproheme to heme *b*, based on the expected reaction $t_{1/2}$ = 140 s for heme *b* formation cited above (7). Moreover, the 14 s half-life for the initial decarboxylation of P2 to yield harderoheme and the circa 300 s lifetime of the radical species overall suggests that the observed EPR signals most likely represent superimposed radical intermediate density from both the decarboxylations of P2 and P4, particularly at the later time points (7). This observation is consistent with prior stopped flow analyses, which showed that the P2 and P4 decarboxylations were similar in rate and not temporally well resolved (8).

Double integration of the 0.5 min sample spectrum and comparison to a TEMPO standard curve indicated that it contained 35 μM of the EPR-active species per 100 μM decarboxylase-coproheme complex initially present, where the complex converts nearly stoichiometrically to decarboxylase-heme *b* under the conditions used. The spectrum showed a partially resolved 4-line signal centered at g = 2.005 with a peak-to-trough linewidth ~20 G (Fig. S6.4), consistent with an amino acid side chain radical (see below) (12).

The Organic Radical is Localized on a Tyrosine Side Chain

To gain more information about the radical species, spectra for the 0.5 min sample were measured as a function of applied microwave power and at varying temperatures (Fig. 6.2B-C). Increasing power yielded a series of similar looking traces that diminished in intensity with $P_{1/2}$ = 190 μW. A value in this range is consistent with an amino acid based radical that is not strongly exchange coupled to the electronic spin of a nearby paramagnetic metal. Coupling would enhance the spin-lattice relaxation for the radical and raise $P_{1/2}$. Values of $P_{1/2}$ for compound I, for example, where the por•+ radical is strongly exchange-coupled to the heme Fe(IV) (S=1/2) are typically >5 mW(13-15). For heme proteins in which the por•+ from compound I migrates to a nearby but still Fe(IV)-exchange-coupled tyrosine, e.g., cytochome P450 cam, $P_{1/2}$ = 1 mW (16). The effect of temperature on the spectrum was likewise characteristic of an organic side chain radical (17), with signal intensity diminishing steadily as the temperature was lowered from 200 to 30 K. The isotropic diminution in spectral intensity with either increasing power or decreasing temperature is suggestive of a single organic radical, rather than a distribution of species.

To test whether the radical species was a tyrosyl, the protein was expressed with all of its tyrosine side chains carbon-deuterated. The deuterium nucleus has an integer spin (I_D = 1) that couples weakly to the electron spin relative to the protium nucleus (I_H = ½); perdeuteration consequently eliminates the doublet hyperfine splitting observed for ^{1}H in the EPR spectra of tyrosyl radicals. Moreover, deuteration narrows the EPR peak-to-trough line width for free tyrosine from 21 to 8 G (12). Consistent with its assignment as a neutral tyrosyl radical, the spectrum measured for the Tyr-deuterated decarboxylase following reaction with 400 eq H_2O_2 (<30 s) displayed no hyperfine features and a significantly narrowed linewidth (7 G) (Fig. 6.2D).

The EPR Spectrum for the Intermediate Can Be Simulated with Hyperfine Coupling Due to the Y145 Methylene Protons and Slight G-anisotropy

Studies of site-specifically deuterated tyrosines have shown that the electron spin of the tyrosyl radical localizes on the ring 1, 3, and 5 carbons (12,18). Coupling of the electron spin to ^{1}H on carbons 3 and 5 is weak and relatively insensitive to the protein environment. Doublet splitting due to each of the two methylene Cβ protons (H_A and H_B, Scheme 6.1), however, constitutes the major contributor to hyperfine structure, and depends on each proton's position relative to the p_z orbital on the ring C1, according to (1):

$$A_H = B_0\rho + B_1\rho\cos^2\theta \qquad (1)$$

A_H is the isotropic hyperfine coupling due to Cβ-H for H_A or H_B, ρ is the ring carbon unpaired electron spin density (ranging over 0.35-0.42 for C1 for known protein tyrosyl radicals), and B_1 is a constant (58 G for tyrosyl radicals) (12,18, 19). $B_0 << B_1$ and is usually neglected (12).

Analysis of the crystal structure for the homopentameric decarboxylase-coproheme complex (PDB ID 5T2K) (9) allowed us to identify an average Θ_A = 45.41° (± 2.20°) and Θ_B = 72.21° (± 2.01°) for Y145 (errors represent ±1 standard deviation).

Inserting each of these angles and $\rho = 0.35\text{-}0.42$ into (1) yielded predicted hyperfine coupling constants $A_{HA} = 10\text{-}12$ G and $A_{HB} = 1.9\text{-}2.3$ G. These ranges and g = 2.005 gave starting values for fitting the spectrum for the intermediate trapped at 30 s (Fig. S6.4). The fit refined to give $A_{HA} = 9.6$ and $A_{HB} = 2.5$ G, each of which is close to the predicted range. A small degree of g-anisotropy ($g_1 = 2.006$, $g_2 = 2.005$, $g_3 = 2.004$) improved the fit, possibly reflecting small differences in the individual subunits of the homopentamer, or delocalization of radical character onto other tyrosines (total of 9 per monomer). Hence, the spectrum appears to be consistent with a radical on residue Y145. Accurate simulation of the X-band EPR spectrum, without making assumptions about the identity or structure of the tyrosine giving rise to the spectrum, the likely degree of g-anisotropy, or the range of values for ρ will require further analysis of the corresponding high-field EPR spectrum, using g_x to solve for θ and ρ, as in reference (19).

Loss of the EPR Radical Signal Specifically in the Y145S Mutant Suggests That Y145 is the Site of the Radical Intermediate

Four aromatic amino acids that could potentially harbor radical electron density (20) surround the pair of reactive propionates: Y145 (propionate 2), and W198, W157, and Y113 (propionate 4) (Fig. 6.1). Substitution of each of the latter 3 by redox-inactive residues had little or no effect on the number of H_2O_2 equivalents required to convert the enzyme-coproheme complex to heme *b*, though there were some differences in HPLC profiles of porphyrin-containing products versus [H_2O_2]. The W198F mutant, for example, accumulated relatively more harderoheme intermediate than WT, while the heme *b* product bound to Y113S was more susceptible to H_2O_2 mediated degradation.

These differences suggested that Y113, W198, and W157 may play some role in the coproheme/heme *b* conversion, but not as an essential catalytic component.

The Y145S mutant, by contrast, exhibited no decarboxylase activity, regardless of the amount of H_2O_2 added (9). Instead, after addition of 3000 eq H_2O_2, 90% of the initially present coproheme had degraded to a product without an observable UV/vis chromophore. These experiments suggested that Y145 was possibly the site of a catalytic radical.

To test this hypothesis and to determine whether the radical formed in a unique and localized manner, coproheme complexes of the W198F, W157F, Y113S, and Y145S mutants were examined for their ability to form radicals during turnover with H_2O_2. Following reaction with 10 eq H_2O_2, the W198F, W157F, and Y113S mutants formed radical species with EPR spectral features that were highly similar to each other and to WT (Fig. S6.4). Small discrepancies in the fitted g-values and hyperfine coupling constants suggest the radical is sensitive to the changes in the chemical environment that these mutations produce (Table S6.1). Spin quantitation of the spectrum measured for the 30 s samples indicated 30, 30, and 42 μM of the radical species had formed in the W198F, W157F, and Y113S mutants (standard deviations for 3 measurements were ≤10% of the measured intensity). For comparison, the WT decarboxylase accumulated 35 μM of the radical species at 30 s. In each case, the radical species diminished in intensity over time, reaching ≤25% of the integrated intensity at 30 s by 150 s (Fig 6.3A-C) and receding to baseline within 300 s.

By contrast, the Y145S-coproheme complex formed no appreciable radical species under the same reaction conditions. Following addition of a large excess of H_2O_2 (300 eq), a small amount of an EPR-observable S=1/2 species formed (3.8 μM per 100 μM protein) (Fig 6.3D). The peak-to-trough linewidth (11 G) was narrower than the spectra in Fig 2A or 3A-C, the spectrum decayed to baseline more rapidly following the addition of H_2O_2 (within 150 s), and the spectrum measured at 30 s lacked any detectable hyperfine splitting (Fig. S6.4, Table S6.1). While the identity/nature of the radical in this mutant is currently unresolved, it is clear this species is off the reaction pathway.

The dependence of product formation on Y145, the formation of a $S = ½$ radical whose microwave power and temperature dependencies are consistent with an organic radical, and the temporal correlation of the radical decay with product formation support the conclusion that Y145 is the site of a mechanistically crucial radical-based intermediate.

Cleavage of the 2-propionate-β-C-H Bond by the Y145 Radical is Partly Rate Limiting

Y145• is well-positioned to remove a hydrogen atom from the coproheme propionate 2 on the carbon β to the tetrapyrrole (Fig. 6.1) (9). A substrate radical at this position would be conjugated to and resonance stabilized by the macrocycle. To test whether C-H bond cleavage occurs at this position, coproheme with deuterium substituted for protium at all of its propionate-β-carbons was prepared. Its reaction with H_2O_2 was studied over time via stopped flow UV/vis and freeze-quench EPR spectroscopies. The reaction exhibited biphasic kinetics in which the first phase was linearly dependent on H_2O_2 concentration and led to heme *b* formation (Fig. 6.4A). The second phase was independent of H_2O_2 and led to loss of the heme *b* chromophore. Second order rate constants determined for the first phase as a function of pH are plotted in Fig. 4B along with data previously measured for unlabeled coproheme.(8) The rate constants in each case had identical though modest (~3-fold) pH dependencies, with a p*K*a = 7.4 and a k_D/k_H kinetic isotope effect (KIE) of approximately 2 across the entire pH range. We conclude that the Cβ-H bond is cleaved during the decarboxylation reaction; because the theoretically expected value for a primary H/D KIE is 7 (21,22), this step likely only partially limits the rate of coproheme/heme *b* conversion. The D-coproheme/H_2O_2 reaction was subsequently monitored over time by freeze-quench EPR (Fig. 6.4C). The amount of Y145• accumulating at 0.5 min dramatically increased, relative to the unlabeled substrate, to 75 μM per 100 μM protein. The Y145• signal likewise took longer (>30 min instead of ~5 min) to return to baseline for the deuterated complex (data shown to 300 s). These results collectively suggest that Y145• forms immediately prior to, and is responsible for, cleavage of the Cβ-D bond.

Y145• Formation is Accompanied by Loss of the High Spin Iron Signal

EPR spectra were remeasured at 15K for the t=0 and 30s samples from Fig. 4C to characterize changes at the iron center that accompany formation of Y145• (Fig. 6.5). The spectrum measured at 0s was largely high spin (S=5/2) and rhombic, similar to spectra previously reported for HemQ-coproheme complexes from *S. aureus* and *Listeria monocytogenes* (23). At 30s, no obvious new signals due to iron species appeared. Instead, ~70% of the doubly integrated spectral intensity was lost from the t=0s high spin signal. At the same time, the S=1/2 signal attributed to Y145• appeared (77K data shown in Fig. 6.2). These data are consistent with the conversion of some of the initially available Fe(III) to an EPR-silent iron species, such as low spin Fe(IV)=O (S = 0), as Y145• forms.

Y145• also Catalyzes the Decarboxylation of the Ferric Harderoheme Intermediate

The data presented above suggest that Y145• facilitates the initial, slower decarboxylation of coproheme to harderoheme. Data presented here and previously also suggest that, if a similar radical mechanism is used for conversion of harderoheme to heme *b*, Y145 is also responsible. Specifically, reactions of the W198F, W157F, and Y113S mutants were not interrupted at the harderoheme/heme *b* interconversion step, and the Y145S mutant did not yield heme *b* (7). To examine directly whether Y145• is also involved in the harderoheme/heme *b* conversion, the decarboxylase-harderoheme complex was generated and its reaction with 10 eq H_2O_2 followed over time by freeze-quench EPR. A radical species with features similar to those in Fig. 2 formed and decayed over time (Fig. 6.6, Fig. S6.4, Table S1). Product analysis identified the end species of the reaction as heme *b* (7). These data suggest that Y145• forms and reacts in the harderoheme-bound enzyme, and may therefore also be responsible for decarboxylating propionate 4.

Discussion

Heme biosynthesis in many bacteria concludes with a pair of oxidative decarboxylations. Coproheme serves as both substrate and cofactor in these reactions, and the two vinyl groups of heme *b* are products. A similar heme- and H_2O_2-dependent reaction is catalyzed by the unusual cytochrome P450, OleT. This enzyme reacts with H_2O_2 to form the catalytic Fe(IV)=O (por+•) species, which in turn directly abstracts a hydrogen atom from the carbon at the □□position relative to the carboxylate group of a fatty acid. For long chain substrates (C_n, $n \geq 20$), this is followed by transfer of an electron and proton to the resulting Fe(IV)-OH (por), yielding Fe(III)por, CO_2, the n-1 alkene and water (24).

Though coproheme decarboxylase catalyzes a similar reaction, its structural constraints are different from those of OleT. Specifically, the two sites of decarboxylation – propionates at peripheral tetrapyrrole positions 2 and 4 – are positioned such that neither has direct access to the distal pocket where H_2O_2 is activated (Fig. 6.1). This suggested two possible mechanisms. First, oxidizing equivalents could be conveyed by diffusion of •OH, generated via homolytic cleavage of a ferric-hydroperoxy intermediate, from the site of the Fe/H_2O_2 reaction to each propionate. Alternatively, the oxidation could proceed through a relay mechanism involving one or more amino acid side chains as intermediaries, possibly dissecting the requisite H-atom transfer reaction into proton and electron transfer steps.

Results reported here clearly support the latter mechanism. Time-resolved freeze quench experiments demonstrated the formation and decay of an EPR-active, S=1/2 species during the course of a single turnover of the decarboxylase-coproheme complex (Fig. 6.2). This species had power- and temperature-dependencies consistent with its assignment as an organic radical. Narrowing of the spectral linewidth and loss of ^{1}H-hyperfine coupling in spectra for the D-Tyr labeled protein allowed assignment of the radical species as a tyrosyl (Fig. S6.3), which mutagenesis confirmed to be localized specifically at the Y145 side chain (Fig. 6.3).

Separation between the sites of oxidant activation and substrate oxidation is a recurring motif in metalloenzyme catalysis. Class 1 ribonucleotide reductase provides a classic example, in which oxidizing equivalents are conveyed from the dinuclear iron cluster where O_2 is reductively activated to a nearby tyrosine and ultimately to a catalytic cysteine residue more than 30 Å away (25). Heme-dependent lignin peroxidases translate the oxidizing power of the catalytic Fe(IV)=O (por+•) species over similar distances and to the protein surface, allowing the enzyme to access large, water-insoluble lignin substrates (26). A heme/alkylperoxide reaction in prostaglandin synthase generates Fe(IV)=O (por+•) which in turn oxidizes a tyrosine side chain to the tyrosyl radical. The tyrosyl specifically abstracts the pro-S hydrogen atom from the C13 position on a large, polyunsaturated arachidonic acid substrate (10). Distinct from OleT, the resulting fatty acyl radical is prevented from transferring an electron to the heme iron; instead, it reacts directly with O_2 to form an intermediate adduct. Heme A synthase and certain cytochrome P450 subtypes are in some ways most analogous to coproheme decarboxylase, since the same heme molecule is both the catalytic moiety and the scaffold for the substrate (3,4). In each case, oxidation of amino acid side chains by Fe(IV)=O (por+•) is proposed to generate amino acid radicals which, in turn, abstract hydrogen atoms from heme methyl substituents. Subsequent transfer of the resulting electron on the methyl carbon to the heme Fe(IV) generates a methyl carbocation, which is primed for nucleophilic attack by either water or carboxylate side chains.

These examples illustrate how, using one or a series of oxidizable amino acid side chains, Fe(IV)=O (por+•) can extend its reach over sometimes long distances. The amino acid intermediary additionally provides a degree of control over what happens after the initial hydrogen atom abstraction from the substrate. In the case of OleT, in which the hydrogen atom transfers directly to Fe(IV)=O (por+•), the resulting substrate radical transfers a second electron to the nearby Fe(IV)=O (por). By contrast, in prostaglandin synthase, the arachidonic acid radical is removed from the analogous Fe(IV)=O (por) species, and instead reacts with O_2. Coproheme decarboxylase appears to use Tyr145 as an intermediary, connecting the oxidizing power of the presumptive Fe(IV)=O (por+•) intermediate to the C□ carbon of each reactive propionate. The resulting propionyl radical electron is then transferred to the Fe(IV).

Though there is no direct evidence as yet for Fe(IV)=O (por+•) as the reactive species, the production of Y145• occurred along with loss of the starting ferric-coproheme S=5/2 signal and without the clear appearance of new EPR-active species (Fig. 5). These observations are consistent with a mechanism in which ferric coproheme first reacts with H_2O_2 to form a ferric-hydroperoxy intermediate. Protonation and heterolytic cleavage of the intermediate would yield Fe(IV)=O (por+•) and water. This high-valent species could subsequently remove a hydrogen atom from Y145 to form Y145•. In cytochrome P450s or peroxidases with a basic ferryl oxygen, H-atom transfer is expected to deliver an electron to the porphyrin radical cation and a proton to the ferryl in a single, concerted step (27-29). While the destination of the proton from Y145 is not clear, concerted rather than sequential proton and electron transfer from Y145 is attractive, in light of the expected p*K*a (~10) and midpoint potential of the neutral tyrosine side chain (30). Hydrogen bonding contact between propionate 2 and Y145 (Fig. 6.1) might serve to modulate this p*K*a and/or supply a conduit through which the electron is conducted to the macrocycle, as proposed for ascorbate peroxidase and heme model complexes (31,32). The resulting low-spin d^4 Fe(IV)=O (por) or Fe(IV)-OH (por) species is expected to have integer spin (S=1), and therefore to be EPR-silent (33).

Once formed, Y145• abstracts a hydrogen atom from a nearby propionate-Cβ-H in a step that appears to be partially rate limiting (Fig. 4). Supporting this conclusion, deuteration of the propionate-β-carbons elicits a two-fold (rather than the theoretically predicted seven-fold) decrease in the second order rate constant for the decarboxylase/H_2O_2 reaction (22). Moreover, about twice as much Y145• accumulates in the time-resolved EPR spectra when the propionate is deuterated, suggesting that this species directly abstracts the H-atom from propionate 2. H-atom transfer is expected to leave behind a Cβ□radical, which we anticipate quickly transfers to the substrate Fe(IV) as CO_2 is lost and a new C-C double bond forms (Scheme 6.2).

Prior work showed that the initial decarboxylation of propionate 2, yielding harderoheme, is slightly slower than the subsequent decarboxylation of propionate 4. While we inferred that the harderoheme reacted with a second molecule of H_2O_2 to form heme *b*, it was not certain whether this reaction utilized the same Y145 radical. To address this question directly we generated the decarboxylase-harderoheme complex and monitored its reaction with H_2O_2 by time-resolved, freeze-quench EPR. A $S = ½$ signal having line width and hyperfine features similar to those of the analogous coproheme intermediate was observed (Fig. 6.6). This suggested that harderoheme's propionate 4 is also decarboxylated using Y145• as an intermediary. Whether the harderoheme reacts in the same orientation as shown in Fig. 1, or whether the propionate first forms a hydrogen bonding interaction with Y145, either by leaving the active site and rebinding in a reactive configuration, or by rotating ~90° *in situ*, is unknown.

Conclusions

Our results support a catalytic model in which the decarboxylase-coproheme complex reacts with H_2O_2 to form an activated intermediate, possibly Fe(IV)=O (por+•), that in turn oxidizes Y145 to Y145•. The tyrosyl radical then abstracts a hydrogen atom from the Cβ□of propionate 2 in a step that partially limits the overall reaction rate. Electron transfer from the Cβ to Fe(IV) occurs with loss of CO_2 and formation of a new vinyl group. A second round of reaction with H_2O_2 generates Y145• again in the harderoheme complex, allowing for a second decarboxylation in turn. This model is reminiscent of mechanisms proposed for heme A synthase or certain cytochrome P450s, both of which undergo oxidative modifications of their methyl side chains, or the initial hydrogen atom transfer from arachidonic acid in prostaglandin synthase. The use of tyrosyl radicals as intermediaries in each case allows for a high degree of reaction control and access of the oxidizing species to otherwise hard-to-reach substrates.

Experimental Procedures

Preparation of the decarboxylase (HemQ) from *Staphylococcus aureus*

Expression and purification of WT and mutant proteins (plasmids available from prior work) were carried out as previously reported (7,9).

Preparation of the Decarboxylase with Deuterated Tyrosine Side Chains

L-tyrosine with deuterium substituted for protium at all of its carbon atoms (D_6-L-Tyr, 98% label incorporation) was obtained from Cambridge Isotopes. The decarboxylase was overexpressed in a tyrosine-auxotrophic strain of *E. coli* C43 (DE3) ML14 (*ΔtyrA*) (Adgene),(34) which had been transfected with the same pET28a-*hemQ* construct used above. M63 minimal growth medium contained (per L): 3 g KH_2PO_4, 7 g K_2HPO_4, 2 g glucose, 2 g NH_4Cl, 10 mg thiamine, 50 mg kanamycin, 10µM $CuSO_4$, 30 µM $FeSO_4$ and 1 mM $MgSO_4$). Prior to inoculation, the medium was supplemented with an amino acid mixture containing (per l) 16 mg His, 35 mg Val, 35 mg Phe, 40 mg Leu, 40 mg Asp, 40 mg Ile, and either 80 mg of unlabeled Tyr or 50 mg D_6-Tyr (L-enantiomers used for all amino acids). A starter culture was generated by inoculating 2 ml of Lysogeny Broth (LB) plus 50 mg/l kanamycin with a single colony of the expression strain from a freshly streaked plate. The culture was grown on a 250 RPM shaker incubator for 10 h at 37°C, and then used to inoculate (1:500) 10 ml of fresh M63+amino acids+kanamycin. After 12 h (37°C, 250 RPM), the 10 ml culture was used to inoculate (1:1000) 6 1lflasks of M63+amino acids+kanamycin. Cultures were grown at 37°C until an OD_{600} of 0.4 was reached. Protein expression was induced by adding IPTG (isopropyl β-D-1-thiogalactopyranoside, 0.5 mM final concentration) and the temperature was lowered to 20°C. Cells were harvested by centrifugation after 16 h and the enzyme purified/substrate-loaded in the same fashion as the unlabeled enzyme.

Generation of Decarboxylase-Substrate Complexes

Purified protein was incubated at 4 °C in the dark with gentle stirring for 24 h with either the substrate ferric coproheme III, the three-propionate-substituted intermediate (ferric 2-vinyl-4,6,7-tripropionic acid heme, commonly named harderoheme isomer III (35) though it is now understood not to be associated with the harderian gland (36)), or deuterated coproheme III (D-coproheme, synthesis described below) in a 1:1 subunit:coproheme ratio. Unbound coproheme was removed by repeated rounds of centrifuge-filtration and the protein-ligand complexes were further purified on an S-200 Sephacryl gel filtration column (0.4 ml/min). Fractions were collected using an AKTA purification system and then screened via UV/Vis spectroscopy (Cary50) for the presence of a ferric porphyrin. Fractions with Rz values ≥0.8 (Rz = $\text{absorbance}_{\text{Soret}}/\text{absorbance}_{280\text{nm}}$) were pooled. For D_6-Tyr-labeled protein, protein with Rz ≥ 0.4 was retained. Bound porphyrin concentrations were determined by the pyridine hemochrome method. Briefly: 50 μl of protein solution (at 50-300 μM) was mixed with 200 μL of 50 mM NaOH containing 20% pyridine by volume. 3 μL of 0.1 M $K_3[Fe(CN)_6]$ was added and the oxidized spectrum was measured; 3−5 mg of solid sodium dithionite ($Na_2S_2O_4$) was then added to yield spectra for the reduced pyridine-bound hemes. Difference spectra (reduced minus oxidized, r-o) were used to determine the concentration of metalloporphyrin released from the protein. For coproheme: $\varepsilon_{r\text{-}o}$ 546 nm = 23.2 mM^{-1} cm^{-1}; for heme *b*, $\varepsilon_{r\text{-}o}$ 556 nm = 28.4 mM^{-1} cm^{-1}. The Bradford and pyridine hemochrome assays for protein and Fe-porphyrin, respectively, were used to determine the cofactor occupancy in the purified complexes.

Biosynthesis, Purification, and Characterization of Deuterium-Labeled Coproheme

Site-specifically deuterated coproheme III was synthesized enzymatically *in vitro* (11). The heme biosynthesis enzymes porphobilinogen synthase (HemB), porphobilinogen deaminase (HemC), uroporphyrinogen III synthase (HemD), uroporphyrinogen III decarboxylase (HemE), coproporphyrinogen oxidase (HemY) and ferrochelatase (HemH) were recombinantly expressed in His_6-tagged forms from synthetic genes in pET 15b or 28a vectors (Genscript). Sequences for the genes encoding HemB, C, D, and E were obtained from the *E. coli* K12 genome in the NCBI data base and used without modification (genome accession number NC_000913.3 at location 388753-389727, 3989825-3990766, 3989088-3989828, and 4197716-4198780 for *hemB*, *C*, *D*, and *E* respectively). Sequences encoding HemY and HemH in *Staphylococcus aureus* Newman were likewise obtained from NCBI (accession number NC_009641.1 at 1923252-1924652 for *hemY* and 1924676-1925599 for *hemH*) and codon-optimized for heterologous expression in *E. coli*. Individual plasmids were transformed into Tuner(DE3) cells (Novagen). Heterologous expression was carried out in 1L flasks of Terrific Broth supplemented with the appropriate antibiotic (kanamycin or ampicillin). Flasks were inoculated 1:100 with a freshly saturated starter culture and grown at 37 °C until an optical density of 0.4-0.6 at 600 nm was reached. IPTG was added to a final concentration of 100 µM, the temperature lowered to 20 °C, and the cells grown overnight. Cell pellets harvested by centrifugation were lysed by sonication in buffer A (50 mM Tris, pH 8, 150 mM NaCl, 5 mM imidazole), the lysates were clarified by centrifugation at 45,000 x g for 1 hour, and the supernatants loaded onto a nickel-nitrilotriacetic acid affinity column (BioRad) equilibrated with buffer A. Protein was eluted by a 300 ml linear gradient from 0-100% buffer B (50 mM Tris, pH 8, 150 mM NaCl, 500 mM imidazole) at 2 ml/min (Akta Prime). The proteins eluted around 40-60% buffer B. Pure fractions were identified via SDS-PAGE, concentrated, dialyzed into 50 mM Tris (pH 8, 150 mM NaCl, with 20% glycerol for HemD), and stored at -80 °C.

Custom-synthesized 3,3,5,5-$^{2}H_4$-aminolevulinic acid (D_4-ALA, Shanghai Artis Company) was used as the labeled starting material to produce [5, 10, 15, 20, 21, 22, 23, 24-$^{2}H_{12}$]-coproporphyrin III (D-coproporphyrin), in which the carbons □ to the propionate carboxylate groups as well as the tetrapyrrole-bridging *meso* carbons are perdeuterated (Scheme 2). Zn-acetate (10 μM), $MgSO_4$ (10 μM), ALA or D_4-ALA (1 mM), dithiothreitol (DTT, 3 mM), and the four enzymes HemB/C/D/E (2 μM) were degassed by repeated cycles of evacuation and argon backfilling on a Schlenk line, then brought into an anaerobic chamber (Coy). Reactants were combined in 50 ml of 50 mM Tris, pH 8 and stirred overnight in the dark at ambient temperatures (expected theoretical yield: 6.25 □moles coproporphyrin). After ~16 h, the reactions were removed from the anaerobic chamber, exposed to O_2 from ambient air, and HemY (350 nM) was added. Reactions were stirred at 37°C in the dark for 1-2 h to fully oxidize the D-coproporphyrinogen to D-coproporphyrin.

The D-coproporphyrin-containing reactions were degassed by repeated cycles of evacuation and N_2 backfilling on a Schlenk line and brought into the anaerobic chamber. HemH (10 μM), DTT (1 mM), and 1.1 eq of ferrous ammonium sulfate were added. After 30 min, the red D-coproheme was removed from the chamber and analyzed by HPLC and mass spectrometry (MS). For final purification, the D-coproheme-containing reaction was loaded onto two 25 ml C18 solid phase extraction columns (Restec product # 26034). The columns were washed with several volumes of H_2O and eluted with methanol, followed by acetonitrile (ACN) with 0.1% trifluoroacetic acid (TFA), and finally methanol. Each column elution step was dried under N_2, reconstituted in DMSO, and analyzed (see below) before combining and storing the pure fractions at -80 °C. Biosynthetically generated hemes and their precursors were analyzed by the methods outlined below.

HPLC

20-25 µl porphyrin- or heme-samples were injected onto a Hypersil Gold PFP 5 µm column (150 × 4.6 mm, Thermo Fisher) attached to an Agillent1100 series HPLC instrument. Solvent A was H_2O with 0.1% TFA and Solvent B was ACN with 0.1% TFA. Samples were run at a flow rate of 2.5 ml/min starting with isocratic 10% B for 3 min, followed by a linear gradient from 10% B to 95% B over 13 min. This was followed by isocratic 95% B for 3 min and a 2 min wash with 10% B. UV/vis absorbance was monitored at 400 nm. Coproporphyrin and coproheme samples were quantified via standard curves (0-20 µM) based on HPLC peak integration.

MS

Tetrapyrrole intermediates and products were analyzed via HPLC in line with electrospray ionization (ESI) MS to verify their expected masses and deuterium incorporation. HPLC was carried out using an Agilent 1290 system and Agilent PLRP-S PSDVB column (3.0 µm particles, 50 mm x 1.0 mm diameter, P/N PL1312-1300). The column was maintained at 50ºC with a flow rate of 0.6 ml/min. Solvent A consisted of water with 0.1% (v/v) formic acid. Solvent B was acetonitrile with 0.1% formic acid. The column was equilibrated to 5% B prior to sample injection. A linear gradient from 5% to 95% B was used from 1.0-4.0 min, followed by 95% B (4.0-5.0 min) and 5% B (5.0-6.0 min). Column eluate was imported into an Agilent 6538 quadrupole time of flight (QTOF) mass spectrometer with an electrospray ionization (ESI) source. Source parameters were: drying gas 8.0 l/min, drying gas heat at 350 ºC, nebulizer 55 psi, capillary voltage 3500 V, capillary exit 100 V. Spectra were collected in positive mode from 50 to 1700 m/z at a rate of 2 Hz.

NMR Spectroscopy

Coproporphyrin III, D-coproporphyrin III, and their aminolevulinic acid precursors were analyzed by NMR in order to assess the position and extent of deuterium label incorporation into the latter. All compounds were characterized by ^{1}H using a Bruker 300MHz NMR and/or a Bruker AVANCE III 500 MHz NMR spectrometer, equipped with a Prodigy^{TM} cryoprobe and SampleJet^{TM} automatic sample loading system. Chemical shifts are reported in ppm (□) relative to the residual solvent peak in the corresponding spectra; deuterium oxide □□4.79, D_4-methanol □□3.31 and coupling constants (*J*) are reported in hertz (Hz) and analyzed using MestReC NMR data processing.

Monitoring Decarboxylase Reactions in Real Time with Stopped Flow UV/Visible spectroscopy (UV/Vis)

Data were measured using a Hi-Tech Scientific stopped-flow spectrometer in single mixing mode with diode array detection. The decarboxylase-ferric-tetrapyrrole complex (5 – 10 µM) was rapidly mixed (<1.5 ms) with variable concentrations of H_2O_2/D_2O_2 or peracetic acid prior to measurement of spectra. Data were measured at varying time points and fit using the Kinetic Studio (Hi-Tech Scientific) software to exponential decay functions to determine rate constants (k_{obs}). For each experimental condition, all data were measured in at least triplicate and averaged. Plots of k_{obs} versus oxidant concentration were fit with linear least squares regression analysis to determine second order rate constants (Kaleidagraph). Reactions were carried out over a range of pH values in either 50 mM potassium phosphate (pH 5.8, 6.6, and 7.4) or 50 mM Tris-Cl (pH 8.2 or 8.8).

Time resolved EPR Spectroscopic Analyses of the Reaction of Decarboxylase-Tetrapyrrole Complexes with H_2O_2

EPR data were measured on a Bruker EMX EPR spectrometer (X-band, 9.37 MHz) using a Bruker Cold Edge (Sumitomo Cryogenics) cryogen-free system with a Mercury iTC controller unit. In all cases, averages of 4 scans are reported. For the reaction time course experiments, 120 μL aliquots of enzyme-substrate complex (200 μM, pH/D 8.8, 298 K) were manually mixed inside the EPR tube with an equal volume of H_2O_2 (D_2O_2) containing either 10 or 300 equivalents of the oxidant and frozen in liquid N_2 at time points between 30-300 s. Organic radical spectra were measured at 77 K, 25 μW microwave power, 100 kHz modulation frequency, and 5 G modulation amplitude. Signals were double integrated over 3250-3450 G (OriginLab) and compared to TEMPO standards (0, 25, 50, and 100 μM) measured under similar conditions for spin quantitation. Fe spectra were measured at 15 K with a 2 mW microwave power over a field of 500 – 3500 G. Spectral g-values were determined via simulations of experimental data sets utilizing Easyspin software (37).

For studies of the dependence of the organic radical EPR signal intensity on temperature, the instrument parameters were the same as above but with temperatures set at intervals between 15 and 200 K. The normalized intensity (I_n) was plotted versus temperature:

$$I_n = \frac{(I_o \; x \; T \; x \; 10^{-\frac{dB}{20}})}{gain} \qquad (2)$$

Here, I_o is the doubly integrated signal, T is temperature, dB is microwave power, and gain is the amplifier gain.

For studies of the power saturation properties of the organic radical EPR signal, data were measured over 0.85 μW-103 mW at 77 K. The power at half saturation ($P_{1/2}$) was determined via nonlinear least squares regression analysis of the log($I/P^{0.5}$) versus P plots using:

$$\log\left(\frac{I}{\sqrt{P}}\right) = -\left(\frac{b}{2}\right)\log\left(P_{\frac{1}{2}} + P\right) + \left(\frac{b}{2}\right)\log\left(P_{\frac{1}{2}}\right) + \log(k) \qquad (3)$$

P is the microwave power, I is the peak-to-trough EPR signal intensity, b is a factor describing the homogeneity of the radical signal (where a value of 1 is non-homogenous and a value of 3 is completely homogenous), and k is an intensity correction factor.

Figures

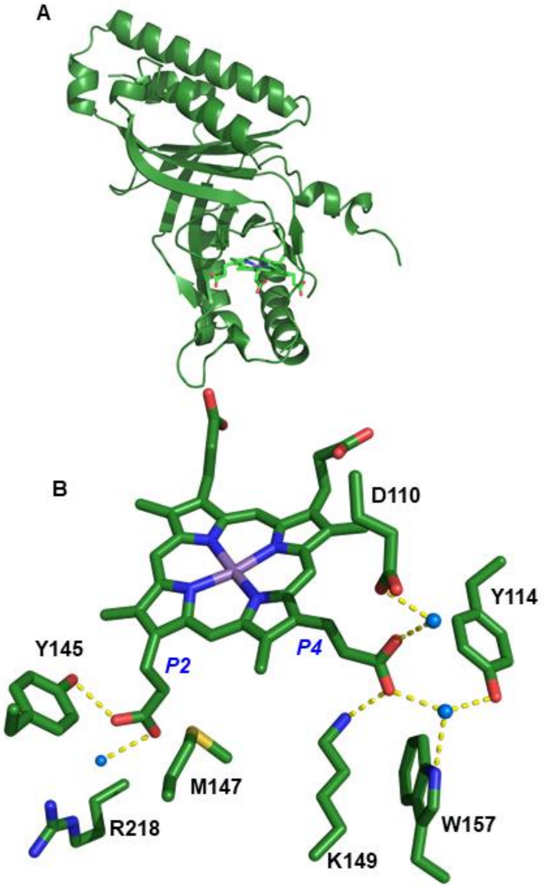

Figure 6.1. Coproheme decarboxylase subunit and active site with the substrate analog, manganese coproporphyrin, bound. A) The subunit structure of coproheme decarboxylase (green cartoon) showing a bound manganese coproheme. The unreactive pair of propionates points toward the solvent exterior and to the right in this diagram. B) Residues hydrogen bonded to reactive propionates 2 (P2) and 4 (P4) are indicated with dashed lines. Y145, Y113, W157, and W159 are all redox active side chains and potential sites of catalytic radical formation. W159, in the foreground of P4 in this view, has been omitted for clarity. K149 and M147 may facilitate a ~90° rotation to place P4 in hydrogen bonding contact with Y145.Three water molecules involved in hydrogen bonding networks to each propionate are included. Atoms are labeled: carbon green, nitrogen blue, oxygen red, and iron purple.

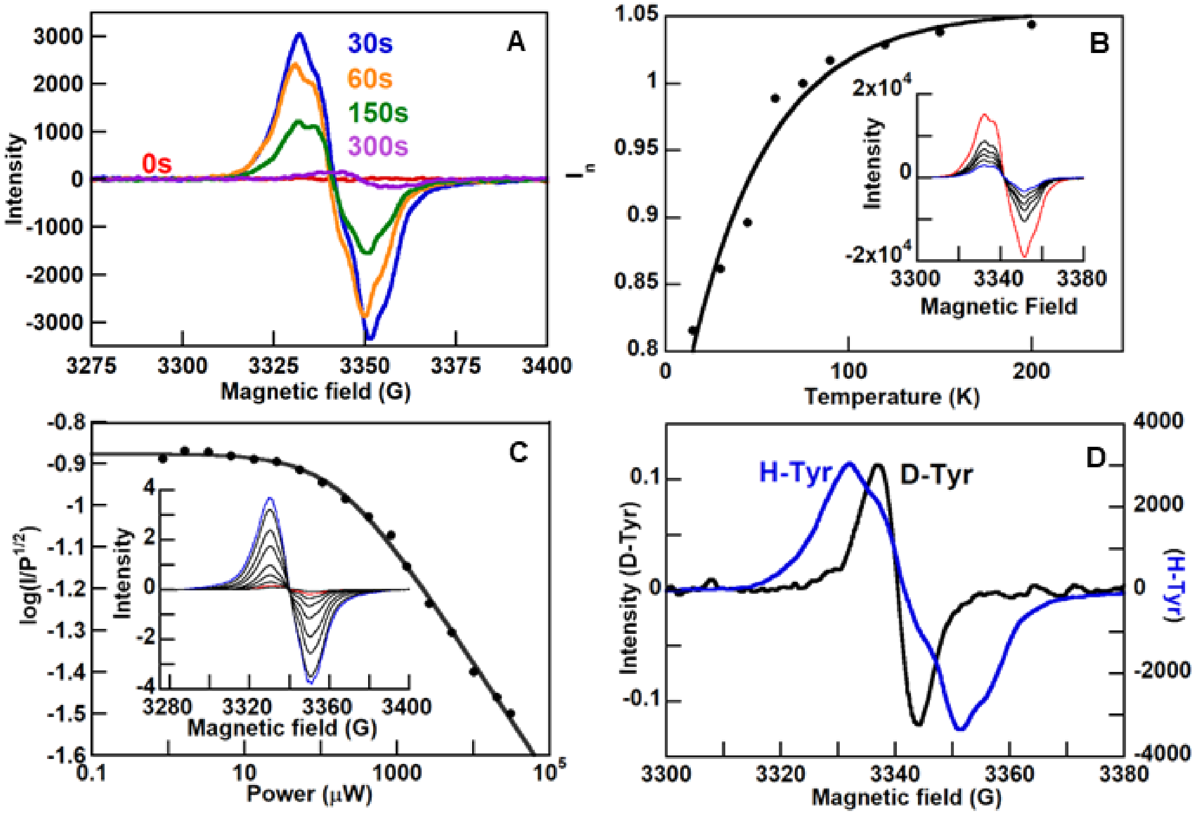

Figure 6.2. Properties of the side chain radical intermediate generated along the pathway to coproheme decarboxylation. A) A radical forms within 30 s of mixing 100 μM decarboxylase-coproheme complex with 10 eq H_2O_2 and then decays to base line over time. Spectra were measured for samples frozen at the indicated time points at 26 μW, 77 K, pH 8.8. Spin quantitation of the 30 s sample spectrum relative to a TEMPO standard curve indicated 35 μM of the radical species. B) The effect of temperature on normalized EPR signal intensity [eq (2)] was measured for the 30 s sample from 15-200K (A). An extrapolated curve illustrates the trend in the data points. Inset: full spectra measured at 30 (red curve), 60, 90, 120, 150, and 200 (blue curve) K are shown, illustrating the isotropic diminution of the signal with decreasing temperature. C) The power saturation behavior for the 30 s sample in (A) was determined from 0.85 μW – 39 mW. The data were fit to eq (3) yielding $P_{1/2}$ = 190 (±30) μW. Inset: full spectra are shown for every other point on the plot, from 1.7 μW (red curve) to 39 mW (blue curve), illustrating the isotropic loss of signal with increasing power. D) The EPR spectrum measured for the sample frozen at 30 s in (A) is overlaid with a sample prepared in a similar manner but with protein in which all the tyrosine side chains were fully deuterated. Upon deuteration, the peak-to-trough line width narrows from 20 G to 7 G and the fine structure is lost, consistent with the radical's assignment as a tyrosyl.

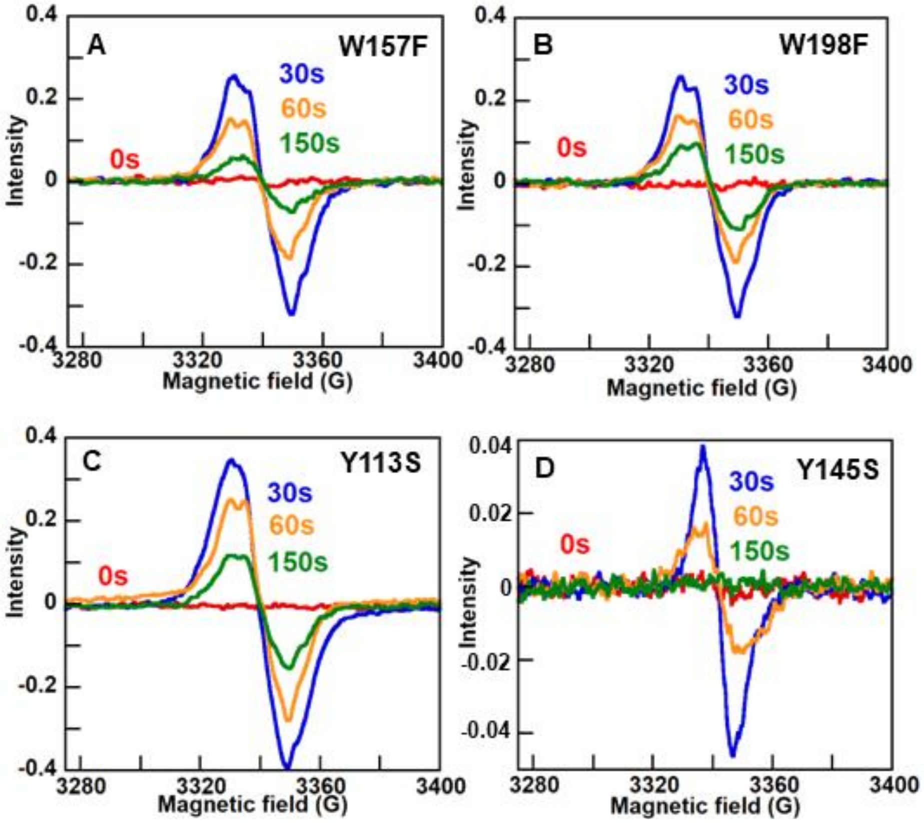

Figure 6.3. The side chain radical intermediate formed in W157F, W198F, and Y113S decarboxylase mutants has similar properties to WT decarboxylase, while Y145S is distinct. 100 □M coproheme complexes of the A) W157F, B) W198F, C) Y113S, and D) Y145S decarboxylase mutants were rapidly mixed with 10 eq H_2O_2 and subsequently frozen at the indicated time points. EPR spectra measured for the first three mutants resemble one another and the 30 s sample measured for the WT enzyme (Fig. 2). By contrast, the Y145S sample had a narrower line width and distinct g-values (see Fig. S3, Table S1, and text). Spin quantitation of the spectra measured for the 30 s samples indicated A) 30, B) 30, C) 42, and D) 3.8 □M of the radical species had formed (compare with WT Fig. 2A, where 35 □M accumulated). The radical species formed in the Y145S sample was not apparent above baseline by 150 s.

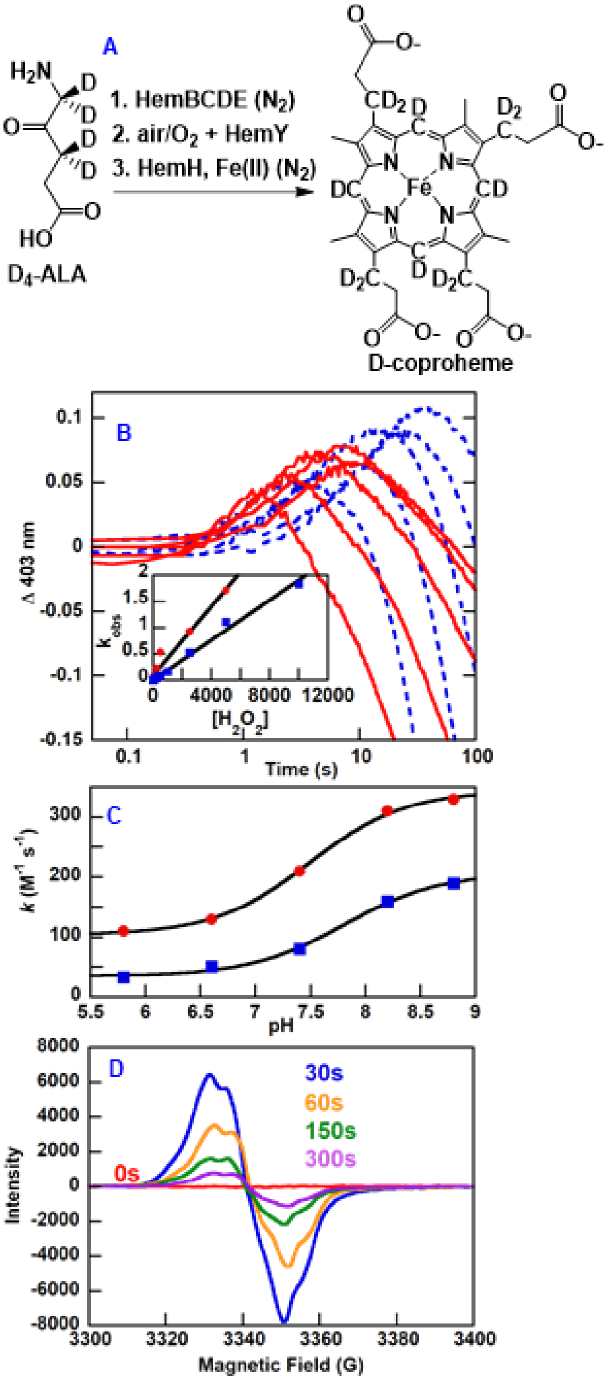

Figure 6.4. The decarboxylation of C□D$_2$-coproheme is ~2-fold slower than C□H$_2$-coproheme and results in substantially greater accumulation of Y145•. A) Summary of the biosynthetic scheme for C□D$_2$-coproheme from D$_4$-ALA, illustrating the expected positions of deuterium label incorporation. B) Reactions of 10 µM decarboxylase-coproheme (red lines) or -C□D$_2$-coproheme (blue dashes) with 15, 25, 50, 100, or 250 eq

H_2O_2 (increasing concentrations, right to left) were monitored over time via stopped flow UV/vis spectroscopy (50 mM potassium phosphate, pH 7.4, 25 °C). The traces measured at 402 nm (shown) were fit to two the sum of two exponentials. The first phase corresponded to the formation of the decarboxylase-heme *b* complex and the second to heme *b* decay (8). Inset: k_{obs} values derived from fits to the initial phase are plotted versus [H_2O_2]. Linear fits to the data yielded second order rate constants 210 and 80 M^{-1} s^{-1} for coproheme (red circles) and C□D_2-coproheme (blue squares) respectively. C) Second order rate constants for the reactions described in (A) were measured as a function of pH, and were fit to the same p*K*a. D) The tyrosyl radical formed during a single turnover of the decarboxylase-D-coproheme complex (100 □M + 10 eq H_2O_2) was monitored at 30 s, along with its subsequent decay. Spectra were measured at 0.026 mW, 77 K, pH 8.8. Spin quantitation of the spectrum measured for the 30 s sample indicated 75 □M of the radical species had formed.

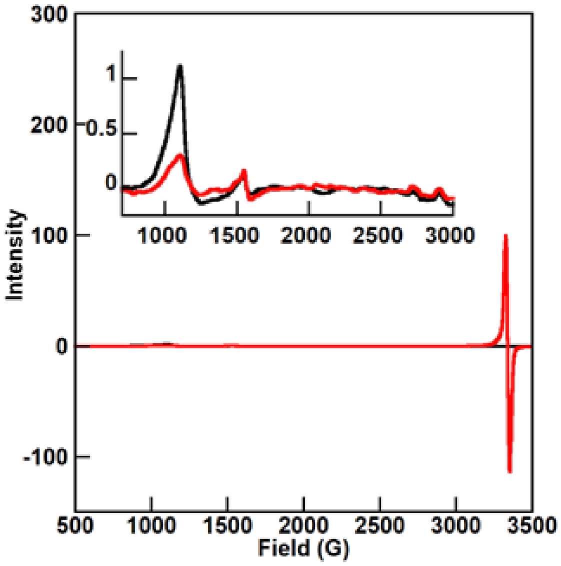

Figure 6.5. Time resolved EPR spectra show a ferric S=5/2 component that diminishes in intensity as the S=1/2 signal due to Y145• forms. The X-band EPR spectrum of the decarboxylase-C□D$_2$-coproheme complex (shown at 77K in Figure 3C) was remeasured at low temperature (15K) and over a broad magnetic field in order to visualize the substrate-bound iron at t=0 (black lines, 100 □M, 0.850 mW, pH 8.8). The 15K spectrum for the sample measured 30 s after the addition of 10 eq of H_2O_2 is shown in red. The 700-3000 G region is shown at an amplified scale in the inset. An S=5/2 signal, attributed to the ferric-C□D$_2$-coproheme, is apparent at both time points, diminishing in intensity from 97 (± 5) □M at 0s to 25 (±5) □M at 30 s. Over the same time interval, the S=1/2 signal attributed to Y145• in Fig. 4C formed [75 (±5) □M].

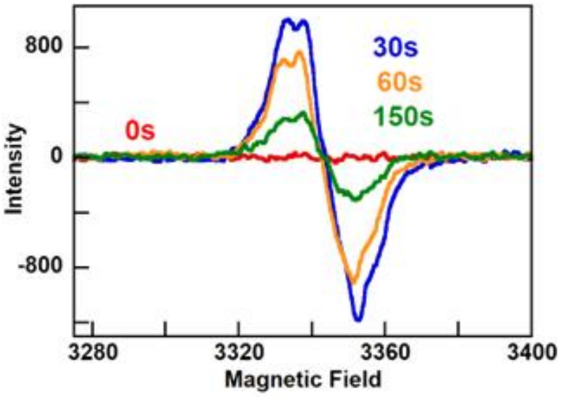

Figure 6.6. The ferric decarboxylase-harderoheme complex is also decarboxylated via a Y145 radical. Tyrosyl radical and its decay were monitored during a single turnover of the decarboxylase-harderoheme complex (100 □M + 10 eq H_2O_2). Spectra were measured at 0.026 mW, 77 K, pH 8.8. Spin quantitation of the spectrum measured for the 30 s sample indicated 12 □M of the radical species had formed. The EPR spectrum for the intermediate and the time required for its decay are similar to those measured for the radical involved in the decarboxylase-coproheme reaction (Fig. 2, Table S1), suggesting that Y145 is also involved in decarboxylating propionate 4.

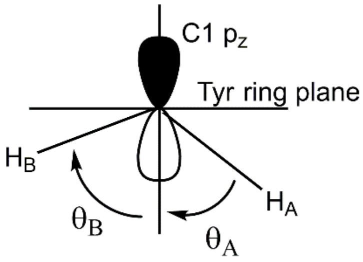
C1 p_z
Tyr ring plane
H_B
H_A
θ_B
θ_A

Scheme 6.1

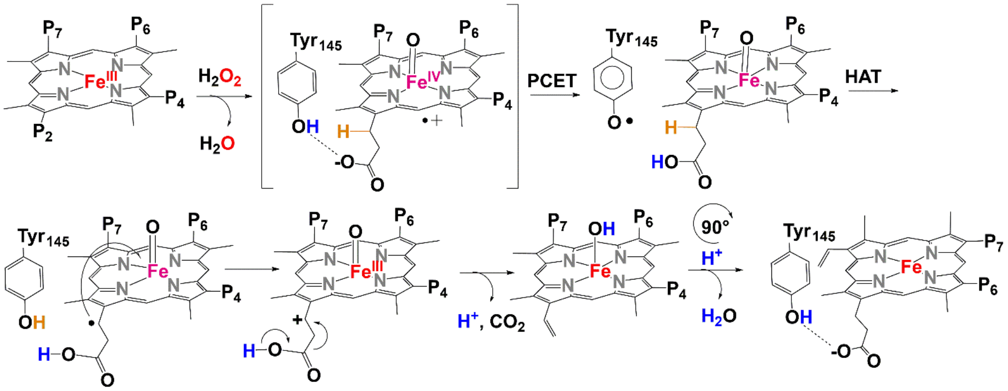
P_7
P_6
P_4
P_2
Fe^{III}
H_2O_2
H_2O
Tyr_{145}
Fe^{IV}
•+
PCET
HAT
-O
HO
90°
H^+
H^+, CO_2

Scheme 6.2. Proposed mechanism for coproheme decarboxylation. The C□-carbon from which an H-atom is transferred is labeled. There is no direct evidence for the intermediacy of a coproheme compound I (shown in brackets) or the subsequent C□-carbocation species; their presence is merely proposed hypothetically.

Associated Content

Acknowledgements

This work was supported by funding from the National Institutes of Health, General Medical Sciences R01GM090260 (J.L.D.) and R15GM114787 (G.S.L.-R.).

Abbreviations

The abbreviations used are: PCET, proton-coupled electron transfer; ALA, aminolevulinic acid; D_4-ALA, 3,3,5,5-$^2H_4$-aminolevulinic acid; KIE, kinetic isotope effect; LB, Lysogeny Broth; ACN, acetonitrile; TFA, trifluoroacetic acid; IPTG, isopropyl β-D-1-thiogalactopyranoside.

Conflicts of Interest

The authors declare no conflicts of interest with the contents of this article. The content is solely the responsibility of the authors and does not necessarily represent the official views of the National Institutes of Health.

References

1. Unno, M., Matsui, T., and Ikeda-Saito, M. (2007) Structure and catalytic mechanism of heme oxygenase. *Nat. Prod. Rep.* **24**, 553-570

2. Wilks, A., and Heinzl, G. (2014) Heme oxygenation and the widening paradigm of heme degradation. *Arch. Biochem. Biophys.* **544**, 87-95

3. Brown, K. R., Brown, B. M., Hoagland, E., Mayne, C. L., and Hegg, E. L. (2004) Heme A synthase does not incorporate molecular oxygen into the formyl group of heme A. *Biochemistry* **43**, 8616-8624

4. Colas, C., and de Montellano, P. R. O. (2003) Autocatalytic radical reactions in physiological prosthetic heme modification. *Chem. Rev.* **103**, 2305-2332

5. Dailey, H., Gerdes, S., Dailey, T., Burch, J., and Phillips, J. (2015) Noncanonical coproporphyrin-dependent bacterial heme biosynthesis pathway that does not use protoporphyrin. *Proc. Nat. Acad. Sci. USA* **112**, 2210-2215

6. Dailey, H., Dailey, T., Gerdes, S., Jahn, D., Jahn, M., O'Brian, M., and Warren, M. (2017) Prokaryotic heme biosynthesis: multiple pathways to a common essential product. *Microbiol. Molec. Bio. Rev.* **81**, e00048-16

7. Celis, A. I., Streit, B. R., Moraski, G. C., Kant, R., Lash, T. D., Lukat-Rodgers, G. S., Rodgers, K. R., and DuBois, J. L. (2015) Unusual peroxide-dependent, heme-transforming reaction catalyzed by HemQ. *Biochemistry* **54**, 4022-4032

8. Streit, B., Celis, A., Shisler, K., Rodgers, K., Lukat-Rodgers, G., and DuBois, J. (2017) Reactions of ferrous coproheme decarboxylase (HemQ) with O-2 and H_2O_2 yield ferric heme *b*. *Biochemistry* **56**, 189-201

9. Celis, A., Gauss, G., Streit, B., Shisler, K., Moraski, G., Rodgers, K., Lukat-Rodgers, G., Peters, J., and DuBois, J. (2017) Structure-based mechanism for oxidative decarboxylation reactions mediated by amino acids and heme propionates in coproheme decarboxylase (HemQ). *J. Am. Chem. Soc.* **139**, 1900-1911

10. Tsai, A. L., Kulmacz, R. J., and Palmer, G. (1995) Spectroscopic evidence for reaction of prostaglandin-H synthase-1 tyrosyl radical with arachidonic acid. *J. Biol. Chem.* **270**, 10503-10508

11. Layer, G., Pierik, A. J., Trost, M., Rigby, S. E., Leech, H. K., Grage, K., Breckau, D., Astner, I., Jaensch, L., Heathcote, P., Warren, M. J., Heinz, D. W., and Jahn, D. (2006) The substrate radical of Escherichia coli oxygen-independent coproporphyrinogen III oxidase HemN. *J. Biol. Chem.* **281**, 15727-15734

12. Barry, B., Eldeeb, M., Sandusky, P., and Babcock, G. (1990) Tyrosine radicals in photosystem II and related model compounds – characterization by isotopic labeling and EPR spectroscopy. *J. Biol. Chem.* **265**, 20139-20143

13. Khindaria, A., and Aust, S. (1996) EPR detection and characterization of lignin peroxidase porphyrin pi-cation radical. *Biochemistry* **35**, 13107-13111

14. Fujii, H., Yoshimura, T., and Kamada, H. (1996) ESR studies of A(1u) and A(2u) oxoiron(IV) porphyrin pi-cation radical complexes. Spin coupling between ferryl iron and A(1u)/A(2u) orbitals. *Inorg. Chem.* **35**, 2373-2377

15. Yeh, H., Gerfen, G., Wang, J., Tsai, A., and Wang, L. (2009) Characterization of the peroxidase mechanism upon reaction of prostacyclin synthase with peracetic acid. Identification of a tyrosyl radical intermediate. *Biochemistry* **48**, 917-928

16. Schunemann, V., Lendzian, F., Jung, C., Contzen, J., Barra, A., Sligar, S., and Trautwein, A. (2004) Tyrosine radical formation in the reaction of wild type and mutant cytochrome P450cam with peroxy acids - A multifrequency EPR study of intermediates on the millisecond time scale. *J. Biol. Chem.* **279**, 10919-10930

17. Di Bilio, A., Crane, B., Wehbi, W., Kiser, C., Abu-Omar, M., Carlos, R., Richards, J., Winkler, J., and Gray, H. (2001) Properties of photogenerated tryptophan and tyrosyl radicals in structurally characterized proteins containing rhenium(I) tricarbonyl diimines. *J. Am. Chem. Soc.* **123**, 3181-3182

18. Bender, C., Sahlin, M., Babcock, G., Barry, B., Chandrashekar, T., Salowe, S., Stubbe, J., Lindstrom, B. Petersson, L. Ehrenberg, A., and Sjoberg, B. (1989) An ENDOR study of the tyrosyl free-radical in ribonucleotide reductase from *Escherichia coli*. *J. Am. Chem. Soc*. **111**, 8076-8083

19. Svistunenko, D. A. and Cooper, C. E. (2004) A new method of identifying tyrosyl radicals in proteins. *Biophys. J.* **84**. 582-595

20. Westerlund, K., Berry, B., Privett, H., and Tommos, C. (2005) Exploring amino-acid radical chemistry: protein engineering and de novo design. *Biochim. Biophys. Acta-Bioenergetics* **1707**, 103-116

21. Roston, D., Islam, Z., and Kohen, A. (2014) Kinetic isotope effects as a probe of hydrogen transfers to and from common enzymatic cofactors. *Arch. Biochem. Biophys.* **544**, 96-104

22. Frey, P. A., and Hegeman, A. D. (2007) *Enzymatic Reaction Mechanisms,* Oxford University Press, Oxford, England, U.K.

23. Hofbauer, S., Dalla Sega, M., Scheiblbrandner, S., Jandova, Z., Schaffner, I., Mlynek, G., Djinovic-Carugo, K., Battistuzzi, G., Furtmüller, P. G., Oostenbrink, C., and Obinger, C. (2016) Chemistry and molecular dynamics simulations of heme *b*-HemQ and coproheme-HemQ. *Biochemistry* **55**, 5398–5412

24. Grant, J. L., Hsieh, C. H., and Makris, T. M. (2015) Decarboxylation of fatty acids to terminal alkenes by cytochrome P450 compound I. *J. Am. Chem. Soc.* **137**, 4940-4943

25. Stubbe, J., Nocera, D. G., Yee, C. S., and Chang, M. C. Y. (2003) Radical initiation in the class I ribonucleotide reductase: Long-range proton-coupled electron transfer? *Chem. Rev.* **103**, 2167-2201

26. Doyle, W. A., Blodig, W., Veitch, N. C., Piontek, K., and Smith, A. T. (1998) Two substrate interaction sites in lignin peroxidase revealed by site-directed mutagenesis. *Biochemistry* **37**, 15097-15105

27. Efimov, I., Badyal, S. K., Metcalfe, C. L., Macdonald, I., Gumiero, A., Raven, E. L., and Moody, P. C. (2011) Proton delivery to ferryl heme in a heme peroxidase: enzymatic use of the Grotthuss mechanism. *J. Am. Chem. Soc.* **133**, 15376-15383

28. Rittle, J., and Green, M. T. (2010) Cytochrome P450 compound I: capture, characterization, and C-H bond activation kinetics. *Science* **330**, 933-937

29. Gumiero, A., Metcalfe, C. L., Pearson, A. R., Raven, E. L., and Moody, P. C. (2011) Nature of the ferryl heme in compounds I and II. *J. Biol. Chem.* **286**, 1260-1268

30. Warren, J. J., Tronic, T. A., and Mayer, J. M. (2010) Thermochemistry of proton-coupled electron transfer reagents and its implications. *Chem. Rev.* **110**, 6961-7001

31. Macdonald, I. K., Badyal, S. K., Ghamsari, L., Moody, P. C., and Raven, E. L. (2006) Interaction of ascorbate peroxidase with substrates: a mechanistic and structural analysis. *Biochemistry* **45**, 7808-7817

32. Warren, J. J., and Mayer, J. M. (2011) Proton-coupled electron transfer reactions at a heme-propionate in an iron-protoporphyrin-IX model compound. *J. Am. Chem. Soc.* **133**, 8544-8551

33. Schultz, C. E., Devaney, P. W., Winkler, H., Debrunner, P. G., Doan, N., Chiang, R., Rutter, R., and Hager, L. P. (1979) Horseradish peroxidase compound I: Evidence for spin coupling between the heme iron and a 'free' radical. *FEBS Lett.* **103**, 102-105

34. Lin, M., Sperling, L., Schmidt, H., Tang, M., Samoilova, R., Kumasaka, T., Iwasaki, T., Dikanov, S., Rienstra, C., and Gennis, R. (2011) A rapid and robust method for selective isotope labeling of proteins. *Methods* **55**, 370-378

35. Lash, T. D., Mani, U. N., Keck, A., and Jones, M. A. (2010) Normal and abnormal heme biosynthesis. 6. Synthesis and metabolism of a series of monovinylporphyrinogens related to harderoporphyrinogen. Further insights into the oxidative decarboxylation of porphyrinogen substrates by coproporphyrinogen oxidase. *J. Org. Chem.* **75**, 3183-3192

36. Gorchein, A., Danton, M., and Lim, C. K. (2005) Harderoporphyrin: a misnomer. *Biomed. Chromatogr.* **19**, 565-569

37. Stoll, S., and Schweiger, A. (2006) EasySpin, a comprehensive software package for spectral simulation and analysis in EPR. *J. Mag. Res.* **178**, 42-55

CHAPTER SEVEN

PRELIMINARY EVIDENCE AND FUTURE DIRECTIONS IN THE INVESTIGATION OF A PROTEIN-PROTEIN INTERACTION BETWEEN CPFC AND CHDC

Background and Statement of the Knowledge Gap

Control Over Metabolite Flux in the Heme *b* Biosynthesis Pathway is Essential

Synthesis (or acquisition) of heme *b*, is essential for almost all living organisms. However, heme *b* and the precursors formed during its biosynthesis can be toxic to the cell if they are allowed to accumulate. This is specifically true for the last three steps of the pathway in both the PPD and the CPD branch (Figure 7.1).

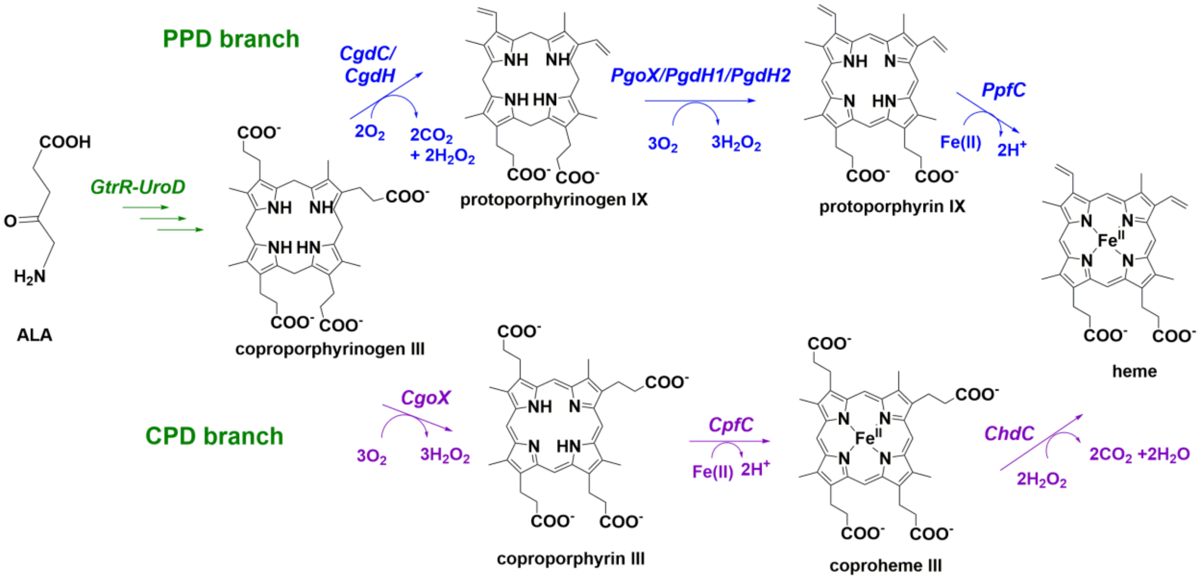
PPD branch
CgdC/ CgdH
$2O_2$
$2CO_2$ + $2H_2O_2$
protoporphyrinogen IX
PgoX/PgdH1/PgdH2
$3O_2$
$3H_2O_2$
protoporphyrin IX
PpfC
Fe(II)
$2H^+$
heme
ALA
GtrR-UroD
coproporphyrinogen III
CPD branch
CgoX
$3O_2$
$3H_2O_2$
coproporphyrin III
CpfC
Fe(II) $2H^+$
coproheme III
ChdC
$2CO_2$ +$2H_2O$
$2H_2O_2$

Figure 7.1. The PPD and CPD branches of heme b biosynthesis both produce toxic intermediates during the process. Protoporphyrin IX and coproporphyrin III are light-sensitive molecules that can participate in radical formation by donating electrons to O_2. Fe (II) and H_2O_2 together can participate in Fenton chemistry, also creating are also toxic reactive oxygen species (ROS). These metabolites must therefore be tightly controlled during heme biosynthesis.

Coproporphyrinogen III and protoporphyrinogen IX are highly reactive molecules which can readily and non-enzymatically be oxidized. The oxidized products, coproporphyin III and PPIX are light-sensitive molecules that are even more reactive, participating in radical chemistry though their donation of electrons to O_2 and generating reactive oxygen species (ROS) such as superoxide (•O_2^-), hydrogen peroxide (H_2O_2) and hydroxyl radicals (HO•). Their detrimental accumulation in human cells is linked to diseases called porphyrias and their toxic effects in bacterial cells have also been well documented[1-2]. In addition, H_2O_2 itself is generated as a by-product during biosynthesis and is required for the ChdC reaction (Figure 7.1). This is all in the presence of ferrous iron

(Fe^{2+}), which can participate in the infamous Fenton reaction, also with generating ROS (Figure 7.2).

$$Fe^{2+} + H_2O_2 \rightarrow Fe^{3+} + HO\bullet + OH^-$$

Figure 7.2.The Fenton reaction. Ferrous iron readily becomes oxidized by H_2O_2 leading to the generation of reactive oxygen species.

It is therefore essential that there be tight regulation of metabolite flux and control over off-pathway reactivity during heme *b* biosynthesis, specifically during the terminal three steps. This regulation has been described for organisms that use the PPD branch (namely eukaryotic organisms and gram-negative bacteria) but not for the organisms that utilize the novel CPD branch (gram-negative bacteria). These mechanisms must be different, as not only the enzymes that carry out these branches are different, but the organisms themselves are structurally different in significant ways.

Regulation and Control in the PPD Branch

The PPD branch of heme *b* biosynthesis is exclusive to eukaryotic and gram-negative organisms. Of significance to heme *b* biosynthesis metabolite flux, these organisms have one thing in common; multiple membranes. Heme *b* biosynthesis enzymes in eukaryotic organisms are distributed in different areas of the cell. The first enzymes of the pathway (GtrR-UroD), which do not produce cytotoxic molecules, are located in the cytoplasm, while the last three enzymes (CgdC, PgoX, and PpfC) are localized in various areas of the mitochondrion[1] (Figure 7.3A).

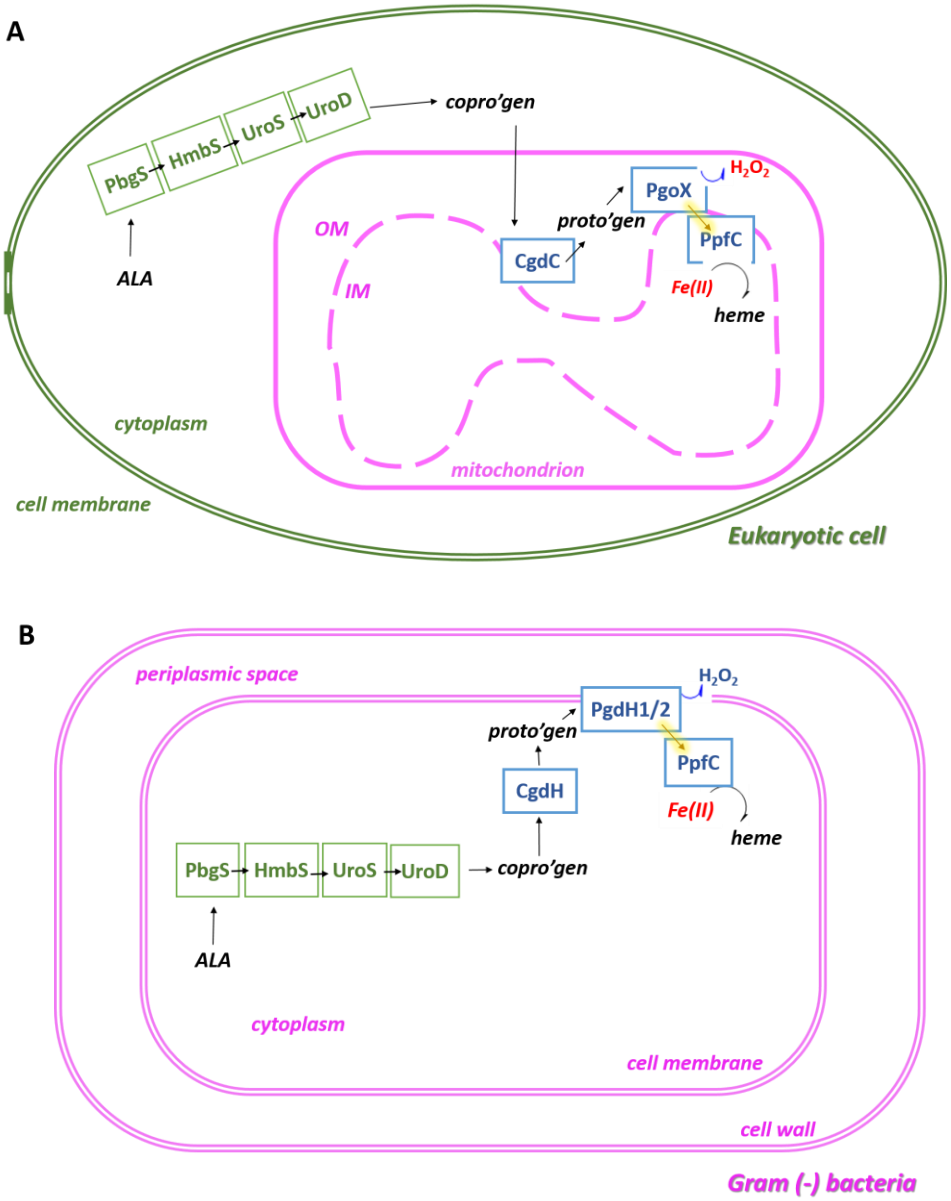
A
PbgS
HmbS
UroS
UroD
copro'gen
ALA
OM
IM
CgdC
proto'gen
PgoX
H_2O_2
PpfC
Fe(II)
heme
cytoplasm
mitochondrion
cell membrane
Eukaryotic cell
B
periplasmic space
PgdH1/2
H_2O_2
proto'gen
PpfC
CgdH
Fe(II)
heme
PbgS
HmbS
UroS
UroD
copro'gen
ALA
cytoplasm
cell membrane
cell wall
Gram (-) bacteria

Figure 7.3. Eukaryotic cells and gram-negative bacteria can compartmentalize the cytotoxic metabolites of heme b biosynthesis in their membrane-bound spaces. (A) Eukaryotic cells control metabolite flux and prevent off pathway reactivity during the synthesis of heme by confining the last three enzymes of this pathway to the mitochondrial inner membrane space and the matrix. (B) Gram-negative bacteria achieve a similar effect by localizing these enzymes to their inner membrane and the periplasmic space that is exists between the inner and outer membrane.

PpfC resides in the mitochondrial matrix and PgoX and CdgC are located in the inner mitochondrial space. This compartmentalization restrains the toxic molecules being produced to a single location and facilitates direct interaction between these terminal enzymes. Biochemical data has shown that CdgC, PgoX, and PpfC must transiently interact, preventing any measurable amount of metabolite leakage from being detected in the cellular mileu[1]. PgoX and PpfC are both membrane-bound proteins, embedded in the inner mitochondrial membrane on their respective sides. PgoX and PpfC are thought to pass substrate/product directly to each other through a channel in PgoX that spans through the mitochondrial membrane[2-4] (Figure 7.3A). This direct interaction is only transiently stable but allows rapid conversion of PPIX to heme *b*, making PPIX concentrations negligible and harmless to the cell [2].

Similarly, gram-negative bacteria are able to compartmentalize their enzymes to drive direct substrate/product delivery. Gram-negative bacteria have two cell membranes that create a periplasmic space in between (Figure 7.3B). Like in eukaryotic cells, all non-toxic producing steps happen in the cytoplasm, while the terminal enzymes reside in the inner cell membrane and the periplasmic space. Membrane compartmentalization again allows for direct transfer of substrate/product to happen between these enzymes, providing control of metabolite flux and preventing off-pathway reactivity.

Less is known about what happens to heme *b* at the end of biosynthesis. It is known that after the last step, heme *b* it remains bound to PpfC, presumably until a heme chaperone takes it to its final destination. Moreover, in eukaryotic cells, heme *b* needs to be exported out of the mitochondria membrane before it can be incorporated into the required hemoprotein. It is speculated that there is more than one heme chaperone and that these pathways of heme trafficking are likely complex[1, 5]. These chaperones and mitochondrial export machinery have yet to become elucidated in eukaryotes as well as in gram-negative bacteria, although bacterioferritin (Bfr) has recently been suggested to be the heme recipient of PpfC in *E. coli* [6].

Regulation and Control in the CPD Branch is Not Known

How metabolite flux and off-pathway reactivity is controlled in the CPD branch of heme *b* biosynthesis has not been described due to the novelty of this discovery. The CPD branch is found in gram-positive organisms, which lack the physical structure of a double membrane. Gram-positive bacteria have a single membrane and a thick, but porous peptidoglycan layer which does not allow formation of a true periplasmic space. These organisms have no way of compartmentalizing the terminal, toxic intermediate-producing enzymes of this pathway. Moreover, the terminal enzymes in the CDP branch are not membrane-bound, but cytosolic, indicating that regulation and control must be quite distinct for the CPD branch (Figure 7.4).

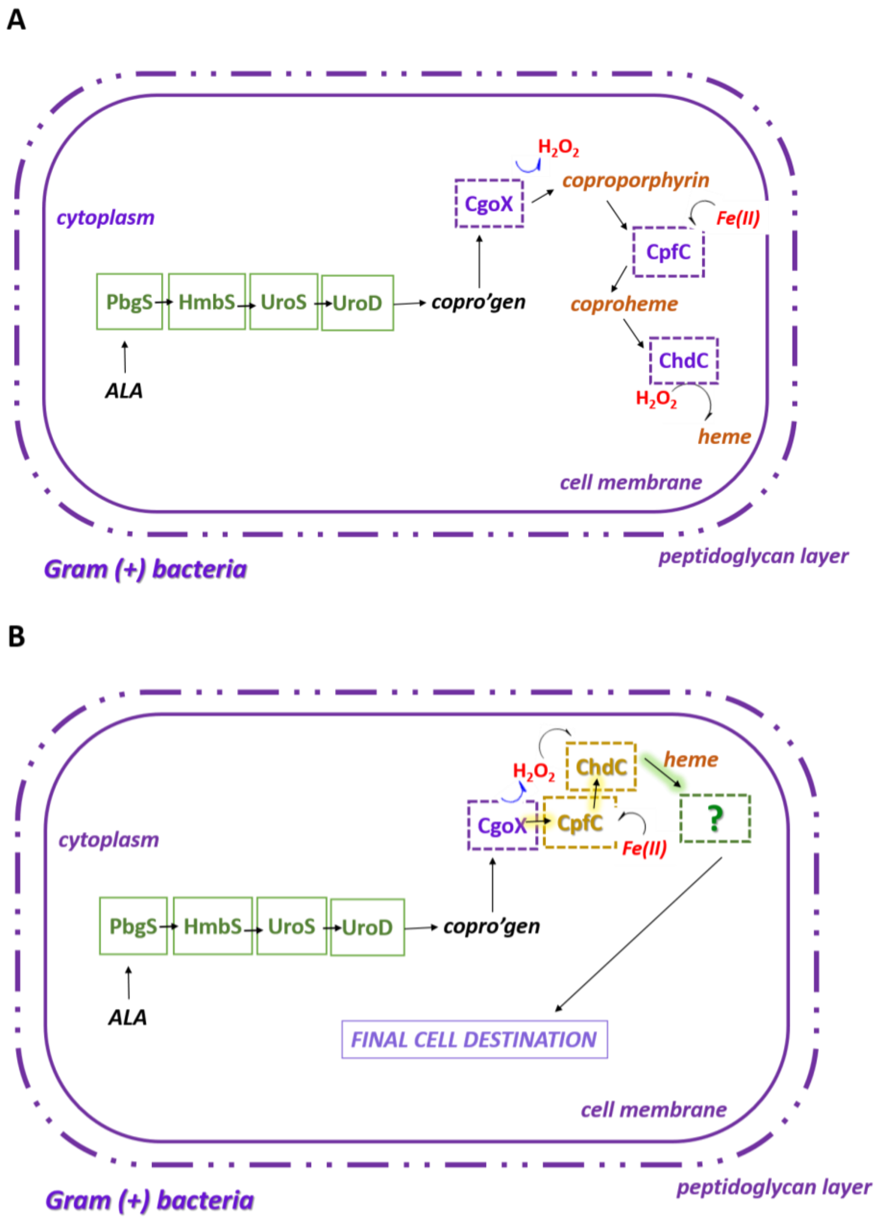
A
H2O2
CgoX
coproporphyrin
cytoplasm
Fe(II)
CpfC
PbgS
HmbS
UroS
UroD
copro'gen
coproheme
ChdC
ALA
H2O2
heme
cell membrane
Gram (+) bacteria
peptidoglycan layer
B
H2O2
ChdC
heme
CgoX
CpfC
?
cytoplasm
Fe(II)
PbgS
HmbS
UroS
UroD
copro'gen
ALA
FINAL CELL DESTINATION
cell membrane
Gram (+) bacteria
peptidoglycan layer

Figure 7.4. Gram-positive bacterial heme b biosynthesis occurs in the cytoplasm without membrane compartmentalization of cytotoxic intermediates. (A) Gram-positive bacteria lack a double membrane as well as a true periplasmic space and their terminal heme biosynthesis enzymes are cytosolic, potentially exposing all cytotoxic metabolites to the cell. (B) We propose that in the absence of a physical barrier, gram-positive bacteria heme biosynthesis enzymes control off-pathway reactivity by forming protein-protein interactions and delivering substrate/products directly to each other. In addition, because the product heme is toxic itself, the final enzyme ChdC transfers heme to a heme-transport protein that safely delivers heme to its final destination.

Given what is known about protein-protein interactions in the PPD branch, as well as many other metabolic pathways, we hypothesize that direct metabolite channeling through protein-protein interactions is used as an alternate mechanism for physical cellular structure compartmentalization in gram-positive organisms (Figure 7.4B). Specifically we focus our efforts at describing protein-protein interactions that occur with ChdC, the last enzyme of the CPD heme *b* biosynthesis pathway. We propose that ChdC must directly interact with CpfC, if even transiently, to obtain newly formed coproheme substrate and that ChdC must have a heme *b* delivery protein partner, which delivers heme *b* to its final cellular destination.

Reasoning

Protein-protein interactions are a common theme in regulation of metabolic pathways. Interaction and direct delivery of substrate/product by metabolic pathway enzymes becomes especially important when the molecules that are being generated can become cytotoxic and are not confined by physical cellular barriers (namely membrane-bound organelles), as is the case during the terminal three steps of the CPD branch in gram-positive bacteria.

Focusing on the last two enzymes in the CDP branch of the heme *b* biosynthesis pathway (Figure 7.1), perhaps the most compelling evidence that ChdC and CpfC interact with each other is the existence of a *cpfC-chdC* gene fusion in the gram-positive bacteria, *P. acnes*[7], which indicates that CpfC and ChdC can at least form a quasi-stable quaternary structure. Another hint comes the CpfC crystal structure which lacks the conserved “active site lip" found in its eukaryotic homolog PpfC. The absence of this "lip" leaves a solvent exposed active site in CpfC which can serve as a channel for substrate/product transfer upon interaction with ChdC, which has been suggested by *in silico* CpfC-ChdC docking studies (no data shown, Dailey 2010[7]).

Our in-depth mechanistic and structural studies of the terminal enzyme ChdC have directed us towards determining the biochemical factors that would allow for a ChdC protein-protein interaction with CpfC. Using and a variety of biochemical tools and *in vivo* phenotype characterization assays, we have used *Staphylococcus aureus* and its enzymes to provide, the first of its kind, preliminary evidence for a CpfC-ChdC protein-protein interaction.

Preliminary Studies

Methods

Reagents and Stocks. Ferric coproporphyrin III chloride (coproheme III, Frontier Scientific) and coproporphyrin III dihydrochloride (Frontier Scientific) were obtained in 10-100 mg ampules and used to generate 5-10 mM stock solutions in dimethylsulfoxide (DMSO). These stocks were further diluted in 50mM Tris, pH8, 150mM NaCl prior to use. The coproporphyrin and coproheme concentrations in these solutions were ascertained by performing a pyridine hemochrome assay for coproheme or ε_{548}=16.8 mM^{-1}cm^{-1} in 0.1M HCl for coproporphyrin[8].

For ferrochelatase (CpfC) reactivity studies, $(NH_4)_2Fe(SO_4)_2 \cdot 6H_2O$ was used as a source of ferrous iron. 10mM stocks were generated prior to use by weighing out the solid and introducing it into an anaerobic atmosphere (COY Chamber). The solid was resuspended in anaerobic water. This stock was further diluted to a 0.1 mM final concentration and placed in a septum-sealed vial to be used for experiments.

For coproheme decarboxylase (ChdC) reactivity studies, hydrogen peroxide (H_2O_2) stock solutions were prepared at 100 µM concentrations in 50 mM potassium phosphate (KPi) buffer, pH 7.4. H_2O_2 concentrations were ascertained by titration with freshly prepared 0.02 M $KMnO_4$, as previously reported[9].

Preparation of the Coproheme Decarboxylase (ChdC) and Coproporphyrin Ferrochelatase (CpfC) Enzymes from *Staphylococcus aureus*. Expression and purification of *Sa*ChdC were carried out as previously reported[9]. The sequences encoding CpfC in *Staphylococcus aureus* Newman was obtained from NCBI (accession number NC_009641.1 at 1924676-1925599 for *hemH*) and codon-optimized for heterologous expression in *E. coli*. The *cpfC* containing plasmid was transformed into Tuner (DE3) cells (Novagen). Heterologous expression was carried out in 1L flasks of Terrific Broth supplemented with the 50mg/L kanamycin. Flasks were inoculated 1:100 with a freshly saturated starter culture and grown at 37 °C until an optical density of 0.4-0.6 at 600 nm was reached. IPTG was added to a final concentration of 1 uM, the temperature lowered to 20 °C, and the cells grown overnight. Cell pellets harvested by centrifugation were lysed by sonication in buffer A (50 mM Tris, pH 8, 150 mM NaCl, 5 mM imidazole), the lysate was clarified by centrifugation at 45,000 x g for 1 hour, and the supernatants loaded onto a nickel-nitrilotriacetic acid affinity column (BioRad) equilibrated to buffer A. Protein was eluted by a 300 mL linear gradient from 0-100% buffer B (50 mM Tris, pH 8, 150 mM

NaCl, 500 mM imidazole) at 2 mL/min (AKTA Prime). The protein eluted around 40-60% buffer B. Pure fractions were identified via SDS-PAGE, concentrated, dialyzed into 50 mM Tris (pH 8, 150 mM NaCl) and stored at -80°C.

UV-Vis Spectroscopy. UV/Vis spectra were measured on a temperature-controlled Cary60 instrument in scanning mode at 20 °C. Samples contained the enzyme and porphyrin concentrations specified in the text. All experiments were performed in 50mM Tris, pH 8, 150mM NaCl.

Determining a coporpoprhyin-CpfC-ChdC Complex Dissociation Constant and protein-porphyrin Dissociation Constants. Values of K_D for equilibrium binding of CpfC or ChdC to coproprohyrin and coproheme were determined by fluorescence quenching (Cary). Tryptophan fluorescence was excited at 295 nm and emission monitored at 340 nm. Quenched emission at 340 nm was plotted versus the concentration of added ligand. Plots were fitted with the Langmuir-Hill equation to determine the K_D.

$$\theta = \frac{[L]^n}{KD + [L]^n}$$

θ is the fraction of ligand-binding sites occupied by the ligand, [L] is the ligand concentration, and n is the Hill coefficient describing cooperativity.

K_D for equilibrium binding of ChdC to coproporphyrin-CpfC was performed using Uv-Vis spectroscopy as described in the text. The Langmuit-Hill equation was again used to determine K_D.

Growth Curve Phenotype Analysis of *S. aureus* ChdC Mutants. *S. aureus* containing ChdC protein variants were streaked on a TSA+ chloramphenicol agar plate and allowed to grow for 18-24hrs. The E120L strain and the strain containing the empty vector (ie, no ChdC) grew as SCVs. These strains were allowed to grow for 24hrs more (48hrs total) in order to obtain fully formed and visible colonies before proceeding. 3mL of RPMI (Cat no. 11879, contains no glucose) + 1% casamino acids+ 2mg/mL glucose+ 10 ug/mL chloroamphenicol were inoculated with a single colony from each strain, separately. This was done in triplicate for each strain. 2 μM hemin was added to the empty vector and E120L strains to obtain similar densities as WT. The cultures were allowed to grow for 16-18hrs at 37 °C, 250rpm. In a 96-well plate, 200 uL of RPMI (Cat no. 11879, contains no glucose) + 1% casamino acids+ 4mg/mL glycerol+ 10 ug/mL chloroamphenicol+ 0 or 1 μM heme were inoculated 1:100 with the overnight cultures. OD600 was measured using a VarioSkan plate reader every 30 min for 20 hrs (37 °C, discontinuous shaking (5sec on, 5 sec off) at 120 rpm, slow speed). Measurements were taken with the plate's lid on and the perimeter of the 96-wellplate covered in parafilm (one layer) to prevent evaporation.

Cellular porphyrin quantification of *S. aureus* ChdC mutants by LC-MS. The procedure for making growth curves was followed up until inoculation in the 96-well plate, at which point in 250 mL flasks, 50-100 mL of RPMI (Cat no. 11879, contains no glucose) + 1% casamino acids+ 4mg/mL glycerol+ 10 ug/mL chloroamphenicol were inoculated 1:100 with the overnight cultures and incubated for 20 hrs at 37, 250rpm. Cells were collected by centrifugation (5,000 rpm, 8 min, 4 °C) and subsequently resuspended in 1 mL 1M HCL:DMSO (1:1 (v/v)) and transferred to Matrix B Lysis tubes

(MP Biomedicals). Porphyrin extraction procedure optimized in out lab was followed as outlined in Choby 2018[10]. To normalize porphyrin content to CFU count, CFUs were enumerated for each sample before cells were collected and lyzed.

Results

Coproporphyrin III can be used as an indicator to visualize a CpfC-ChdC complex.

Heme *b* and its porphyrin precursors have unique UV-Vis absorption spectra. Their spectrum is not only unique to the porphyin itself, but also to the environment in which that porphyrin is found. As such, UV-Vis spectroscopy can indicate a change in a porphyrin's location (ie. in solvent versus enzyme-bound) or chemical changes to that porphyrin.

The spectral features of the substrate and product of CpfC (coproporphyrin III and coproheme III) were analyzed in the absence or presence of CpfC and ChdC, individually (Figure 7.5). As expected, coproporphyrin and coproheme each had distinct features from each other when in solution. Also as expected, these signals were further distinct when bound to CpfC or ChdC (Figure 7.5, Table 7.1).

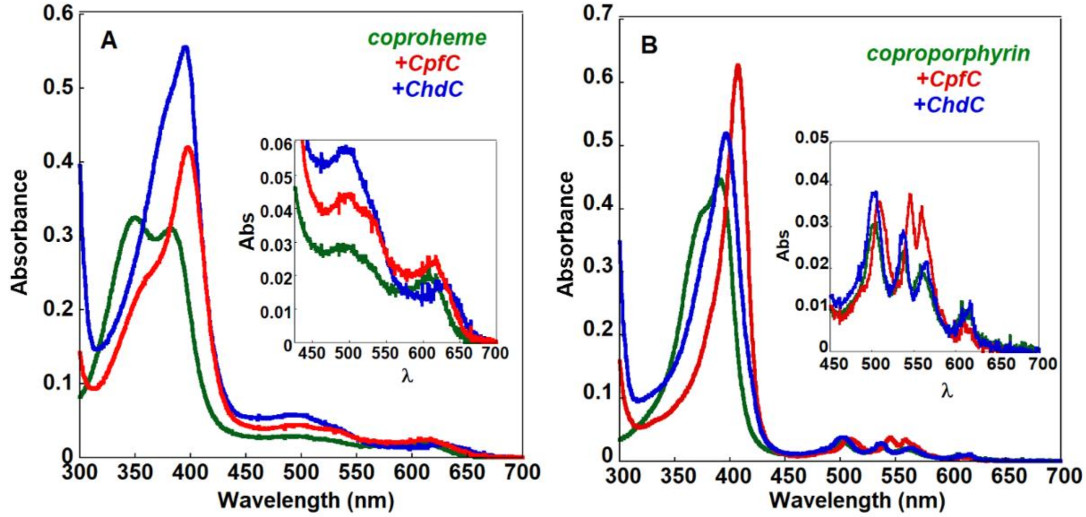

Figure 7.5. UV-Vis spectra of coproporphyrin and coproheme in the absence and presence of CpfC or ChdC. UV-Vis spectra of 5uM coproporphyrin or coproheme in the absence or presence of the specified enzyme (50 mM Tris-HCl, pH 8, 150mM NaCl). As seen with many other porphyrin-binding enzymes, the active site environment of CpfC and ChdC modifies the pi to pi* electron transition energy in the porphyrin macrocycle and thus its spectra. These changes provide a signature of where the porphyrin is located. These unique spectral features are summarized in Table 7.1.

In the presence of *both* CpfC and ChdC, the UV-Vis spectrum of coproheme was very similar to that of coproheme bound to ChdC alone, reflecting the enzyme-porhyrin complex with the highest affinity to be coproheme-ChdC and not coproheme-CpfC (Figure 7.6A). Addition of both enzymes to coproporphyin led to the formation of an intense, sharp peak (Figure 7.6B). This peak was undoubtedly distinct from coproporphyrin bound to either enzyme individually, strongly suggesting the sharing of coproporphyrin between CpfC and ChdC and thus an interaction between these enzymes. Formation of this complex is specific to the CpfC-ChdC pair, as substituting ChdC for another enzyme does not yield the observed spectral feature (data not shown).

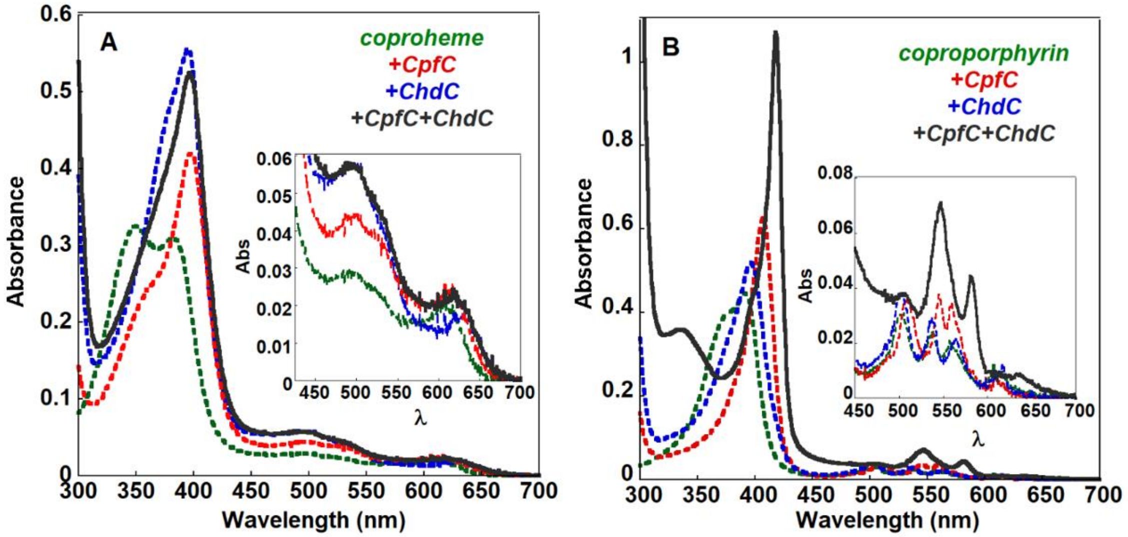

Figure 7.6. UV-Vis spectra of coproporphyrin can be used to visualize the formation of a CpfC-ChdC complex. Distinct UV/vis spectra measured for 5 μM coproheme (A) or 5 μM coproporphyrin (B) alone (green) or in complex with saturating amounts of CpfC (red), ChdC (blue), or CpfC-ChdC togethter (grey) 50 mM Tris-Cl, pH 8, 15 mM NaCl). The inset shows the visible bands on an amplified scale.

Table 7.1. Summary of coproheme and coproporphyrin UV-Vis spectral features (50 mM Tris, pH 8, 150 mM NaCl) in solution or when enzyme-bound

Porphyrin	Enzyme(s)	Soret (max absorbance peak)
Coproporphyrin	--	392 nm, 370 nm shoulder
Coproporphyrin	CpfC	405 nm (sharp)
Coproporphyrin	ChdC	396nm
Coproporphyrin	CpfC and ChdC	418 nm (sharp)
Coproheme	--	383, 350 nm
Coproheme	CpfC	398 nm
Coproheme	ChdC	394 nm (broad)
Coproheme	CpfC and ChdC	395 nm (sharp)

Determining the Affinity of the CpfC-ChdC Complex in the Presence of Coproporphyrin. To determine the affinity of the coproporphyrin-CpfC-ChdC complex, 5 μM coproporphyrin bound to excess CpfC (20 μM, to ensure complete binding) was titrated with increasing concentrations of ChdC and spectral changes were monitored (Figure 7.7).

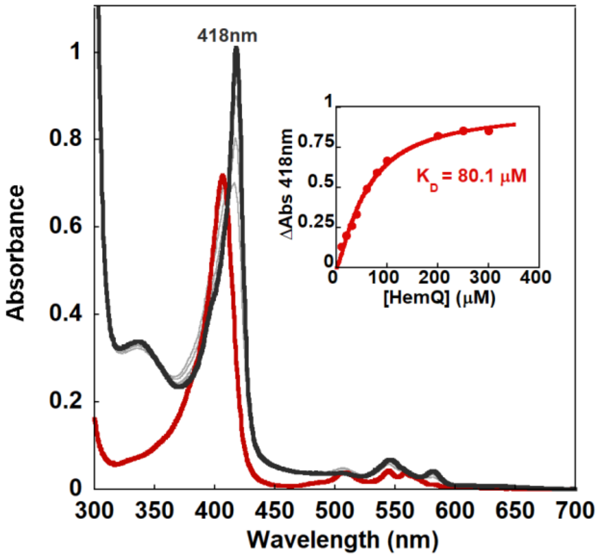

Figure 7.7. The affinity of the CpfC-ChdC complex in the presence of coproporphyrin is consistent with a transient protein-protein interaction. A pre-formed coproporphyrin-CpfC complex was generated by equilibrating 5 μM coproporphyrin with 20 μM CpfC (red spectrum). ChdC was added titrimetrically (grey spectra) until the spectral changes ceased (black spectrum). The inset shows the change in absorbance at 418 nm, which was fit to the Langmuir-Hill equation to determine a K_D for [coproporphyrin-CpfC] with ChdC.

Absorbance at 418 nm was plotted against concentration of ChdC the data was fit to the Hill equation to obtain a dissociation constant (K_D) value (Figure 7.7, inset). The obtained K_D value of 80.1 μM reflects the affinity of coproporphyrin-bound CpfC for ChdC and is a composite of (1) the affinity of CpfC for coproprophyrin, (2) the affinity of ChdC for coproporphyin, and (3) the affinity of CpfC for CdhC. Because coproprphyrin is required to observe this interaction, the affinity of the CpfC-ChdC complex alone (in the absence of porphyrin) could not be determined. An estimate of the affinity constant for the

CpfC-ChdC complex alone was calculated by taking the affinity of the individual components to form the complex as a whole (see below).

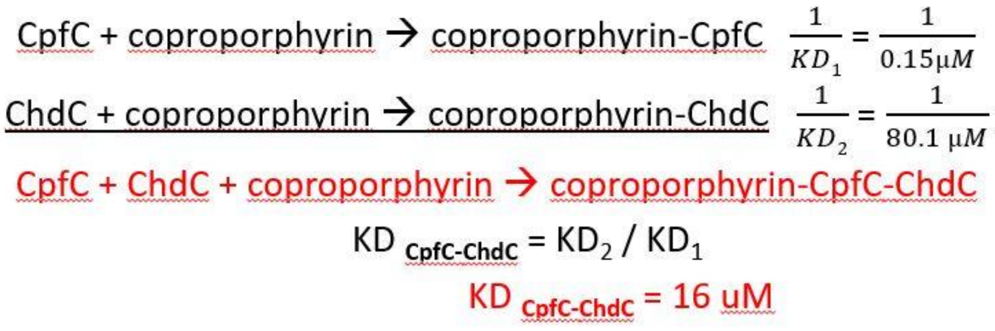

CpfC + coproporphyrin → coproporphyrin-CpfC $\frac{1}{KD_1} = \frac{1}{0.15\mu M}$

ChdC + coproporphyrin → coproporphyrin-ChdC $\frac{1}{KD_2} = \frac{1}{80.1\ \mu M}$

CpfC + ChdC + coproporphyrin → coproporphyrin-CpfC-ChdC

$KD_{CpfC\text{-}ChdC} = KD_2 / KD_1$

$KD_{CpfC\text{-}ChdC} = 16\ uM$

Given the affinity constant of CpfC for coproporphyrin of 0.15 µM (Table 7.2), a K_D of 16.5 ± 6.3 µM was calculated for the coproporphyin-CpfC-ChdC complex. A K_D of this magnitude is consistent with a transient protein-protein interaction[11].

Table 7.2. K_D values calculated for enzyme-porphyrin complexes

Enzyme	Ligand	K_D (µM)	Hill coefficient (n)
CpfC	Coproporphyrin III (substrate)	0.15	1
CpfC	Coproheme III (product)	1.8	1.9
ChdC	Coproheme III (substrate)	0.52	1.3 (1.1)
ChdC	Heme *b* (product)	1.7	--
ChdC	Coproporphyrin III	0.54	1.4
Coproporphyrin-CpfC	HemQ	80.1	1
Coproporphyrin-ChdC	HemH	49.7	1

The CpfC-CdhC Complex Does Not Enhance Intrinsic Reactivity CpfC. CpfC catalyzes insertion of ferrous iron into coproporphyrin to yield coproheme (Figure 7.1).

The progress of reaction can be monitored by measuring the decrease in coproporphyrin-bound CpfC Soret absorbance (405 nm) over time upon addition of Fe(II). Production of coproheme is visualized by the shift in Soret from 405nm to 396nm (Figure 7.8A). To test whether complexation between CpfC and ChdC enhanced CpfC reactivity, 5 μM coproporphyrin was bound 10 uM CpfC in the presence of 100 μM ChdC and 10 uM Fe(II) was added to start the reaction (Figure 7.8B).

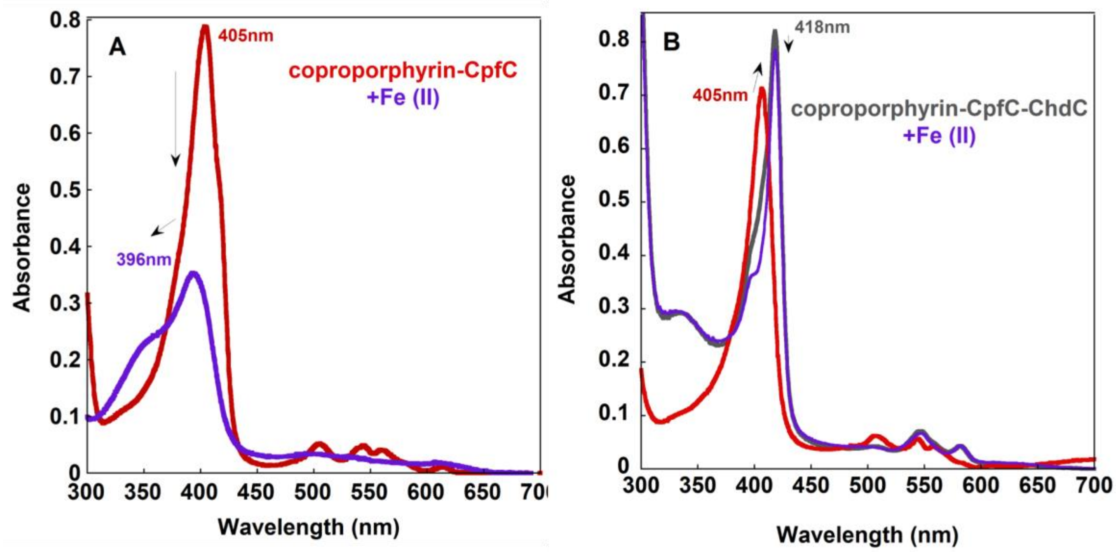

Figure 7.8. The CpfC-ChdC complex does not affect the intrinsic reactivity of CpfC. 5 μM coproporphyrin was bound to 10 μM ChdC and reacted with 10uM Fe(II) in the absence or presence of 100uM ChdC. The first spectrum was recorded prior to addition of Fe(II) or HemQ (red). (A) In the absence of ChdC, the reaction is complete within mixing time (purple). (B) In the presence of ChdC, the coproporphyrin-CpfC-ChdC complex peak at 418 nm forms quickly (gray) and upon addition of Fe(II), little to no change is observed (purple).

In the absence of ChdC, addition of Fe(II) led to the expected decrease in 405nm and a shift towards 396nm. The reaction was complete within mixing time and the final blue spectrum was obtained (Figure 7.8A). In the presence of ChdC, the complex (indicated by the 418nm peak) was allowed to form prior to addition of iron. Reacting the coproporphyrin-CpfC-ChdC complex with Fe(II), led to no significant spectral changes, indicating less reactivity by CpfC. These results suggest that formation of the coproporphyrin-CpfC-ChdC complex does not enhance the intrinsic reactivity of CpfC and furthermore inhibits it, perhaps by shielding the porphyrin from the surrounding mileu.

The CpfC-ChdC complex does not enhance intrinsic reactivity CpfC. ChdC catalyzes the oxidative decarboxylation of coproheme to yield heme *b* in a H_2O_2-dependent manner (Figure 7.1). Upon addition of excess H_2O_2, conversion of coproheme to heme can be observed spectroscopically by monitoring a shift in the coproheme Soret from 394nm to 410nm. To determine whether CpfC has an enhancing effect on reactivity of ChdC, 5 μM coproheme-bound ChdC was reacted with excess H_2O_2 in the presence of 0-20 μM CpfC (Figure 7.9).

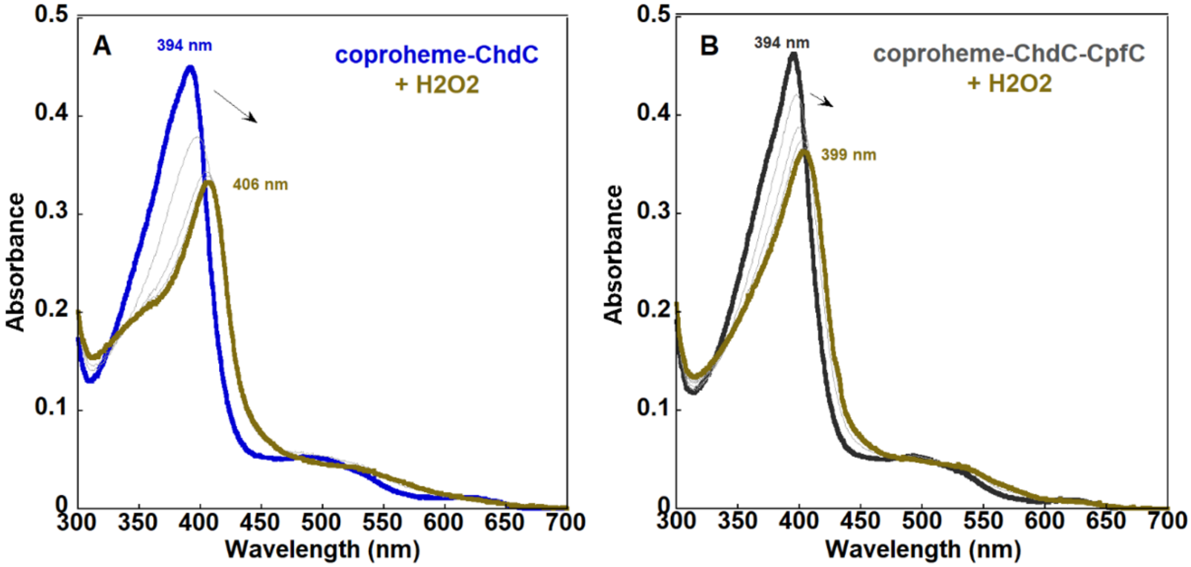

Figure 7.9. The CpfC-ChdC complex does not affect the intrinsic reactivity of ChdC. 5 μM coproheme was bound to 10 μM ChdC. (A) Spectral changes were monitored after the addition of excess H_2O_2 or (B) excess H_2O_2 in the presence of 10 μM CpfC. In the presence of CpfC, there is incomplete conversion of coproheme to heme as can be seen by the incomplete shift from 304 nm to 406 nm.

The presence of CpfC did not enhance ChdC reactivity and instead yielded incomplete conversion of coproheme to heme, as could be seen by the incomplete shift of the Soret from 394 nm to 406 nm. The magnitude of perturbation to the completion of reaction was positively correlated with CpfC concentration, suggesting that in the presence of CpfC, coproheme is shielded from the outer-protein environment and thus is it less able to react with H_2O_2.

These results demonstrate that the CpfC-ChdC complex does not enhance intrinsic enzyme reactivity of either CpfC or ChdC, and suggests that the main purpose of this protein-protein interaction is to protect and safely deliver substrate/product to ChdC. Furthermore, they indicate that this interaction must be short-lived in order for reactivity to ensue post substrate delivery.

The E120L ChdC Residue is Responsible for the CpfC-ChdC Protein-Protein Interaction. Structural studies of ChdC in the presence and absence of substrate reveal a labile loop near its active site. Composed of residues ~110-140, this structure is found in an open conformation in the absence of coproheme and hugging the active site in its presence (Figure 7.10A). It has been hypothesized that this loop acts as an "active-site gate" serving as a regulator of substrate entry and product egress[12-13]. To determine whether this loop could also be responsible for ChdC's interaction with CpfC, point mutations were made to polar residues on this loop (Table 7.4, Figure 7.10B). These proteins variants were inserted into *chdC*-deficient strains of *S. aureus* (*ΔchdC*), which were subsequently phenotypically characterized.

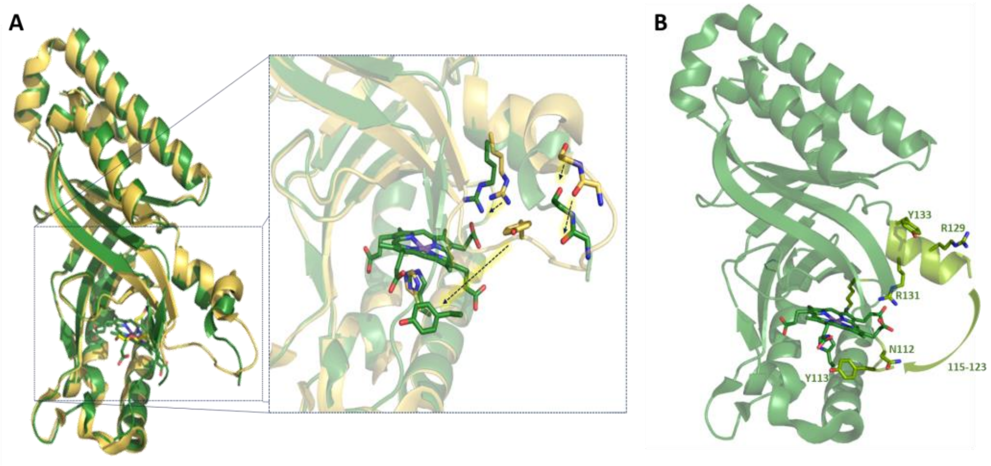

Figure 7.10. ChdC's active site gate may play a role in a CpfC-ChdC protein-protein interaction. (A) Superimposed structures of apo-ChdC (tan, PDBID 1TOT) and coproheme-bound ChdC (green, PDBID 5T2K) reveal a mobile active site loop (amino acids ~110-130) that closes in towards the active site to enclose the coproheme, upon it binding. (B) This mobile loop was hypothesized to play a role in ChdC protein-protein interactions and point mutations along this loop were inserted on ChdC to test this hypothesis. Note: The location of residues 114-124 could not be crystalographically mapped, are missing in the 5T2K structure, and are represented by the green arrow.

Table 7.4. List of point mutations inserted on ChdC's active site gate

ChdC protein variants in *ΔchdC S. aureus*
WT
Y113F
D121V
K182A
R131A
K129A
Y133F
N112L
Y145S
E120L
empty vector control

Out of all the mutants analyzed, only those containing the E120L and N112L ChdC mutation exhibited a growth deficiency in iron/heme deficient conditions (Figure 7.11A). Interestingly, this growth deficiency was complemented in the presence of exogenous hemin for the E120L strain, but not for the N112L strain (Figure 7.11B), whose growth deficit became even more pronounced under these conditions.

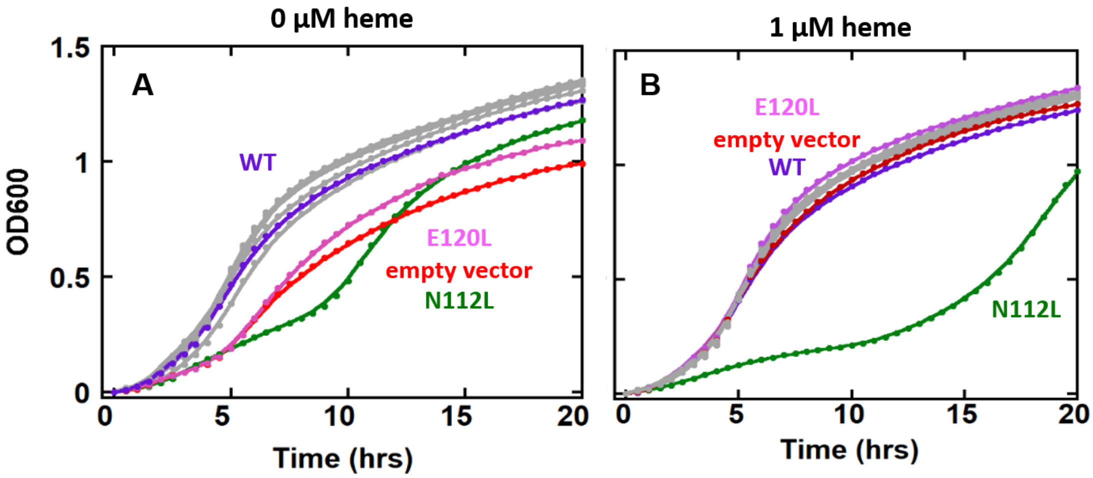

Figure 7.11. E120L and N112L ChdC protein variants in *ΔchdC S. aureus* exhibit a growth deficiency relative to WT. Growth curves of ChdC *S. aureus* mutants in heme deficient or heme-replete (1 μM) media were obtained. (A) In the absence of heme, most mutants displayed a WT-like growth phenotype (purple and gray lines), while the E120L and N112L ChdC mutants displayed a growth deficit that, was similar to the chdC-knock out strain or contained a greater lag-phase, respectively. (B) In the presence of exogenous heme, the chdC knock-out strain and the E120L strain display WT-like growth curves, while the growth deficit of N112L becomes exacerbated.

To further characterize these strains, the cellular concentrations of heme *b* and its coproporphyrin and coproheme precursors were analyzed via LC-MS (Figure 7.12). The N112L porphyrin profile showed that this mutant was deficient in coproheme and accumulated significantly higher levels of heme, relative to WT (no significant change in coproporphyrin levels were observed). In agreement with the exacerbation of growth deficit in the presence of exogenous heme, these results suggest that the N112L strain growth deficiency is likely due to toxic levels of intracellular heme. The fact that this mutation did not affect the production of heme further indicates that neither the ability of ChdC to obtain coproheme from CpfC nor its ability to catalyze its reaction is impaired by this mutation.

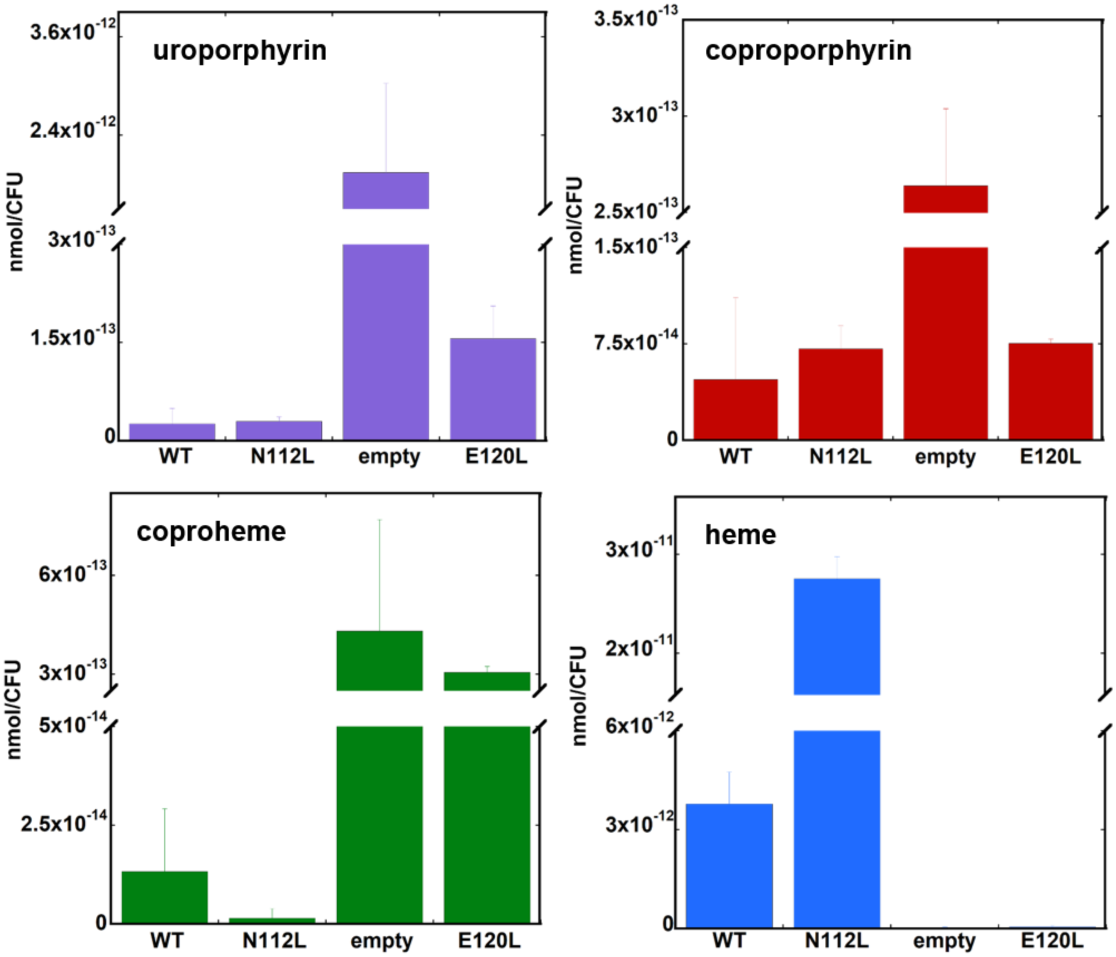

Figure 7.12. Porphyrin profiles for the E120L and N112L ChdC *S. aureus* strains. ChdC mutant *S. aureus* strains were grown to stationary phase in heme-deficient media and their intracellular porphyrins were extracted and quantified by LC-MS. Concentrations of uroporphyrin, coproprophyrin, coproheme, and heme, normalized to CFUs, were plotted for the WT, N112L, E120L ChdC and empty vector containing strains.

The E120L mutant had a similar porphyrin profile to *ΔchdC.* The E120L porphyrin profile revealed that this mutant was heme-deficient and accrued significantly higher levels of coproheme, relative to WT (no significant change in coproporphyrin levels were observed)(Figure 7.12). These results could be interpreted to say that the E120L mutation causes a complete loss in ChdC catalytic activity, leading to a heme auxotroph phenotype, like that documented for *ΔchdC*[14]. However, due to the lack of proximity of the E120 residue to the active site pocket, as well as the instability of the active site loop, on which it resides, we do not favor this conclusion. Instead, we propose that E120 in ChdC is responsible for the CpfC-ChdC interaction and that the exhibited phenotype by the E120L mutant is due an interruption in coproheme delivery from CpfC to ChdC.

Future Directions

The phenotype changes observed in the E120L ChdC *S. aureus* mutant could be reasoned in four ways; (1) Mutation to E120 disrupts ChdC catalytic activity, (2) Mutation to E120 significantly reduces or eliminates ChdC's affinity for coproheme, (3) Mutation to E120 disrupts ChdC's ability to oligomerize or fold properly, or (4) Mutation to E120 eliminates ChdC ability to interact with CpfC.

To confirm the hypothesis that E120 plays a role in the CpfC-ChdC protein-protein interaction, the recombinant E120L *Sa*ChdC protein variant will be overexpressed in *E. coli* and purified via procedures outlined for the WT enzyme[9]. To demonstrate that the E120L mutation does not disrupt ChdC catalytic activity, analysis of E120L ChdC catalytic reactivity (ability to convert coproheme to heme) and catalytic efficiency (number of H_2O_2 equivalents required for full conversion of coproheme to heme) via UV-Vis spectroscopy and HPLC product quantification will be conducted. We expect that this protein variant will have catalytic activity and catalytic efficiency similar to WT. It is possible that mutation of this residue causes a decrease in ChdC's affinity for coproheme, making this protein variant less catalytically competent than WT. This will be determined by measuring the affinity of E120L ChdC for coproheme by calculating a K_D equilibrium constant using Trp fluorescence changes measurements as previously described (see methods and Celis 2017[12]). Lastly, to exclude the possibility that the E120L ChdC mutant is unable to oligomerize or fold properly, its structural integrity will be questioned by measuring thermal denaturation curves ($\theta = 222$ nm) using circular dichroism (CD) spectroscopy and performing high-resolution separation size exclusion chromatography (BioRad Enrich SEC column and FPLC high-pressure system) analyses[15]. We expect that the CD spectrum, CD thermal denaturation curve, and SEC elution profile of E120L ChdC will not be significantly different than that of the WT enzyme.

The most convincing evidence that E120 is essential for a CpfC-ChdC protein-protein interaction will come from UV-Vis spectroscopy analysis. Again using coproporphyrin to visualize this interaction, we expect that in the presence of coproporphyrin and CpfC E120L ChdC will not be able to form the 418 nm Soret that has been attributed to the formation of the coproporphyrin-CpfC-ChdC complex.

Finally, follow up experiments to determine the significance of the N112 residue on ChdC will also be conducted. It is our hypothesis that the N112 residue also participates in ChdC protein-protein interactions, but with a heme chaperone, and not CpfC. We hypothesize that the heme accumulation phenotype exhibited by the N112L *S. aureus* mutant can be explained with this hypothesis. If heme can be synthesized but not delivered to the cellular location in need, then the cell will continue to synthesize heme, leading to its accumulation. Alternatively, we hypothesize that ChdC itself can have a heme-biosynthesis regulatory role and that the N112L mutation impairs that regulation.

Deciphering the role of N112 will be part of a larger study, which is to find the yet unidentified heme chaperone for the CPD heme *b* biosynthesis branch in gram-positive bacteria.

References

1. Hamza, I.; Dailey, H. A., One ring to rule them all: trafficking of heme and heme synthesis intermediates in the metazoans. *Biochim Biophys Acta* **2012,** *1823* (9), 1617-32.

2. Gillam, M. E., Hunter, G.A., Ferreira, G.C., The Ultimate Step of Heme Biosynthesis: Orchestration Between Iron Trafficking and Porphyrin Synthesis. In *Handbook of Porphyrin Science*, Ferreira, G. C., Ed. World Scientific: 2014; Vol. 26, pp 129-189.

3. Ferreira, G. C., Organization of the Terminal Two Enzymes of the Heme Biosynthetic Pathway. *J.Biol.Chem* **1998,** *263* (8), 38835-3839.

4. Koch, M., Crystal structure of protoporphyrinogen IX oxidase: a key enzyme in haem and chlorophyll biosynthesis. *EMBO Journal* **2004,** *23* (8), 1720-1728.

5. Yuan, X.; Rietzschel, N.; Kwon, H.; Walter Nuno, A. B.; Hanna, D. A.; Phillips, J. D.; Raven, E. L.; Reddi, A. R.; Hamza, I., Regulation of intracellular heme trafficking revealed by subcellular reporters. *Proc Natl Acad Sci U S A* **2016,** *113* (35), E5144-52.

6. Haskamp, V.; Karrie, S.; Mingers, T.; Barthels, S.; Alberge, F.; Magalon, A.; Muller, K.; Bill, E.; Lubitz, W.; Kleeberg, K.; Schweyen, P.; Broring, M.; Jahn, M.; Jahn, D., The radical SAM protein HemW is a heme chaperone. *J Biol Chem* **2018,** *293* (7), 2558-2572.

7. Dailey, T. A.; Boynton, T. O.; Albetel, A. N.; Gerdes, S.; Johnson, M. K.; Dailey, H. A., Discovery and Characterization of HemQ: an essential heme biosynthetic pathway component. *J Biol Chem* **2010,** *285* (34), 25978-86.

8. Lobo, S. A.; Scott, A.; Videira, M. A.; Winpenny, D.; Gardner, M.; Palmer, M. J.; Schroeder, S.; Lawrence, A. D.; Parkinson, T.; Warren, M. J.; Saraiva, L. M., Staphylococcus aureus haem biosynthesis: characterisation of the enzymes involved in final steps of the pathway. *Mol Microbiol* **2015,** *97* (3), 472-87.

9. Celis, A. I.; Streit, B. R.; Moraski, G. C.; Kant, R.; Lash, T. D.; Lukat-Rodgers, G. S.; Rodgers, K. R.; DuBois, J. L., Unusual Peroxide-Dependent, Heme-Transforming Reaction Catalyzed by HemQ. *Biochemistry* **2015,** *54* (26), 4022-32.

10. Choby, J. E.; Grunenwald, C. M.; Celis, A. I.; Gerdes, S. Y.; DuBois, J. L.; Skaar, E. P., Staphylococcus aureus HemX Modulates Glutamyl-tRNA Reductase Abundance To Regulate Heme Biosynthesis. *MBio* **2018,** *9* (1).

11. Perkins, J. R.; Diboun, I.; Dessailly, B. H.; Lees, J. G.; Orengo, C., Transient protein-protein interactions: structural, functional, and network properties. *Structure* **2010,** *18* (10), 1233-43.

12. Celis, A. I.; Gauss, G. H.; Streit, B. R.; Shisler, K.; Moraski, G. C.; Rodgers, K. R.; Lukat-Rodgers, G. S.; Peters, J. W.; DuBois, J. L., Structure-Based Mechanism for Oxidative Decarboxylation Reactions Mediated by Amino Acids and Heme Propionates in Coproheme Decarboxylase (HemQ). *J Am Chem Soc* **2017,** *139* (5), 1900-1911.

13. Celis, A. I.; DuBois, J. L., Substrate, product, and cofactor: The extraordinarily flexible relationship between the CDE superfamily and heme. *Archives of Biochemistry and Biophysics* **2015,** *574*, 3-17.

14. Mayfield, J. A.; Hammer, N. D.; Kurker, R. C.; Chen, T. K.; Ojha, S.; Skaar, E. P.; DuBois, J. L., The Chlorite Dismutase (HemQ) fromStaphylococcus aureusHas a Redox-sensitive Heme and Is Associated with the Small Colony Variant Phenotype. *Journal of Biological Chemistry* **2013,** *288* (32), 23488-23504.

15. Mourino, S.; Giardina, B. J.; Reyes-Caballero, H.; Wilks, A., Metabolite-driven Regulation of Heme Uptake by the Biliverdin IXbeta/delta-Selective Heme Oxygenase (HemO) of Pseudomonas aeruginosa. *J Biol Chem* **2016,** *291* (39), 20503-15.

CHAPTER EIGHT

THE TRUE FINAL STEP IN HEME B BIOSYNTHESIS; EXPLORING THE ROLE OF CHDC IN THE DELIVERY OF HEME B TO ITS FINAL DESTINATION

Background and Introduction

Heme *b* must not only be biosynthesized, but delivered to the necessary recipient proteins in order to fulfill cellular needs. As mentioned in previous chapters, this process must be tightly regulated and controlled, as the reactivity that makes this molecule such a versatile co-factor can also be detrimental to the cell. This is especially true in organisms like gram-positive bacteria that lack membrane-bound structures for toxic molecule compartmentalization.

What happens in gram-positive bacteria after the final heme-forming reaction occurs is not known. We hypothesize that after catalysis, ChdC does not release heme into the cellular milieu and that it instead remains heme-bound until it can hand it off to another protein. We propose that this heme-recipient protein is a heme trafficking chaperone that will safely deliver heme to its final cellular destination. Alternatively, it is also possible that ChdC itself is this heme cellular delivery agent, playing a double role as a coproheme decarboxylase and a heme chaperone. Experiments to explore the former hypothesis are proposed here.

Targeted search for the gram-positive bacterial heme chaperone; Interrogating HemW

Exploring the idea of a gram-positive bacterial heme chaperone led us to consider HemW as a possibility. HemW is one of three known heme-binding proteins in the gram-positive group of lactic acid bacteria[1] and was proposed to be involved in heme-trafficking in *Lactococcus lactis*[2]. HemW enzymes share a high sequence similarity with and have been widely misannotated as coproporphyrnigen dehydrogenases (CgdH, formerly known as the coproporphyrin oxidase/dehydrogenase, HemN)[2-3]. However, HemWs do not catalyze the CgdH reaction *in vivo* nor *in vitro* and, as a group, display conserved sequence and structural differences relative to canonical CgdHs[2].

HemWs have a truncated N-terminus and lack the conserved fourth Cys of the CgdH [4Fe-4S] cluster CX3CX2CXC motif, which is replaced by a Phe. Instead of a [4Fe-4S] cluster, the *Ll*HemW described by Abicht et al. 2012 was found to have a [2Fe-2S]. In the presence of this cluster this enzyme is a dimer and in its absence it is a momomer. *Ll*HemW was further shown to have the ability to bind heme, independent of [Fe-S] cluster content, and to transfer heme specifically to *L. lactis* cell membranes in a NADH-dependent manner[2].

To determine whether HemW could be the CDP branch heme biosynthesis chaperone, we searched for a *cgdH* gene sequence in the *S. aureus* genome. As a gram-positive organism, *S. aureus* uses the CPD branch of heme *b* biosynthesis and thus has no requirement for a canonical CgdH, yet indeed has a gene annotated as *cgdH*. Sequence alignments with canonical CgdHs and *Ll*HemW reveal that *Sa*CgdH in fact has the defining sequence characteristics of a HemW (Figure 8.1).

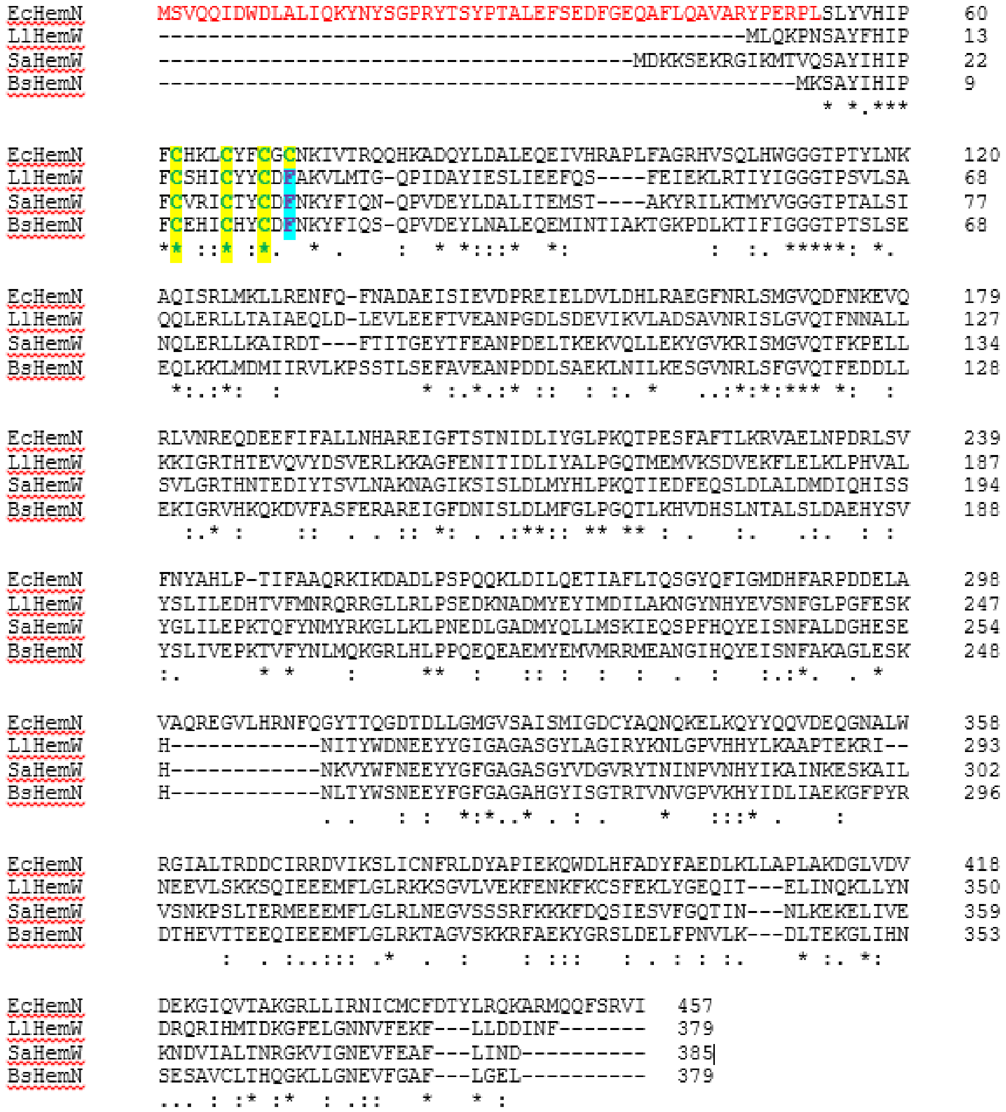

```
EcHemN      MSVQQIDWDLALIQKYNYSGPRYTSYPTALEFSEDFGEQAFLQAVARYPERPLSLYVHIP    60
LlHemW      -----------------------------------------------MLQKPNSAYFHIP    13
SaHemW      --------------------------------------MDKKSEKRGIKMTVQSAYIHIP    22
BsHemN      ---------------------------------------------------MKSAYIHIP    9
                                                                 * *.***

EcHemN      FCHKLCYFCGCNKIVTRQQHKADQYLDALEQEIVHRAPLFAGRHVSQLHWGGGTPTYLNK    120
LlHemW      FCSHICYYCDFAKVLMTG-QPIDAYIESLIEEFQS----FEIEKLRTIYIGGGTPSVLSA    68
SaHemW      FCVRICTYCDFNKYFIQN-QPVDEYLDALITEMST----AKYRILKTMYVGGGTPTALSI    77
BsHemN      FCEHICHYCDFNKYFIQS-QPVDEYLNALEQEMINTIAKTGKPDLKTIFIGGGTPTSLSE    68
            ** ::* :*.  * .    :  * *:::*  *:           :  :. *****: *.

EcHemN      AQISRLMKLLRENFQ-FNADAEISIEVDPREIELDVLDHLRAEGFNRLSMGVQDFNKEVQ    179
LlHemW      QQLERLLTAIAEQLD-LEVLEEFTVEANPGDLSDEVIKVLADSAVNRISLGVQTFNNALL    127
SaHemW      NQLERLLKAIRDT---FTITGEYTFEANPDELTKEKVQLLEKYGVKRISMGVQTFKPELL    134
BsHemN      EQLKKLMDMIIRVLKPSSTLSEFAVEANPDDLSAEKLNILKESGVNRLSFGVQTFEDDLL    128
             *:.:*:  :           * :.*.:* ::  : :. *   ..:*:*:*** *:  :

EcHemN      RLVNREQDEEFIFALLNHAREIGFTSTNIDLIYGLPKQTPESFAFTLKRVAELNPDRLSV    239
LlHemW      KKIGRTHTEVQVYDSVERLKKAGFENITIDLIYALPGQTMEMVKSDVEKFLELKLPHVAL    187
SaHemW      SVLGRTHNTEDIYTSVLNAKNAGIKSISLDLMYHLPKQTIEDFEQSLDLALDMDIQHISS    194
BsHemN      EKIGRVHKQKDVFASFERAREIGFDNISLDLMFGLPGQTLKHVDHSLNTALSLDAEHYSV    188
              :.* :    ::  . . :: *: . .:**:: ** ** : .   :.   .:.  : :

EcHemN      FNYAHLP-TIFAAQRKIKDADLPSPQQKLDILQETIAFLTQSGYQFIGMDHFARPDDELA    298
LlHemW      YSLILEDHTVFMNRQRRGLLRLPSEDKNADMYEYIMDILAKNGYNHYEVSNFGLPGFESK    247
SaHemW      YGLILEPKTQFYNMYRKGLLKLPNEDLGADMYQLLMSKIEQSPFHQYEISNFALDGHESE    254
BsHemN      YSLIVEPKTVFYNLMQKGRLHLPPQEQEAEMYEMVMRRMEANGIHQYEISNFAKAGLESK    248
            :.      * *    :     **  :   :: :  :  :  .  :   :.:*.  . *

EcHemN      VAQREGVLHRNFQGYTTQGDTDLLGMGVSAISMIGDCYAQNQKELKQYYQQVDEQGNALW    358
LlHemW      H------------NITYWDNEEYYGIGAGASGYLAGIRYKNLGPVHHYLKAAPTEKRI--    293
SaHemW      H------------NKVYWFNEEYYGFGAGASGYVDGVRYTNINPVNHYIKAINKESKAIL    302
BsHemN      H------------NLTYWSNEEYFGFGAGAHGYISGTRTVNVGPVKHYIDLIAEKGFPYR    296
                         . .   : :  *:*..* . : .    *   :::* .    :

EcHemN      RGIALTRDDCIRRDVIKSLICNFRLDYAPIEKQWDLHFADYFAEDLKLLAPLAKDGLVDV    418
LlHemW      NEEVLSKKSQIEEEMFLGLRKKSGVLVEKFENKFKCSFEKLYGEQIT---ELINQKLLYN    350
SaHemW      VSNKPSLTERMEEEMFLGLRLNEGVSSSRFKKKFDQSIESVFGQTIN---NLKEKELIVE    359
BsHemN      DTHEVTTEEQIEEEMFLGLRKTAGVSKKRFAEKYGRSLDELFPNVLK---DLTEKGLIHN    353
                 :  . :..::: .*  .  :    : :::   : . : : :.    * :. *:

EcHemN      DEKGIQVTAKGRLLIRNICMCFDTYLRQKARMQQFSRVI   457
LlHemW      DRQRIHMTDKGFELGNNVFEKF---LLDDINF-------   379
SaHemW      KNDVIALTNRGKVIGNEVFEAF---LIND----------   385
BsHemN      SESAVCLTHQGKLLGNEVFGAF---LGEL----------   379
            ... : :* :*  : .::   *   * :
```

Figure 8.1. Clustal O(1.2.4) sequence alignment of a canonical CgdH from *E. coli* (*Ec*HemN), *Ll*HemW, *Sa*CgdH (HemW), and *Bs*CgdH (HemW). The N-terminus (shown in red) of canonical CgdH proteins is missing in the characterized HemW heme-chaperone from *L. lactis* (*Ll*HemW). *Ll*HemW is also missing the fourth Cys residue in the CX3CX2CXC motif (shown in green with yellow highlight) of canonical CgdHs, and it is replaced by a Phe (shown in purple with blue highlight). Sequences of the annotated CgdH/HemN proteins from the common representative gram-positive organisms, *S. aureus* and *B. subtilis*, share these sequence differences, indicating that these proteins are likely HemWs and not canonical CgdHs.

Specifically, *Sa*CgdH lacks 36 N-terminal amino acids of canonical CgdHs and the fourth Cys residue of the CX3CX2CXC [4Fe-4S] motif, which is replaced by a Phe. Given these results, we propose that *Sa*CgdH should be annotated as a HemW and that it is a heme biosynthesis heme chaperone in gram-positive bacteria. We hypothesize that ChdC transfers heme to HemW and that this happens via a direct protein-protein interaction between the two enzymes.

Preliminary and Proposed Experiments

Expression and Purification of *Sa*HemW. The sequence encoding HemW (CgdH, formerly known as HemN) in *Staphylococcus aureus* Newman was obtained from NCBI (accession number NC_009641.1) and codon-optimized for heterologous expression in *E. coli*. The *SahemW(cgdH)* containing plasmid (ATUM) was transformed into Tuner (DE3) cells (Novagen). Heterologous expression will be carried out in 1 L flasks of Terrific Broth supplemented with the 50 mg/L kanamycin. Purification of HemW will proceed as for *Sa*CpfC in Chapter 7 of this thesis. Because the air sensitivity of *Sa*HemW is unknown, we will begin with aerobic purification and adopt anoxic conditions if the [2Fe-2S] cluster (characterized and quantified by EPR) proves unstable. We expect heme-free/apo-*Sa*HemW to be present in the cytosolic fraction of the cell lysate; heme-bound *Ll*HemW was found to migrate to an *L. lactis* membrane vesicle fraction[2]. This His-tagged *Sa*HemW is estimated to have a molecular weight of 46.3 kDa and a pI of 6.0 (ExPASy ProtParam). Post-purification, anaerobic incubation with $Fe(NH_4)_2(SO_4)_2$ and Na_2S (as an iron and sulfur source, respectively) might be required to obtain full [Fe-S] cluster formation and incorporation into *Sa*HemW (to be experimentally determined), where one [2Fe-2S] cluster per protein is expected and the cluster-loaded protein should be dimeric. It is suggested that purification and experiments are conducted in a buffer of pH 7.5-8.

Characterization of the *Sa*HemW [Fe-S] Cluster via EPR. Characterization of this cluster could be the first indication that *Sa*HemW is really a HemW and not a canonical HemN. This will be carried out by using electron-plasma resonance spectroscopy. We expect that *Sa*HemW will have a [2Fe-2S], and not a [4Fe-4S], cluster, like that described for *Ll*HemW. The composition of the cluster should be directly reflected by the the EPR spectrum.

Analysis of SAM Binding and Cleavage Capacity of *Sa*HemW. To determine whether HemW binds SAM, purified *Sa*HemW will be incubated with ^{14}C-SAM and then passed through a desalting column to remove any unbound material. ^{14}C-SAM-bound *Sa*HemW will then be analyzed by LC-MS and/or NMR. Liquid scintillation counting can also be used for analysis[3], if this instrument is made available. For SAM cleavage, purified *Sa*HemW will be incubated with sodium dithionite and SAM anaerobically. Reactions will be stopped by addition of 5% formic acid. Production of 5'deoxyadenosine and consumption pf SAM will be monitored via HPLC.

Characterization of Heme-Binding Properties of *Sa*HemW. UV/Vis spectra of HemW in the absence and presence of heme will be measured on a Cary60 instrument. Absorbance wavelength and intensity of Soret and Q-bands of the heme-bound form of

*Sa*HemW will be determined. Samples containing greater concentrations of enzyme to porphyrin should be used to ensure complete binding.

Values of K_D for equilibrium binding of *Sa*HemW to heme will be determined by tryptophan fluorescence quenching (excitation = 295 nm, emission = 340 nm) (Cary). Plotting and calculation of K_D will be done as specified in the Chapter 7 of this thesis.

The extinction coefficient at the Soret band maximum of the heme-HemW complex should be determined by the pyridine-hemochrome method as was previously done in Celis et al. 2015 (Chapter 3 in this thesis).

Measurement of Heme-Association and Heme-Dissociation Constants. A heme-trafficking function is consistent with a significantly faster rate of heme dissociation than that of myoglobin ($k_{\text{off (heme)}} = 8.4 \times 10^7\ \text{s}^{-1}$) [4]. Kinetic association $k_{\text{on (heme)}}$ and dissociation $k_{\text{off (heme)}}$ rates of heme to *Sa*HemW will be determined using a stopped-flow spectrometer (Hi-Tech SF-61DX2). *Sa*HemW will be rapidly mixed with heme and spectra will be collected from 30-700nm in diode array mode. Rate constants (k_{obs}) will be calculated by fitting single-exponential curves of changes at the determined heme-bound *Sa*HemW absorbance maxima (Soret) versus time using the KineticAssay software from Tgk Scientific and the following equation:

$$\text{Equation 1} \qquad \Delta Abs = \Delta Abs_1 \exp(-k_1 t)$$

Second-order rate constants will then determined from fits of k_{obs} versus heme concentration to the following equation:

$$\text{Equation 2} \quad k_{obs} = k_{on}\,[heme] + k_{off}$$

Equation 3 $$K_d = \frac{k_{OFF}}{k_{ON}}$$

Where k_{on} is the rate of heme association and k_{off} is the rate of dissociation. Kinetic values of the dissociation constants K_{d} can then be determined using equation 3.

In vitro Heme Transfer Experiments by UV-Vis. These experiments are inspired by those performed by Bahkta and Wilks 2006[4] and Lansky et al. 2006[5] and will be conducted to determine (1) whether *Sa*HemW can accept heme from *Sa*ChdC, (2) the extent of heme transfer, and (3) whether heme transfer is unidirectional, as should be the case if HemW is the ChdC heme recipient.

To determine whether heme bound to ChdC is transferred to HemW, the spectrum of heme-bound ChdC will be recorded once, then recorded again after an equimolar amount of apo-HemW is added to the solution. It has previously been reported that the heme-bound ChdC spectrum is a broad Soret ~406 nm with an extinction coefficient of $\varepsilon_{416} = 76.6\ \text{mM}^{-1}\ \text{cm}^{-1}$ [6]. If heme transfer from ChdC to HemW occurs, we expect that the Soret will shift from ~406nm to the Soret assigned to heme-bound *Sa*HemW. If the Soret peaks of the two bound enzymes are very close, difference spectra should be plotted to see changes indicative of heme transfer.

In vitro Heme Transfer Analysis by SEC and SDS-PAGE**.** To differentiate between heme-transfer and heme-sharing, the extent of heme transfer will be assessed using size-exclusion chromatography (SEC) followed by SDS-PAGE analysis. Following the transfer event, as monitored by UV-Vis, the reaction mixture will be loaded to a SEC column

(ENRich BioRad) and separated using an FPLC system. Absorbance of fractions collected will be monitored at 400 nm for heme and 280 nm for protein. The spectra obtained will be compared to the respective fractions analyzed by SDS-PAGE. This procedure will be repeated using another heme-binding enzyme, thought to not interact with ChdC, as a negative control. If HemW is the ChdC heme recipient, we expect that there will be full heme transfer from ChdC to HemW. Thus, all fractions containing absorbance ~400 nm should correspond a to single HemW band on the SDS-PAGE gel and should not contain any significant amount of ChdC. A published sample figure taken from Lansky et al 2006[5], where PhuS is the heme-delivery protein, pa-HO is the heme-recipient protein, and BpHO is the negative control, is shown below (solid line = 280 nm, dashed line = 400 nm).

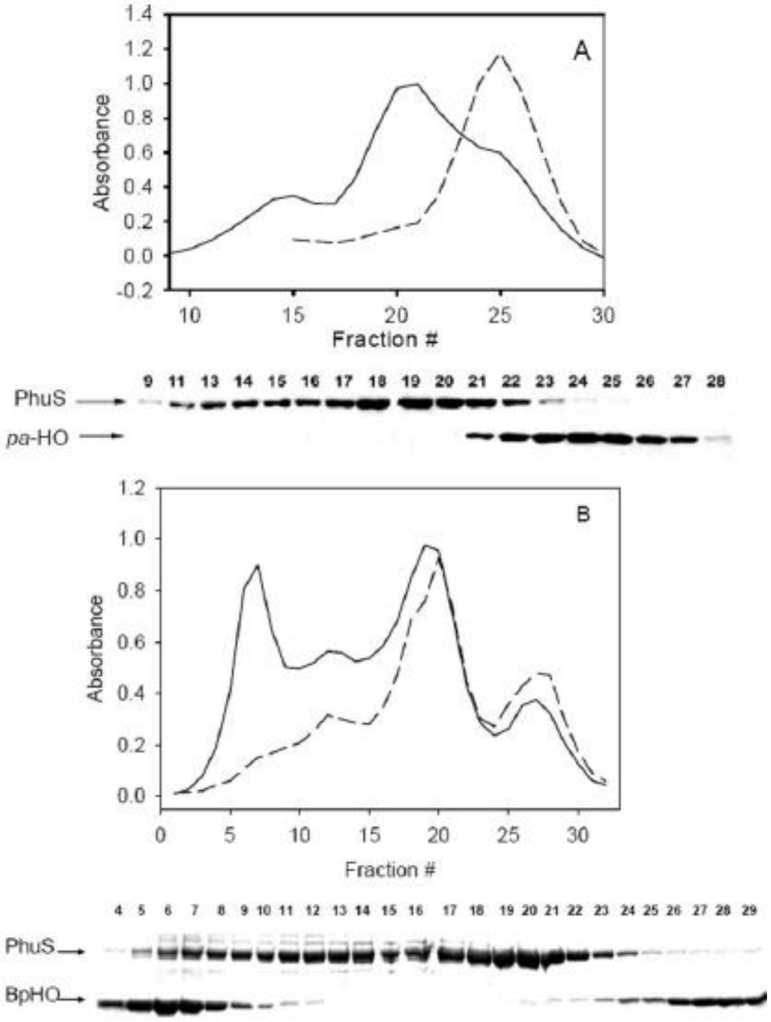

Figure 8.2. Sample figure showing analysis of heme-transfer from PhuS to pa-HO or BpHO by SEC and SDS-PAGE. The extent of heme transfer from ChdC to HemW can be analyzed as was done with for the heme-delivery protein PhuS and the protein-recipient protein pa-HO (A) or the negative control protein BpHO (B)[5]. A single protein band for the heme-recipient protein on the SDS-PAGE gel corresponding to the heme-containing fractions on the SEC chromatogram is indicative of complete transfer of heme.

Determining Rate of Heme Transfer. The protein myoglobin uses heme as a cofactor and has a heme binding constant of $k_{on} = 1.3 \times 10^{-8}$ μM. This is usual for enzymes that use heme as a cofactor but significantly greater than most heme-trafficking enzymes (~10^{-1} μM). To determine whether heme transfer is ChdC to HemW-specific, the transfer rate from ChdC to HemW will be measured using stopped flow UV-Vis spectroscopy and compared to the rate of transfer from ChdC to myoglobin. Because the affinity for and rate of binding of heme to myoglobin is so large, we expect to see some heme transfer from ChdC to myoglobin. However, if HemW is the true heme recipient of heme from ChdC, we expect that the rate of heme transfer from ChdC to HemW will be significantly faster than that of ChdC to myoglobin[4].

Preliminary Studies with N112L ChdC. It was previously hypothesized that a helical loop near the active site of ChdC acts as an "active site gate" and might be responsible for ChdC protein-protein interactions. To test this hypothesis, residues along this loop were mutated and the resulting ChdC protein variants were inserted in *chdC*-deficient strains of *S. aureus* (*ΔchdC*) and subsequently phenotypically characterized. The *S. aureus* mutant containing a mutation on residue N112L displayed a growth deficiency that was not complemented (and was instead exacerbated) by addition of exogenous heme (Figure 7.11). Analysis of this strain's cellular heme and coproheme content (its porphyin profile) revealed that it was deficient in coproheme and accumulated heme, relative to WT (Figure 7.12). These results indicated that this mutation did not affect ChdC catalytic activity but that it could perhaps disturb the ability of ChdC to deliver heme to its final cellular destination, leaving the cell feeling "hungry" for heme and signaling for production of more.

Assessing the Role of the N112 Residue of ChdC in Heme Transfer to HemW. Given the results obtained in our phenotype characterization of the N112L ChdC-*S. aureus* mutant, we hypothesized that this residue in ChdC is important for delivery of ChdC-bound heme to a heme chaperone. To test this hypothesis, site-directed mutagenesis will be performed on the WT plasmid and inserted into *E. coli* (Tuner DE3). N112L ChdC will be heterologously expressed and purified as outlined for the WT enzyme and other ChdC protein variants[7]. The heme binding properties of N112L ChdC will be analyzed and the ability of this protein variant to transfer heme will be assessed as was done with WT ChdC. We expect that if the N112L residue to ChdC plays a role in heme transfer to HemW, then impaired or no heme transfer will be observed.

An Untargeted Approach to Finding the Gram-Positive Bacterial Heme Chaperone

The experiments outlined above might provide compelling evidence that HemW is the gram-positive bacterial heme biosynthesis heme chaperone. Less excitingly, they might instead indicate that (1) HemW is a heme chaperone, but is not ChdC's interaction partner or (2) that *Sa*HemW is not a heme chaperone at all. Whether the results are positive or negative, an untargeted search for the gram-positive bacteria heme biosynthesis chaperone would be greatly informative. It could confirm the hypothesis that HemW is the heme biosynthesis chaperone, it could provide us with the identity of the correct heme chaperone (if HemW is not it), or it could provide us with identities of alternate chaperones (as there may be more than one).

This untargeted approach could be taken by conducting proteomic analyses of *S. aureus* cell lysates to identify heme-binding proteins as was done by Wang et al 2014[8]. This search could be facilitated by having two different kinds of samples to pick out differences from; one where the chaperone would presumably be overexpressed. These samples could be cells grown in heme-deficient versus heme-replete conditions, WT *S.*

aureus versus *ΔchdC-S. aureus* (a similar ± heme case), or WT *S. aureus* versus N112L-ChdC-*S. aureus*.

The same set of samples could be analyzed by conducting quantitative reverse transcriptase PCR (qtPCR) as was done in Choby et al 2017[9], to look for proteins that might be upregulated in heme deficient samples or in the N112L mutant strain versus WT.

Conclusions

The heme-paradox is the concept that heme is a versatile cofactor that is essential to aerobic life and that at the same time this versatile reactivity can be toxic to the cell. In order to deal with this paradox, organisms must have tightly regulated heme biosynthesis pathways, including handling of the final heme product. The destiny of heme after the final biosynthesis step in gram-positive bacteria is not known. We propose that ChdC must hand off heme to a heme-trafficking protein that delivers heme to its final cellular destination. We further propose that HemW may be this heme-chaperone and have outlined experiments to test this hypothesis here. An untargeted approach to find ChdCs heme-deliver partner is also suggested. Lastly, it is possible that ChdC itself is this heme-trafficking/heme-chaperone protein. This hypothesis should also be considered.

References

1. Hederstedt, L., Heme Proteins in Lactic Acid Bacteria. *Advances in Microbial Physiology* **2013,** *62*, 1-43.

2. Abicht, H. K.; Martinez, J.; Layer, G.; Jahn, D.; Solioz, M., Lactococcus lactis HemW (HemN) is a haem-binding protein with a putative role in haem trafficking. *Biochem J* **2012,** *442* (2), 335-43.

3. Haskamp, V.; Karrie, S.; Mingers, T.; Barthels, S.; Alberge, F.; Magalon, A.; Muller, K.; Bill, E.; Lubitz, W.; Kleeberg, K.; Schweyen, P.; Broring, M.; Jahn, M.; Jahn, D., The radical SAM protein HemW is a heme chaperone. *J Biol Chem* **2018,** *293* (7), 2558-2572.

4. Wilks, M. N. B. a. A., The Mechanism of Heme Transfer from the Cytoplasmic Heme Binding Protein PhuS to the δ-Regioselective Heme Oxygenase of Pseudomonas aeruginosa. *Biochem J* **2006,** *45* (38), 11642-11649.

5. Lansky, I. B.; Lukat-Rodgers, G. S.; Block, D.; Rodgers, K. R.; Ratliff, M.; Wilks, A., The cytoplasmic heme-binding protein (PhuS) from the heme uptake system of Pseudomonas aeruginosa is an intracellular heme-trafficking protein to the delta-regioselective heme oxygenase. *J Biol Chem* **2006,** *281* (19), 13652-62.

6. Celis, A. I.; Streit, B. R.; Moraski, G. C.; Kant, R.; Lash, T. D.; Lukat-Rodgers, G. S.; Rodgers, K. R.; DuBois, J. L., Unusual Peroxide-Dependent, Heme-Transforming Reaction Catalyzed by HemQ. *Biochemistry* **2015,** *54* (26), 4022-32.

7. Celis, A. I.; Gauss, G. H.; Streit, B. R.; Shisler, K.; Moraski, G. C.; Rodgers, K. R.; Lukat-Rodgers, G. S.; Peters, J. W.; DuBois, J. L., Structure-Based Mechanism for Oxidative Decarboxylation Reactions Mediated by Amino Acids and Heme Propionates in Coproheme Decarboxylase (HemQ). *J Am Chem Soc* **2017,** *139* (5), 1900-1911.

8. Wang, N.; Zhang, J.; Yang, X.; Li, N.; Yu, G.; Han, J., Cao, K,; Guo, Z.; Syn, X.; and He, Q. Proteomic analysis of putative heme-binding proteins in *Streptococcus pyogenes*. *Metallomics* **2014,** *6*, 1451-1459.

9. Choby, J. E.; Grunenwald, C. M.; Celis, A. I.; Gerdes, S. Y.; DuBois, J. L.; Skaar, E. P., Staphylococcus aureus HemX Modulates Glutamyl-tRNA Reductase Abundance To Regulate Heme Biosynthesis. *MBio* **2018,** *9* (1).

CHAPTER NINE

CONCLUDING REMARKS

Heme *b* is a versatile cofactor that is essential for almost all aerobic life. Because of its importance, the biosynthesis of heme *b* has been extensively studied and well-documented for over 60 years. The development and accessibility of genome sequencing and bioinformatics tools led to the discovery that the established pathway for making this molecule was not universal[1-2]. It is now known that there are at least two pathways of heme *b* biosynthesis, which share a similar beginning and only “branch out” for the final three steps. The terminal steps of these two branches are different in the order in which they are performed, in the enzymes that catalyze them, and in the heme precursors that are formed along the way. The canonical pathway uses protoporphyrin IX as the intermediate to get to heme and thus has been designated as the protoporphyrin-dependent (PPD) branch. The newly characterized pathway uses coproporphyrin III as the intermediate instead, and thus was termed the coproporphyrin-dependent (CPD) branch. The PPD branch is exclusively found in gram-negative organisms (*E. coli)* and eukaryotes, while the CPD branch is unique to gram-positive bacteria (*S. aureus*, *B. subtilis*).

The discovery of the CPD branch of heme *b* biosynthesis came as a result of discovering the enzyme that is unique to it, now called coproheme decarboxylase (ChdC), but formerly known as HemQ. Although first classified as a chlorite dismutase enzyme, it readily became evident that ChdC had a role in heme *b* biosynthesis and not chlorite detoxification[3-4]. Once its role was deciphered and the novel CPD branch of heme *b* biosynthesis was elucidated, understanding the unique ChdC reaction became our goal. The aim of this research project was to characterize the ChdC catalyzed reaction at the molecular level, the structural level, and the cellular level. The contents of this thesis exemplify our approach towards this multi-level characterization and the contributions that we have added to the field.

Through our work with the recombinant ChdC enzyme from *S. aureus*, we demonstrated that ChdC catalyzes the oxidative decarboxylation of the ring A- and ring B- propionate groups of coproheme III to yield the final product of the CPD branch, heme *b*. This reaction is H_2O_2-dependent and proceeds in a sequential and clockwise fashion, specifically generating the mono-vinyl harderoheme III intermediate during the process. With rapid mixing UV-Vis analyses, we showed that, although ChdC receives its coproheme substrate in the ferrous form, the coproheme iron is quickly oxidized to Fe (III) prior to reactivity with ChdC to yield ferric heme *b* as the product. We solved and crystallographically characterized the first ever coproheme-bound ChdC enzyme structure.

Structural analysis allowed us to identify the specific ChdC amino acid residues that made direct contact with each of the reactive propionates and suggested residues that might be essential for catalysis. Site-directed mutagenesis experiments allowed us to develop a structurally based mechanism for the ChdC reaction. In this reaction mechanism, we proposed that post binding of H_2O_2 to Fe(III), this reaction proceeds through the high-valent Fe(IV) intermediate (Compound I), which oxidizes a nearby Tyr residue (Tyr 145S, *Sa* numbering), producing a Tyr radical (Tyr•). This radical then abstracts an H-atom at the β-position of the ring A-propionate group, promoting decarboxylation and the production of a vinyl group at that position, creating harderoheme III. This process occurs one more time, with another molecule of H_2O_2. This time decarboxylation happens to the ring B-propionate group, again leaving a vinyl group at that position and creating the final product heme *b*. Through EPR characterization of the Tyr• in the WT and various Tyr protein variants of ChdC, along with other spectroscopic studies, we concluded that Tyr145, and only Tyr145 is responsible for both decarboxylation events.

Comparison the coproheme-bound ChdC (PDBID 5T2K) structure and the structure of a canonical, and highly structurally similar Cld (PDBID 3Q09) revealed that coproheme binds in a similar location, but in a different orientation relative to the heme in the Cld. Comparison of coproheme-bound ChdC with apo-ChdC (PDBID 1T0T) highlights a mobile structural helical loop composed of amino acids ~110-140. This helical structure is away from the active site in the absence of substrate, and moves closes in towards it in its presence. We have hypothesized that this loop can act as an “active site gate”, allowing for substrate entry and product egress.

Because heme, as well as its porphyrin precursors, is reactive and cytotoxic if allowed to accumulate, we have further hypothesized that this structural loop might be involved in substrate/product delivery though direct protein-protein interactions with other enzymes. Specifically, we hypothesize that ChdC might interact with CpfC, the preceding enzyme in the pathway, and a yet unidentified heme chaperone, which would be responsible for the safe delivery of heme to its final cellular destination. Using UV-Vis spectroscopy, we have provided preliminary evidence for a CpfC-ChdC interaction and through phenotype characterization of *S. aureus* strains containing ChdC point mutants (residues mutated along the active site gate), we have proposed that mutation to the E120 residue on ChdC disrupts this interaction. Future studies to provide evidence for this role have been proposed here.

Also part of understanding the role of ChdC at the cellular level, we have hoped to determine the fate of ChdC's heme product. A literature search for gram-positive bacterial heme chaperones identified the heme-binding, SAM-containing enzyme, HemW, as a potential candidate. HemW was shown to be a misannotaed CgdH enzyme (the coproporphyrin dehydrogenase enzyme in the PPD branch of the pathway) in *L. lactis*[5] .Gram-positive organisms use the CPD branch of heme *b* biosynthesis and thus have no requirement for a canonical CdgH, yet indeed, most contain a gene annotated as *cdgH*. Using the gene from *S. aureus*, we have proposed that *Sa*CdgH is a misannotated HemW and that HemW is the heme biosynthesis heme-chaperone in gram-positive bacteria. We have hypothesized that ChdC transfers heme to HemW and that this happens via a direct protein-protein interaction between the two enzymes. Experiments to determine whether this hypothesis is correct have been proposed in this thesis.

Lastly, a big question in the field relates to the cellular source of the H_2O_2, required for the ChdC reaction. Historically, it has been stated that CgoX uses O_2 as an electron acceptor and produces H_2O_2 during its catalytic reaction, making it the perfect candidate as the source of this molecule. If this is the case, we propose that CgoX must directly interact with ChdC to deliver this powerful oxidant. However, it must be noted that production of H_2O_2 by CgoX has not been experimentally shown and most of what is known about this enzyme's reaction comes from studies of the PPD branch homolog, PgoX. While PgoX and CgoX are structurally similar, they are not identical and contain significant differences which have been outlined in Chapter 1 of this thesis. Important to this discussion is the significant larger active site of CgoX relative to PgoX (1173 Å vs 450-550 Å, respectively)[6]. It has been noted that this larger active site serves to accommodate the FAD co-factor and the larger coproporporphyrinogen substrate. Not as obvious, is that this active site is spacious enough to also accommodate another large molecule, as crystallization of this enzyme with acifluoren has shown (PDBID 3I6D). Although completely speculative at the moment, we propose that the true electron acceptor of the CgoX reaction has yet to be determined and that it could potentially be NAD(P). If this is true, then NADH, and not H_2O_2, might be the biological oxidant the ChdC reaction. The use of this less powerful and recyclable oxidant for the ChdC reaction makes more sense from the biological perspective but also remains to be experimentally tested.

It is my belief that this thesis contains answer to questions which have allowed for the expansion of the heme *b* biosynthesis field and that these questions have been answered using a wide-variety of biochemical and analytical techniques. Simultaneously, the work presented here has given rise to many more questions to answer. It is my hope that they too will be answered (perhaps in someone else's thesis) and continue to provide greater depth and biochemical understanding of heme *b* biosynthesis in gram-positive bacteria.

References

1. Dailey, H. A.; Gerdes, S.; Dailey, T. A.; Burch, J. S.; Phillips, J. D., Noncanonical coproporphyrin-dependent bacterial heme biosynthesis pathway that does not use protoporphyrin. *Proc Natl Acad Sci U S A* **2015,** *112* (7), 2210-5.

2. Bali, S.; Lawrence, A. D.; Lobo, S. A.; Saraiva, L. M.; Golding, B. T.; Palmer, D. J.; Howard, M. J.; Ferguson, S. J.; Warren, M. J., Molecular hijacking of siroheme for the synthesis of heme and d1 heme. *Proc Natl Acad Sci U S A* **2011,** *108* (45), 18260-5.

3. Mayfield, J. A.; Hammer, N. D.; Kurker, R. C.; Chen, T. K.; Ojha, S.; Skaar, E. P.; DuBois, J. L., The Chlorite Dismutase (HemQ) fromStaphylococcus aureusHas a Redox-sensitive Heme and Is Associated with the Small Colony Variant Phenotype. *Journal of Biological Chemistry* **2013,** *288* (32), 23488-23504.

4. Dailey, T. A.; Boynton, T. O.; Albetel, A. N.; Gerdes, S.; Johnson, M. K.; Dailey, H. A., Discovery and Characterization of HemQ: an essential heme biosynthetic pathway component. *J Biol Chem* **2010,** *285* (34), 25978-86.

5. Abicht, H. K.; Martinez, J.; Layer, G.; Jahn, D.; Solioz, M., Lactococcus lactis HemW (HemN) is a haem-binding protein with a putative role in haem trafficking. *Biochem J* **2012,** *442* (2), 335-43.

6. Qin, X., Structural insight into unique properties of protoporphyrinogen oxidase from Bacillus subtilis. *Journal of Structural Biology* **2010,** *170* (1), 76-82.

REFERENCES CITED

Abicht, H. K.; Martinez, J.; Layer, G.; Jahn, D.; Solioz, M., Lactococcus lactis HemW (HemN) is a haem-binding protein with a putative role in haem trafficking. *Biochem J* **2012,** *442* (2), 335-43.

Adams, P. D.; Afonine, P. V.; Bunkóczi, G.; Chen, V. B.; Davis, I. W.; Echols, N.; Headd, J. J.; Hung, L. W.; Kapral, G. J.; Grosse-Kunstleve, R. W.; McCoy, A. J.; Moriarty, N. W.; Oeffner, R.; Read, R. J.; Richardson, D. C.; Richardson, J. S.; Terwilliger, T. C.; Zwart, P. H., PHENIX: a comprehensive Python-based system for macromolecular structure solution. *Acta Crystallogr D Biol Crystallogr* **2010,** *66* (Pt 2), 213-21.

Amy Medlock, L. S., Tamara A. Dailey, Harry A. Dailey, and William N. Lanzilotta, Substrate interactions with human ferrochelatase. *Proc Natl Acad Sci U S A* **2001,** *104* (6), 1789-1793.

Arnould, S., and Camadro, J. M. (1998) The domain structure of protoporphyrinogen oxidase, the molecular target of diphenyl ether-type herbicides, *Proc. Natl. Acad. Sci. USA 95*, 10553-10558.

Ayala, M., Roman, R., and Vazquez-Duhalt, R. (2007) A catalytic approach to estimate the redox potential of heme-peroxidases, *Biochem. Biophys. Res. Commun. 357*, 804-808.

Bali, S., Rollauer, S., Roversi, P., Raux-Deery, E., Lea, S. M., Warren, M. J., and Ferguson, S. J. (2014) Identification and characterization of the 'missing' terminal enzyme for siroheme biosynthesis in alpha-proteobacteria, *Mol. Microbiol. 92*, 153-163.

Bali, S.; Lawrence, A. D.; Lobo, S. A.; Saraiva, L. M.; Golding, B. T.; Palmer, D. J.; Howard, M. J.; Ferguson, S. J.; Warren, M. J., Molecular hijacking of siroheme for the synthesis of heme and d1 heme. *Proc Natl Acad Sci U S A* **2011,** *108* (45), 18260-5.

Barry, B., Eldeeb, M., Sandusky, P., and Babcock, G. (1990) Tyrosine radicals in photosystem II and related model compounds – characterization by isotopic labeling and EPR spectroscopy. *J. Biol. Chem.* **265**, 20139-20143.

Bates, R. G., and Covington, A. K. (1968) Behavior of the glass electrode and other pH-responsive electrodes in biological media, *Ann. N Y Acad. Sci. 148*, 67-80.

Bender, C., Sahlin, M., Babcock, G., Barry, B., Chandrashekar, T., Salowe, S., Stubbe, J., Lindstrom, B. Petersson, L. Ehrenberg, A., and Sjoberg, B. (1989) An ENDOR study of the tyrosyl free-radical in ribonucleotide reductase from *Escherichia coli. J. Am. Chem. Soc*. **111**, 8076-8083.

Berry, E.A.; Trumpower, B.L. (1987) Simultaneous determination of hemes a, b, and c from pyridine hemochrome spectra, *Anal. Biochem. 161*, 1-15.

Blanc, B.; Mayfield, J. A.; McDonald, C. A.; Lukat-Rodgers, G. S.; Rodgers, K. R.; DuBois, J. L., Understanding how the distal environment directs reactivity in chlorite dismutase: Spectroscopy and reactivity of Arg183 mutants. *Biochemistry* **2012,** *51* (9), 1895-1910.

Boynton, T. O.; Daugherty, L. E.; Dailey, T. A.; Dailey, H. A., Identification of Escherichia coli HemG as a Novel, Menadione-Dependent Flavodoxin with Protoporphyrinogen Oxidase Activity. *Biochemistry* **2009,** *48* (29), 6705-6714.

Boynton, T. O.; Gerdes, S.; Craven, S. H.; Neidle, E. L.; Phillips, J. D.; Dailey, H. A., Discovery of a gene involved in a third bacterial protoporphyrinogen oxidase activity through comparative genomic analysis and functional complementation. *Appl Environ Microbiol* **2011,** *77* (14), 4795-801.

Brown, K. R., Brown, B. M., Hoagland, E., Mayne, C. L., and Hegg, E. L. (2004) Heme A synthase does not incorporate molecular oxygen into the formyl group of heme A. *Biochemistry* **43**, 8616-8624.

Celis, A. I., Geeraerts, Z., Ngmenterebo, D., Machovina, M. M., Kurker, R. C., Rajakumar, K., Ivancich, A., Rodgers, K. R., Lukat-Rodgers, G. S., and DuBois, J. L. (2015) A dimeric chlorite dismutase exhibits O2-generating activity and acts as a chlorite antioxidant in *Klebsiella pneumoniae* MGH 78578, *Biochemistry 54*, 434-446.

Celis, A. I.; DuBois, J. L., Substrate, product, and cofactor: The extraordinarily flexible relationship between the CDE superfamily and heme. *Archives of Biochemistry and Biophysics* **2015,** *574*, 3-17.

Celis, A. I.; Gauss, G. H.; Streit, B. R.; Shisler, K.; Moraski, G. C.; Rodgers, K. R.; Lukat-Rodgers, G. S.; Peters, J. W.; DuBois, J. L., Structure-Based Mechanism for Oxidative Decarboxylation Reactions Mediated by Amino Acids and Heme Propionates in Coproheme Decarboxylase (HemQ). *J Am Chem Soc* **2017,** *139* (5), 1900-1911.

Celis, A. I.; Streit, B. R.; Moraski, G. C.; Kant, R.; Lash, T. D.; Lukat-Rodgers, G. S.; Rodgers, K. R.; DuBois, J. L., Unusual Peroxide-Dependent, Heme-Transforming Reaction Catalyzed by HemQ. *Biochemistry* **2015,** *54* (26), 4022-32.

Choby, J. E.; Grunenwald, C. M.; Celis, A. I.; Gerdes, S. Y.; DuBois, J. L.; Skaar, E. P., Staphylococcus aureus HemX Modulates Glutamyl-tRNA Reductase Abundance To Regulate Heme Biosynthesis. *MBio* **2018,** *9* (1).

Choinowski, T.; Blodig, W.; Winterhalter, K. H.; Piontek, K., The crystal structure of lignin peroxidase at 1.70 angstrom resolution reveals a hydroxy group on the C-beta of tryptophan 171: A novel radical site formed during the redox cycle. *J Mol BIol* **1999,** *286* (3), 809-827.

Choudhury, K.; Sundaramoorthy, M.; Hickman, A.; Yonetani, T.; Woehl, E.; Dunn, M. F.; Poulos, T. L., Role of the proximal ligand in peroxidase catalysis - crystallographic, kinetic, and spectral studies of cytochrome-c peroxidase proximal ligand mutants. *J Biol Chem* **1994,** *269* (32), 20239-20249.

Colas, C., and de Montellano, P. R. O. (2003) Autocatalytic radical reactions in physiological prosthetic heme modification. *Chem. Rev.* **103**, 2305-2332.

Colin, J.; Wiseman, B.; Switala, J.; Loewen, P.; Ivancich, A., Distinct role of specific tryptophans in facilitating electron transfer or as [Fe(IV)=O Trp(+▪)] intermediates in the peroxidase reaction of *Bulkholderia pseudomallei* catalase-peroxidase: A multifrequency EPR spectroscopy investigation. *J Am Chem Soc* **2009,** *131* (24), 8557-8563.

Corrigal, A. V., Purification of and Kinetic Studies on a Cloned Protoporphyrinogen Oxidase from the Aerobic BacteriumBacillus subtilis. *Archives of Biochemistry and Biophysics* **1998,** *358* (2), 251-256.

D’Antonio, J., and Ghiladi, R. A. (2011) Reactivity of Deoxy- and Oxyferrous Dehaloperoxidase B from Amphitrite ornata: Identification of Compound II and Its Ferrous–Hydroperoxide Precursor, *Biochemistry 50*, 5999-6011.

D’Antonio, J., D’Antonio, E. L., Thompson, M. K., Bowden, E. F., Franzen, S., Smirnova, T., and Ghiladi, R. A. (2010) Spectroscopic and Mechanistic Investigations of Dehaloperoxidase B from *Amphitrite ornata*, *Biochemistry 49*, 6600-6616.

Dailey, H. A. (1997) Enzymes of heme biosynthesis, *J. Biol. Inorg. Chem. 2*, 411-417.

Dailey, H. A. (2002) Terminal steps of haem biosynthesis, *Biochem. Soc. Trans. 30*, 590-595.

Dailey, H. A., Altered Orientation of Active Site Residues in Variants of Human Ferrochelatase.Evidence for a Hydrogen Bond Network Involved in Catalysis. *Biochem J* **2007,** *46* (27), 7973-7979.

Dailey, H. A.; Dailey, T. A.; Gerdes, S.; Jahn, D.; Jahn, M.; O'Brian, M. R.; Warren, M. J., Prokaryotic Heme Biosynthesis: Multiple Pathways to a Common Essential Product. *Microbiol Mol Biol Rev* **2017,** *81* (1).

Dailey, H. A.; Gerdes, S.; Dailey, T. A.; Burch, J. S.; Phillips, J. D., Noncanonical coproporphyrin-dependent bacterial heme biosynthesis pathway that does not use protoporphyrin. *Proc Natl Acad Sci U S A* **2015,** *112* (7), 2210-5.

Dailey, T. A.; Boynton, T. O.; Albetel, A. N.; Gerdes, S.; Johnson, M. K.; Dailey, H. A., Discovery and Characterization of HemQ: an essential heme biosynthetic pathway component. *J Biol Chem* **2010,** *285* (34), 25978-86.

Degroot, D. C. (1967) Titrimetric determination of sodium dithionite with potassium hexacyanoferrate(3) as reagent and methylene blue as indicator, *Zeits. Analyt. Chemie Fresenius 229*, 335.

Di Bilio, A., Crane, B., Wehbi, W., Kiser, C., Abu-Omar, M., Carlos, R., Richards, J., Winkler, J., and Gray, H. (2001) Properties of photogenerated tryptophan and tyrosyl radicals in structurally characterized proteins containing rhenium(I) tricarbonyl diimines. *J. Am. Chem. Soc.* **123**, 3181-3182.

Doyle, W. A., Blodig, W., Veitch, N. C., Piontek, K., and Smith, A. T. (1998) Two substrate interaction sites in lignin peroxidase revealed by site-directed mutagenesis. *Biochemistry* **37**, 15097-15105.

Draganova, E. B.; Adrian, S. A.; Lukat-Rodgers, G. S.; Keutcha, C. S.; Schmitt, M. P.; Rodgers, K. R.; Dixon, D. W., Corynebacterium diphtheriae HmuT: dissecting the roles of conserved residues in heme pocket stabilization. *J Biol Inorg Chem* **2016, ASAP**.

Du, J., Sono, M., and Dawson, J. (2010) Functional Switching of Amphitrite ornata Dehaloperoxidase from O-2-Binding Globin to Peroxidase Enzyme Facilitated by Halophenol Substrate and H_2O_2, *Biochemistry 49*, 6064-6069.

Dunford, H. B., *Heme Peroxidases*. Wiley-VCH: 1999; p 528.

Efimov, I., Badyal, S. K., Metcalfe, C. L., Macdonald, I., Gumiero, A., Raven, E. L., and Moody, P. C. (2011) Proton delivery to ferryl heme in a heme peroxidase: enzymatic use of the Grotthuss mechanism. *J. Am. Chem. Soc.* **133**, 15376-15383.

English, A. M., and Tsaprailis, G. (1995) Catalytic Structure–Function Relationships in Heme Peroxidases, *Adv. Inorg. Chem. 43*, 79-125.

Erman, J. E.; Vitello, L. B.; Miller, M. A.; Kraut, J., Active-site mutations in cytochrome-c peroxidase - a critical role for histidine-52 in the rate of formation of Compound-I. *J Am Chem Soc* **1992,** *114* (16), 6592-6593.

Erman, J. E.; Vitello, L. B.; Miller, M. A.; Shaw, A.; Brown, K. A.; Kraut, J. (1993) Histidine 52 is a critical residue for rapid formation of cytochrome c peroxidase compound I, *Biochemistry 32*, 9798-9806.

Ferreira, G. C., Organization of the Terminal Two Enzymes of the Heme Biosynthetic Pathway. *The journal of biological chemistry* **1998,** *263* (8), 38835-3839.

Ferreira, G. C., Organization of the Terminal Two Enzymes of the Heme
Frey, P. A., and Hegeman, A. D. (2007) *Enzymatic Reaction Mechanisms*, Oxford University Press, Oxford, England, U.K.

Fujii, H., Yoshimura, T., and Kamada, H. (1996) ESR studies of A(1u) and A(2u) oxoiron(IV) porphyrin pi-cation radical complexes. Spin coupling between ferryl iron and A(1u)/A(2u) orbitals. *Inorg. Chem.* **35**, 2373-2377.

Gillam, M. E., Hunter, G.A., Ferreira, G.C., The Ultimate Step of Heme Biosynthesis: Orchestration Between Iron Trafficking and Porphyrin Synthesis. In *Handbook of Porphyrin Science*, Ferreira, G. C., Ed. World Scientific: 2014; Vol. 26, pp 129-189.

Gilski, M.; Borek, D.; Chen, Y.; Collart, F.; Joachimiak, A.; Otwinowski, Z. Crystal Structure of APC35880 protein from *Bacillus stearothermophilus*. *To be published* **2004**.

Goblirsch, B. R.; Streit, B. R.; DuBois, J. L.; Wilmot, C. M., Structural features promoting dioxygen production by *Dechloromonas aromatica* chlorite dismutase. *J Biol Inorg Chem* **2010,** *15* (6), 879-888.

Goblirsch, B., Kurker, R. C., Streit, B. R., Wilmot, C. M., and DuBois, J. L. (2011) Chlorite Dismutases, DyPs, and EfeB: 3 Microbial Heme Enzyme Families Comprise the CDE Structural Superfamily, *J. Mol. Biol. 408*, 379-398.

Gonzalez,A.;Tsai,Y.**2010**.http://smb.slac.stanford.edu/facilities/software/xds/#autoxds_script

Gorchein, A., Danton, M., and Lim, C. K. (2005) Harderoporphyrin: a misnomer. *Biomed. Chromatogr.* **19**, 565-569

Grant, J. L., Hsieh, C. H., and Makris, T. M. (2015) Decarboxylation of fatty acids to terminal alkenes by cytochrome P450 compound I. *J. Am. Chem. Soc.* **137**, 4940-4943.

Grant, J. L.; Mitchell, M. E.; Makris, T. M., Catalytic strategy for carbon-carbon bond scission by the cytochrome P450 OleT. *PNAS* **2016,** *113* (36), 10049-10054.

Guallar, V., Heme Electron Transfer in Peroxidases: The Propionate e-Pathway. *J Phys Chem B* **2008,** *112* (42), 13460-13464.

Gumiero, A., Metcalfe, C. L., Pearson, A. R., Raven, E. L., and Moody, P. C. (2011) Nature of the ferryl heme in compounds I and II. *J. Biol. Chem.* **286**, 1260-1268.

Hammes-Schiffer, S., Proton-coupled electron transfer: Moving together and charging forward. *J Am Chem Soc* **2015,** *137* (28), 8860-71.

Hamza, I.; Dailey, H. A., One ring to rule them all: trafficking of heme and heme synthesis intermediates in the metazoans. *Biochim Biophys Acta* **2012,** *1823* (9), 1617-32.

Haskamp, V.; Karrie, S.; Mingers, T.; Barthels, S.; Alberge, F.; Magalon, A.; Muller, K.; Bill, E.; Lubitz, W.; Kleeberg, K.; Schweyen, P.; Broring, M.; Jahn, M.; Jahn, D., The radical SAM protein HemW is a heme chaperone. *J Biol Chem* **2018,** *293* (7), 2558-2572.

Hayashi, T., Dejima, H., Matsuo, T., Sato, H., Murata, D., and Hisaeda, Y. (2002) Blue myoglobin reconstituted with an iron porphycene shows extremely high oxygen affinity, *J. Am. Chem. Soc. 124*, 11226-11227.

Hederstedt, L., Heme Proteins in Lactic Acid Bacteria. *Advances in Microbial Physiology* **2013,** *62,* 1-43.

Henderstedt, M. H. a. L., Bacillus subtilis HemY Is a Peripheral Membrane Protein Essential for Protoheme IX Synthesis Which Can Oxidize Coproporphyrinogen III and Protoporphyrinogen IX. *Journal of Bacteriology* **1994,** *176* (19), 5962-5970.

Hiner, A. N.; Raven, E. L.; Thorneley, R. N.; García-Cánovas, F.; Rodríguez-López, J. N. (2002) Mechanisms of compound I formation in heme peroxidases, *J. Inorg. Biochem. 91*, 27-34.

Hobbs, C., Dailey, H. A., and Shepherd, M. (2016) The HemQ coprohaem decarboxylase generates reactive oxygen species: implications for the evolution of classical haem biosynthesis, *Biochem J.* in press.

Hofbauer, S., Dalla Sega, M., Scheiblbrandner, S., Jandova, Z., Schaffner, I., Mlynek, G., Djinovic-Carugo, K., Battistuzzi, G., Furtmüller, P. G., Oostenbrink, C., and Obinger, C. (2016) Chemistry and molecular dynamics simulations of heme *b*-HemQ and coproheme-HemQ. *Biochemistry* **55**, 5398–5412.

Hofbauer, S.; Gruber, C.; Pirker, K.; Schaffner, I.; Furtmuller, P.; Obinger, C.; Hagmuller, A.; Gysel, K.; Mlynek, G.; Kostan, J.; Djinovic-Carugo, K.; Bellei, M.; Battistuzzi, G.; Daims, H., Understanding chlorite dismutase from *Candidatus Nitrospira defluvii. J Biol Inorg Chem* **2014,** *19*, S253-S253.

Hofbauer, S.; Howes, B. D.; Flego, N.; Pirker, K. F.; Schaffner, I.; Mlynek, G.; Djinovic-Carugo, K.; Furtmueller, P. G.; Smulevich, G.; Obinger, C., From chlorite dismutase towards HemQ-the role of the proximal H-bonding network in haeme binding. *Biosci. Rep.* **2016,** *36* , e00312.

Hofbauer, S.; Mlynek, G.; Millazo, L.; Pühringer, D.; Maresch, D.; Schaffner, I.; Furtmüller, P.G.; Smulevich, G.; Djinović-Carugo, K.; Obinger, C. Hydrogen peroxide-mediated conversion of coproheme to heme *b* by HemQ - Lessons from the first crystal structure and kinetic studies. *FEBS J* **2016**, Ahead of print.

Hu, S.; Smith, K.; Spiro, T. (1996) Assignment of protoheme resonance raman spectrum by heme labeling in myoglobin, *J. Am. Chem. Soc*. *118*, 12638-12646.

Ilka U. Heinemann, M. J., Dieter Jahn, The biochemistry of heme synthesis. *Archives of Biochemistry and Biophysics* **2008,** *474* (2), 238-251.

Kato, K., Identification of a gene essential for protoporphyrinogen IX oxidase activity in the cyanobacterium Synechocystis sp. PCC6803. *PNAs* **2010,** *107* (36), 16649-16654.
Khindaria, A., and Aust, S. (1996) EPR detection and characterization of lignin peroxidase porphyrin pi-cation radical. *Biochemistry* **35**, 13107-13111.

Kobayashi, K.; Masuda, T.; Tajima, N.; Wada, H.; Sato, N., Molecular phylogeny and intricate evolutionary history of the three isofunctional enzymes involved in the oxidation of protoporphyrinogen IX. *Genome Biol Evol* **2014,** *6* (8), 2141-55.

Koch, M., Crystal structure of protoporphyrinogen IX oxidase: a key enzyme in haem and chlorophyll biosynthesis. *EMBO Journal* **2004,** *23* (8), 1720-1728.

Kuhner, M.; Haufschildt, K.; Neumann, A.; Storbeck, S.; Streif, J.; Layer, G. (2014) The alternative route to heme in the methanogenic archaeon *Methanosarchia barkeri, Archaea.* vol. 2014, Article ID 327637, 13 pages, 2014

LaMattina, J. W.; Nix, D. B.; Lanzilotta, W. N., Radical new paradigm for heme degradation in Escherichia coli O157:H7. *Proc Natl Acad Sci U S A* **2016,** *113* (43), 12138-12143.

Lansky, I. B.; Lukat-Rodgers, G. S.; Block, D.; Rodgers, K. R.; Ratliff, M.; Wilks, A., The cytoplasmic heme-binding protein (PhuS) from the heme uptake system of Pseudomonas aeruginosa is an intracellular heme-trafficking protein to the delta-regioselective heme oxygenase. *J Biol Chem* **2006,** *281* (19), 13652-62.

Lash, T. D. (2005) The enigma of coproporphyrinogen oxidase: how does this unusual enzyme carry out oxidative decarboxyations to afford vinyl groups? *Bioorg. Med. Chem. Lett. 15*, 4506-4509.

Lash, T. D., Mani, U. N., Keck, A., and Jones, M. A. (2010) Normal and abnormal heme biosynthesis. 6. Synthesis and metabolism of a series of monovinylporphyrinogens related to harderoporphyrinogen. Further insights into the oxidative decarboxylation of porphyrinogen substrates by coproporphyrinogen oxidase. *J. Org. Chem.* **75**, 3183-3192.

Lash, T. D.; Mani, U. N.; Drinan, M. A.; Zhen, C.; Hall, T.; Jones, M. A. (1999) Normal and abnormal heme biosynthesis. 1. Synthesis and metabolism of di- and monocarboxylic porphyrinogens related to coproporphyrinogen-III and harderoporphyrinogen: A model for the active site of coproporphyrinogen oxidase, *J. Org. Chem. 64*, 464.

Layer, G., Pierik, A. J., Trost, M., Rigby, S. E., Leech, H. K., Grage, K., Breckau, D., Astner, I., Jaensch, L., Heathcote, P., Warren, M. J., Heinz, D. W., and Jahn, D. (2006) The substrate radical of Escherichia coli oxygen-independent coproporphyrinogen III oxidase HemN, *J. Biol. Chem. 281*, 15727-15734.

Layer, G.; Grage, K.; Teschner, T.; Schunemann, V.; Breckau, D.; Masoumi, A.; Jahn, M.; Heathcote, P.; Trautwein, A. X.; Jahn, D., Radical S-adenosylmethionine enzyme coproporphyrinogen III oxidase HemN: functional features of the [4Fe-4S] cluster and the two bound S-adenosyl-L-methionines. *J Biol Chem* **2005,** *280* (32), 29038-46.

Layer, G.; Pierik, A. J.; Trost, M.; Rigby, S. E.; Leech, H. K.; Grage, K.; Breckau, D.; Astner, I.; Jaensch, L.; Heathcote, P.; Warren, M. J.; Heinz, D. W.; Jahn, D., The substrate radical of Escherichia coli oxygen-independent coproporphyrinogen III oxidase HemN. *J Biol Chem* **2006,** *281* (23).

Layer, G.; Reichelt, J.; Jahn, D.; Heinz, D. W. (2010) Structure and function of enzymes in heme biosynthesis, *Protein Sci. 19*, 1137-1161.

Lecerof, D.; Fodje, M. N.; Alvarez Leon, R.; Olsson, U.; Hansson, A.; Sigfridsson, E.; Ryde, U.; Hansson, M.; Al-Karadaghi, S., Metal binding to Bacillus subtilis ferrochelatase and interaction between metal sites. *J Biol Inorg Chem* **2003,** *8* (4), 452-8.

Lee, W. C.; Reniere, M. L.; Skaar, E. P.; Murphy, M. E. P. (2008) Ruffling of metalloporphyrins bound to IsdG and IsdI, two heme-degrading enzymes in *Staphylococcus aureus*, *J. Biol. Chem. 283*, 30957-30963.

Lesuisse, E., Iron use for haeme synthesis is under control of the yeast frataxin homologue (Yfh1). *Human Molecular Genetics* **2003,** *12* (8), 879-889.

Lin, M., Sperling, L., Schmidt, H., Tang, M., Samoilova, R., Kumasaka, T., Iwasaki, T., Dikanov, S., Rienstra, C., and Gennis, R. (2011) A rapid and robust method for selective isotope labeling of proteins. *Methods* **55**, 370-378.

Lobo, S. A., Scott, A., Videira, M. A., Winpenny, D., Gardner, M., Palmer, M. J., Schroeder, S., Lawrence, A. D., Parkinson, T., Warren, M. J., and Saraiva, L. M. (2015) *Staphylococcus aureus* haem biosynthesis: characterisation of the enzymes involved in final steps of the pathway, *Mol. Microbiol. 97*, 472-487.

Lobo, S.A.L.; Scott, A.; Videira, M. A. M.; Winpenny, D.; Gardner, M.; Palmer, M.J.; Schroeder, S.; Lawrence, A. D.; Parkinson, T.; Warren, M.J.; Saraiva, L.M. (2015) *Staphyloccocus aureus* haem biosynthesis: characterisation of the enzymes involved in final steps of the pathway, *Mol. Microbiol., Epub ahead of print*

Lukat-Rodgers, G. S.; Rodgers, K. R.; Caillet-Saguy, C.; Izadi-Pruneyre, N.; Lecroisey, A., Novel heme ligand displacement by CO in the soluble hemophore HasA and its proximal ligand mutants: implications for heme uptake and release. *Biochemistry* **2008,** *47*, 2087-2098.

Luo, J.; Lim, C. K. (1993) Order of uroporphyrinogen III decarboxylation on incubation of prophobilinogen and uroporphyrinogen III with erythrocyte uropophyrinogen decarboxylase, *Biochem. J. 289*, 529-532.

Macdonald, I. K., Badyal, S. K., Ghamsari, L., Moody, P. C., and Raven, E. L. (2006) Interaction of ascorbate peroxidase with substrates: a mechanistic and structural analysis. *Biochemistry* **45**, 7808-7817.

Mak, P.; Podstawka, E.; Kincaid, J.; Proniewicz, L. (2004) Effecrs of systematic peripheral group deuteration on the low-frequency resonance Raman spectra of myoglobin derivatives, *Biopolymers 75,* 217-228.

Matsui, T., Nambu, S., Goulding, C., Takahashi, S., Fujii, H., and Ikeda-Saito, M. (2016) Unique coupling of mono- and dioxygenase chemistries in a single active site promotes heme degradation, *Proc. Natl. Acad. Sci. USA 113*, 3779-3784.

Matsui, T., Nambu, S., Ono, Y., Goulding, C. W., Tsurnoto, K., and Ikeda-Saitot, M. (2013) Heme Degradation by Staphylococcus aureus IsdG and IsdI Liberates Formaldehyde Rather Than Carbon Monoxide, *Biochemistry 52*, 3025-3027.

Matsui, T., Unno, M., and Ikeda-Saito, M. (2010) Heme oxygenase reveals its strategy for catalyzing three successive oxygenation reactions, *Acc. Chem. Res. 43*, 240-247.

Matsui, T.; Iwasaki, M.; Sugiyama, R.; Unno, M.; Ikeda-Saito, M. (2010) Dioxygen activation for the self-degradation of heme: reaction mechanism and regulation of heme oxygenase, *Inorg. Chem. 49*, 3602-3609.

Mayfield, J. A.; Hammer, N. D.; Kurker, R. C.; Chen, T. K.; Ojha, S.; Skaar, E. P.; DuBois, J. L., The Chlorite Dismutase (HemQ) fromStaphylococcus aureusHas a Redox-sensitive Heme and Is Associated with the Small Colony Variant Phenotype. *Journal of Biological Chemistry* **2013,** *288* (32), 23488-23504.

McCoy, A. J.; Grosse-Kunstleve, R. W.; Adams, P. D.; Winn, M. D.; Storoni, L. C.; Read, R. J., Phaser crystallographic software. *J Appl Crystallogr* **2007,** *40* (Pt 4), 658-674.

Mielcarek, A.; Blauenburg, B.; Miethke, M.; Marahiel, M. A., Molecular insights into frataxin-mediated iron supply for heme biosynthesis in Bacillus subtilis. *PLoS One* **2015,** *10* (3), e0122538.

Mourino, S.; Giardina, B. J.; Reyes-Caballero, H.; Wilks, A., Metabolite-driven Regulation of Heme Uptake by the Biliverdin IXbeta/delta-Selective Heme Oxygenase (HemO) of Pseudomonas aeruginosa. *J Biol Chem* **2016,** *291* (39), 20503-15.

Nagaraj, V. A.; Arumugam, R.; Prasad, D.; Rangarajan, P. N.; Padmanaban, G., Protoporphyrinogen IX oxidase from Plasmodium falciparum is anaerobic and is localized to the mitochondrion. *Mol Biochem Parasitol* **2010,** *174* (1), 44-52.

Okamura, M. Y.; Paddock, M. L.; Graige, M. S.; Feher, G., Proton and electron transfer in bacterial reaction centers. *Biochim Biophys Acta* **2000,** *1458* (1), 148-163.

Ortiz de Montellano P.R., *Cytochrome P450: Structure, Mechanism and Biochemistry*. 3rd ed.; Kluwer Academic/Plenum: New York, 2005.

Panek, H.; O'Brian, M. R. (2002) A whole genome view of prokaryotic haem biosynthesis, *Microbiology 148*, 2273-2282.

Patil, P. V., and Ballou, D. P. (2000) The Use of Protocatechuate Dioxygenase for Maintaining Anaerobic Conditions in Biochemical Experiments, *Analyt. Bioch. 286*, 187-192.

Pelletier, H.; Kraut, J., Crystal-structure of a complex between electron-transfer partners, cytochrome-c peroxidase and cytochrome-c. *Science* **1992,** *258* (5089), 1748-1755.

Perkins, J. R.; Diboun, I.; Dessailly, B. H.; Lees, J. G.; Orengo, C., Transient protein-protein interactions: structural, functional, and network properties. *Structure* **2010,** *18* (10), 1233-43.

Pfister, T. D., Gengenbach, A. J., Syn, S., and Lu, Y. (2001) The role of redox-active amino acids on compound I stability, substrate oxidation, and protein cross-linking in yeast cytochrome c peroxidase, *Biochemistry 40*, 14942-14951.

Pires, R. H., Venceslau, S. S., Morais, F., Teixeira, M., Xavier, A. V., and Pereira, I. A. C. (2006) Characterization of the Desulfovibrio desulfuricans ATCC 27774 DsrMKJOP complex - A membrane-bound redox complex involved in the sulfate respiratory pathway, *Biochemistry 45*, 249-262.

Podstawka, E.; Mak, P.; Kincaid, J., Proniewicz, L. (2006) Low frequency resonance Raman spectra of isolated alpha and beta subunits of hemoglobin and their deuterated analoges, *Biopolymers 83*, 455-466.

Poulos, T. L., Heme enzyme structure and function. *Chem Rev* **2014,** *114* (7), 3919-62. (b) Cherifi, G.; Baxter, E.L.; Doukov, T.; Cohen, A.E.; McPhillips, S.E.; Song, J.; Meharenna, Y.T; Soltis, S.M.; Poulos, T.L. Crystal structure of the pristine peroxidase ferryl center and its relevance to proton-coupled electron transfer. *PNAS*, **2016**, *112 (5)*, 1226-1231.

Poulos, T. L.; Fenna, R. E. (1994) Metalloenzymes involving amino acid residue related radicals, *Metal Ions Biol. Syst, 30*, 25-75.

Presi, P., Stark, K. D., Stephan, R., Breidenbach, E., Frey, J., and Regula, G. (2009) Risk scoring for setting priorities in a monitoring of antimicrobial resistance in meat and meat products, In *Int J Food Microbiol*, pp 94-100, Netherlands.

Qin, X., Structural insight into unique properties of protoporphyrinogen oxidase from Bacillus subtilis. *Journal of Structural Biology* **2010,** *170* (1), 76-82.

Rand, K.; Noll, C.; Schiebel, H. M.; Kemken, D.; Duelcks, T.; Kalesse, M.; Heinz, D. W.; Layer, G. (2010) The oxygen-independent coproporphyrinogen III oxidase HemN utilizes harderoporphyrinogen as a reaction intermediate during conversion of coproporphyrinogen III to protoporphyrinogen IX, *Biol. Chem. 391*, 55-63.

Reece, S.Y.; Hodgkiss, J.M., Stubbe, J.; Nocera, D.G. Proton-coupled electron transfer: the mechanistic underpinning for radical transport and catalysis in biology. *Philos Trans R Soc Lond B Biol Sci* **2006**, *361* (1472), 1351-1364.

Rittle, J.; Green, M. T., Cytochrome P450 compound I: capture, characterization, and C-H bond activation kinetics. *Science* **2010,** *330* (6006), 933-7.

Rodriguez-Lopez, J. N. L., D.J.; Hernandez-Ruiz, J.; Hiner, A.N.P.; Garcia-Canovas, F.; Thorneley, R.N.F Mechanism of Reaction of Hydrogen Peroxide with Horseradish Peroxidase: Identification of Intermediates in the Catalytic Cycle. *J Am Chem Soc* **2001,** *123* (48), 11838-11847.

Roston, D., Islam, Z., and Kohen, A. (2014) Kinetic isotope effects as a probe of hydrogen transfers to and from common enzymatic cofactors. *Arch. Biochem. Biophys.* **544**, 96-104.

Rwere, F.; Mak, P.; Kincaid, J. (2008) Resonance raman interrogation of the consequences of heme rotational disorder in myoglobin and its ligated derivatives, *Biochemistry 47*, 12869-12877.

Rwere, F.; Mak, P.; Kincaid, J. (2008) The impact of altered protein-heme interactions on the resonance Raman spectra of heme proteins. Studies of heme rotational disorder, *Biopolymers 89*, 179-186.

Rwere, F.; Mak, P.; Kincaid, J. (2014) Resonance Raman determination of vinyl group disposition in different derivatives of native myoglobin and its heme-disoriented form, *J. Raman Spec. 45*, 97-104.

Salam Al-Karadaghi, M. H., Stanislav Nikonov, Crystal structure of ferrochelatase: the terminal enzyme in heme biosynthesis. *Structure* **1997,** *5* (11), 1501-1510.

Schultz, C. E., Devaney, P. W., Winkler, H., Debrunner, P. G., Doan, N., Chiang, R., Rutter, R., and Hager, L. P. (1979) Horseradish peroxidase compound I: Evidence for spin coupling between the heme iron and a 'free' radical. *FEBS Lett.* **103**, 102-105.

Schunemann, V., Lendzian, F., Jung, C., Contzen, J., Barra, A., Sligar, S., and Trautwein, A. (2004) Tyrosine radical formation in the reaction of wild type and mutant cytochrome P450cam with peroxy acids - A multifrequency EPR study of intermediates on the millisecond time scale. *J. Biol. Chem.* **279**, 10919-10930.

Sharp, K. H.; Mewies, M.; Moody, P. C.; Raven, E. L., Crystal structure of the ascorbate peroxidase-ascorbate complex. *Nat Struct Biol* **2003,** *10* (4), 303-7.

Shepherd, M.; Dailey, T. A.; Dailey, H. A., A new class of [2Fe-2S]-cluster-containing protoporphyrin (IX) ferrochelatases. *Biochem J* **2006,** *397* (1), 47-52.

Singh, R.; Grigg, J. C.; Armstrong, Z.; Murphy, M. E. P.; Eltis, L. D., Distal heme pocket residues of B-type dye-decolorizing peroxidase, arginine but not aspartate is essential for peroxidase activity. *J Biol Chem* **2012,** *287* (13), 10623-10630.

Sivaraja, M.; Goodin, D. B.; Smith, M.; Hoffman, B. M., Identification by ENDOR of Trp191 as the free-radical site in cytochrome c peroxidase compound ES. *Science* **1989,** *245* (4919), 738-40.

Skaar, E. P.; Gaspar, A. H.; Schneewind, O. (2004) IsdG and IsdI, heme-degrading enzymes in the cytoplasm of Staphyloccocus aureus, *J. Biol. Chem. 279*, 436-443.

Smulevich, G., Feis, A., and Howes, B. D. (2005) Fifteen years of Raman spectroscopy of engineered heme containing peroxidases: What have we learned? *Acct. Chem. Res. 38*, 433-440.

Soderberg, C.; Gillam, M. E.; Ahlgren, E. C.; Hunter, G. A.; Gakh, O.; Isaya, G.; Ferreira, G. C.; Al-Karadaghi, S., The Structure of the Complex between Yeast Frataxin and Ferrochelatase: Characterization and pre-steady state reaction of ferrous iron delivery and heme synthesis. *J Biol Chem* **2016,** *291* (22), 11887-98.

Spiro, T. G.; Soldatova, A. V.; Balakrishnan, G., CO, NO and O2 as vibrational probes of heme protein interactions. *Coord Chem Rev* **2013,** *257*, 511-527.

Spiro, T. G.; Wasbotten, I. H., CO as a vibrational probe of heme protein active sites. *J Biol Inorg Chem* **2005,** *99* (1), 34-44.

Stephenson, J. R.; Stacey, J. A.; Morgenthaler, J. B.; Friesen, J. A.; Lash, T. D.; Jones, M. A. (2007) Role of aspartate 400, arginine 262, and arginine 401 in the catalytic mechanism of human corpoporphyrinoen oxidase, *Protein Sci. 16*, 401-410.

Stoll, S., and Schweiger, A. (2006) EasySpin, a comprehensive software package for spectral simulation and analysis in EPR. *J. Mag. Res.* **178**, 42-55

Streit, B. R., Blanc, B., Lukat-Rodgers, G. S., Rodgers, K. R., and DuBois, J. L. (2010) How Active-Site Protonation State Influences the Reactivity and Ligation of the Heme in Chlorite Dismutase, *J. Am. Chem. Soc. 132*, 5711-5724.

Streit, B. R., Decarboxylation involving a ferryl, propionate, and a tyrosyl group in a radical relay yields heme b. *Journal of Biological Chemistry* **2018,** *293* (11), 3989-3999.

Streit, B., Celis, A., Shisler, K., Rodgers, K., Lukat-Rodgers, G., and DuBois, J. (2017) Reactions of ferrous coproheme decarboxylase (HemQ) with O-2 and H_2O_2 yield ferric heme *b*. *Biochemistry* **56**, 189-201.

Streit, B., Kant, R., Tokmina-Lukaszewska, M., Celis, A., Machovina, M., Skaar, E., Bothner, B., and DuBois, J. (2016) Time-resolved Studies of IsdG Protein Identify Molecular Signposts along the Non-canonical Heme Oxygenase Pathway, *J. Biol. Chem. 291*, 862-871.

Stubbe, J., Nocera, D. G., Yee, C. S., and Chang, M. C. Y. (2003) Radical initiation in the class I ribonucleotide reductase: Long-range proton-coupled electron transfer? *Chem. Rev.* **103**, 2167-2201.

Sun, J., Wilks, A., Ortiz de Montellano, P. R., and Loehr, T. M. (1993) Resonance Raman and EPR spectroscopic studies on heme-heme oxygenase complexes, *Biochemistry 32*, 14151-14157.

Sun, S. F., Sono, M., Wang, C. X., Du, J., Lebioda, L., and Dawson, J. H. (2014) Influence of heme environment structure on dioxygen affinity for the dual function *Amphitrite ornata* hemoglobin/dehaloperoxidase. Insights into the evolutional structure-function adaptations, *Arch. Biochem. Biophys. 545*, 108-115.

Svistunenko, D. A. and Cooper, C. E. (2004) A new method of identifying tyrosyl radicals in proteins. *Biophys. J.* **84**. 582-595.
Takahashi, S., Wang, J., Rousseau, D. L., Ishikawa, K., Yoshida, T., Host, J. R., and Ikeda-Saito, M. (1994) Heme-heme oxygenase complex. Structure of the catalytic site and its implication for oxygen activation, *J. Biol. Chem. 269*, 1010-1014.

Teraoka, J., and Kitagawa, T. (1981) Structural implication of the heme-linked ionization of horseradish peroxidase probed by the iron-histidine stretching Raman line, *J. Biol. Chem. 256*, 3969-3977.

Tommos, C.; Skalicky, J. J.; Pilloud, D. L.; Wand, A. J.; Dutton, P. L., De novo proteins as models of radical enzymes. *Biochemistry* **1999,** *38* (29), 9495-9507.

Traylor, T. G.; Traylor, P. S., Reactions of dioxygen and its reduced forms with heme proteins and model porphyrin complexes. In *Active Oxygen in Biochemistry*, Valentine, J. S.; Foote, C. S.; Greenberg, A.; Liebman, J. F., Eds. Springer Netherlands: 1995; pp 84-187.

Tsai, A. L.; Kulmacz, R. J.; Palmer, G., Spectroscopic evidence for reaction of prostaglandin-H synthatase-1 tyrosyl radical with arachidonic-acid. *J Biol Chem* **1995,** *270* (18), 10503-10508.

Uchida, K.; Susai, Y.; Hirotani, E.; Kimura, T.; Yoneya, T.; Tekeuchi, H.; Harada, I. (1988) 4-vinyl and 2,4-divinyl deuteration effects on the low frequency resonance Raman bands of myoglobin: correlation with the structure of vinyl group, *J. Biol. Chem. 103*, 979-985.

Unno, M., Matsui, T., and Ikeda-Saito, M. (2007) Structure and catalytic mechanism of heme oxygenase. *Nat. Prod. Rep.* **24**, 553-570.

Valentine, J. S., Dioxygen Reactions. In *Bioinorganic Chemistry*, University Science Books: Mill Valley, CA, 1994; pp 253-311.

Valentine, J. S., Foote, C. S., Greenberg, A., and Liebman, J. F. (1995) *Active Oxygen in Biochemistry*, Vol. 3, Springer

Wang, N.; Zhang, J.; Yang, X.; Li, N.; Yu, G.; Han, J., Cao, K,; Guo, Z.; Syn, X.; and He, Q. Proteomic analysis of putative heme-binding proteins in *Streptococcus pyogenes*. *Metallomics* **2014,** *6*, 1451-1459.

Warren, J. J., and Mayer, J. M. (2011) Proton-coupled electron transfer reactions at a heme-propionate in an iron-protoporphyrin-IX model compound. *J. Am. Chem. Soc.* **133**, 8544-8551.

Warren, J. J.; Tronic, T. A.; Mayer, J. M., Thermochemistry of proton-coupled electron transfer reagents and its implications. *Chem Rev* **2010,** *110* (12), 6961-7001.

Westerlund, K., Berry, B., Privett, H., and Tommos, C. (2005) Exploring amino-acid radical chemistry: protein engineering and de novo design. *Biochim. Biophys. Acta-Bioenergetics* **1707**, 103-116.

Whittaker, J. W., Free radical catalysis by galactose oxidase. *Chem Rev* **2003,** *103* (6), 2347-2363.

Wilks, A. (2002) Heme oxygenase: Evolution, structure, and mechanism, *Antioxidants & Redox Signaling 4*, 603-614.

Wilks, A., Heinzl, G. (2014) Heme oxygenation and the widening paradigm of heme degradation, *Arch. Biochem. Biophys. 544*, 87-95.

Wilks, M. N. B. a. A., The Mechanism of Heme Transfer from the Cytoplasmic Heme Binding Protein PhuS to the δ-Regioselective Heme Oxygenase of Pseudomonas aeruginosa. *Biochem J* **2006,** *45* (38), 11642-11649.

Winn, M. D.; Ballard, C. C.; Cowtan, K. D.; Dodson, E. J.; Emsley, P.; Evans, P. R.; Keegan, R. M.; Krissinel, E. B.; Leslie, A. G.; McCoy, A.; McNicholas, S. J.; Murshudov, G. N.; Pannu, N. S.; Potterton, E. A.; Powell, H. R.; Read, R. J.; Vagin, A.; Wilson, K. S., Overview of the CCP4 suite and current developments. *Acta Crystallogr D Biol Crystallogr* **2011,** *67* (Pt 4), 235-42.

Wolfsberg, M., Van Hook, W. A., Paneth, P., and Rebelo, L. P. N. (2014) *Isotope Effects in the Chemical, Geological, and Bio Sciences*, Springer, 484 pp.

Yeh, H., Gerfen, G., Wang, J., Tsai, A., and Wang, L. (2009) Characterization of the peroxidase mechanism upon reaction of prostacyclin synthase with peracetic acid. Identification of a tyrosyl radical intermediate. *Biochemistry* **48**, 917-928.

Yuan, X.; Rietzschel, N.; Kwon, H.; Walter Nuno, A. B.; Hanna, D. A.; Phillips, J. D.; Raven, E. L.; Reddi, A. R.; Hamza, I., Regulation of intracellular heme trafficking revealed by subcellular reporters. *Proc Natl Acad Sci U S A* **2016,** *113* (35), E5144-52.